UNIVERSIDADE FEDERAL DE SANTA CATARINA
CENTRO TECNOLÓGICO
PROGRAMA DE PÓS-GRADUAÇÃO EM ENGENHARIA MECÂNICA

André Miazaki da Costa Tourinho

A study on the role of muscle contraction on the self-sustained oscillations of the pharyngoesophageal segment in tracheoesophageal speech

Florianópolis
2022

André Miazaki da Costa Tourinho

A study on the role of muscle contraction on the self-sustained oscillations of the pharyngoesophageal segment in tracheoesophageal speech

Tese submetida ao Programa de Pós-Graduação em Engenharia Mecânica da Universidade Federal de Santa Catarina para a obtenção do título de Doutor em Engenharia Mecânica.
Orientador: Prof. Andrey Ricardo da Silva, Ph.D.

Florianópolis
2022

Ficha de identificação da obra elaborada pelo autor,
através do Programa de Geração Automática da Biblioteca Universitária da UFSC.

Tourinho, André Miazaki da Costa
A study on the role of muscle contraction on the self sustained oscillations of the pharyngoesophageal segment in tracheoesophageal speech / André Miazaki da Costa Tourinho ; orientador, Andrey Ricardo da Silva, 2022.
207 p.

Tese (doutorado) - Universidade Federal de Santa Catarina, Centro Tecnológico, Programa de Pós-Graduação em Engenharia Mecânica, Florianópolis, 2022.

Inclui referências.

1. Engenharia Mecânica. 2. Fala traqueoesofágica. 3. Segmento faringoesofágico. 4. Auto-oscilação. I. da Silva, Andrey Ricardo. II. Universidade Federal de Santa Catarina. Programa de Pós-Graduação em Engenharia Mecânica. III. Título.

André Miazaki da Costa Tourinho

A STUDY ON THE ROLE OF MUSCLE CONTRACTION ON THE SELF-SUSTAINED OSCILLATIONS OF THE PHARYNGOESOPHAGEAL SEGMENT IN TRACHEOESOPHAGEAL SPEECH

O presente trabalho em nível de Doutorado foi avaliado e aprovado por banca examinadora composta pelos seguintes membros:

Prof. Byron D. Erath, Ph.D.
Clarkson University

Prof. Scott L. Thomson, Ph.D.
Brigham Young University

Prof. Júlio Apolinário Cordioli, Dr.
Universidade Federal de Santa Catarina

Certificamos que esta é a **versão original e final** do trabalho de conclusão que foi julgado adequado para obtenção do título de Doutor em Engenharia Mecânica.

ICP-Edu
Documento assinado digitalmente
Henrique Simas
Data: 17/11/2022 14:00:55-0300
CPF: ***.194.639-**
Verifique as assinaturas em https://v.ufsc.br

Prof. Henrique Simas, Dr.
Coordenador do Programa

ICP-Edu
Documento assinado digitalmente
Andrey Ricardo da Silva
Data: 16/11/2022 15:16:34-0300
CPF: ***.554.909-**
Verifique as assinaturas em https://v.ufsc.br

Prof. Andrey Ricardo da Silva, Ph.D.
Orientador

Florianópolis, 12 de setembro de 2022.

Acknowledgements

I would like to thank my advisor, Andrey R. da Silva, for all the assistance and support given throughout the development of this thesis. I am also thankful for the financial support given by CAPES, CNPq, and FINEP, which enabled the development of this research project.

I am very grateful for the help given by the team from CEPON: Luis Roberto Medina dos Santos, Elisa Gomes Vieira, and Fabiana Barroso Thomaz. Their assistance in helping me understand the pharyngoesophageal segment and its function was very valuable. Likewise, the discussions with the patients of GAL (Grupo de Acolhimento a Pacientes com Câncer de Cabeça e Pescoço) were instrumental in helping me understand the life of a laryngectomee. I am very thankful to them for welcoming me in their meetings and taking the time to talk to me. Additionally, I would like to thank prof. Ana Carolina de Assis Moura Ghirardi from the Phonoaudiology Department of UFSC for the very helpful discussions on the pharyngoesophageal segment.

I would like to thank the people from the Laboratório de Vibrações e Acústica (LVA). I would specially like to thank the friends and colleagues who worked in the voice prosthesis project (Andressa, Bárbara, Camila, Guilherme, João, Maria Júlia, Nivaldo, Tanaka, and Tobias), not only for their support, but for being able to make the day-to-day life in the lab very enjoyable.

Finally, I would like to thank my family, who have always offered me nothing but support and encouragement.

"See first, think later, then test. But always see first.
Otherwise you will only see what you were expecting."
Wonko the Sane

Resumo

Apesar de todo o progresso sendo feito no tratamento do câncer de laringe, a remoção cirúrgica da laringe ainda se faz necessária em muitos casos. Os pacientes que passam por esta cirurgia perdem as pregas vocais e, consequentemente, a capacidade de fala. Para estes pacientes, a fala traqueoesofágica talvez seja o método mais vantajoso de reestabelecer a comunicação vocal. Contudo, nem todos são capazes de produzir a voz traqueoesofágica. Isto geralmente está associado ao nível de contração muscular (a tonicidade) do segmento faringoesofágico, que é a principal fonte sonora na fala traqueoesofágica. Embora os pontos básicos acerca da fisiologia da fala traqueoesofágica sejam conhecidos atualmente, existem áreas pouco exploradas e muitas perguntas ainda não foram respondidas, inclusive a respeito do papel da tonicidade do segmento faringoesofágico na produção da voz traqueoesofágica. Mais especificamente, a mecânica da auto-oscilação do segmento faringoesofágico recebeu pouca atenção na literatura. A presente tese busca contribuir para o preenchimento desta lacuna. Um modelo matemático da fonação traqueoesofágica é proposto com base em uma revisão do que se sabe atualmente sobre a anatomia do segmento faringoesofágico e sobre a fisiologia da fala traqueoesofágica. A despeito de sua simplicidade, o modelo é capaz de reproduzir diferentes formas do segmento faringoesofágico que são observadas em estudos de videofluoroscopia. A relação entre a tonicidade do segmento faringoesofágico e sua forma durante a fonação é descrita na literatura e esta relação é verificada com o modelo simplificado. Uma análise de estabilidade linear também foi conduzida para identificar a tonicidade mínima necessária para que ocorra a auto-oscilação do segmento faringoesofágico. Um modelo experimental da fonação traqueoesofágica também foi desenvolvido, fornecendo uma abordagem complementar ao modelo matemático. Com o modelo experimental, verificou-se que a frequência de oscilação aumenta com a tonicidade, mas mudanças na tensão longitudinal não levaram a alterações consideráveis na frequência. Isto levanta a questão de se o controle da frequência fundamental de fonação ocorre por meio de alterações de tonicidade. Tendências da tonicidade mínima necessária para auto-oscilação foram identificadas e comparações com o modelo matemático foram feitas.

Palavras-chave: Fala traqueoesofágica. Segmento faringoesofágico. Auto-oscilação.

Resumo expandido

Introdução

Uma grande quantidade de pessoas são diagnosticadas com câncer de laringe todos os anos. Uma parcela considerável dessas pessoas precisará passar por uma cirurgia, chamada de laringectomia total, para tratar o tumor. Nesta operação a laringe é removida, o que implica a perda das pregas vocais e, consequentemente, da capacidade de produção da voz laríngea. No entanto, atualmente existem diversos métodos de reabilitação da fala. Dentre eles, a fala traqueoesofágica talvez seja o mais vantajoso. Na fala traqueoesofágica, uma prótese é utilizada na ligação entre a traqueia e o esôfago. A prótese atua como uma válvula unidirecional, impedindo a passagem do conteúdo do esôfago para a traqueia, mas permitindo a passagem de ar da traqueia para o esôfago quando o laringectomizado (pessoa que passou por uma laringectomia total) fecha o traqueostoma e expira. O redirecionamento do ar da traqueia para o esôfago resulta em um escoamento de ar através do segmento faringoesofágico, induzindo sua auto-oscilação. A oscilação do segmento faringoesofágico, por sua vez, produz som, possibilitando a fala. A despeito das várias vantagens da fala traqueoesofágica sobre outros métodos de reabilitação vocal, o método ainda apresenta limitações. Para o presente trabalho a limitação mais relevante é a de que nem todos os laringectomizados são capazes de produzir a voz traqueoesofágica. A razão mais comum para isto está relacionada ao nível de contração muscular (tonicidade) no segmento faringoesofágico. Uma tonicidade excessiva (hipertonicidade) impede a produção da voz traqueoesofágica assim como uma tonicidade muito baixa (hipotonicidade), embora este segundo caso seja muito mais raro que o primeiro. Desta forma, a compreensão do papel da musculatura do segmento faringoesofágico em sua auto-oscilação é de grande importância para o aprimoramento da fala traqueoesofágica como método de reabilitação vocal.

Objetivos

A presente tese tem como objetivo geral propor um modelo matemático e um modelo experimental do segmento faringoesofágico na produção da voz traqueoesofágica. Estes modelos serão usados para estudar o papel da contração muscular na produção da voz traqueoesofágica. Em específico, será estudada a relação entre a tonicidade e a forma do segmento faringoesofágico durante a fonação, assim como a tonicidade mínima que é necessária para a produção da voz traqueoesofágica.

Metodologia

O processo de modelagem do segmento faringoesofágico tem início com uma revisão bibliográfica a respeito da anatomia do segmento faringoesofágico pós-laringectomia e da fisiologia da voz traqueoesofágica. Esta revisão levou à proposta de se representar o segmento faringoesofágico como um tubo colapsável. Um tubo colapsável é um tubo flexível ligado em suas extremidades a tubos rígidos. Através dos tubos passa um escoamento de fluido e o tubo flexível está sujeito a uma pressão externa, que tende a fechá-lo. Neste contexto, o tubo flexível representa o segmento faringoesofágico, enquanto que os tubos rígidos representam o esôfago e a faringe. A pressão externa exerce o papel da tonicidade e uma tensão longitudinal no tubo exerce o papel de cargas longitudinais atuando no segmento faringoesofágico. Tanto o modelo matemático como o modelo experimental se baseiam nesta ideia, mas o modelo matemático trabalha com uma representação simplificada: a de um canal colapsável. Um canal colapsável é um canal bidimensional onde um trecho de uma das laterais é substituído por uma membrana flexível, sobre a qual atua uma pressão externa. O modelo matemático foi usado para obter soluções de regime permanente, para avaliar como a tonicidade do segmento faringoesofágico afeta a forma do segmento durante a fonação. Também comparou-se soluções de regime permanente obtidas com o modelo matemático com dados retirados de imagens de tomografia. As equações governantes também foram linearizadas para avaliar a estabilidade das soluções de regime permanente para diferentes combinações de parâmetros do modelo. Isto permite a estimativa da tonicidade mínima necessária para que ocorra a auto-oscilação. O modelo experimental proposto, por sua vez, é essencialmente um tubo colapsável, sendo que para aplicar a pressão externa ao tubo flexível o sistema de tubo flexível e tubos rígidos foi colocado no interior de uma câmara pressurizada. O experimento é conduzido impondo uma tensão longitudinal inicial ao tubo flexível e mantendo uma vazão de ar constante. A pressão da câmara é então elevada gradativamente, enquanto se monitora a vazão de entrada para o tubo flexível, a pressão na câmara e as pressões a montante e a jusante do tubo flexível. Este procedimento permite a identificação da tonicidade mínima necessária para que ocorra a auto-oscilação, além de permitir analisar como o aumento da pressão afeta a oscilação do tubo. Diferentes combinações de vazão (12 vazões distintas foram consideradas) e tensão longitudinal (5 valores distintos) foram testadas, sendo que em cada caso a pressão na câmara sempre foi elevada gradativamente até um valor limite. Para cada combinação se identifica a pressão na câmara que levou à auto-oscilação, assim como se registra como o comportamento do sistema varia com esta pressão por meio da medição da pressão a jusante do tubo flexível.

Resultados e Discussão

As soluções de regime permanente do modelo matemático sugerem a relação entre a tonicidade do segmento faringoesofágico e sua forma durante a fonação. Caso o segmento apresente tonicidade muito baixa, ele permanece basicamente aberto, com suas paredes razoavelmente afastadas uma da outra. Conforme a tonicidade aumenta, o segmento tende a fechar. A princípio isto se inicia pelo meio do segmento, mas conforme a tonicidade cresce, o ponto de área mínima se desloca a jusante. Quando a tonicidade já está elevada, a parte inferior do segmento começa a inflar, e a constrição formada mais a jusante se torna mais estreita. Esta mesma tendência já havia sido descrita em estudos de videofluoroscopia, demonstrando a coerência do modelo. Comparações das soluções de regime permanente com dados obtidos de imagens de tomografia mostram semelhanças qualitativas, mas divergiram quantitativamente. Estas diferenças eram esperadas, uma vez que não se conhece a distribuição de tonicidade dos laringectomizados dos quais as imagens foram obtidas. A análise de estabilidade forneceu uma expressão simplificada da tonicidade mínima necessária para auto-oscilação do segmento faringoesofágico, em termos do diâmetro equivalente do segmento, do comprimento do segmento, da tensão longitudinal atuando sobre ele, da densidade do ar e da velocidade média do escoamento de ar. O modelo experimental evidenciou como a oscilação do segmento faringoesofágico é afetada pela tonicidade do segmento faringoesofágico, assim como com a tensão longitudinal. Para tensões longitudinais baixas e vazões baixas, a auto-oscilação tinha início a pressões da câmara relativamente elevadas e com frequências relativamente altas. Conforme se testava vazões maiores, o comportamento era alterado e, para uma certa vazão, a auto-oscilação subitamente se iniciava a pressões baixas e com frequências mais baixas. Nestes casos, conforme a pressão na câmara aumentava, a oscilação do tubo se modificava. A frequência de oscilação crescia, e a forma de onda das flutuações de pressão a jusante do tubo flexível era modificada consideravelmente. Tensões longitudinais mais elevadas geralmente levaram a um comportamento similar a este segundo caso, ou seja, as oscilações tinham início a pressões baixas e, conforme a pressão na câmara era elevada, a frequência de oscilação crescia e a forma de onda das flutuações de pressão se modificava. Curvas identificando a menor pressão da câmara que era necessária para a auto-oscilação foram construídas em termos da vazão e da tensão longitudinal. Exceção feita aos casos em que a auto-oscilação tinha início a altas pressões da câmara, ou em que houve o término das oscilações com o aumento da pressão, foi identificado um padrão claro, onde um aumento da vazão reduz a pressão limiar, assim como uma redução da tensão longitudinal. Mais especificamente, observou-se o mesmo comportamento qualitativo previsto pelo modelo matemático, muito embora discrepâncias quantitativas tenham sido observadas. Dada a natureza simplificada do modelo matemático, estas discrepâncias eram esperadas. Com o modelo experimental também se observou que o parâmetro que mais influenciou a frequência de oscilação foi a pressão na câmara, contudo, as variações de frequência foram relativamente pequenas, sendo da ordem de uma oitava ou menos.

Considerações Finais

Com o modelo matemático proposto, foi possível demonstrar que a correlação feita em estudos de imagem entre a forma do segmento faringoesofágico durante a fonação e sua tonicidade possui de fato uma fundamentação física. Também foi possível propor uma expressão simplificada para a tonicidade mínima necessária para a fonação, determinando um critério para a falha na produção da voz traqueoesofágica devido a hipotonicidade do segmento faringoesofágico. O modelo experimental corroborou a expressão simplificada sugerida pelo modelo matemático na maior parte das combinações de parâmetros testadas. Contudo, para outras combinações, o modelo matemático não representou adequadamente o comportamento do modelo experimental. Tendo em vista as simplificações envolvidas, estas discrepâncias eram esperadas. Uma possível causa para elas é um acoplamento acústico (que não está presente no modelo matemático) com a cavidade de ar no tubo rígido a jusante do tubo flexível. Estudos futuros podem elucidar esta questão. Com o modelo experimental também foi observado que a frequência de oscilação era mais fortemente afetada pela pressão na câmara, que representa a tonicidade do segmento faringoesofágico. Uma vez que não se sabe até que ponto um laringectomizado é capaz de voluntariamente controlar a tonicidade de seu segmento, isto levanta a questão de como um laringectomizado é capaz de ajustar a frequência de fonação. Este ponto também sugere como caminho para trabalhos futuros uma melhora na representação da tonicidade nos modelo matemático e experimental. Tendo em vista o impacto positivo que um melhor entendimento da mecânica envolvida na fala traqueoesofágica traria a milhares de laringectomizados, acredita-se que mais estudos na área (avaliando, por exemplo, a falha na produção da voz traqueoesofágica devido a hipertonicidade) seriam de grande valor.

Palavras-chave: Fala traqueoesofágica. Segmento faringoesofágico. Auto-oscilação.

Abstract

Despite the continuous progress being made in the treatment of laryngeal cancer, the complete surgical excision of the larynx remains necessary in many cases. Patients who undergo surgery will lose their vocal folds, and consequently their ability to speak. For these patients, tracheoesophageal speech might be the most advantageous method to reestablish vocal communication. However, not every patient is able to produce the so-called tracheoesophageal voice. This failure is usually associated with the amount of muscle contraction (tonicity) in the pharyngoesophageal segment, which is the main source of sound in tracheoesophageal speech. While the most basic aspects regarding the physiology of tracheoesophageal speech are currently known, some areas are still little explored and many questions remain, including on the role played by pharyngoesophageal segment tonicity on the tracheoesophageal voice. In particular, the mechanics of the self-sustained oscillations of the pharyngoesophageal segment has received very little attention. The present thesis aims to address this. A simplified mathematical model for tracheoesophageal phonation is proposed based on a review of the literature on the anatomy of the pharyngoesophageal segment and the physiology of tracheoesophageal speech. The model is capable of reproducing several different pharyngoesophageal segment shapes that are observed in imaging studies with only few parameters. The relationship between tonicity with the shape of the pharyngoesophageal segment during phonation that is reported in the literature is verified with the model. Additionally, a linear stability analysis is conducted to identify the minimum amount of tonicity required for the onset of self-sustained oscillations of the pharyngoesophageal segment. An experimental model of tracheoesophageal phonation has also been developed, providing a complementary approach to the mathematical model. It was observed that the oscillation frequency increases with tonicity, but changes with longitudinal tension were not as large, raising the question of whether frequency control in tracheoesophageal speech might happen by changes in tonicity. Trends in the minimum tonicity required for self-sustained oscillations to occur were identified, and comparisons to the mathematical model were made.

Keywords: Tracheoesophageal speech. Pharyngoesophageal segment. Self-sustained oscillations.

List of Figures

List of Tables

List of abbreviations and acronyms

CT	Computed tomography
EMG	Electromyography
FFT	Fast Fourier Transform
MRI	Magnetic resonance imaging
PES	Pharyngoesophageal segment
PIV	Particle image velocimetry
SPVP	Sound-producing voice prosthesis
TE	Tracheoesophageal

List of symbols

a	Collapsible channel width
a_j	Coefficients of a Chebyshev series
f	Frequency
h	Vertical position of the membrane
$\hat{h}$	Dimensionless h
$\tilde{h}$	Eigenfunction related to the vertical position of the membrane
h_{min}	Minimum of h_s
h_s	Steady-state membrane configuration
l	Length of the membrane
l_1	Length of the rigid segment upstream of the membrane
L_1	Ratio of lengths of the upstream rigid section and the membrane
l_2	Length of the rigid segment downstream of the membrane
L_2	Ratio of lengths of the downstream rigid section and the membrane
m	Mass per unit area
M	Dimensionless membrane inertia
N	Order of the highest term in a truncated Chebyshev series
p	Pressure
$\hat{p}$	Dimensionless p
p_1	Pressure upstream of the flexible tube
p_2	Pressure downstream of the flexible tube
p_c	Characteristic value of p
p_e	External pressure
$\bar{p}_e$	Mean value of $p_e(x)$
P_e	Dimensionless external pressure
$\bar{P}_e$	Mean value of $P_e(x)$
p_o	Pressure at the outlet of the collapsible channel
q	Dimensionless flux per unit breadth (out-of-plane direction)
$\tilde{q}$	Eigenfunction related to the flux
q_s	Steady-state flux
Q	Flow per unit breadth (out-of-plane direction)
Q_v	Volumetric flow rate
R	Modified Reynolds number
t	Time
T	Dimensionless membrane tension
$\hat{t}$	Dimensionless t
t_c	Characteristic value of t
u	Velocity component in the x direction
$\hat{u}$	Dimensionless u

U	Mean velocity at the inlet
v	Velocity component in the y direction
$\hat{u}$	Dimensionless v
v_c	Characteristic value of v
x	Horizontal cartesian coordinate
$\hat{x}$	Dimensionless x
y	Vertical cartesian coordinate
$\hat{y}$	Dimensionless y
κ	Curvature of the membrane
λ	Eigenvalue
ν	Kinematic viscosity
ρ	Density
τ	Longitudinal membrane tension
ψ_j^0	Chebyshev polynomial of order j
ψ_j^m	m-th integral of ψ_j^0

Contents

1 Introduction

This thesis is concerned with voice production by laryngectomees, who are individuals who have had their larynges surgically removed due to cancer. The surgical removal of the larynx happens in a procedure called total laryngectomy.

Since the larynx contains the vocal folds, its excision will preclude voice production. However, there are different ways for laryngectomees to speak, even without the vocal folds. One of these methods is called tracheoesophageal (TE) speech. In TE speech a prosthesis is placed connecting the trachea to the esophagus. The prosthesis allows the passage of air from the trachea to the esophagus, and the airflow sets the pharyngoesophageal segment (PES) into self-sustained oscillations. These oscillations produce the TE voice, allowing vocal communication to occur. Therefore, in TE speech, the PES plays a role that is analogous to that of the vocal folds in laryngeal speech.

TE speech is the most common type of speech rehabilitation method today (VERKERKE; THOMSON, 2014). However, the TE voice does not have the same quality as the laryngeal voice, and the method still has some drawbacks. Therefore, it is desirable to study the mechanics of the TE voice, since this may aid the process of overcoming these obstacles.

Several aspects in the mechanics of the vocal folds and the laryngeal voice have been made clearer with mathematical models, as well as with experimental *in vitro* models. In the present thesis, these two methods of investigation are applied to TE speech. While the production of the TE voice is in many ways analogous to the production of the laryngeal voice, the anatomical structures are completely different, as are many aspects of the physiology involved. Therefore, a considerable part of the knowledge gained in the mechanics of the laryngeal voice does not translate directly to the TE voice. It is then important to first review what is currently known about the anatomy of the PES and the physiology of TE speech, so that the proposed models may be useful.

What is hoped to achieve with the mathematical and experimental models is to better understand the effect muscle contraction has on the TE voice. This understanding is important since failure in producing the TE voice is often associated with issues regarding muscle contraction.

This introductory chapter presents the context in which this thesis is inserted. It covers the topics of total laryngectomy (Section 1.1), voice rehabilitation after surgery (Section 1.2), and TE speech (Section 1.3). This initial presentation is followed by a description of the objectives of the thesis (Section 1.4), where the main questions to be answered by the models are listed. A final section exposes the organization and structure of the thesis (Section 1.5).

1.1 Total laryngectomy and its consequences

The main reason for someone to go through a total laryngectomy is laryngeal cancer. In 2020, it is estimated that there were over 180 000 new cases of laryngeal cancer worldwide and almost 100 000 fatalities associated with the disease (WHO, 2020). In Brazil, it is estimated that there will be 7 650 new cases for each year of the triennium 2020–2022 (INCA, 2019). While the incidence of laryngeal cancer is not particularly high compared to different types of cancer[1], in absolute terms the number of people diagnosed each year with the disease is clearly considerable.

Treatment options for laryngeal cancer are essentially the same as that for different types of cancer — surgery, chemotherapy, radiotherapy, or a combination of these procedures (GENDEN et al., 2007).

With regard to surgical treatments, it should be noted that total laryngectomy is not the only surgical procedure used for laryngeal cancer. There are also partial laryngectomies and a "near-total" laryngectomy[2]. However, for the purposes of this work, total laryngectomy is the most relevant, and the term "laryngectomy" will be used as a synonym for total laryngectomy.

In a total laryngectomy, the entire larynx is removed and the trachea is separated from the pharynx, being connected to a surgically created opening in the neck, called a tracheostoma (see Section 2.3 for a detailed description of the procedure). Post-surgery, the reconstructed PES consists essentially of a tube with an inner layer of mucosa surrounded by a layer of muscle. Figure 1 shows schematically the anatomy of a person before and after surgery.

A total laryngectomy causes a number of drastic changes in the life of a laryngectomee. Since the connection between the lungs and the upper respiratory tract (which includes the nose and oral cavities) is lost, the laryngectomee does not breathe through the nose, but through the tracheostoma. This has several consequences. For instance, many of the functions usually performed by the nose are completely lost, such as warming, humidifying, and filtering the air that is inhaled. To compensate for this, laryngectomees often wear a heat and moisture exchange device on the tracheostoma (LEWIS, 2019).

Figure 2 shows a heat and moisture exchanger open and closed. When open, it allows the passage of air from the trachea to the outside of the body through the filtering element. Should a laryngectomy wish to occlude the tracheostoma (to produce the TE voice, for instance), he/she may press down the button on the heat and moisture exchanger, and seal it. These devices can be held in place by different means, such as adhesives, buttons, or laryngectomy tubes (Figure 3).

1 For the sake of comparison, there were over two million new cases of lung cancer, as well as breast cancer in 2020 (WHO, 2020).

2 See Ferreiro-Argüelles et al. (2008) for descriptions of different types of partial laryngectomies, and Genden et al. (2007) for the "near-total" laryngectomy.

Figure 1 – Changes in anatomy due to a total laryngectomy.

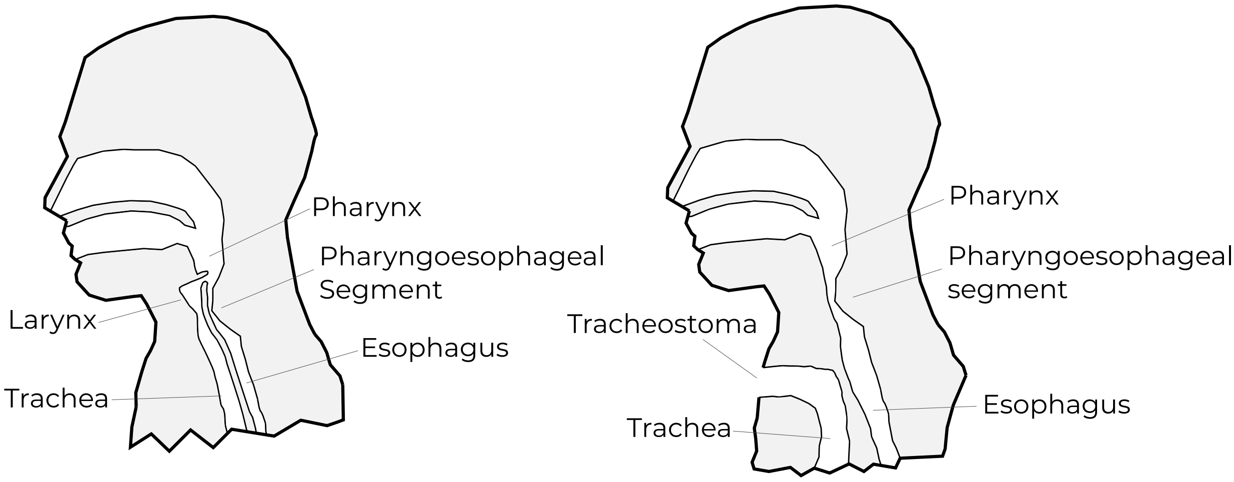

(a) Before surgery.

(b) After surgery.

Source – Author.

Figure 2 – Heat and moisture exchange device.

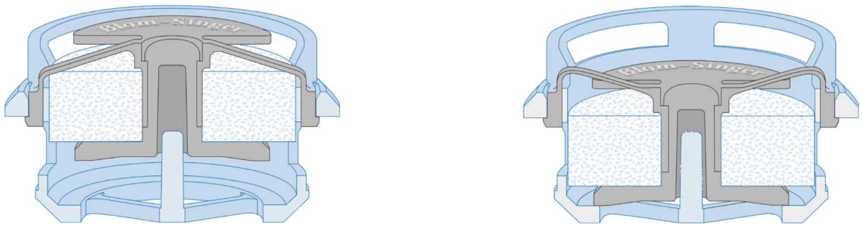

(a) Open.

(b) Closed.

Source – InHealth (2018).

Figure 3 – Devices to secure the heat and moisture exchange device on the tracheostoma.

(a) Adhesive.

(b) Button.

(c) Laryngectomy tube.

Source – Atos (2021a).

Several other life changes caused by total laryngectomy may be listed, such as an impaired sense of smell (WARD et al., 2010), a higher likelihood of swallowing issues (MACLEAN; COTTON; PERRY, 2009), and even the inability to swim, since submerging the tracheostoma would fill the lungs with water[3]. Considering all of the

[3] However, it should be mentioned that there are special devices to allow for a laryngectomee to swim. See Kress and Schäfer (2021b).

drawbacks associated with a total laryngectomy, it is not surprising that several studies have argued in favor of larynx preserving treatments (FORASTIERE et al., 2003), such as chemoradiation, and shown a decrease on the number of total laryngectomies performed in comparison to alternative treatments (GENDEN et al., 2007; CHEN; FEDEWA; ZHU, 2011; TIMMERMANS et al., 2016).

Unfortunately, larynx preserving alternatives also have their own drawbacks, and the decision of which treatment to adopt is not a simple one (CHEN; FEDEWA; ZHU, 2011). Moreover, patients treated with chemoradiation may need to undergo a total laryngectomy due to recurrent tumor, and a total laryngectomy may provide a better survival rate and quality of life for individuals with extensive laryngeal cancer (BOZEC et al., 2020). Therefore, it is likely that total laryngectomy will remain a common form of treatment for years to come.

For the purposes of the present work, the most relevant consequence of a total laryngectomy is the loss of speech associated with the excision of the vocal folds. Vocal communication is so prevalent in social interactions that it is no surprise that its loss has a significant impact in a laryngectomee's quality of life (SOUZA et al., 2020). In order to mitigate this effect, several methods of vocal rehabilitation have been developed over time. A brief presentation of them is made in the following section.

1.2 Vocal rehabilitation

Methods of voice rehabilitation following total laryngectomy date back as far as the nineteenth century. The first successful laryngectomy was performed by Billroth in 1873 (LORENZ, 2017). The procedure was reported by one of Billroth's assistants, Carl Gussenbauer, in a medical conference in 1874. In his presentation, he also described a prosthesis he had designed to restore the patient's voice. Since then, a wide variety of devices and methods have been developed with the goal of restoring voice after a total laryngectomy. The interested reader is referred to Lorenz (2017), and Verkerke and Thomson (2014) for a historical overview of voice rehabilitation methods. Here, the presentation is restricted to methods which are still commonly used.

Pseudo-whispering is a method of vocal communication that does not require any device. The laryngectomee uses the air in the oral cavity and the pharynx to articulate voiced sounds. As the name implies, the resulting voice is weak and aphonic, and allows for fluent communication only in relatively quiet settings (LORENZ, 2017). Brown et al. (2003) indicate that this method is rarely used, and that the speech produced has poor intelligibility.

Esophageal speech is another method of speech rehabilitation that does not require any external device. In this method, the laryngectomee moves air from the mouth into the esophagus and later expels it (Figure 4). When the air is exiting the esophagus, it sets the PES into self-sustained oscillations. These oscillations produce sound in a manner that is analogous to the oscillations of the vocal folds in laryngeal speech.

Esophageal speech is an old technique, dating back to the nineteenth century, when different reports of laryngectomees who "spontaneously" recovered the ability to speak appeared (DAMSTÉ, 1958; LORENZ, 2017). In spite of being a well established method of rehabilitation, esophageal speech has several drawbacks. Gates et al. (1982) describe the resulting voice as a "harsh voice of low pitch and loudness that is adequate for communication in small groups and quiet settings". There is also a limit on the amount of air that the person is able to move into the esophagus, which in turn limits speech to a few syllables at a time (LORENZ, 2017). Additionally, esophageal speech requires training and there is no guarantee of success. While there is some uncertainty with regard to the success rate of esophageal speech, with Brown et al. (2003) indicating that published success rates range from 14% to 75%, it is evident that a certain amount of skill is required for obtaining a fluent esophageal speech. The training necessary to obtain such skill does impose an obstacle to the method.

While the present work is not particularly concerned with esophageal speech, it will be mentioned and discussed further throughout the thesis. The reason for this is that both the esophageal voice and the TE voice are generated by the self-sustained oscillations of the PES. Therefore, in certain points, both methods are very closely related.

Figure 4 – Esophageal speech.

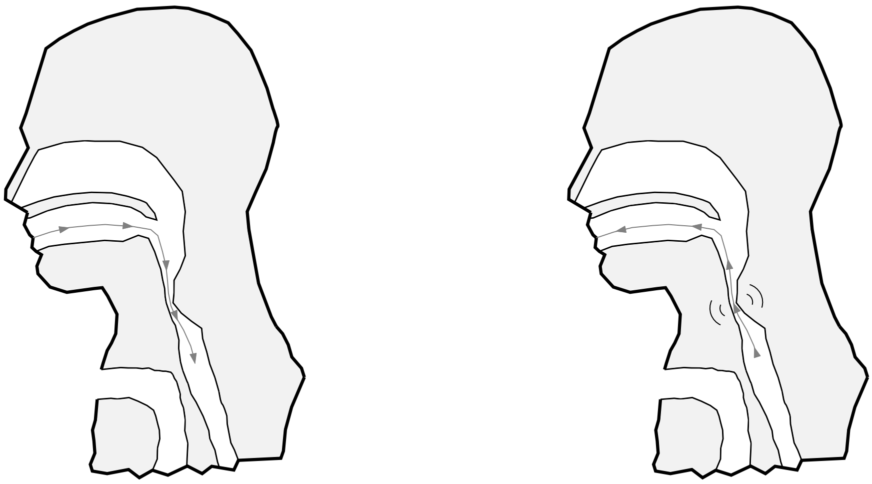

(a) Air intake. (b) Expelling air from the esophagus.

Source – Author.

Another well known method of vocal rehabilitation for laryngectomees is electrolarynx speech. The electrolarynx is an electromechanical device whose purpose is to acoustically excite the vocal tract (MELTZNER; HILLMAN, 2005). Presently its most common form consists of a hand-held device that is pressed against the neck (Figure 5). A vibrating coupler disk sets pharyngeal tissue into vibration, which acoustically excites the vocal tract (FUCHS; HAGMULLER; KUBIN, 2016). Although the resulting voice is functional, it has a distinct "mechanical", or "robotic" quality to it. Meltzner and Hillman (2005) indicate that the lack of frequency variation, the competing noise directly radiated from the device (and not filtered through the vocal tract), and an improper sound spectrum are commonly cited as contributors to the low quality of the resulting voice.

Figure 5 – Electrolarynx speech.

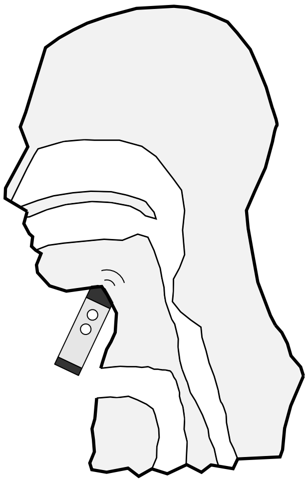

Source – Author.

The last method of speech rehabilitation that will be presented is TE speech. Due to its significance for the present thesis, the method is discussed separately, in Section 1.3 below.

1.3 Tracheoesophageal speech

In TE speech, a prosthesis is placed in an opening between the trachea and the esophagus (Figure 6a). The prosthesis acts as a check valve—it allows the passage of air from the trachea to the esophagus, but prevents food, liquids, and any content of the esophagus from entering the trachea and, consequently, the lungs. To produce the TE voice, the laryngectomee occludes the tracheostoma and exhales. The air flows through the prosthesis into the esophagus, where it sets the PES into self-sustained oscillations, producing the TE voice (Figure 6b).

The use of a TE puncture (the opening connecting the trachea to the esophagus), to restore voice is not a particularly recent development[4]; however, widespread interest in TE speech only began after the development of the silicone TE prosthesis by Blom and Singer in the late 1970's (BLOM, 1998; MAHIEU, 1988; SINGER; BLOM, 1980). Different types of prostheses have been proposed since then[5].

[4] Guttman (1932 apud MAHIEU, 1988) reports the remarkable case of a laryngectomee who, dissatisfied with his artificial larynx, punctured his own trachea with a heated ice pick. The procedure had to be repeated two additional times in order to make the opening permanent, but the laryngectomee was indeed able speak.

[5] See Mahieu (1988) and Lorenz (2017) for a historical overview. Blom (1998) describes the evolution

Figure 6 – TE speech.

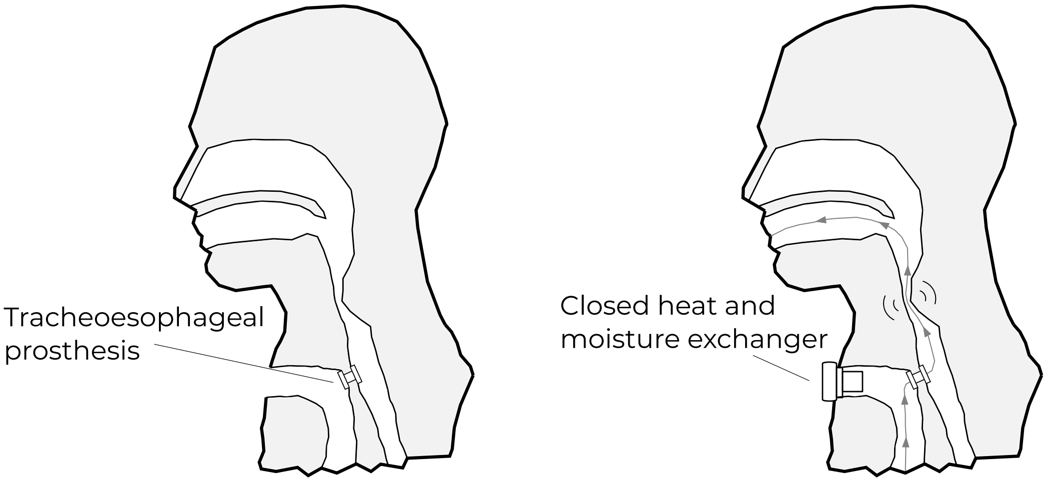

(a) Placement of the prosthesis. (b) Phonation.

Source – Author.

Figure 7 shows two different prostheses that are commercially available. Both of them use a flap as the valve element (Figure 8), which is a common type of prosthesis encountered today.

Figure 7 – Examples of TE prostheses.

(a) Blom-Singer Classic Indwelling, Sterile. (b) Provox Vega.

Source – (a) InHealth (2021), and (b) Atos (2021b).

TE speech has been described as the most successful and most widely used method of voice restoration available at the moment (VERKERKE; THOMSON, 2014). It offers many solutions to the issues associated with its closest predecessor—esophageal speech. The use of the lungs as the source of air provides two obvious changes: (i) a considerably larger volume of air is available for phonation, and (ii) air intake and exhalation is far more intuitive than in esophageal speech. Therefore, it is no surprise that TE speech is associated with better a voice quality and higher success rates[6] when compared to esophageal

of the Blom and Singer prostheses. The website by Kress and Schäfer (2021a) contains detailed information on recent prostheses.

[6] Mahieu (1988) indicates that published success rates for TE speech range from 56% to 93%, which is similar to the range of 58–94% mentioned by Chone, Gripp, et al. (2005). Op de Coul et al. (2000) report a success rate of 95%.

Figure 8 – Section view of a typical prosthesis.

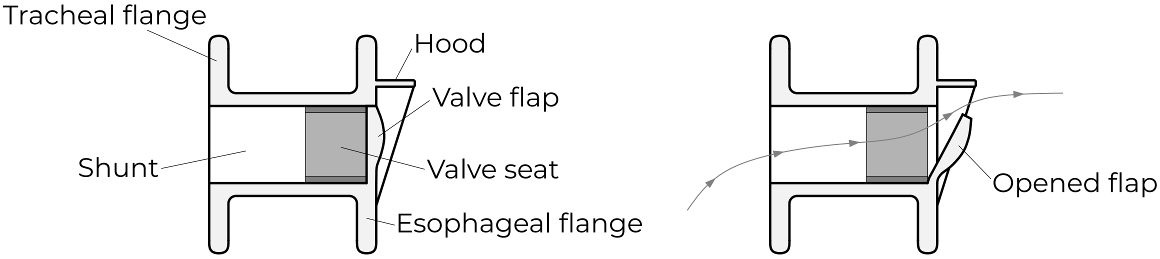

(a) Valve flap closed. (b) Valve flap opened.

Source – Author.

speech (VAN AS, 2001). These advantages evidently have an impact on the quality of life of a laryngectomee. Souza et al. (2020) conducted a study with 95 laryngectomees registered at the Brazilian National Cancer Institute from 2004 to 2012, and found that those who used TE speech reported a better quality of life in comparison to those who used esophageal speech or an electrolarynx.

However, despite the several advantages offered by TE speech, the method still has several drawbacks. One of which if the fact that the prosthesis has to be replaced periodically. Balm et al. (2011) mention that the lifespan of the prostheses varies considerably in the literature; however, they point to a range of 4–6 months in most of the Western world, and larger values (10–18 months) in Mediterranean areas and the USA (the USA is considered separately from the other western countries in the study). However, considerably lower values have been observed by Op de Coul et al. (2000), who report an overall median lifespan of about 3 months, and Lewin et al. (2017) who report an overall median lifespan of about 2 months.

The need for frequent prosthesis replacement places a heavy financial burden on the TE speaker[7]. This issue is obviously exacerbated in developing countries (STAFFIERI et al., 2006). For instance, in the previously mentioned study of Souza et al. (2020), about half of the laryngectomees had less than 8 years of formal education, which likely corresponds to lower incomes. Even in the case of a country with a public health system that is able to provide the prostheses to the laryngectomees, the financial issue is not entirely solved since the state still has to accommodate the additional cost. Therefore, efforts to lower costs and increase the lifespan of the prostheses are still needed.

Another drawback of TE speech concerns the quality of the TE voice. Even though the TE voice is in general of a higher quality than the voice produced by an electrolarynx or esophageal speech, it still differs considerably from the laryngeal voice both in subjective as well as objective criteria (VAN AS; HILGERS, et al., 1998; VAN AS, 2001). In a subjective test, the TE male voice was judged to be more deviant, uglier, more unsteady, weaker,

[7] A recent purchase was made by the state of Santa Catarina (Brazil) at a price of R$ 2 025.00 per prosthesis (SES, 2019).

duller, breathier, lower, and deeper than the laryngeal male voice (VAN AS; HILGERS, et al., 1998; VAN AS, 2001). For the female voice, there is also the additional issue that the female TE voice is of an unnaturally low pitch, being comparable to that of the male voice (VERKERKE; THOMSON, 2014).

A third issue is that some laryngectomees are not able to produce the TE voice. This is usually associated to the tonicity of the muscles of the PES (MAHIEU, 1988; VERKERKE; THOMSON, 2014). Tonicity may be defined as the "slightly tense state of a healthy muscle when it is not fully relaxed" (COLLIN, 2005)[8].

Tonicity may vary in intensity from very small (hypotonicity) to very large (hypertonicity). A PES that is either hypotonic or hypertonic leads to issues in voice production. Hypertonicity is the most common cause for failure in TE voice production (BALM et al., 2011). Hypotonicity is usually associated with a weak and breathy voice (BLOM; REMACLE, 1998), but may preclude phonation in extreme cases (MCIVOR et al., 1990). Different approaches to deal with hypertonicity and hypotonicity of the PES have been proposed. They are out of the scope of this introduction, but will be discussed further in Section 2.7.

To conclude the present section, it should be mentioned that there are efforts being made to address issues related to voice production in TE speech. One of them is the modern Sound-producing voice prosthesis (SPVP) described by Verkerke and Thomson (2014), in which a membrane element is included in the TE prosthesis. This membrane element oscillates with the airflow, and acts as the sound source. This allows for the control of certain properties of the resulting voice by changes in design of the membrane element. At the moment these SPVP are still at a research phase, and to the best of the author's knowledge there is no commercial prosthesis that makes use of the idea.

1.4 Objectives

The preceding sections have shown that total laryngectomy is likely to continue to exist as a form of treatment for laryngeal cancer in the foreseeable future. Therefore, a number of people will continue to benefit from voice rehabilitation methods; in particular, from the most advantageous option at the moment: TE speech.

It was also pointed out that, while superior to the alternatives, the TE voice is still inferior to the laryngeal voice, in terms of quality and intelligibility. Additionally, some people are not able to produce the TE voice. The tonicity of the PES plays an important role in these issues. Even the aforementioned SPVP is not exempt of considerations of tonicity, since in "normotonic and hypertonic patients, interference with PES vibrations

[8] There are some issues when considering this definition for the purposes of TE speech. As will be seen in Section 2.6, there is an additional contraction of the musculature of the PES during TE speech, rather than only a "slightly tense state". However, the term is well established in the literature, and will be used throughout the thesis.

will occur" (VERKERKE; THOMSON, 2014), requiring interventions to the PES.

A better understanding of the mechanics of TE speech would be of considerable help in solving these issues, either by improvements in the design of prostheses, or by a better understanding of the consequences of specific surgical decisions on the TE voice. However, unlike laryngeal speech, the literature on the mechanics of TE speech is still quite scarce (Section 2.8). Therefore, there is a need for additional research in this area.

The present thesis seeks to help in solving this. Here, both a mathematical model as well as an experimental *in vitro* model are proposed to study TE speech. More specifically, the focus of the study is the effect of the tonicity of the muscles of the PES on its self-sustained oscillations during TE phonation. These points are highlighted below:

General objective

(i) To propose mathematical and experimental models of the PES for the study of TE speech.

Specific objectives

(i) To study the effect of tonicity on the observed shape of the PES during phonation.

Previous imaging studies have correlated the tonicity of the PES with its shape during phonation. For example, it was noticed that if the tonicity of the PES is sufficiently high, its the lowest part tends to inflate during phonation. Other characteristics are discussed in Section 2.6. While several imaging studies refer to this correlation, only one work was found that provided a test of the correlation, which suggests a need for further work on the matter.

(ii) To study the tonicity required for the self-sustained oscillations of the PES.

Given that failure in TE phonation is commonly associated with the tonicity of the PES, it is natural to attempt to predict the range of tonicities that leads to the self-sustained oscillations of the PES, and to study how this range changes with other properties of the system (such as the flow rate, for example).

While the threshold of hypertonicity is certainly more important, determining the hypotonicity threshold is a more tractable problem at the moment, and is the one that will be addressed in this work.

1.5 Structure of the thesis

To give the reader an overall view of the thesis, this section presents the organization of the remaining chapters and sections.

Chapter 2 presents the literature review. This review briefly covers the mechanics of laryngeal speech, and the subject of collapsible tubes; however, the main purpose of the review is to present in detail what is currently known about the PES and its functioning.

The mathematical model, which is based on the collapsible channel of Stewart (2017), is described in Chapter 3. The formulation is presented, as is the method of solution. The relationship between parameters of the model and physiological quantities are also discussed. Finally, results of the model are interpreted in light of TE phonation.

Chapter 4 describes the experimental model of the PES. The experimental setup is described, highlighting how the several constituents of the model relate to TE phonation. The results are then presented, and comparisons are made to the theoretical model.

The final chapter of the thesis (Chapter 5) presents the conclusions drawn from the present work, its main contributions, as well as suggestions for future work.

2 Literature review

The goal of the present chapter is to lay the foundation for the development of the models of TE phonation. In this regard, much of the discussion focuses on the PES and on TE speech; however, other topics need to be addressed to provide the necessary background to assess several decisions that were made during the development of the models.

Since TE speech bears a strong resemblance to laryngeal speech, it is natural to provide a review of the research on the mechanics of laryngeal speech. This is done in Section 2.1.

Sections 2.2 to 2.8 compose the main part of this chapter. The PES is discussed in detail, both before and after a total laryngectomy. While some points in these sections may appear peripheral to this work (such as the physiology of the PES prior to surgery), it is felt that they provide an understanding of the PES that could not be gained by discussing the post-laryngectomy PES, and TE speech, alone. Additionally, a lot of valuable information on the PES is scattered across studies focusing on swallowing, dysphagia, esophageal speech, and TE speech. It was hoped for the present review to also serve as a starting point for future studies on the PES conducted at the Laboratory of Vibrations and Acoustics. Therefore, the scope of the review was made broad.

Both the mathematical model and the experimental model proposed in this work are based on the literature on collapsible tubes. Therefore, a brief exposition of it is made in Section 2.9, at the end of the chapter.

2.1 The mechanics of laryngeal speech

This section presents a brief review of laryngeal speech. The review is not meant to be extensive—the idea is to provide an overall view of laryngeal speech, in particular of the self-sustained oscillations of the vocal folds, of mathematical models of phonation, and of self-oscillatory experimental models.

Several anatomical structures are involved in the production of the laryngeal voice. The lungs, trachea, larynx, and vocal tract all play a part in the process; however, the main source of sound is the oscillatory motion of the vocal folds. The vocal folds are a pair of protuberant structures that project towards the interior of the laryngeal airway. Figure 9 shows a sideways view of the larynx, as well as the PES. Figure 10 shows two section views of the larynx. In Figure 10a the cutting plane is the coronal plane, while in Figure 10b it is the transverse plane.

The vocal folds are indicated in Figure 10a as “true vocal folds” to distinguish them from the ventricular vocal folds. The ventricular vocal folds are also protuberances towards the inside of the laryngeal airway. While they are likely to exert some influence on voice production (ZHANG; ZHAO, et al., 2002; MATSUMOTO et al., 2021), it is not

Figure 9 – Sideways view of larynx and PES.

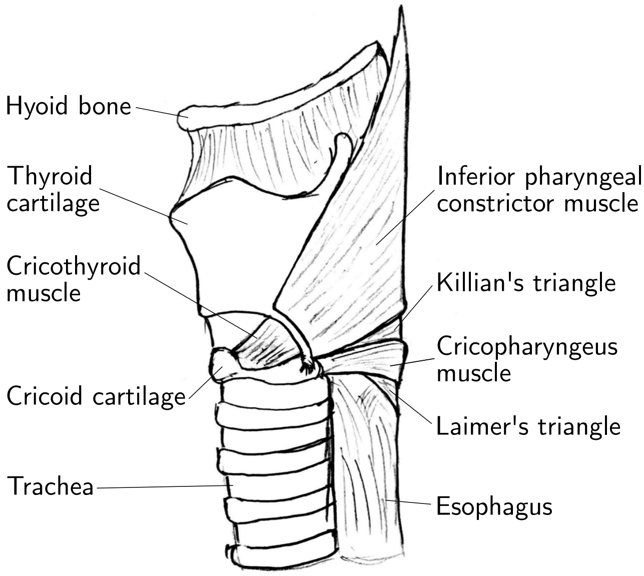

Source – Tourinho et al. (2021).

nearly as significant as that of the vocal folds.

As Figure 10 shows, the anterior part of each vocal fold is attached to the thyroid cartilage, while the posterior part attaches to the arytenoid cartilages. Movement the arytenoid cartilages is one way to change the positioning, or posturing, of the vocal folds, which results in changes of the voice produced. For instance, activation of the interarytenoid muscle (a muscle that connects the posterior part of the arytenoid cartilages) results in an approximation of the arytenoid cartilages, tending to close the glottis. Many different mechanisms for changing vocal fold posturing exist, and the vocal folds may be rotated, approximated, elongated, shortened, etc. These will not be discussed here, but the reader is referred to Zhang (2016) for an additional discussion[1].

While earlier theories supposed that voice production was analogous to whistling, or that the oscillation of the vocal folds was caused by nerve impulses, today the myoelastic-aerodynamic theory is widely accepted (VAN DEN BERG, 1958). The basic premise of the theory is that the self-sustained oscillation of the vocal folds is due to the flow of air provided by the lungs through the trachea (VAN DEN BERG, 1958). Mechanical properties of the tissue affect this oscillation, and resonances in the vocal cavities play a significant part in shaping the resulting sound. Fant (1970) made this last point explicit in his “source-filter” theory, which considers a division of the complete system in an acoustic source, corresponding to the sound generated directly by the vocal folds, and an acoustic filter, corresponding to the effect of the vocal tract.

Under this framework, the earliest mathematical model of phonation is that of

[1] It is worth remarking that while vocal fold posturing is a fairly sophisticated process, the same is not true for the PES, as will be seen in Sections 2.2–2.7.

Figure 10 – Section view of the larynx.

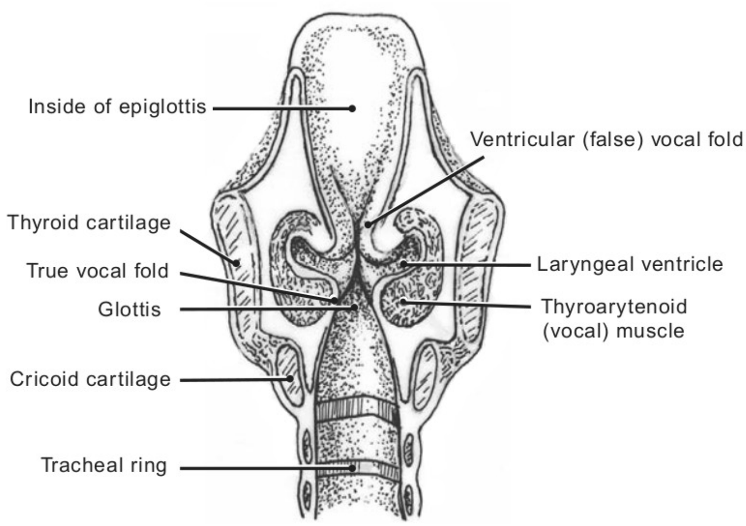

(a) Coronal plane.

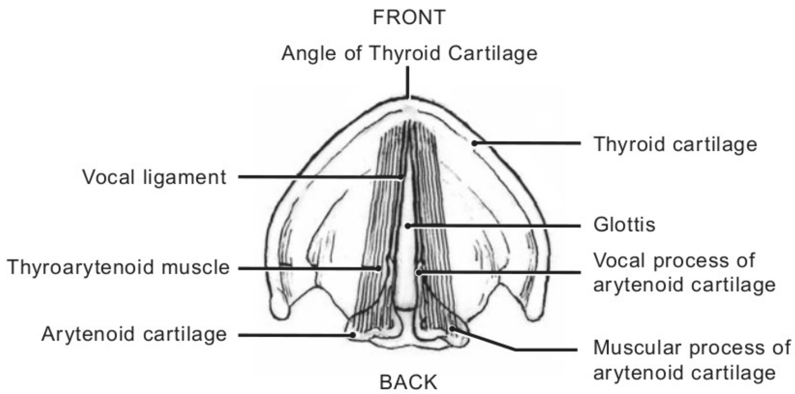

(b) Transverse plane.

Source – Adapted from Raphael, Borden, and Harris (2011).

Flanagan and Landgraf (1968). In this model, each vocal fold is modeled by a lumped mass element attached to a linear spring and a viscous damper element. The movement of the masses is assumed to be symmetric, therefore only one mass is considered. The path from the lungs to the vocal folds, as well as the effect of the vocal tract, are modeled by lumped acoustic elements. The airflow is modeled as a force acting on the mass. The expression for this force was determined based on experimental data. To model the complete closure of the glottis during oscillation, Flanagan and Landgraf (1968) tested two different methods: a hard boundary collision and a viscous boundary collision.

In the model of Flanagan and Landgraf (1968), the vocal tract influences the behavior of the vocal folds in an exaggerated manner, with self-sustained oscillations resulting mainly from the lumped acoustic circuits (ERATH; ZAÑARTU, et al., 2013). A second limitation of the model is that it does not represent the out-of-phase movement of the vocal folds that is typically observed during phonation. In an oscillation cycle, the vocal folds begin to open from the inferior part, and they also begin to close from the inferior part, with the superior part lagging behind. This vertical phase difference is also referred to as the mucosal wave (ZHANG, 2016), since it corresponds to a wave traveling on the surface of the vocal folds, from the inferior part to the superior. Figure 11 illustrates this, showing the vocal folds at different instants of an oscillation cycle. The vocal folds are shown from a front view (coronal plane) as well as top view (transverse plane).

Figure 11 – Out-of-phase motion of the vocal folds.

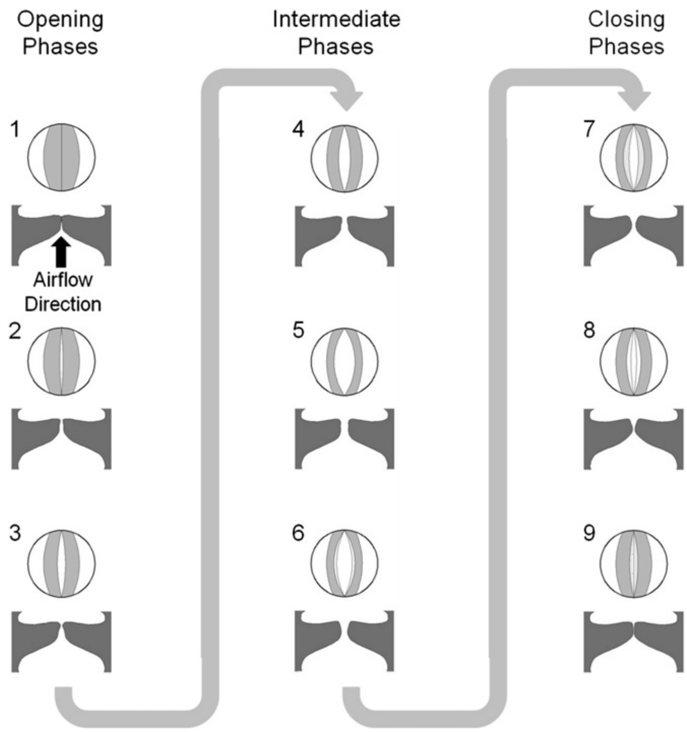

Source – Erath, Zañartu, et al. (2013).

In order to address the limitations of the model of Flanagan and Landgraf (1968), Ishizaka and Flanagan (1972) proposed the two-mass model for the vocal folds shown in Figure 12. In the model, each vocal fold is represented by a pair of masses connected to each other by a spring (movement of the two vocal folds is again assumed to be symmetric). Besides the additional mass, several modifications were made from the model of Flanagan and Landgraf (1968): the use of nonlinear anchoring springs, increased damping and an additional stiffness to contact, a different formulation for the airflow, etc. The model of Ishizaka and Flanagan (1972) was very influential, and several works that followed modeled the vocal folds in a very similar manner (LUCERO, 1993; PELORSON et al., 1994; STEINECKE; HERZEL, 1995; JIANG; ZHANG; STERN, 2001; BAILLY; HENRICH; PELORSON, 2010).

One of the notable contributions of the model is that it is able to represent the difference in phase between the inferior and superior parts of each vocal fold. The importance in this point is that this vertical phase difference “is generally considered as the

Figure 12 – Vocal folds model of Ishizaka and Flanagan (1972).

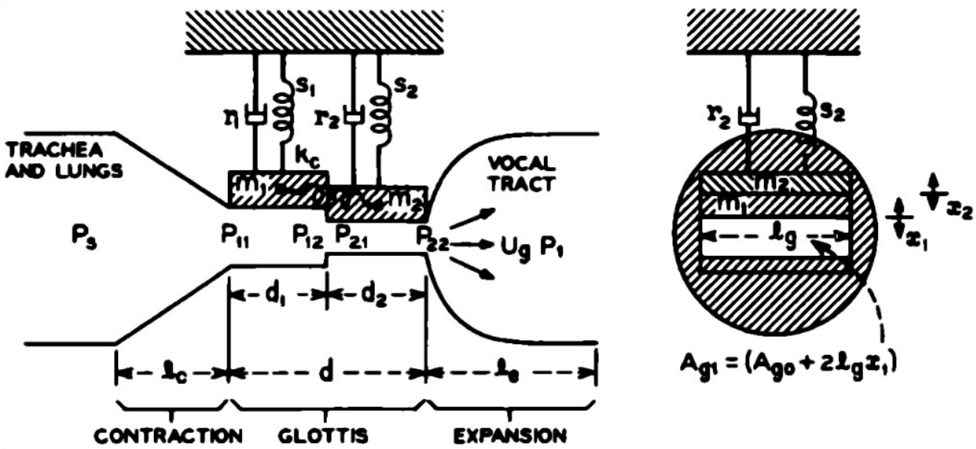

Source – Ishizaka and Flanagan (1972).

primary mechanism for phonation onset” (ZHANG, 2016). The basic idea is explained by Titze (1988) and by Thomson, Mongeau, and Frankel (2005). During the part of the oscillation cycle where the glottis is opening, the glottis will take a convergent shape (Figure 13a) and during closing, it will take a divergent shape (Figure 13b). The pressure downstream of the glottis is zero (any acoustic loading by the vocal tract is neglected here for simplicity).

For the convergent shape, when the glottis is opening, the fluid velocity is increasing along the glottis and pressure decreasing (neglecting viscous effects). The pressure is reduced from a positive value in the inferior part of the glottis to zero on the superior part. The flow remains attached throughout the glottis, separating only at the expansion downstream from the vocal folds.

For the divergent shape, when the glottis is closing, the fluid is decelerating along the glottis and pressure is increasing. Therefore, since the pressure must increase to zero, it must take a negative value in the glottis, and at a certain point along the glottis the flow separates due to the adverse pressure gradient.

Past the separation point, the pressure near the surface of the vocal folds is approximately zero. Since the pressure is positive during the opening phase, the work done by it on the vocal folds surface will be positive due to the direction of tissue velocity (see Figure 13). During closing, the work done by the pressure on the vocal folds will be nearly zero past the separation point, and positive in the region where the pressure is negative. Therefore, the convergent shape during opening and the divergent shape during closing allow for a net transfer of energy from the flow to the vocal folds in an oscillation cycle.

It should be noted that the above explanation is quite simplified, and for this net transfer of energy to occur, there is no real need for the pressure to be negative during the closing of the glottis. It is only required for the pressure to be smaller during closing than during opening. In the finite element simulations of Thomson, Mongeau, and Frankel

(2005) the spatially averaged pressure over the vocal folds surface did not become negative, and regions of negative pressure did not contribute much to the energy transferred.

Figure 13 – Schematic representation of the glottis upon opening and closing.

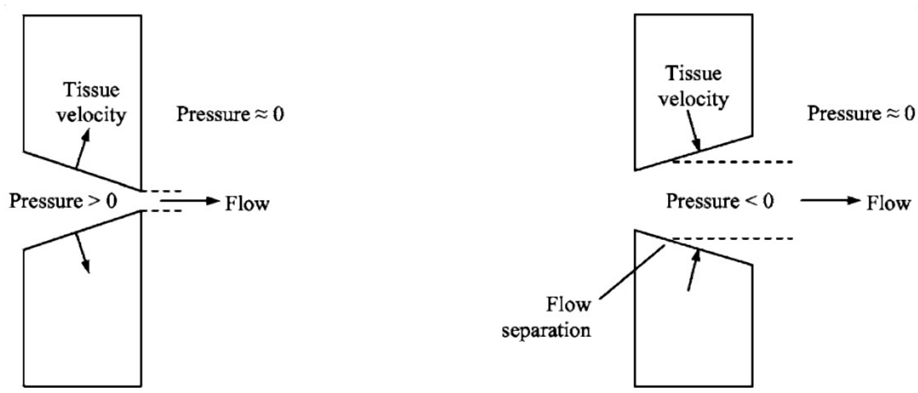

(a) Opening. (b) Closing.

Source – Thomson, Mongeau, and Frankel (2005).

Titze (1988) proposed a lumped-parameter model to study the above mechanism, as well as that of the acoustic coupling with the vocal tract. The mucosal wave was modeled by the one-dimensional wave equation (with constant propagation velocity). The d'Alembert solution for the wave propagating towards positive x, i.e. $\xi(t - x/c)$, was linearized in x around the midpoint of the vocal fold. This procedure results in a straight line representing the surface of the vocal folds. Moreover, the vocal folds will always open in a convergent shape and close in a divergent shape. The position of the midpoint of the vocal folds was set to follow the equation for a mass-spring-damper system, and fluid flow and acoustic coupling with the vocal tract were also modeled by lumped-parameter elements. This model was also influential in subsequent work in the mechanics of phonation (LUCERO, 1999; LUCERO; KOENIG, 2007).

With the model, Titze (1988) derived a simple expression for the phonation threshold pressure[2]. This expression was then tested experimentally with an artificial model of a hemilarynx[3] (TITZE; SCHMIDT; TITZE, 1995), which was one of the earliest self-oscillating models of the vocal folds. The experimental model is shown schematically in Figure 14. Good agreement between experimental results and the expression derived by the theoretical model was observed for sufficiently high values of the prephonatory half-width. This experimental model was further explored by Chan, Titze, and Titze (1997).

While all the models discussed thus far have proved to be highly useful, none of them considered explicitly the layered structure of the vocal folds (HIRANO, 1974). In each vocal fold, there is a layer of muscle at its base (vocalis muscle), which is covered by

[2] The minimum pressure produced by the lungs that will result in the self-sustained oscillations of the vocal folds

[3] A lateral half of a larynx.

Figure 14 – Artificial hemilarynx model of Titze, Schmidt, and Titze (1995). Distance ξ_o corresponds to the prephonatory half-width.

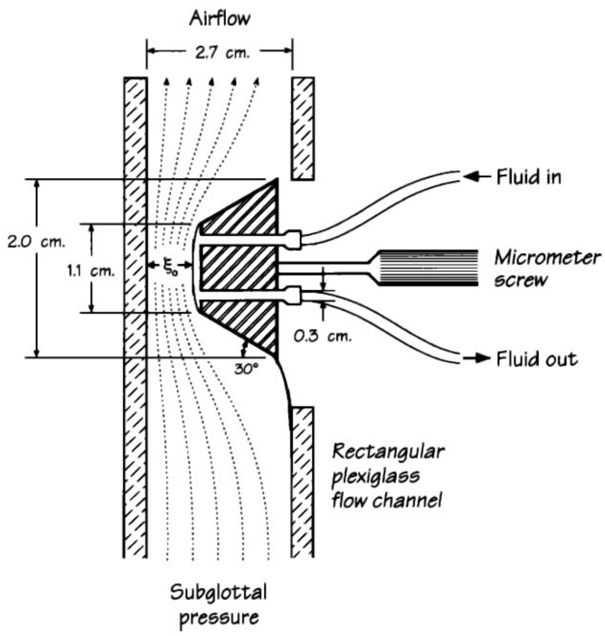

Source – Titze, Schmidt, and Titze (1995).

the elastic conus. On top of the elastic conus sits a layer of mucosa, which can be divided into a very thin outer layer of epithelium and an inner layer of lamina propria. The layer of muscle and the elastic conus are tightly connected to each other, and roughly move as a unit during phonation. The layer of mucosa is only loosely connected to the elastic conus, and it does not necessarily move as a unit with the elastic conus and the vocalis muscle. As Hirano (1974) argues, to achieve an improved description of the mechanics phonation, the vocal folds should be considered at least as a two-layered structure—the "body", composed of the vocalis muscle and elastic conus, and the "cover", composed of the lamina propria and the epithelium.

Based on the model of Ishizaka and Flanagan (1972) and the discussion above, Story and Titze (1995) proposed a simplified layered structure model of the vocal folds. The model consists of two masses, similar to the model of Ishizaka and Flanagan (1972), sitting on top of an addition mass. The mass on the base represents the body, while the two masses on top represent the cover. This change permits the relative motion between the body and cover, but keeps the system reasonably simple.

Different self-oscillating experimental models of the vocal folds were proposed in the beginning of the twenty-first century. Thomson, Mongeau, and Frankel (2005) used synthetic vocal folds made of silicone rubber attached to an acrylic base. Artificial vocal folds have been widely used since (ZHANG; NEUBAUER; BERRY, 2006b,a; NEUBAUER et al., 2007; MCPHAIL; CAMPO; KRANE, 2019), and have been further developed to include multiple layers (MURRAY; THOMSON, 2012), to consider a Magnetic resonance imaging (MRI) based geometry (PICKUP; THOMSON, 2010), and MRI measurements have been performed with them (TAYLOR et al., 2019).

Šidlof et al. (2011) also proposed a variation on the silicone vocal folds described above. While in the works cited above, the deformation of the silicone itself was used to mimic the movement of the vocal folds, in the work of Šidlof et al. (2011) one of the silicone vocal folds was fixed to a rigid wall of the conduit, while the other was fixed to a moving base that was supported by springs. Oscillation was mostly due to the compliance of the springs, and the silicone rubber was considered to be stiff enough that its elasticity would only play a significant role during collision of the vocal folds.

Figure 15 – Synthetic vocal folds of Thomson, Mongeau, and Frankel (2005).

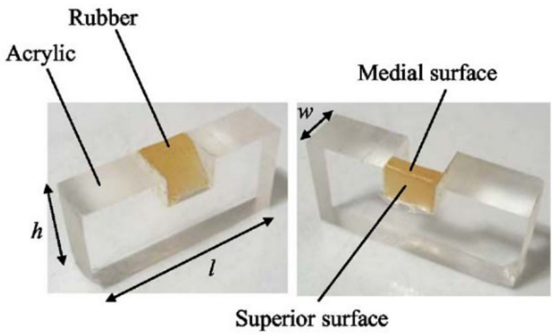

Source – Thomson, Mongeau, and Frankel (2005).

Chan and Titze (2006) modified the artificial hemilarynx used by Titze, Schmidt, and Titze (1995) and Chan, Titze, and Titze (1997). They replaced the fluid that was injected between the metal body and the silicone membrane with a viscoelastic biomaterial.

While the use of liquid contained in a membrane was dropped by Chan and Titze (2006), it was picked up by Ruty et al. (2007), although in a very different manner than that found in the work of Titze, Schmidt, and Titze (1995). The artificial model of Ruty et al. (2007) consisted of a pair of half-brass cylinders, which were covered by elastic tubes (Figure 16). Pressurized water was injected in the cavity formed between the elastic tube and the half-cylinders. These were then positioned together in a support, which also formed a conduit through which air would flow through. With this system, Ruty et al. (2007) studied the accuracy of two low-order lumped parameter models by comparing predictions of the oscillation threshold pressure and oscillation frequency, for different parameters combinations, with experimental results. They report that the models were able to reproduce the same general qualitative behavior of the experimental results, but within a large error range. Like the artificial vocal folds in the work of Thomson, Mongeau, and Frankel (2005), the experimental vocal folds model of Ruty et al. (2007) continued to be explored in subsequent work (LUCERO; VAN HIRTUM, et al., 2009; HAAS et al., 2016; LUIZARD; PELORSON, 2017; LUCERO; PELORSON; VAN HIRTUM, 2020).

Around the time the artificial vocal folds models of Thomson, Mongeau, and Frankel

Figure 16 – Artificial vocal folds of Ruty et al. (2007).

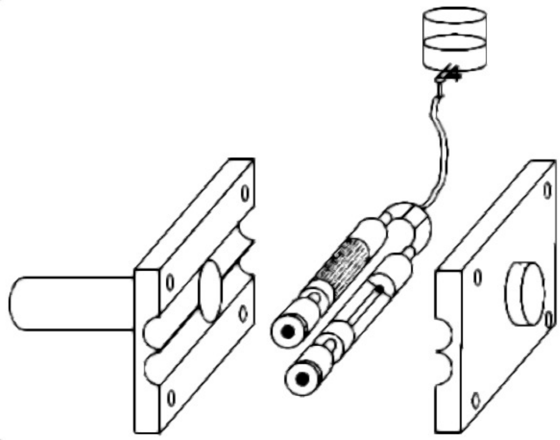

Source – Adapted from Ruty et al. (2007).

(2005) and Ruty et al. (2007) were proposed, Fulcher et al. (2006) described a simplified mathematical model of phonation. This model was based on the model of Ishizaka and Flanagan (1972) and the vertical phase difference discussed above; however, instead of considering a model with two masses, Fulcher et al. (2006) considered a single mass model. The reasoning for this was that, in the two-mass model, instead of using the position of each mass as the pair of coordinates, one may use the position of the center of mass and a coordinate for the relative position between the masses. They considered that the only significant role of the coordinate for the relative position is to keep the aerodynamic forces in phase with the velocity of the vocal folds, so that these aerodynamic forces would do positive work both in the opening phase of the glottis as in the closing phase[4]. The model was then reduced to a one degree of freedom, with an external force (representing aerodynamic forces) that was always in phase with the velocity. In an analogy with dry friction damping, Fulcher et al. (2006) referred to this forcing as a "negative Coulomb damping".

Zañartu, Mongeau, and Wodicka (2007) proposed significant improvements on the model of Fulcher et al. (2006). The external force was reworked in terms of the Bernoulli equation and a time-varying discharge coefficient that was determined based on data by Park and Mongeau (2007). In addition to this, acoustic coupling with the subglottal and the supraglottal tracts was considered, as was a collision force to model vocal fold contact.

Howe and McGowan (2010) later indicated that the point of flow separation changes throughout an oscillation cycle, and this change would provide a considerably larger variation on the surface forces when compared to the discharge coefficient alone. They went on to model flow separation in the glottis using a two-dimensional free streamline model, and to calculate the aerodynamic production of sound. McGowan and Howe (2010)

[4] As mentioned above, this is not necessarily the case. The force may be out-of-phase with the velocity during closing (positive pressure), and the force may still produce net work if the pressure during closing is lower than during opening.

provided a complementary analysis to this work by assessing the effect of suction forces.

To conclude this section, it is important to point out that the brief overview presented here is limited to works that illustrated important anatomical or physiological aspects of laryngeal phonation, or whose approach was closer to that intended for the present work. Continuum-based models have not been addressed (XUE et al., 2014), and a vast amount of simplified models has been left out (ERATH; ZAÑARTU, et al., 2013). Additionally, the important subject of aeroacoustics has not been addressed (MCGOWAN, 1988; HOWE; MCGOWAN, 2013), neither were experiments with excised larynges (DOLLINGER et al., 2011), or in which the artificial vocal folds performed a prescribed motion (MONGEAU et al., 1997; TRIEP et al., 2011). The reader is referred to Zhang (2016) for a comprehensive overview of the field, and Hixon, Weismer, and Hoit (2020) for detailed descriptions of the anatomy and physiology involved.

2.2 The PES prior to a total laryngectomy

The present section focuses on the PES before a total laryngectomy. An extensive presentation is made. While it may be argued that only the anatomy and physiology of the PES after a total laryngectomy are relevant to TE speech, no such (detailed) description was found in the literature. One must not only understand the PES before surgery, but also the surgical procedure of a total laryngectomy, so that by deduction, the post-laryngectomy PES may be properly understood. Additionally, while some details discussed in the following subsections were not considered in the models used in the present thesis (such as the detailed discussions of Subsections 2.2.2 and 2.2.3), it was judged best to present them nonetheless, so that the models may be put under proper perspective.

2.2.1 Basic anatomy

The PES is a sphincter connecting the pharynx to the esophagus[5]. The PES already appeared in Figure 9 at the beginning of Section 2.1—it consists of the uppermost part of the cervical esophagus, the cricopharyngeus muscle, and part of the inferior pharyngeal constrictor muscle. This region is sometimes described as being part of the hypopharynx (MICHAELS; HELLQUIST, 2001).

The three muscles mentioned above have been associated with the PES in large part due to esophageal manometry studies (SINGH; HAMDY, 2005), since there are no clear-cut anatomical boundaries demarcating the sphincter. In an esophageal manometry exam, a catheter with pressure sensors along its length is inserted in the esophagus through

[5] In the literature, this region is referred to by several different names, such as upper esophageal sphincter (SINGH; HAMDY, 2005; BELAFSKY; KUHN, 2014) and pharyngoesophageal sphincter (HALL, 2016). For laryngectomees, it is also referred to as neolarynx (DISANTIS et al., 1984). In analogy with the glottis in laryngeal speech, the space inside the walls of the PES often called neo-glottis or pseudo-glottis in the literature (VAN AS, 2001; MAHIEU, 1988).

the nostrils (BRASSEUR; DODDS, 1991). Figure 17 schematically illustrates the exam. Since the PES is normally closed, the inner walls of the PES compress the catheter and a higher pressure is read in the PES when compared to the pharynx or the esophagus.

Figure 17 – Esophageal manometry exam.

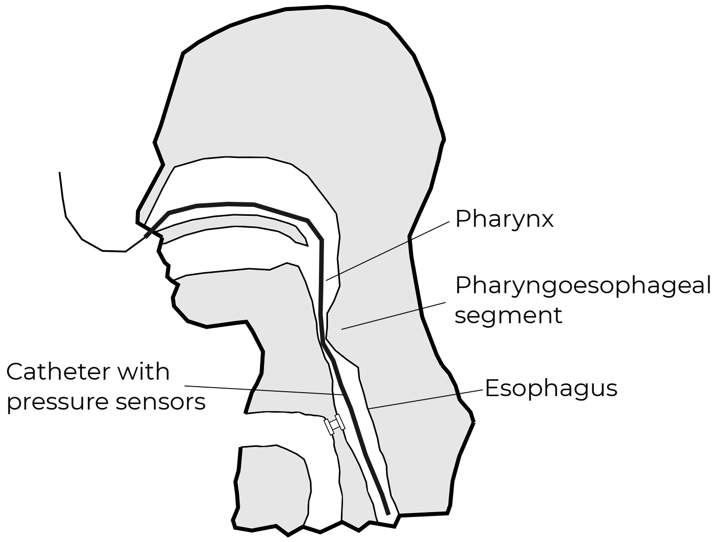

Source – Author.

By the use of esophageal manometry, the length of the PES can be estimated. There is some variation in the typical lengths reported in the literature. For example, Singh and Hamdy (2005) indicate a length of 20–40 mm, Hamaker and Cheesman (1998) indicate a range of around 40–60 mm, and Belafsky and Kuhn (2014) mention a length of about 25–45 mm.

Much like the esophagus, the PES is composed of an inner layer of mucosa. This layer of mucosa may be surrounded by either muscle or cartilage, depending on the region. In the part of the PES that corresponds to the uppermost part of the esophagus, the layer of mucosa is entirely surrounded by muscle, while at the level of the cricopharyngeus and lower part of the inferior pharyngeal constrictor, it is surrounded posteriorly by these muscles and anteriorly by the cricoid cartilage and the cricoarytenoid muscle. These structures are shown in Figure 18. Considering the importance of the layer of muscle and the layer of mucosa to the post-laryngectomy PES, these will be discussed separately, in Subsections 2.2.2 and 2.2.3, respectively.

Additional views of the PES and pharynx are shown in Figures 19 and 20. Figure 19 shows the pharynx and pharyngoesophageal junction opened, while Figure 20 shows the interior of this region, seen from behind. Here, the posterior wall of the pharynx, PES, and esophagus are opened.

The most prominent anatomical structures that neighbor the PES are the larynx anteriorly, the vertebral column and prevertebral muscles posteriorly, and the lobes of the thyroid gland laterally. Figure 21 shows schematically a transverse cut on the neck, on

Figure 18 – Sagittal cut of the esophageal region.

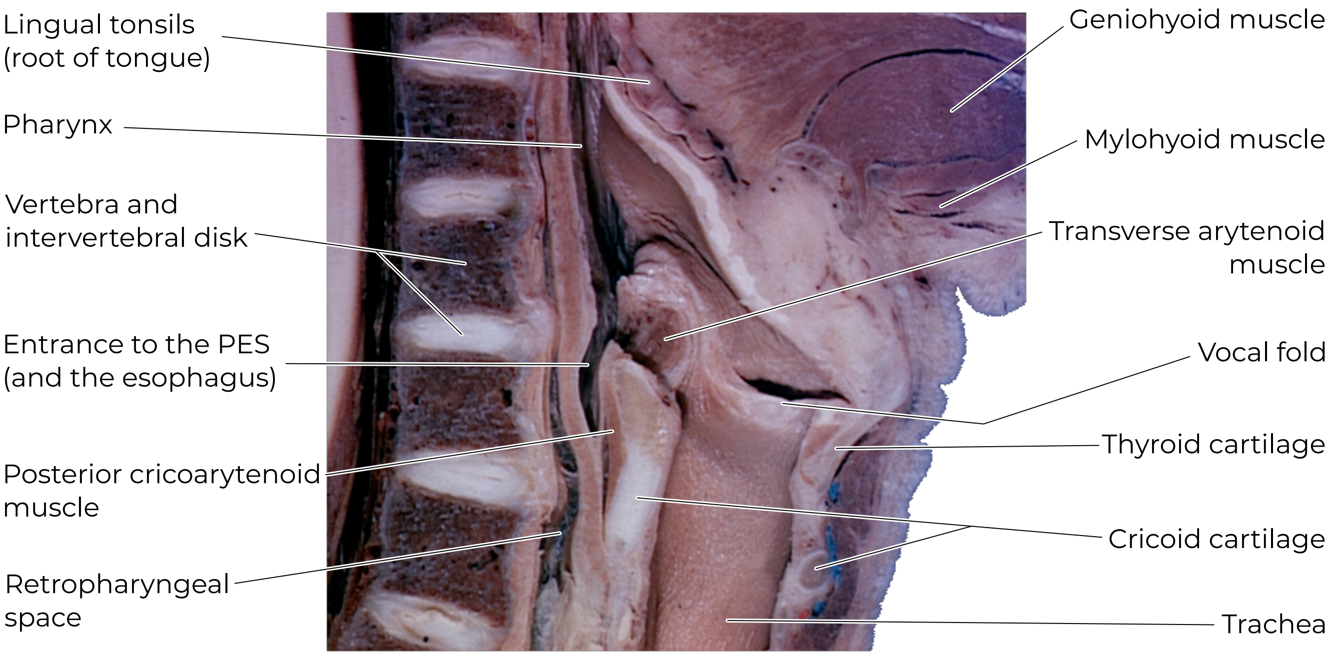

Source – Adapted from Bassett (2021a).

Figure 19 – Posterior view of the inside of the pharynx and esophagus.

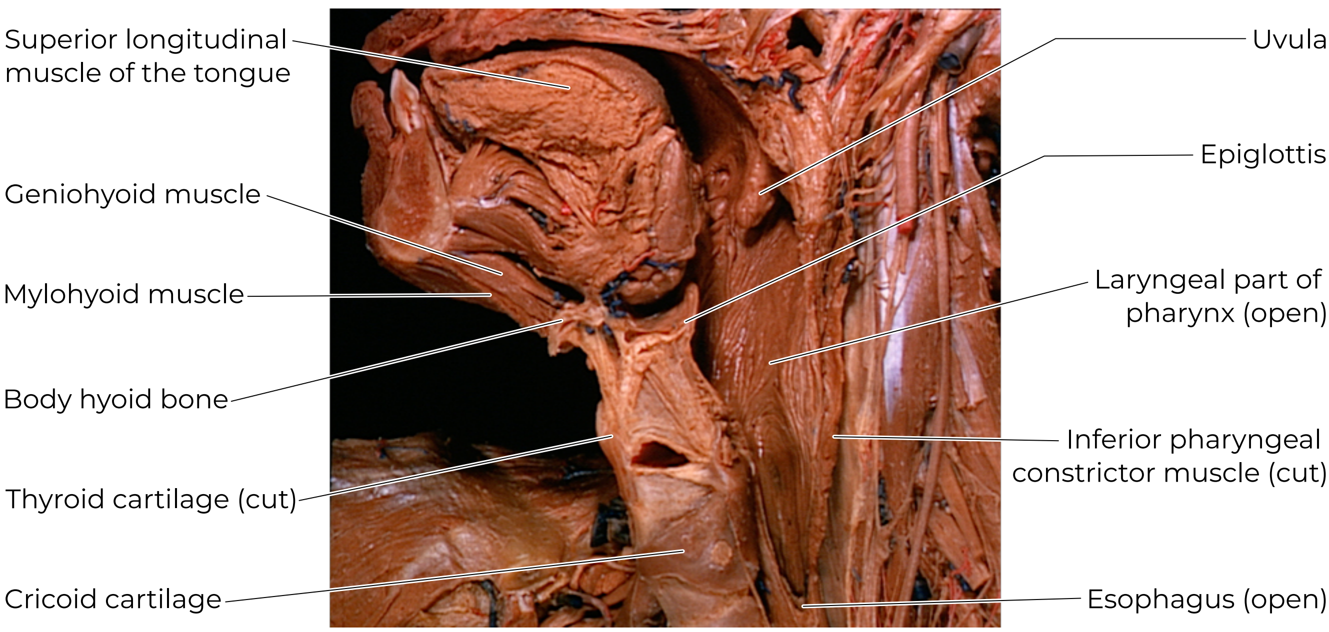

Source – Adapted from Bassett (2021c).

the level of the C6 vertebra. It is slightly below the PES (or near its inferior border), but it illustrates the position of the prevertebral muscles, vertebral column, and thyroid gland relative to the esophagus.

In Figure 21, it can also be seen that the esophagus is separated from the vertebral column by a fascial space. At the level of the PES, this space is composed of the buc-

Figure 20 – Posterior view of the inside of the pharynx and esophagus.

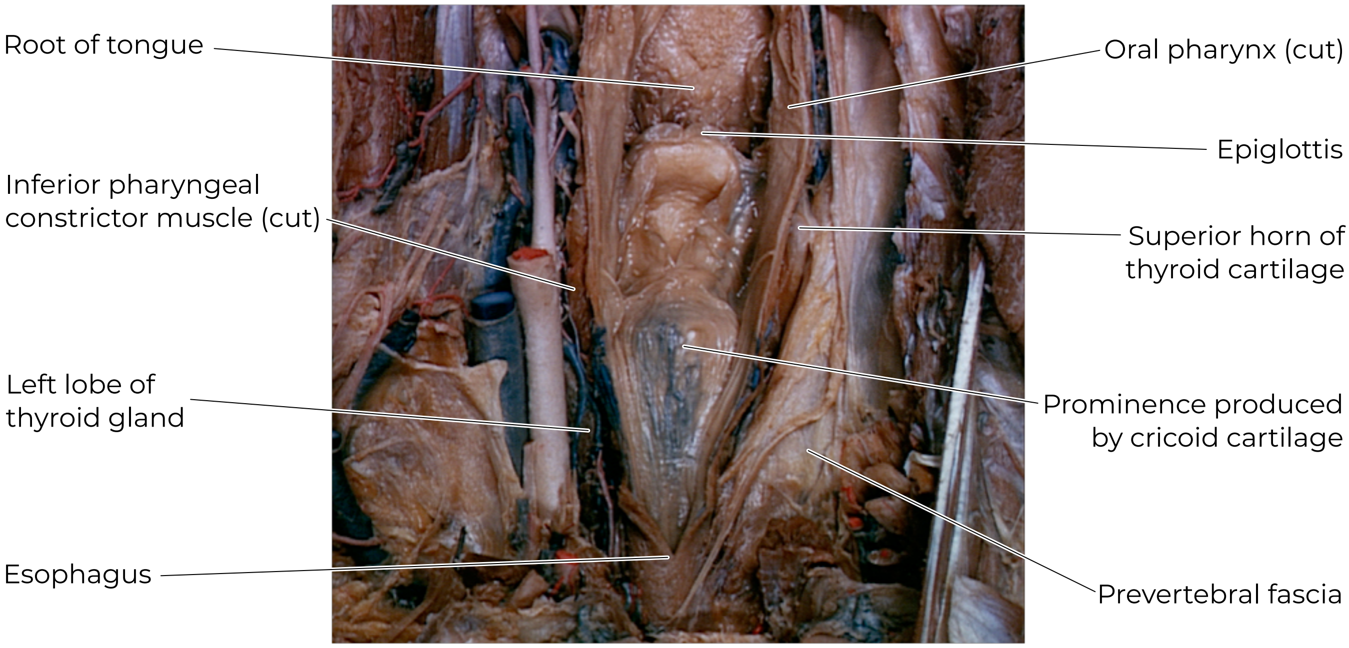

Source – Adapted from Bassett (2021b).

copharyngeal fascia (GRAY, 1918), the alar fascia, and the prevertebral fascia. Between the buccopharyngeal fascia and the alar fascia lies the retropharyngeal space, between the alar fascia and the prevertebral fascia lies the so-called danger space (GUIDERA et al., 2014)[6].

It is also worth pointing out that the thyroid gland is composed of two lobes connected by the thyroid isthmus. It sits anterior to the larynx; however, its lobes extend to the sides of the PES and esophagus (Figures 21 and 22).

2.2.2 Layer of muscle

The uppermost muscle that composes the PES is the inferior pharyngeal constrictor[7]. This muscle is attached to the sides of the thyroid cartilage (Figure 9), and the the muscle fibers arising from each side meet at a median raphe[8] on the posterior wall (Figure 22).

Mu and Sanders (2001) indicate that the inferior pharyngeal constrictor is com-

[6] There is some discussion on the terminology used for these layers, see Guidera et al. (2014).

[7] In the literature, it is common to find differences in what is meant by inferior pharyngeal constrictor. Probably the most common meaning is that the inferior pharyngeal muscle corresponds to the most caudal of the pharyngeal constrictors, and is composed of two parts—the thyropharyngeus and the cricopharyngeus (GATES, 1980; SIVARAO; GOYAL, 2000). In the present work, the nomenclature used by Mu and Sanders (1998) is adopted, and the term inferior pharyngeal constrictor is used to mean only the thyropharyngeus.

[8] A seam; in anatomy, the line of union of the halves of any various symmetrical parts. (DORLAND, 2011)

Figure 21 – Transverse cut at the level of the C6 vertebra.

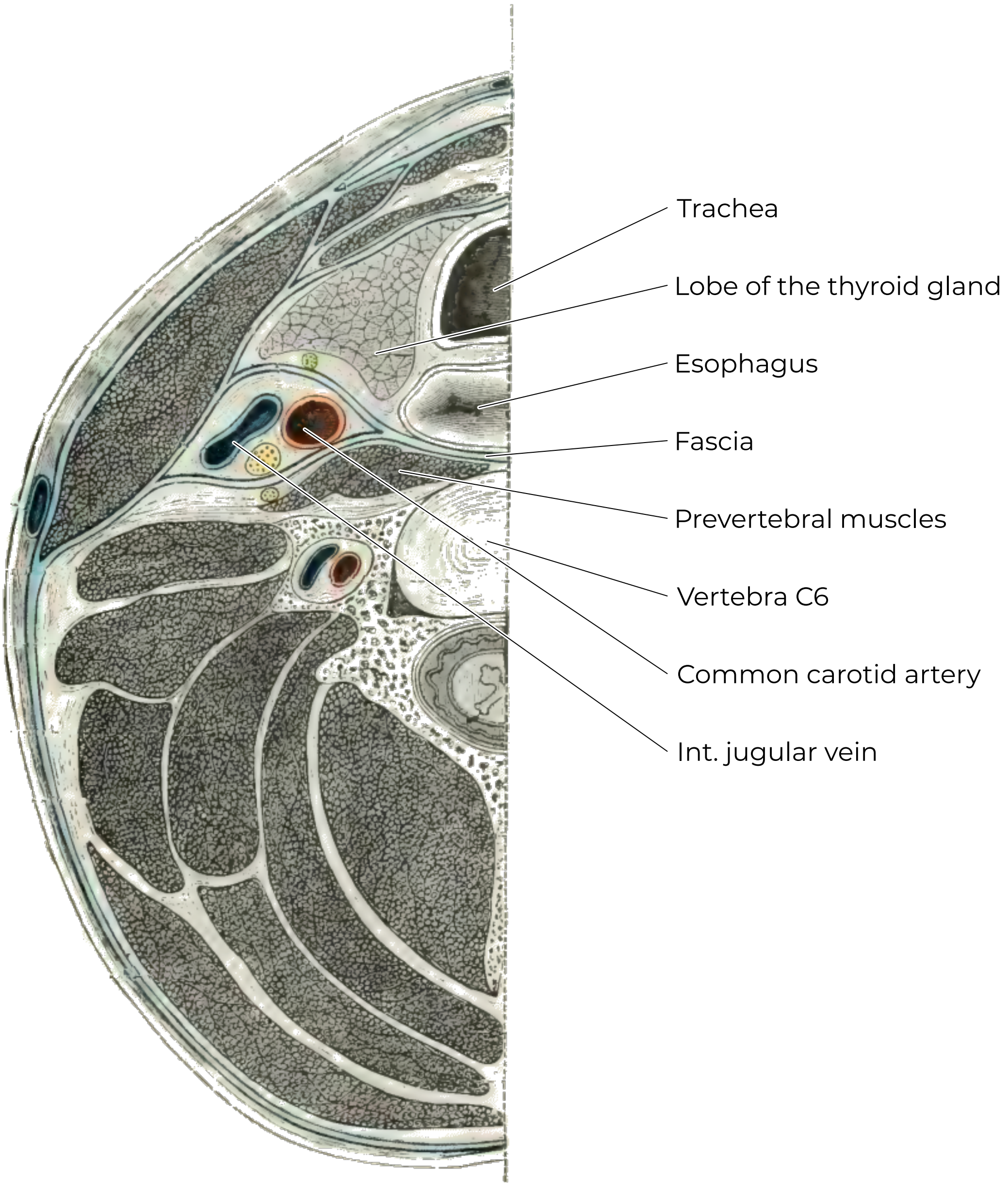

Source – Adapted from Gray (1918).

posed of two neuromuscular compartments: rostral[9], and caudal[10]. Each compartment is innervated by a separate branch of the pharyngeal branch of the vagus nerve. They also present differences in fiber-type distribution (fast-twitch fibers against slow-twitch fibers). Based on fiber-type distribution, Mu and Sanders (2001) divided the muscle in two layers: a "slow" inner layer, and a "fast" outer layer. In the rostral compartment, the fast outer layer is thicker than in the caudal compartment. Likewise, in the caudal compartment the slow inner layer is thicker than in the rostral compartment.

The proportion of fast-twitch fibers and slow twitch fibers in each layer also changes

9 Direction toward the oral and nasal region. (DORLAND, 2011)
10 Synonym of inferior. (DORLAND, 2011)

Figure 22 – Posterior view of the inside of the neck.

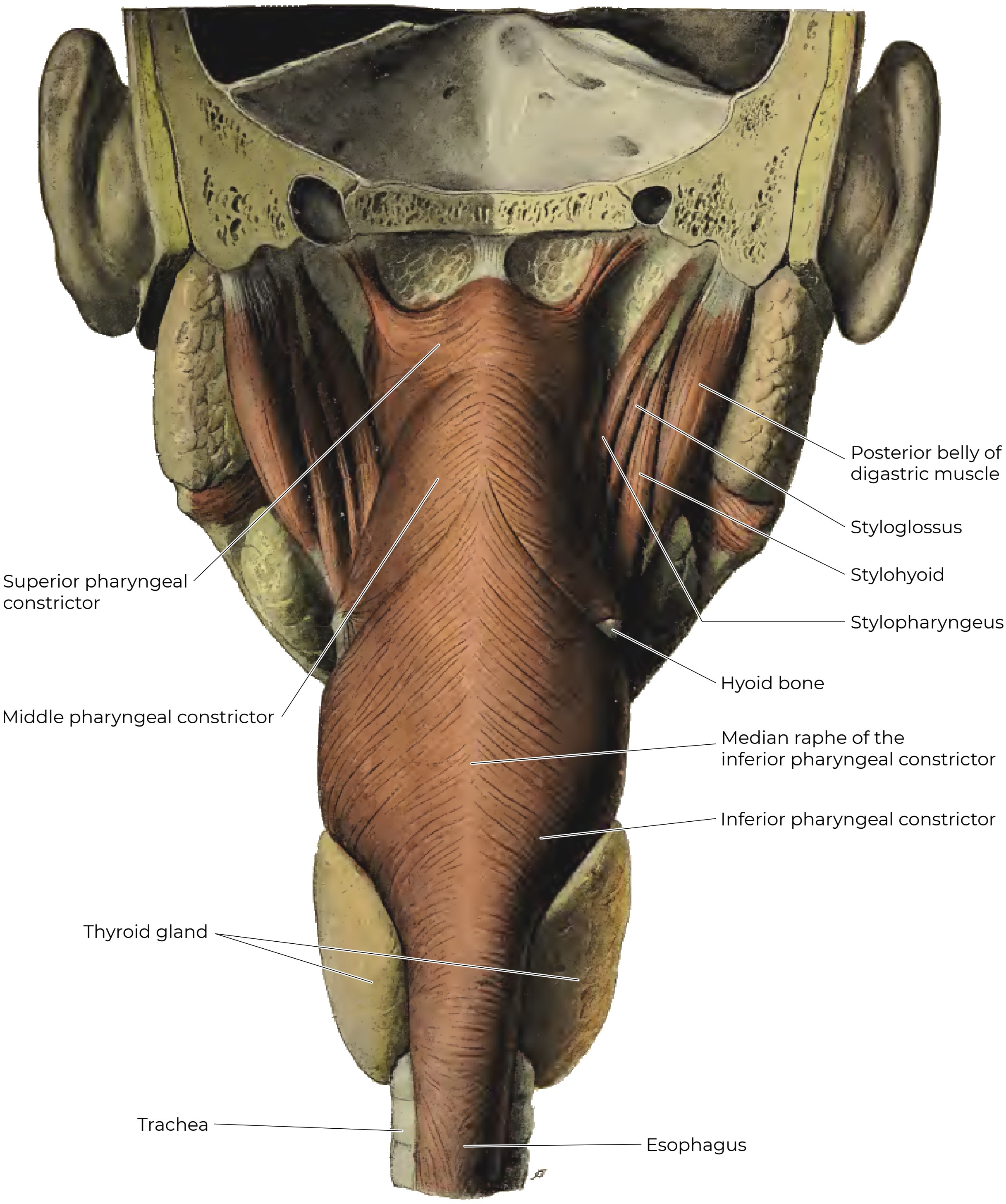

Source – Adapted from Sobotta (1928).

along the inferior pharyngeal constrictor. The slow inner layer of the caudal compartment is composed by a larger proportion of slow-twitch fibers than the slow inner layer of the rostral compartment (84% against 57%), while the fast outer layer of the caudal compartment is composed of fewer fast-twitch fibers when compared to the fast outer layer of the rostral compartment (46% against 71%).

Mu and Sanders (2001) argue that since slow-twitch fibers are associated mostly with fine movements and postural adjustments, the larger proportion of this type of fibers in the inferior part of the muscle would be associated with the sphincter action of the pharyngoesophageal segment.

It should be stressed that these differences between rostral and caudal compartments, and fast layer and slow layer are not abrupt. The fiber-type distribution changes smoothly from different parts of the muscle, as can be seen in Figure 23 which shows a sagittal cut of the inferior pharyngeal constrictor.

Figure 23 – Fiber-type distribution in the inferior pharyngeal constrictor muscle.

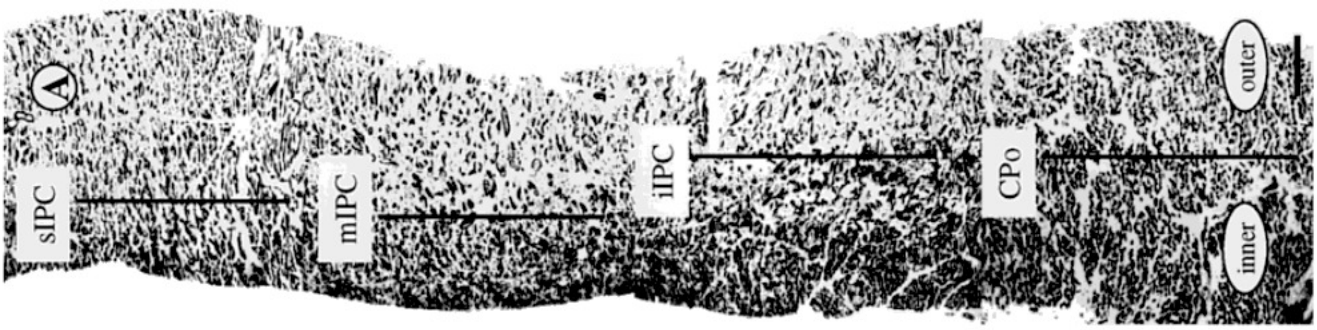

Source – Adapted from Mu and Sanders (2001).

In the figure, the slow-twitch fibers are stained darker. Also, the following acronyms are used: sIPC for the superior part of the inferior pharyngeal constrictor, mIPC for the middle part of the inferior pharyngeal constrictor, iIPC for the inferior part of the inferior pharyngeal constrictor, CPo for the oblique compartment of the cricopharyngeus. The rostral compartment corresponds to the sIPC and the mIPC, while the caudal compartment to the iIPC.

The cricopharyngeus muscle is located below the inferior pharyngeal constrictor. It attaches to the sides of the cricoid cartilage (Figure 9) but, unlike the inferior pharyngeal constrictor, does not possess a median raphe.

This muscle is innervated by the pharyngeal plexus and the recurrent laryngeal nerve (MU; SANDERS, 1998), and Mu and Sanders (2002) indicate that the cricopharyngeus is divided in two neuromuscular compartments: the oblique cricopharyngeus, and the horizontal cricopharyngeus (Figure 25). These authors note that, like the inferior pharyngeal constrictor, the cricopharyngeus displays a slow inner layer and a fast outer layer. The oblique compartment contains an overall smaller proportion of slow-twitch fibers, when compared to the horizontal compartment (69% and 76% respectively). It should be stressed once again that the fiber-type distribution changes smoothly throughout the muscle (Figure 24), as was the case for the inferior pharyngeal constrictor.

Figure 24 – Fiber-type distribution in the cricopharyngeus muscle.

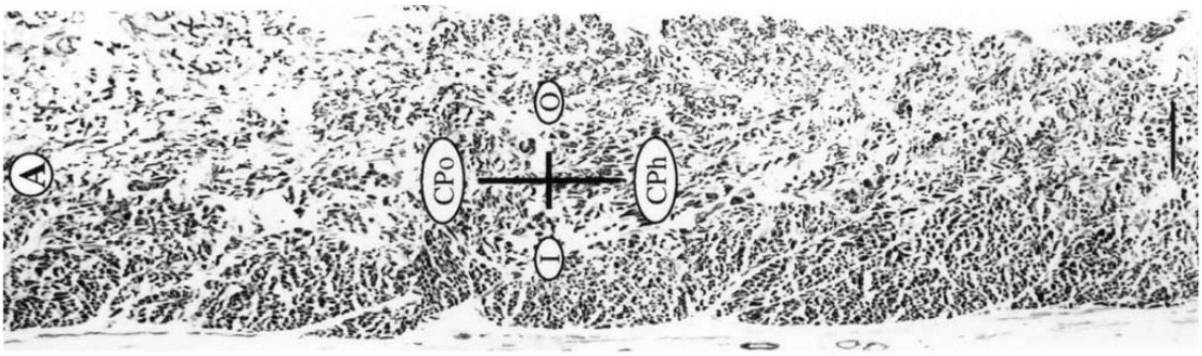

Source – Adapted from Mu and Sanders (2002).

In the figure, the slow-twitch fibers are stained darker. Also, the following acronyms are used: CPo for the oblique compartment of the cricopharyngeus, CPh for the horizontal compartment of the cricopharyngeus, I for the inside direction (towards the mucosa), O for the outside direction.

The PES is also commonly identified with the uppermost part of the cervical esophagus. The muscle layer of the esophagus is composed of two sub-layers—an internal one with fibers oriented in the circular direction, and an outer one where the orientation is longitudinal (MARTINI; TIMMONS; TALLITSCH, 2012). According to Mu and Sanders (1998), the cervical esophagus is innervated by multiple nerve branches of the recurrent laryngeal nerve. Also, there is a predominance of slow-twitch fibers in a similar proportion to that found in the cricopharyngeus.

Figure 25 shows a posterior view of the opened muscle layer of the PES, along with the middle pharyngeal constrictor. In this figure, the inferior pharyngeal constrictor and the cricopharyngeus have been detached from the thyroid cartilage and cricoid cartilage respectively.

The region between the oblique fibers and horizontal fibers in the transition from the inferior pharyngeal constrictor (and the oblique compartment of the cricopharyngeus) to the cricopharyngeus has been identified as an anatomically weak zone, called Killian's triangle, or Killian's dehiscence (GATES, 1980). This region is shown in Figure 9.

Kelly and Kuncl (1996) remark that in their study, the presence of the Killian's triangle was not universal (the observed proportion was less than one third). When present, there were noticeable variations in the size of the triangle, and it was often covered by a fat pad. It is also worthwhile to mention that Yamamoto et al. (2020) indicate that in the transition between the inferior pharyngeal constrictor and the cricopharyngeus there is a region of overlap between these two muscles, with the inferior pharyngeal constrictor covering the upper half of the cricopharyngeus. Since Killian's triangle corresponds to a region of sparser muscle fibers in the PES, it might participate less in the muscle contraction that leads to closing the PES, which in turn would affect how this contraction is longitudinally distributed.

A second structure present in the region is Laimer's triangle (GATES, 1980), which

Figure 25 – Posterior view of the opened muscles of the PES.

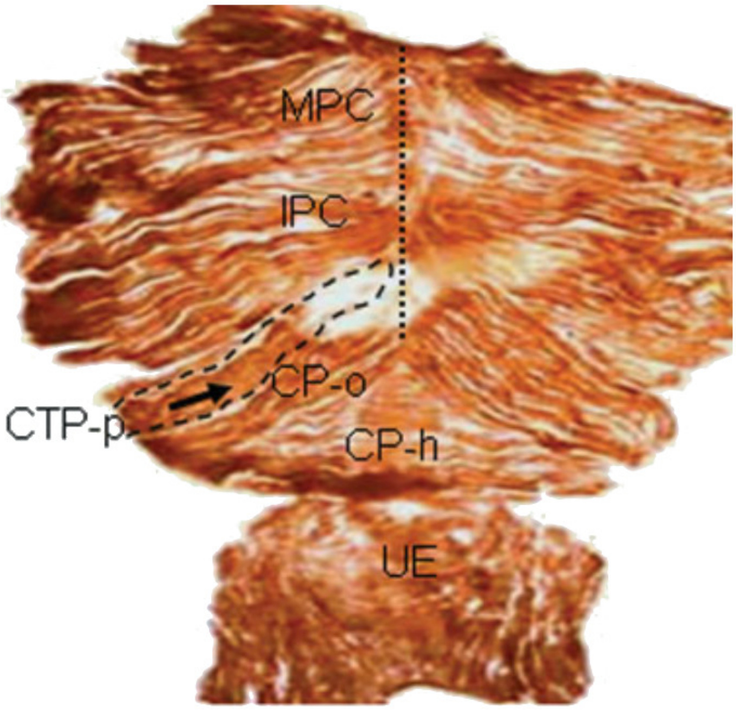

Source – Adapted from Mu and Sanders (2008).

MPC: middle pharyngeal constrictor, IPC: inferior pharyngeal constrictor, CP-o: oblique compartment of the cricopharyngeus, CP-h: horizontal compartment of the cricopharyngeus, UE: upper esophagus, and CTP-p: pharyngeal portion of the "cricothyropharyngeus". The dotted line indicates the median raphe in the middle pharyngeal constrictor and the inferior pharyngeal constrictor.

is also shown in Figure 9. The longitudinal layer of the esophagus, when approaching the PES from below, separates posteriorly in two branches which connect to the sides of the cricoid cartilage. The region delimited by these two branches and the cricopharyngeus forms Laimer's triangle.

It is important to note that the longitudinal layer of the esophagus connects not only to the cricoid cartilage. Wang et al. (2007) observed four superior insertions of the longitudinal esophageal layer: (i) on the posterior part of the cricoid lamina, (ii) on the lateral cricoid surface, (iii) continuous with longitudinal pharyngeal muscles (namely, the palatopharyngeus muscle), and (iv) with the muscular pharyngoesophageal wall.

Finally, it should also be mentioned that Mu and Sanders (2008) also report a distinct muscle, which had not been previously described in the literature. They named this muscle as cricothyropharyngeus. The muscle is a small band-like muscle that originates from the cricoid arch, attaches by loose connective tissue to the most inferior part of the thyroid inferior horn, and inserts into the median raphe. This muscle already appeared in Figure 25, and is shown in a lateral view in Figure 26.

The cricothyropharyngeus was present in 83% of the human specimens they analyzed, and was not identified in any of the animal specimens. Mu and Sanders (2008) argue that since it has its own topographic location, innervation pattern and fiber-type

Figure 26 – Lateral view of the cricothyropharyngeus.

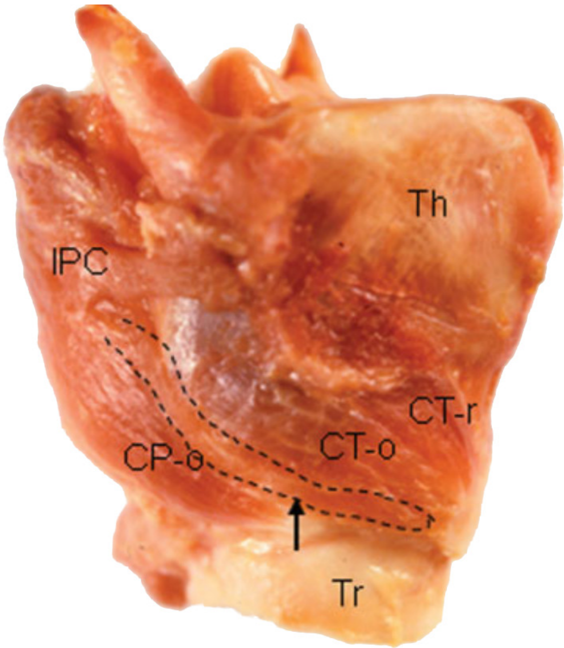

Source – Adapted from Mu and Sanders (2008).

In the figure, the cricothyropharyngeal muscle is shown by the dotted lines. Also, the following acronyms are used: Th for the thyroid cartilage, IPC for the inferior pharyngeal constrictor, CT-r for the rectus belly of the cricothyroid muscle, CT-o for the oblique belly of the cricothyroid muscle, CP-o for the oblique compartment of the cricopharyngeus, and Tr for the trachea.

distribution, it should be considered as a separate muscle in the PES. However, besides the paper by Mu and Sanders (2008), no other study mentioning this muscle has been found.

Given its attachments and position, its contraction could pull the posterior wall of inferior pharyngeal constrictor anteriorly. Therefore, if it is indeed a distinct entity, it could play an important role in how the PES closes.

2.2.3 Layer of mucosa

Inside the layer of muscle lies the tube of mucosa or, more precisely, mucosa and submucosa[11].

The mucosa and submucosa of the esophagus are described in detail in many anatomy textbooks (MARTINI; TIMMONS; TALLITSCH, 2012). The mucosa is composed of a layer of epithelium, the lamina propria, and muscularis mucosae. The epithelium is the innermost layer, and it is usually moistened by glandular secretions. The lamina propria, which covers the epithelium, is a layer of areolar tissue which may contain blood vessels and nerve endings. Outside the lamina propria is the muscularis mucosae, which is a layer of smooth muscle. This layer is a single layer of longitudinal smooth muscle that is very

[11] Along the text, the layer of mucosa and submucosa will usually be referred to simply as mucosa. If the more precise meaning is to be intended, the text will do so explicitly.

thin, or even absent, in the pharynx, but gradually thickens towards the stomach. The submucosa is a layer of connective tissue that wraps the muscularis mucosae. Towards the outer layer of the esophagus, lies the muscularis externa, which is the muscle layer that was discussed in more depth previously. In the esophagus, the outermost layer is a layer of connective tissue called adventitia.

As one moves towards the hypopharynx, some changes take place in this composition. Donald (2010) indicates that "instead of the thick submucosal layer and well-developed muscularis mucosae characteristic of the esophagus, the pharynx possesses a dearth of the former and a replacement of the muscularis mucosae by a dense layer of elastic tissue". Yamamoto et al. (2020) points out that the muscularis mucosae reaches an upper site behind the cricoid cartilage. This is also shown in the diagram of Kawamoto-Hirano et al. (2016) (Figure 27).

Figure 27 – Elastic laminae of the lower pharynx.

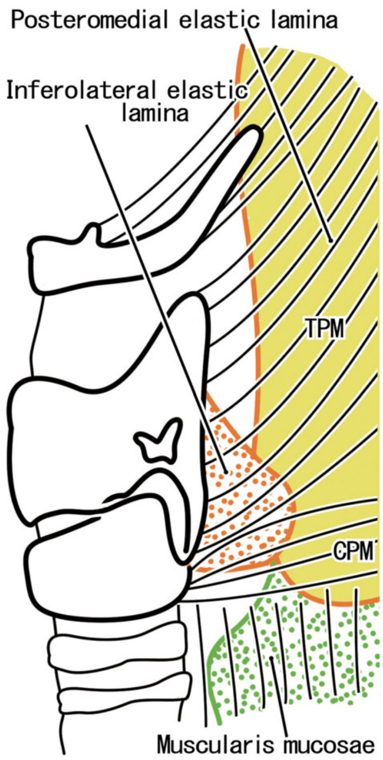

Source – Kawamoto-Hirano et al. (2016).

In the figure, the following acronyms are used: TPM for the thyropharyngeus (inferior pharyngeal constrictor, see Footnote 7), and CPM for the cricopharyngeus.

Figure 27 also shows two elastic membranes situated at the level of the submucosa of the PES and the hypopharynx. These are described by Kawamoto-Hirano et al. (2016), who named them "inferolateral elastic lamina", and "posteromedial elastic lamina". The inferolateral lamina, which appears to have been first identified by Wang et al. (2007), is a membrane of elastic tissue connecting the lateral part of the PES to the posterior border of the thyroid cartilage. The posteromedial elastic lamina covers the inside of the palatopharyngeus, the stylopharyngeus, and the pharyngeal constrictor muscles, depending on the site (KAWAMOTO-HIRANO et al., 2016). The inferolateral lamina is continuous with the posteromedial lamina. The presence of these structures is in agreement with the "dense layer of elastic tissue" in the above quote from Donald (2010).

It is important to stress that a comprehensive and unified description of all the layers that constitute the mucosa of the PES has not been found (unlike that for the esophagus, which can be found in a number of anatomy or histology books). For the hypopharynx, Michaels and Hellquist (2001) give a brief description, in which they mention a layer of epithelium, a layer of submucosa and the layer of muscle corresponding to the inferior pharyngeal constrictor. No mention is made of the layer of elastic tissue described above.

Referring to the pharynx in general, Duvvuri and Myers (2009) indicate that the pharyngeal wall is composed of mucosa, submucosa, pharyngobasiliar fascia, constrictor muscles, and buccopharyngeal fascia. However, Donald (2010) mentions a "dearth" of submucosa in the pharynx, but it is not clear whether the layer of submucosa gradually disappears as one moves from the esophagus to the oral cavity. In the hypopharynx and PES, no reference suggesting an absence of the submucosa has been found.

2.2.4 Phisiology

The main function of the PES is to prevent air from entering the digestive tract, and to prevent esophageal contents from refluxing into the pharynx (SIVARAO; GOYAL, 2000). Therefore, the musculature of the PES must maintain a resting tone in order for the sphincter to remain closed.

This resting tone may be assessed by esophageal manometry, and it is reported that the resting pressure varies significantly depending on several factors. It is nearly eliminated during sleep, but in events of acute stress it increases considerably. Sivarao and Goyal (2000) indicate that resting tone varies even with head position or laryngeal phonation (with higher pitched notes being associated with higher resting tone).

Welch, Luckmann, et al. (1979) used an esophageal manometry probe with eight side holes, which allowed for the measurement of pressure in eight different directions. By slowly moving the probe along the PES, the spatial distribution of pressure in the closed PES could be constructed. Figure 28 shows this distribution for one of the subjects in the study. The two distributions that appear in the figure are actually the same—one is rotated to reveal details that were hidden by the orientation of the plot.

The figure shows that higher pressures occur in the anterior-posterior direction rather than laterally. Also, the pressure peak near the pharynx happens in the anterior direction, while the peak nearer the esophagus happens in the posterior direction. Welch, Luckmann, et al. (1979) speculate that the PES would contract like the jaws of a vise. The movable jaw would correspond to the cricoid cartilage sitting anteriorly, while the fixed jaw would correspond to the sphincteric muscles. These jaws would be partially offset, so

Figure 28 – Pressure distribution in the PES of someone who did not undergo a total laryngectomy.

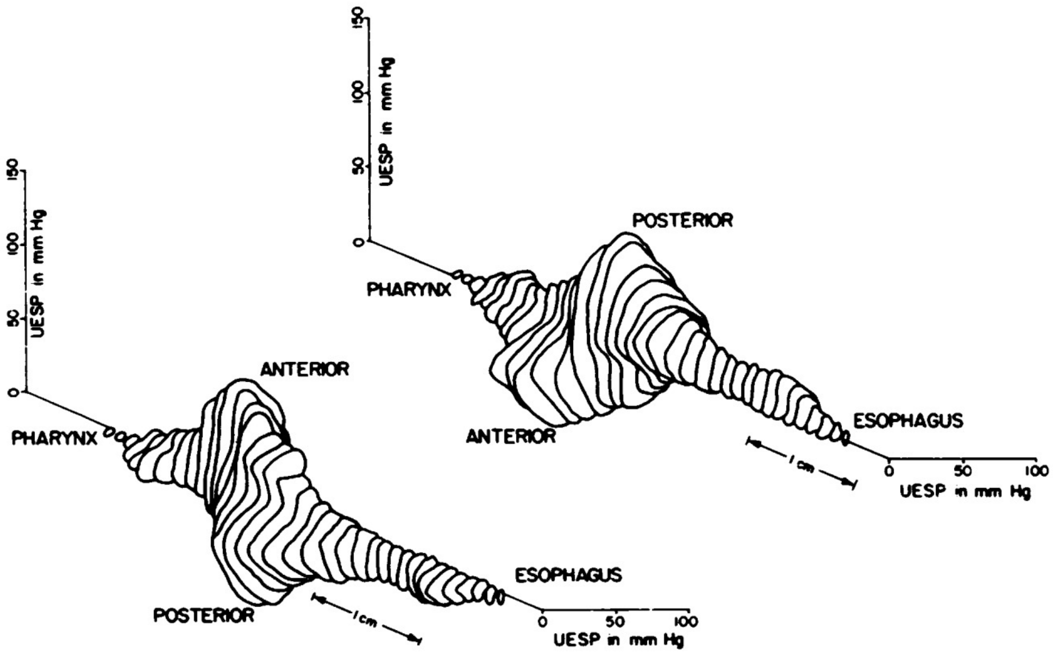

Source – Welch, Luckmann, et al. (1979).

that the peaks do not align. The analogy, however, is not perfect since when the inferior pharyngeal constrictor and cricopharyngeus contract, the posterior wall of the PES is pulled forward, while the sidewalls are pulled forward and inward (HIXON; WEISMER; HOIT, 2020). The forward projection of the posterior wall is also noticeable in imaging exams during TE phonation (Section 2.6).

Asoh and Goyal (1978), performing experiments with opossums, noticed that even after eliminating nerve commands with a neurectomy, a small amount of muscle contraction remained, which the authors attribute to the elasticity of the muscles. Sivarao and Goyal (2000) indicate that there has been some debate over how much of PES closure is due to electrical activity in the muscles and how much is due to this “passive” contraction.

Obviously, the PES does not remain closed at all times. It opens during deglutition, belching, and vomiting. While the mechanisms that govern the opening of the PES during these processes lie outside the scope of the present thesis[12], some points need to be presented as they are relevant for the discussion of the functioning of the PES during tracheoesophageal speech.

The opening of the PES is commonly associated with two factors: relaxation of the musculature of the PES, and contraction of suprahyoid muscles. Relaxation of the musculature of the PES has been noted by a cessation of electrical activity in the cricopha-

[12] The reader is referred to the works of Kahrilas et al. (1986), Shaker, Ren, Kern, et al. (1992), and Sivarao and Goyal (2000) for additional information.

ryngeus, and a decrease in intraluminal pressure immediately after the onset of swallowing (SIVARAO; GOYAL, 2000). Contraction of the suprahyoid muscles causes a movement of the hyoid bone (Figure 9) and of the larynx in the superior and anterior directions. As the movement of the posterior wall of the pharynx is hindered by the prevertebral fascia, this movement of the larynx results in the opening of the PES (SIVARAO; GOYAL, 2000).

During belching, PES opening is also associated with the relaxation of the PES musculature and movement of the hyoid bone; however, the movement of the hyoid bone is considerably different. The amplitude of motion is significantly smaller than during swallowing, and there is next to no movement in the superior direction (SHAKER; REN; KERN, et al., 1992). This reduced movement of the hyoid bone has led Lang (2006) to suggest that PES opening during belching may be mostly due to the "distracting effects" of the air in the esophagus, rather than movement of the hyoid bone and larynx, as is the case for swallowing.

A last point worth of mention is that the opening of the PES during either swallowing or belching is normally initiated by reflexes of the PES (LANG; SHAKER, 1997; SIVARAO; GOYAL, 2000). One reflex that bears significance to the present thesis is a belching reflex observed by Kahrilas et al. (1986), in which a sudden distention of the cervical esophagus leads to the relaxation of the PES. This reflex has been observed both by injection of air in the esophagus, as by a rapid inflation of a balloon in the esophagus. This reflex is referred by Lang (2006) as the "esophago-UES relaxation reflex"[13]. It should be noted that for the PES to relax, the inflation must be sudden. A slow inflation of the esophagus has the opposite effect, and the musculature contracts (LANG; SHAKER, 1997).

Other reflexes that may play a part in TE speech are the pharyngo-UES contractile reflex and the pulmonary-UES contractile reflex (LANG; SHAKER, 1997). The pharyngo-UES contractile reflex increases contraction of the PES upon stimulation of the pharynx. Rapid pulse water injection in the pharynx, as well as slow and continuous injection has been shown to activate this reflex (SHAKER; REN; XIE, et al., 1997). Lang (2006) states that air puffs can also activate the pharyngo-UES contractile reflex.

The pulmonary-UES contractile reflex, refers to an increase in cricopharyngeus contraction upon inflation of the lungs, with Lang and Shaker (1997) indicating that tidal volume is positively correlated with cricopharyngeus Electromyography (EMG) activity.

2.2.5 Stricture

An additional point regarding the anatomy of the PES needs to be presented given its significance to the correct interpretation of videofluoroscopic and radiographic images of the PES during tracheoesophageal phonation.

[13] As mentioned in Section 2.2, the PES is also called Upper Esophageal Sphincter, or UES.

In the preceding section, it was mentioned that during deglutition the musculature of the PES relaxes. Therefore, one would expect that the walls of the tube of mucosa would maintain a relatively flat inner surface as the bolus passes through the PES. That is indeed the case for most individuals; however, in some people a small protrusion on the posterior wall is observed while swallowing. Figure 29 illustrates this protrusion, which will be referred to as stricture in the present thesis[14].

Figure 29 – Lateral radiographic image of a stricture on the PES during swallowing.

Source – Dantas, Cook, et al. (1990).

Dantas, Cook, et al. (1990) have performed esophageal manometry concurrently with videofluoroscopic image acquisition in individuals with and without stricture. The manometry data indicated a complete relaxation of the musculature of the PES in individuals with stricture in the PES. The authors concluded that, besides the stricture itself, the mechanisms required for PES opening were normal in individuals with stricture. Therefore, they discard the possibility of failure of relaxation of the musculature of the PES, and argue that the stricture is the result of an abnormal stiffening of part of the PES.

The work of Leaper, Zhang, and Dawes (2005) also weakens the argument of the protrusion arising from failure of relaxation of the musculature of the PES. They dissected 31 cadavers and found the protrusion in 9 of them. Therefore, at least for these 9 subjects,

[14] This term is the one used by McIvor et al. (1990). Other names commonly used are "cricopharyngeal bar" (DANTAS; COOK, et al., 1990), and "cricopharyngeal protrusion" (LEAPER; ZHANG; DAWES, 2005). In the literature regarding tracheoesophageal speech, one also finds the terms "cricopharyngeal bar" (FOUQUET; GONÇALVES; BEHLAU, 2009) or "neoglottic bar" (VAN AS; OP DE COUL, et al., 2001) being used to indicate a protrusion arising from the posterior wall of the PES. However, in these cases there is no differentiation of whether the neoglottic bar arises from muscle contraction or not. This difference is relevant for the present thesis, and the term *stricture* will be used for the cases where the protrusion exists without muscle contraction.

there is no possibility of the protrusion arising due to muscular contraction. They describe two types of stricture, which they name the *ridge* and the *fold*. The ridge corresponds to a small "bump" on the posterior wall of the PES, with clearly identifiable borders. The fold, on the other hand, was a tongue-like fold of tissue protruding to the inside of the PES. The ridge and the fold are shown in Figure 30.

Figure 30 – The two types of stricture observed by Leaper, Zhang, and Dawes (2005).

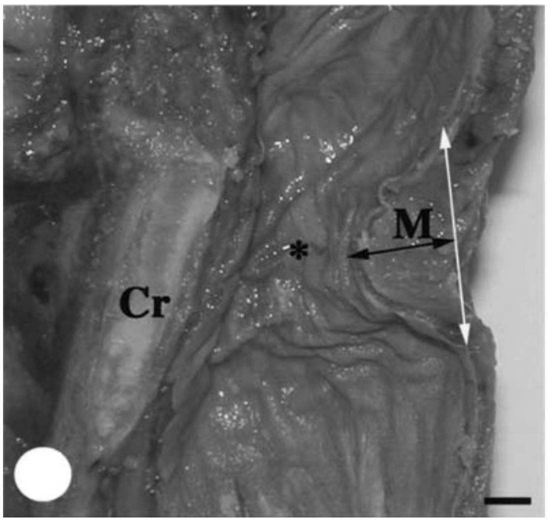

(a) The ridge.

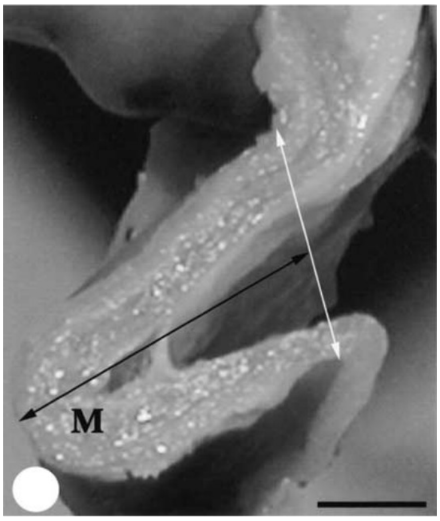

(b) The fold.

Source – Adapted from Leaper, Zhang, and Dawes (2005).

In the figure, M is used to indicate the cricopharyngeus muscle, Cr the cricoid cartilage, and the asterisk marks the lumen of the PES. The black line indicates a length of 2 mm.

It is important to stress that muscle contraction may produce a constriction on the PES, visible in videofluoroscopic images (this is common in images taken during tracheoesophageal phonation). The key difference here is the presence of the protrusion when the musculature is relaxed (during deglutition, or in cadavers).

2.3 Total laryngectomy

The purpose of this subsection is to provide a brief overview of the total laryngectomy. The main focus is the description of the surgical steps most relevant to elucidating the anatomy of the PES after surgery. It should also be stressed that different surgeons may perform the surgery differently, and that the location and extension of the tumor affects how the surgery is carried out.

The description given below is based mainly on Schwartz, Hollinshead, and Devine (1963), Tucker (1990), Donald (2010), and Holsinger and Bhayani (2011). Between these authors there were differences in how particular steps of the surgery were described, and also in the order in which they appeared. An attempt was made to provide a "common ground" description, with an appropriate discussion in points where there were significant differences.

The procedure begins with an incision on the neck, deep enough to cut through the platisma muscle[15]. While Schwartz, Hollinshead, and Devine (1963) describe three different shapes for the incision, and favor a T-shaped one, most references describe a U-shaped incision, as shown in Figure 31. The skin flaps are then pulled open to provide access to the interior of the neck.

Figure 31 – U-shaped incision on the neck.

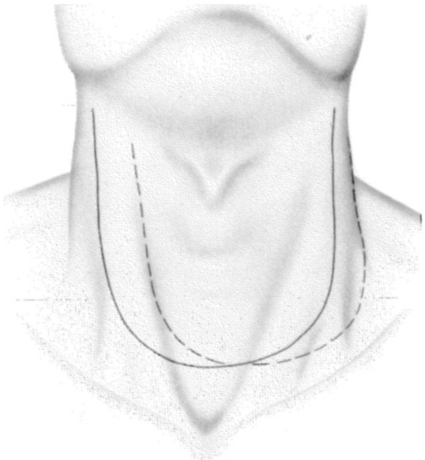

Source – Tucker (1990).

The strap muscles, also called infrahyoid muscles, are then dissected at the level of, or below, where the tracheostoma is expected to be. This group of muscles is composed of the sternohyoid, sternothyroid, omohyoid, and thyrohyoid. They are shown in Figure 32, and they anchor the hyoid bone to the sternum, clavicle, and scapula (DORLAND, 2011).

Next, the thyroid gland (Figures 21 and 22) is addressed. The procedure here is dependent on the extent of the tumor. From the description given by Schwartz, Hollinshead, and Devine (1963), Tucker (1990), Donald (2010), and Holsinger and Bhayani (2011), the most common scenario seems to be the one where the lobe located on the same side of the tumor is removed, and the one on the opposite side is preserved. In this case, the isthmus is transected during the laryngectomy, separating the two lobes. The lobe on the side of the tumor is removed, while the one on the opposite side is reflected to the side, exposing part of the larynx and the trachea.

The suprahyoid muscles are then released from the hyoid bone. These muscles connect the hyoid bone to the skull. The digastric muscle, the stylohyoid, the mylohyoid, and the genoihyoid muscle compose this muscle group (Figure 32). The cut is made at the level of the hyoid bone, with care not to perforate the pharynx. Any other structures

[15] A flat muscle running from the collarbone to the lower jaw (COLLIN, 2005). It covers the anterior part of the neck, just beneath the skin.

Figure 32 – Muscles on the anterior portion of the neck.

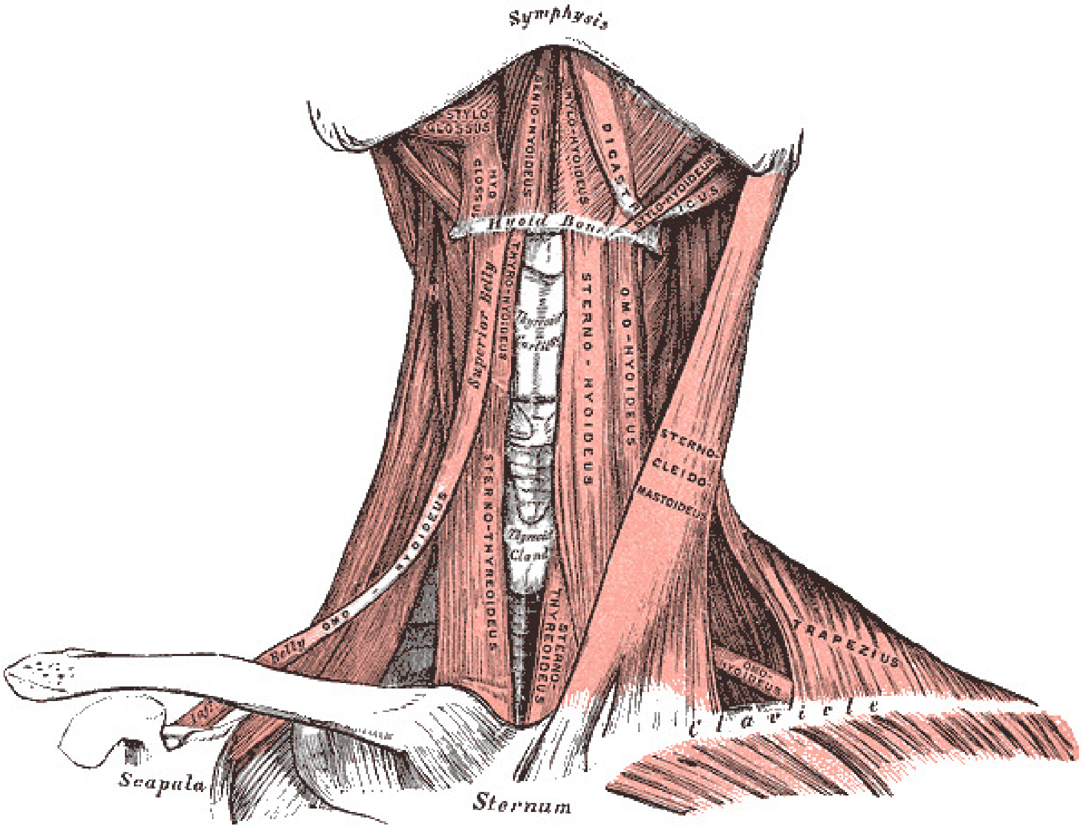

Source – Gray (1918).

which attach to the hyoid bone from above are also removed in this step (this includes the middle pharyngeal constrictor[16]).

The inferior pharyngeal constrictor and the cricopharyngeus are then separated from the thyroid and cricoid cartilages respectively. The separation is made following the posterior edge of the thyroid cartilage.

The mucosa of the pyriform sinus (Figure 33) may be preserved on the side opposite to the tumor (HOLSINGER; BHAYANI, 2011). To do so, the mucosa is separated from the inner surface of the thyroid cartilage, in order not to be removed along with the larynx. This procedure is also recommended by Freeman and Hamaker (1998), who indicate that as much mucosa as possible should be conserved.

The larynx may now be removed. The manner in which this step is performed depends on where the tumor is located, as well as its extension. The descriptions given by Schwartz, Hollinshead, and Devine (1963), Tucker (1990), Donald (2010), and Holsinger and Bhayani (2011) diverge in some details regarding the removal of the larynx. The description given by Tucker (1990) will be presented.

[16] The middle pharyngeal constrictor is located in the pharynx, just above the inferior pharyngeal constrictor, as shown in Figure 22.

Figure 33 – Posterior view on the inside of the pharynx, with the mucosa opened.

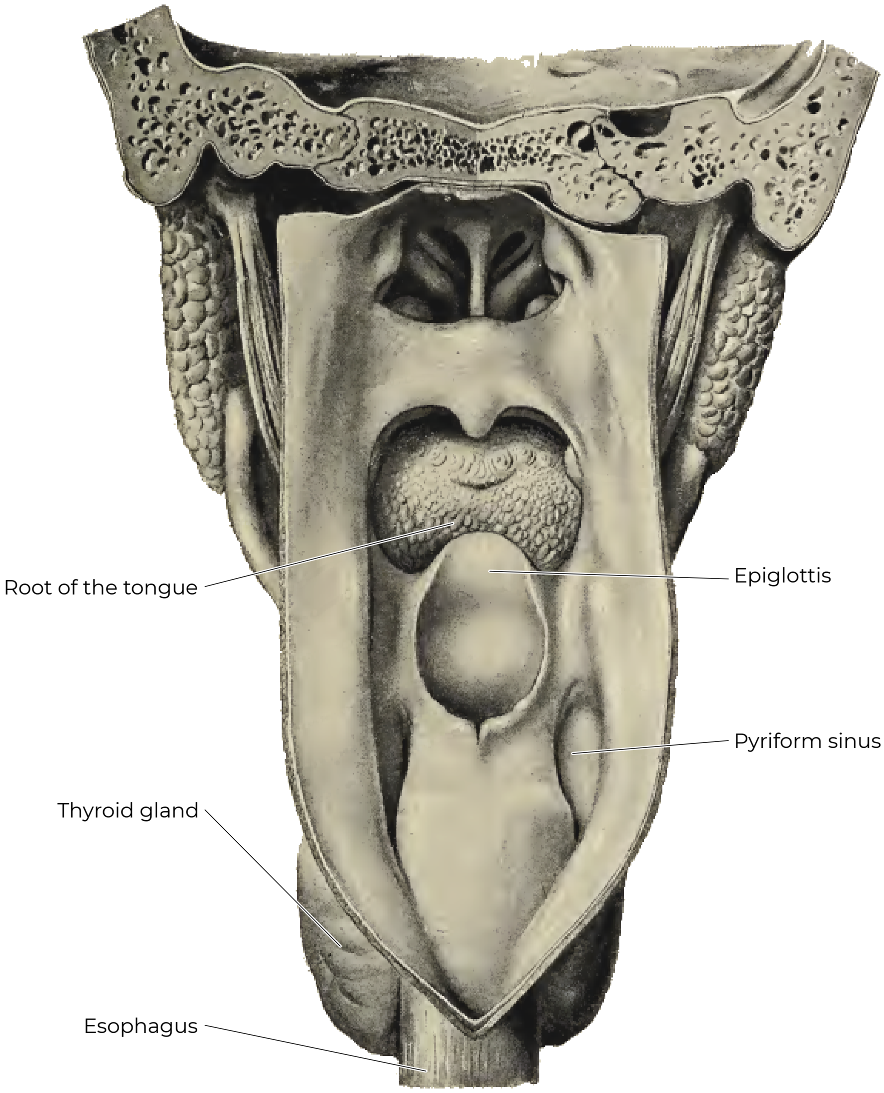

Source – Sobotta (1928).

The trachea is cut at a point below the second tracheal ring. The cut may be on a bevel (DONALD, 2010), or forming a "tongue-like superior projection" of the posterior wall of the trachea (Figure 34), as proposed by Tucker (1990). The cut on the posterior wall of the trachea lies near the inferior border of the cricoid cartilage, and the trachea is cut in this manner to increase the area of the tracheostoma.

The larynx is then pulled upwards from below (Figure 35). A transverse incision is made in the mucosa of the PES, near the lower border of the cricoid cartilage. The cut is then continued superiorly, following the border of the thyroid cartilage on each side.

While the cut is being made, the larynx is still being pulled from below (Figure 36). Eventually, the epiglottis will be visible. The epiglottis is then grasped, and the larynx

Figure 34 – Dissection of the trachea.

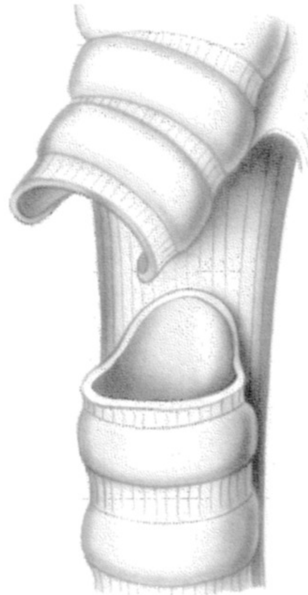

Source – Tucker (1990).

Figure 35 – Pulling the end of the trachea upwards.

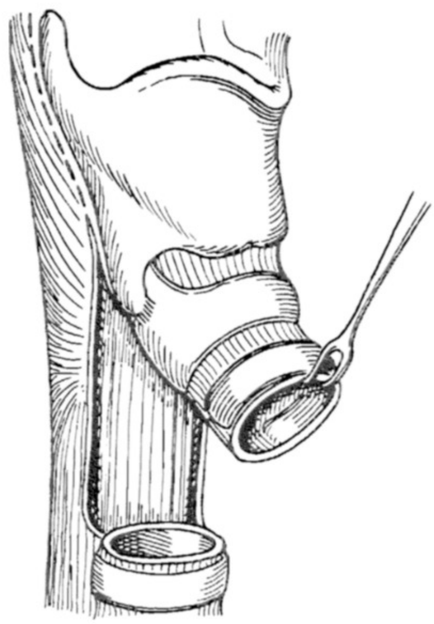

Source – Tucker (1990).

is inverted. The upper part of the cut on the mucosa of the PES is made across the attachment of the base of the tongue. This cut is made anterior to the epiglottis and inferior to the hyoid bone (TUCKER, 1990). The larynx is then completely removed.

The opening made on the mucosa of the PES must then be closed. In this point there seems to be considerable differences in the procedure adopted by different surgeons. Schwartz, Hollinshead, and Devine (1963), Donald (2010), and Holsinger and Bhayani

Figure 36 – Removal of the larynx.

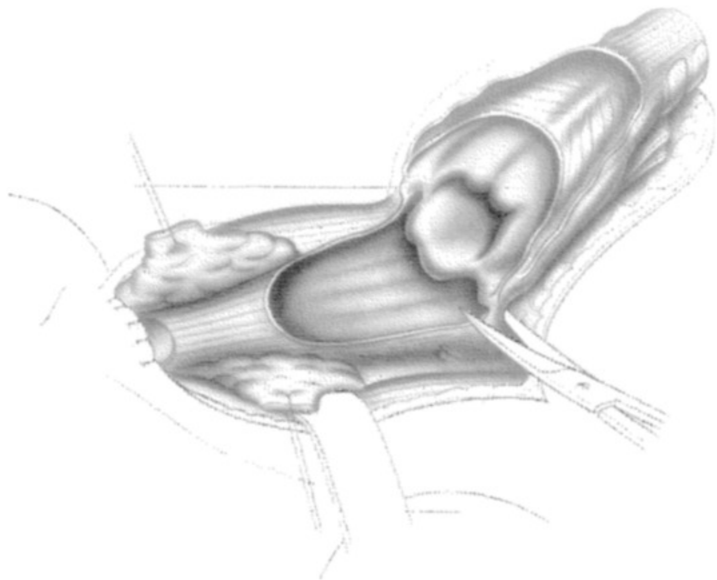

Source – Tucker (1990).

(2011) suggest closing first the layer of mucosa, then a layer of muscle, as illustrated in Figure 37. These authors do not make the distinction between the cricopharyngeus muscle and the inferior pharyngeal constrictor. It is presumed that the muscle layer discussed above is composed of both muscles.

Figure 37 – Closing of the PES during a total laryngectomy.

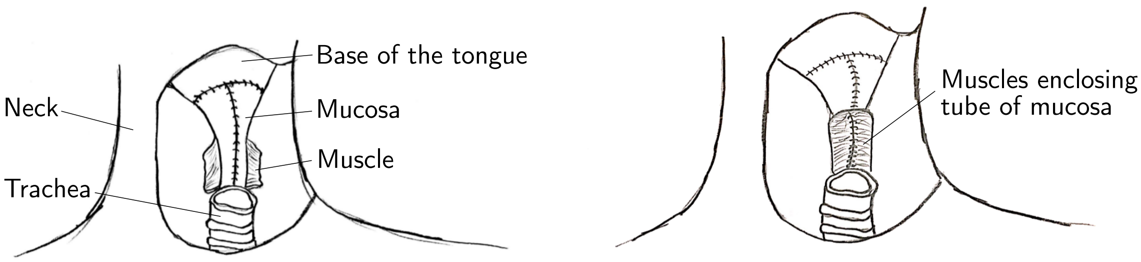

(a) Closing the layer of mucosa. (b) Closing the layer of muscle.

Source – Tourinho et al. (2021).

On the other hand, Tucker (1990) recommends not closing the layer of muscle, as “this may interfere with development of a good vibratory segment”. Tucker (1990) does not cite any reference for this statement.

Hamaker and Cheesman (1998) suggest that there should be a layer of muscle enclosing the mucosa; however, they indicate that it should be composed mainly of the inferior pharyngeal constrictor, with a small contribution from the middle pharyngeal constrictor and “virtually none” from the cricopharyngeus.

Additional steps taken during closure of the PES also differ. Schwartz, Hollinshead, and Devine (1963), Tucker (1990), and Donald (2010) do not mention any additional step. However, Holsinger and Bhayani (2011) point out that, besides the constrictor muscles, the strap muscles, the musculature of the sternocleidomastoid, and even the thyroid gland may be used to form a layered closure over the suture line. Hamaker and Cheesman (1998) suggest suturing the suprahyoid muscles to the upper part of the closed layer of muscle, since this would "enhance the potential of muscle control" of the PES. Simpson, Smith, and Gordon (1972) suggest making a connection between the suprahyoids to the constrictors, forming an "upper anchor structure". They also suggest bringing together the longitudinal layer of the esophagus and posterior wall of the trachea with the lower portion of the cricopharyngeus (which has been closed over the layer of mucosa), forming a "lower anchor structure"[17].

After completing the closure, the PES may be flooded with saline to ensure that there are no leaks (HOLSINGER; BHAYANI, 2011). The tracheostoma may then be formed. First, the anterior wall of the trachea is sewn to the skin of the neck (Figure 38). The skin flaps that were opened and raised are lowered and closed, completing the surgery.

Figure 38 – Anchoring the anterior wall of the trachea to the skin to form the tracheostoma.

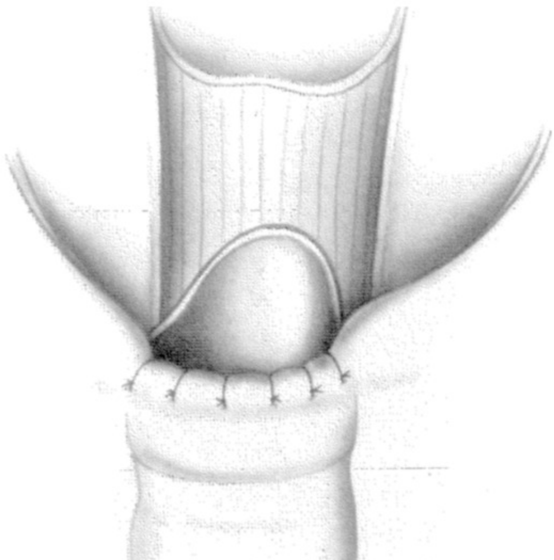

Source – Tucker (1990).

Freeman and Hamaker (1998) recommend forming the stoma in a slightly different manner. They suggest placing the horizontal component of the neck incision (Figure 31) not at the level of the anterior part of the tracheostoma, as in Figure 38, but on the posterior one. An additional small incision is made for the rest of the tracheostoma.

[17] The procedure described by Simpson, Smith, and Gordon (1972) also differs in the fact that it maintains the cornua of the hyoid bone, and most of the musculature connected to it.

To conclude the present section, it is interesting to discuss the survey conducted by Maclean, Cotton, and Perry (2008). In this work, 56 short questionnaires were sent to head and neck surgeons in Australia, questioning them about their particular technique of performing the total laryngectomy. Half of the questionnaires were returned. Of these, 57.7% perform a closure composed of mucosa and muscle (Figure 37), while 19.2% perform a mucosa only closure. 15.4% stated that the closure type was dependent on the features of the tumor, and the remaining ones opt for a “double layer mucosa closure”. With regard to the suprahyoids, only 34.9% of the respondents reattach them during closure of the PES. Two respondents considered important preserving the hyoid bone if possible. While these results cannot be used to determine what is the most common method of performing a laryngectomy, they illustrate how much the procedure may change depending on the surgeon.

2.4 Tracheoesophageal puncture

After having described the total laryngectomy, the only anatomical modification associated with TE speech that remains to be discussed is the tracheoesophageal puncture. The TE puncture is an opening connecting the trachea to the esophagus, where the tracheoesophageal prosthesis will be placed (Figure 6b). The puncture may be formed during the total laryngectomy, in which case it is called a primary tracheoesophageal puncture. When the opening is formed after the total laryngectomy, in a separate procedure, it is called a secondary tracheoesophageal puncture.

The primary procedure is described by Hamaker, Singer, et al. (1985). The puncture is performed after the removal of the larynx, but prior to the closure of the PES. A hemostat[18] is placed inside the esophagus through the opening in the mucosa of the PES. The tip of the hemostat is pressed against the anterior wall of the esophagus, towards the trachea, 8 mm below where the trachea was cut. A 4 mm horizontal incision is then made through the opened trachea, at the point where the tip of the hemostat is marking. A separation between the esophagus and the trachea may occur, in which case the trachea and the esophagus are sutured together. The PES is then closed.

The secondary procedure is described by Singer and Blom (1980). In this procedure, an esophagoscope is introduced in the esophagus through the mouth of the laryngectomee, with the tip 20 mm inferior to the tracheostoma. The puncture is made 3 to 5 mm below the superior part of the tracheostoma, using the opening on the esophagoscope as a guide.

A recent review (CHAKRAVARTY et al., 2018) found that the outcomes of a primary and a secondary procedure are reasonably similar, with no significant difference in voice outcomes, although the primary puncture is associated with higher success rates. On the other hand, pharyngocutaneous fistula formation was found to be more prevalent

[18] A surgical clamp with the appearance of a pair of scissors.

in primary puncture.

2.5 Anatomy of the PES after total laryngectomy

The anatomy of the post-laryngectomy PES may be deduced from the discussion on the total laryngectomy in Section 2.3. Considering the differences in how the procedure might be adopted, it is not possible to specify a unique set o features that compose the post-laryngectomy PES.

In its simplest possible form, the PES will be a tube of mucosa with a layer of muscle being present only on the posterior wall (Figure 37a). Very commonly however, the layer of muscle will wrap around the tube of mucosa (Figure 37b).

The suprahyoid muscles may be connected to the layer of muscle in an attempt to increase muscle control. Although rare, the longitudinal layer of the esophagus may be sutured to the layer of muscle. Additional structures such as the strap muscles and even a thyroid lobe may also be connected to the PES during surgery.

In terms of the neighboring anatomical structures, the main difference is that the larynx is evidently no longer present. The strap muscles, which ran near the larynx before the laryngectomy (Figure 32), are also cut. Therefore, anteriorly, the most prominent structure will be the platisma muscle and the skin of the neck. The thyroid gland is also affected by surgery, and it is likely that there will be only one lobe, or that the gland may be removed completely. Therefore, the main neighboring structure to the sides of the PES has also been either removed, or substantially changed. On the other hand, posteriorly there is no change. The vertebral column and the prevertebral muscles are still located posterior to the PES, separated from it by a fascial space.

A stricture (Section 2.2.5) may also be present in the PES after a laryngectomy. It may have been present prior to the surgery, but it may also occur due to loss of excised mucosa during surgery, or fibrosis secondary to delayed healing (SIMPSON; SMITH; GORDON, 1972). Sweeny et al. (2012) indicate that reported stricture rates vary from 13 to 50% following pharyngeal reconstruction, with their own study observing the development of stricture in 19% of 263 total laryngectomy patients.

2.6 The physiology of tracheoesophageal speech

Before discussing the physiological processes involved in TE speech, it is important to mention that even after a total laryngectomy, the PES maintains its function as a sphincter. It remains normally closed, but opens during swallowing, belching, and vomiting, as was the case before the operation.

The processes involved in each of these actions are evidently affected by surgery. While it is out of the scope of the present thesis to review how each of them is affected, it is fruitful to at least see how surgery affects the resting tone of the PES.

The work of Welch, Luckmann, et al. (1979) provides much insight into this. This work has been discussed in Subsection 2.2.4, where the spatial distribution of intraluminal pressure that they measured in the PES was shown. Welch, Luckmann, et al. (1979) performed the same measurements with laryngectomees. Figure 39 shows the results of the measurement made with one laryngectomee.

Figure 39 – Pressure distribution in the PES of a laryngectomee.

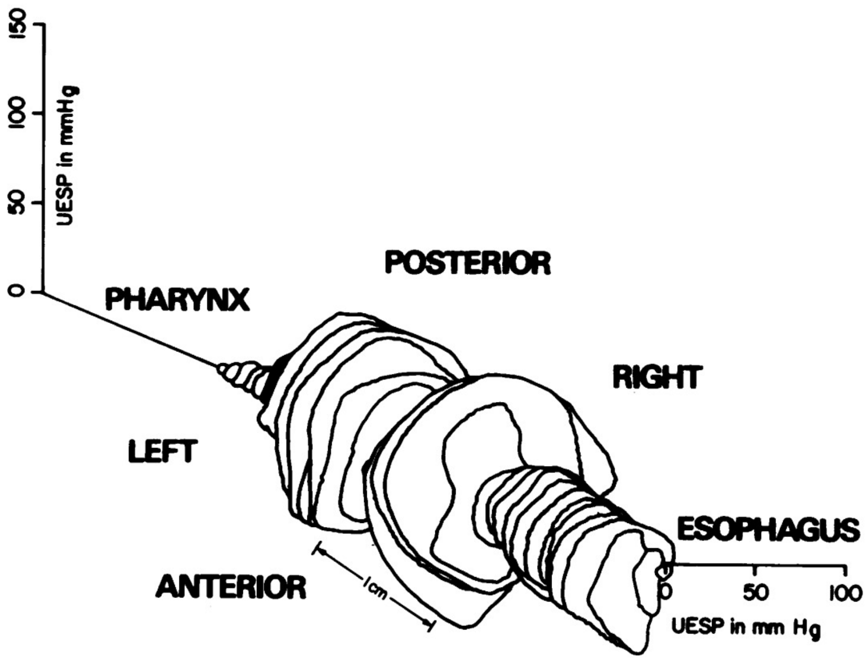

Source – Welch, Luckmann, et al. (1979).

Compared to Figure 28, the distribution is far more axisymmetric. Two lobes of high pressure are identified, as was the case for the subject who had not undergone a total laryngectomy. However, the pressures in the anterior-posterior direction are almost the same as those in the lateral direction.

Welch, Luckmann, et al. (1979) do not explore the reason behind the two lobes of higher pressure beyond their vise analogy (Subsection 2.2.4). One possibility would be that one lobe is associated with the inferior pharyngeal constrictor, and the other with the cricopharyngeus. The part of the PES composed of the cervical esophagus would correspond to the region of nearly uniform pressure in the distribution, and the valley between the lobes could be due to the region of sparse musculature between the inferior pharyngeal constrictor and the cricopharyngeus (Killian's triangle). This, however, is merely speculation, and further studies would be required to properly explain this distribution.

Welch, Luckmann, et al. (1979) compared the average maximum pressure taken among the group of laryngectomees and the group which had not undergone surgery. They indicate that there was a reduction from 16.1 kPa in the no-surgery group to 6.8 kPa in the group of laryngectomees. They also indicate that there was no significant difference in the length of the high pressure zone between the two groups. The reduction in the intraluminal resting to pressure between laryngectomees and non laryngectomees was also observed by Winans, Reichbach, and Waldrop (1974).

The contraction of the PES is essential to the production of sound in alaryngeal phonation. The PES was shown to be the sound source in esophageal speech (Section 1.2) in a series of studies conducted from the 1930's to the 1960's (SIMPSON; SMITH; GORDON, 1972). It is also generally accepted that the process is analogous to laryngeal phonation, in the sense that the PES is set into oscillatory motion by the airflow passing through it (VERKERKE; THOMSON, 2014).

Despite the basic mechanism of sound production being similar to that of the vocal folds, there are many differences between the two processes. For example, there is a considerable change in the shape of the PES during phonation. Figure 40 illustrates this. Figure 40a shows a saggital plane CT image of a laryngectomee at rest, while Figure 40b shows the same subject during phonation. Figure 41 is similar to Figure 40, but the images were obtained with a different subject. Both subjects are fluent TE speakers.

These images had been previously obtained at the Centro de Pesquisas Oncológicas (CEPON). A Canon Aquilion Prime SP Star, with the capability of perform 160 slices per rotation was used. Conduction of the imaging examination was approved by the ethics committee of the Universidade Federal de Santa Catarina (UFSC, 2018). In the figures, the lumen of the tube composed by pharynx, PES, and esophagus has been highlighted in yellow. The PES (more specifically, constrictions in the region of the PES) is marked by red arrowheads. The yellow arrowhead indicates part of a lung, not to be confused with the esophagus.

The main structures of pharynx, esophagus, trachea, and prosthesis are easily identified in the figures (which can be compared to the schematic drawings of Figures 1b and 6). For the subject at rest (Figures 40a and 41a), the PES is seen as a closed region between the pharynx and the esophagus.

In order to provide a more thorough illustration of the region, the lumen of the pharynx, PES, and esophagus was segmented from the images and the three-dimensional reconstructions of the lumen in Figures 40 and 41 are shown in Figures 42 and 43 respectively. The reconstructed region corresponds to the region marked by the yellow contour in Figures 40 and 41.

During phonation, the most inferior part of the PES dilates, and a constriction is formed just below the pharynx. This constriction appears to project from the posterior wall towards the lumen.

It is also interesting to note that the esophagus of both subjects closes just below the prosthesis. It is not known whether this is a general phenomenon, nor the reason for this to occur. One possibility is that the trachea was pushed back as the participants closed

Figure 40 – CT scans of Subject 1 at rest and during phonation.

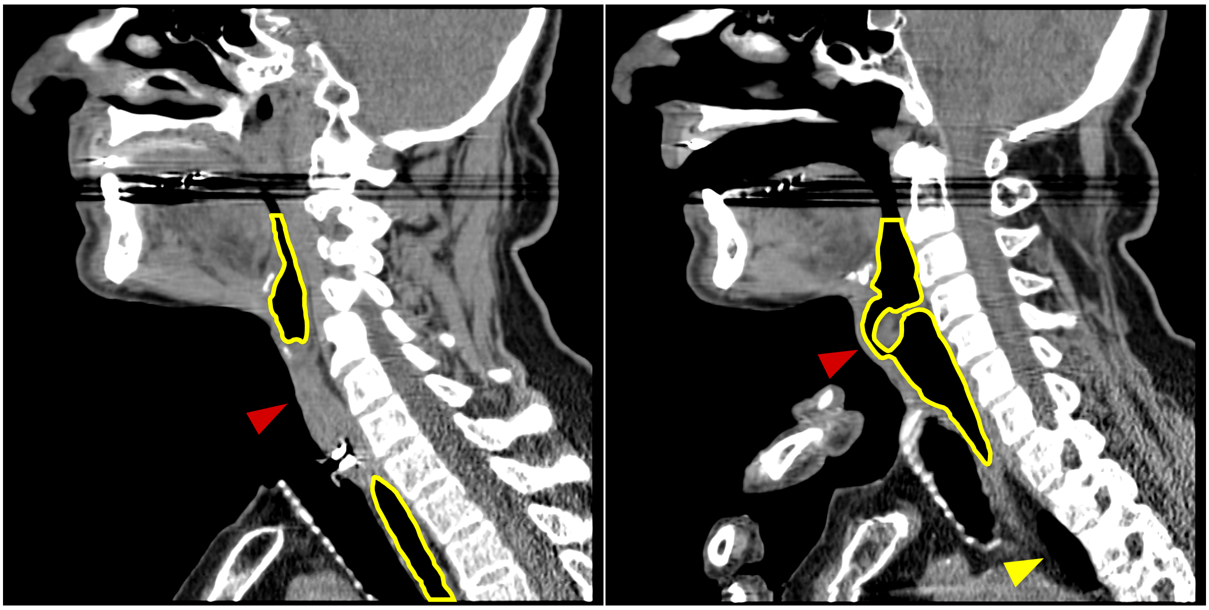

(a) At rest. (b) During phonation of the vowel /a/.

Source – Tourinho et al. (2021).

The yellow contour indicates the lumen of the pharynx, PES and esophagus. The red arrowhead indicates bulges in the PES. The yellow arrowhead indicates a lung. Images (a) and (b) are not from the same sagittal plane.

Figure 41 – CT scans of Subject 2 at rest and during phonation.

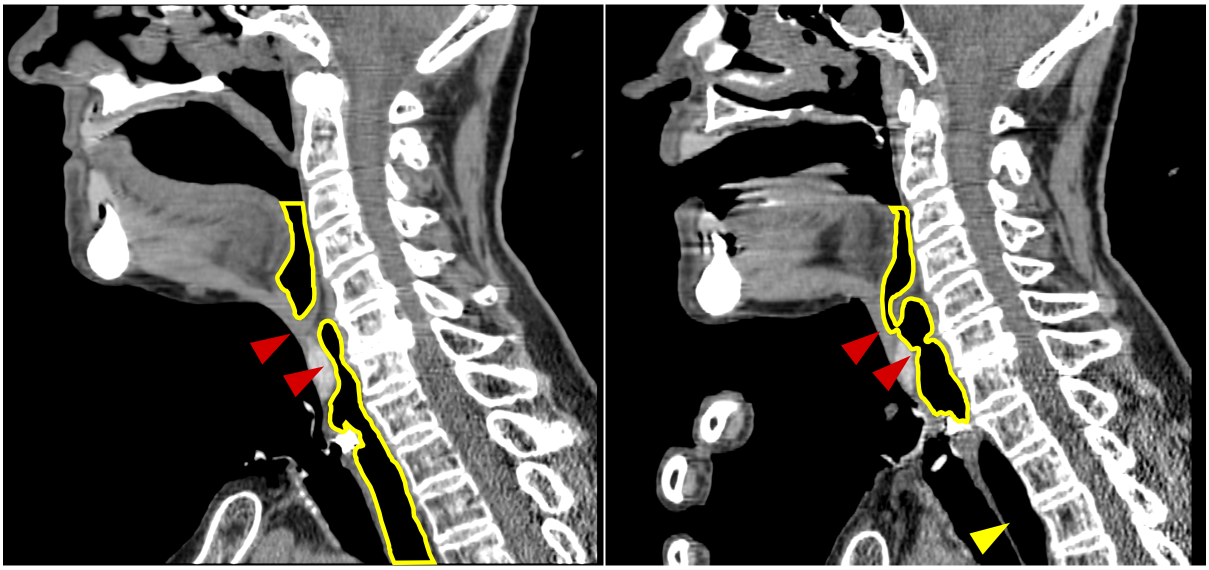

(a) At rest. (b) During phonation of the vowel /a/.

Source – Tourinho et al. (2021).

The yellow contour indicates the lumen of the pharynx, PES and esophagus. The red arrowhead indicates bulges in the PES. The yellow arrowhead indicates a lung. Images (a) and (b) are not from the same sagittal plane.

the heat and moisture exchange device at their tracheostoma (Section 1.1) to phonate;

Figure 42 – Lumen of pharynx, PES, and esophagus reconstructed from CT scans of Subject 1.

(a) At rest. (b) During phonation of the vowel /a/.

Source – Tourinho et al. (2021).

Figure 43 – Lumen of pharynx, PES, and esophagus reconstructed from CT scans of Subject 2.

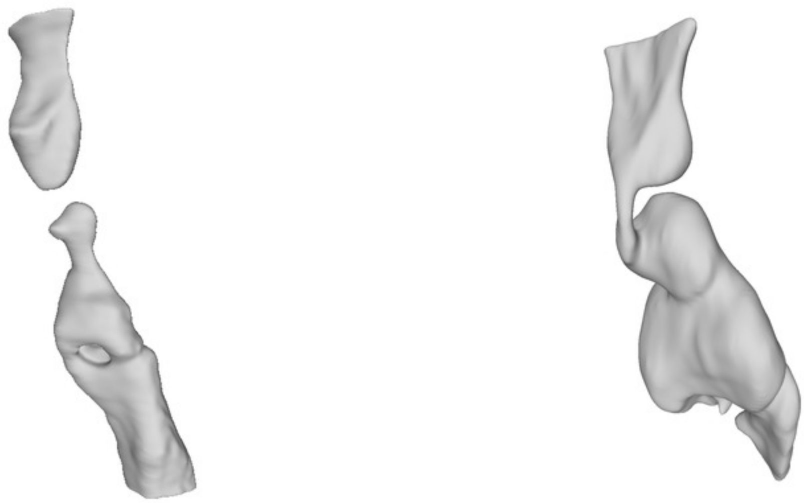

(a) At rest. (b) During phonation of the vowel /a/.

Source – Tourinho et al. (2021).

however, at the moment this is merely speculation.

While this basic description fits the images of both subjects, several differences are readily visible. First, the closed part of the PES at rest for Subject 1 is much longer than that for Subject 2 (it is about 50 mm for Subject 1 and 10 mm for Subject 2).

Also, while the PES of Subject 1 presents one bulge, or constriction, during phonation, the PES of Subject 2 seems to present two constrictions. In fact, a second narrowing is already noticeable in the PES for Subject 2 at rest. This second constriction could be explained in two ways: it could be the case of stricture (Subsection 2.2.5); or it could result from muscle contraction, only that the contraction is not strong enough to completely close the PES at that point.

Published images of the PES during alaryngeal phonation[19] show even larger variations (MAHIEU, 1988; MCIVOR et al., 1990; SLOANE et al., 1991; OMORI et al., 1994; VAN WEISSENBRUCH et al., 2000; VAN AS; OP DE COUL, et al., 2001; FOUQUET; GONÇALVES; BEHLAU, 2009; FOUQUET; BEHLAU; GONÇALVES, 2013). For instance, Figure 44 illustrates a PES in which there is no inflation of its most inferior part.

Figure 44 – Videofluoroscopy image of the PES during phonation.

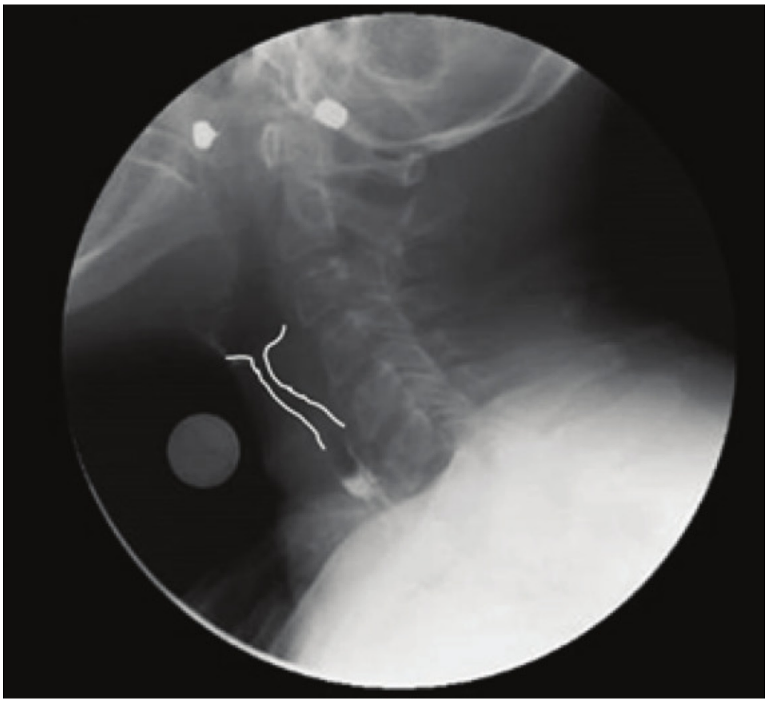

Source – Fouquet, Behlau, and Gonçalves (2013).

Figure 45 illustrates another example—that of a hypotonic PES during an attempt at esophageal phonation. The subject could not produce the esophageal voice, unless the anterior part of the neck was pressed with the hand (Figure 45b).

The various differences in shape that are observed in imaging studies have been attributed to differences in tonicity of the PES among the different subjects (MCIVOR

[19] Some of these studies consider the esophageal voice (Section 1.2). Since PES vibration is the main source of sound in both the esophageal voice as in the TE voice, many of the observations for one case apply to the other.

Figure 45 – Hypotonic PES during attempts at esophageal phonation.

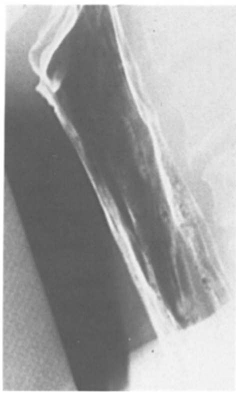

(a) Without the hand pressing the neck.

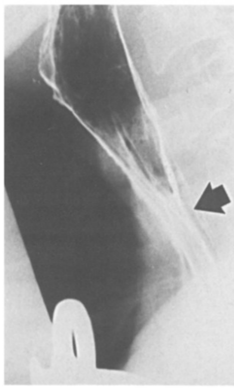

(b) With the hand pressing the neck.

Source – McIvor et al. (1990).

et al., 1990; SLOANE et al., 1991; VAN AS; OP DE COUL, et al., 2001). McIvor et al. (1990), studying esophageal speakers, considers five categories, based on the appearance of the PES on videofluoroscopic images. These are: hypotonic, good esophageal speakers, hypertonic, spasm, and stricture. In the hypotonic group, the walls of the PES remain widely separated during an attempt at phonation (Figure 45a), and there is no voice produced. Good esophageal speakers presented one "vibrating PES" during phonation, with a length of up to 30 mm. In the hypertonic group, one or two narrow segments were formed and the esophagus dilated. The quality of the resulting voice was variable in this group. The case of spasm was similar to the hypertonic group, but the constrictions were even narrower. In this case, the air is "released in sudden explosive bursts" (MCIVOR et al., 1990) and no voice is produced. Subjects in the stricture group presented a narrowing in the PES that persisted with the same contour both at an attempt at phonation and during swallowing. Similar descriptions are given by Sloane et al. (1991) and van Weissenbruch et al. (2000).

The work of Morgan et al. (1992) corroborates the link between tonicity of the PES with its observed shape during phonation. Using videofluoroscopy they classified 18 esophageal speakers in four groups: hypotonic, tonic, hypertonic, and spasm. Then they performed esophageal manometry measurements of the resting tone of the PES of these laryngectomees. As expected, the intraluminal pressures were smallest for the hypotonic group, and increased continuously up to the spasm group.

The presence of two constrictions in the PES, which was described by McIvor et al. (1990) in the hypertonic group, has also been observed by other authors. Simpson, Smith, and Gordon (1972), studying esophageal speakers, noticed that the second constriction could be due to stricture, to what they call "pseudo-stricture", or due to voluntary control. The case of "pseudo-stricture" is a projection of the posterior wall of the PES into the lumen. During swallowing, either it disappears, or there was only a small defect. They speculate if this could happen due to unsutured fibers of the inferior pharyngeal constrictor and cricopharyngeus that have retracted posteriorly. The case of voluntary contraction involved a pulling of the preserved part of the hyoid bone backwards (part of the hyoid was preserved during surgery).

Omori et al. (1994) indicate that two constrictions were observed in the majority of the participants in their study (23 out of 25). The superior constriction closed the lumen completely and oscillated during phonation, while the lower one neither closed the lumen completely nor oscillated. These authors hypothesize that the superior constriction arises due to the inferior pharyngeal constrictor, and the inferior one due to the cricopharyngeus.

The prevalence of two constrictions that was observed in the study of Omori et al. (1994) is likely not universal. In the study of van As, Op de Coul, et al. (2001) two constrictions were observed only in the minority of participants (3 out of 30). This was also the case for the study of Fouquet (2012), in which two constrictions were observed only in 4 of a total of 30 subjects.

The correlation between the tonicity of the PES with its shape during alaryngeal phonation implies that the musculature of the PES contracts during phonation. This has been corroborated by electromyographic (EMG) studies (SHIPP, 1970; PRUSZEWICZ et al., 1992; MOHRI et al., 1994; OMORI et al., 1994; NISHIZAWA et al., 2001).

Mohri et al. (1994), besides EMG, also measured the pressures in the trachea and in the PES during TE phonation. They observed a pattern that was common to all 7 subjects that participated in the study. First there is an activation of the PES musculature, which is noted by a sudden rise in the amplitude of the EMG signal during inspiration. Then there is a sudden reduction in the amplitude of EMG signal. This reduction is very brief and coincides with the onset of vibration of the PES. The amplitude of the EMG signal rises once again, now to an even higher level. This higher level is maintained throughout the entire phonatory process, and gradually returns to the resting level afterwards.

It is interesting to note that this pattern is consistent with the reflexes of the PES (Subsection 2.2.4). The increased activity upon inspiration is consistent with the pulmonary-UES contractile reflex, in which a distention of the lungs causes an increase in the contraction of the PES. The brief drop in EMG activity is consistent with the esophago-UES relaxation reflex—the sudden injection of air through the prosthesis would be analogous to the injections of air in the esophagus in the experiment of Kahrilas et al. (1986). It could also be speculated that the final rise in the amplitude of the EMG signal could be due to the pharyngo-UES contractile reflex, and the air that has passed through the PES into the pharynx would activate this reflex.

Given that TE speakers possess some control over the pitch of the resulting voice (this will be further discussed below), it is somewhat questionable that TE phonation is an entirely involuntary process. On the other hand, the control in pitch could arise due to the contraction of other muscles of the pharynx, that could potentially stretch the PES longitudinally, without directly changing its tonicity.

To the best of the author's knowledge, there is no published study indicating whether TE speakers are able to voluntarily change PES contraction. It was seen that most activity in the PES prior to a total laryngectomy is involuntary and regulated by reflexes, which suggests a limited, or absent, control of the musculature. Furthermore, if a laryngectomee is capable of contracting the PES voluntarily, it would certainly be to a limited amount, since otherwise an individual with hypertonicity could relax the musculature at will and speak normally.

Omori et al. (1994) measured EMG signals for each of the two bulges that were seen in the participants of their study. The EMG signal of both constrictions showed an increase in amplitude about one second before the onset of phonation, and continued throughout the entire phonatory process. The increase in amplitude before the onset of phonation is consistent with the pattern indicated by Mohri et al. (1994), as is the maintenance of the high EMG activity; however, the brief drop in amplitude just before PES vibration was not observed.

Interestingly, the EMG signal associated with the upper bulge presented a larger amplitude when compared to the lower one. While this could potentially suggest a larger increase in contraction in the upper bulge than the lower one, this may not be the case, since it is not known whether a given change in EMG amplitude results in the same increase in muscle contraction in both bulges. To the best of the present author's knowledge, there is no study indicating if during TE phonation PES contraction is considerably different from that which occurs at rest (whose spatial distribution is shown in Figure 39).

Nishizawa et al. (2001), studying esophageal speakers, measured EMG signals not only in the inferior constrictor, but also in the geniohyoid muscle (one of the suprahyoid muscles). The authors indicate that the geniohyoid muscle is activated during esophageal phonation. However, no clear pattern of activation appears and the study was conducted with only two subjects, which leaves the role of the suprahyoid muscles still unclear.

It is worth mentioning that the observation that some longitudinal fibers of the esophageal musculature are continuous with longitudinal fibers of the pharyngeal musculature (Subsection 2.2.2), as well as the fact that the mucosa of the post-laryngectomy PES is connected to the root of the tongue, suggest that longitudinal tension may play a part on the dynamics of TE phonation. However, no mention of this effect has been found in the literature.

Endoscopic imaging studies have also been carried out (MOHRI et al., 1994; DWORKIN et al., 1998; VAN AS; TIGGES, et al., 1999; KOTBY et al., 2009; SCHWARZ et al., 2011; HÜTTNER et al., 2015; ARENAZ BÚA et al., 2017). With this method, the uppermost section of the PES is visible, as shown in Figure 46, which shows images obtained during phonation, at different moments in time.

van As, Tigges, et al. (1999) classified the observed shape of the open section of the

Figure 46 – Endoscopic images of the PES during phonation.

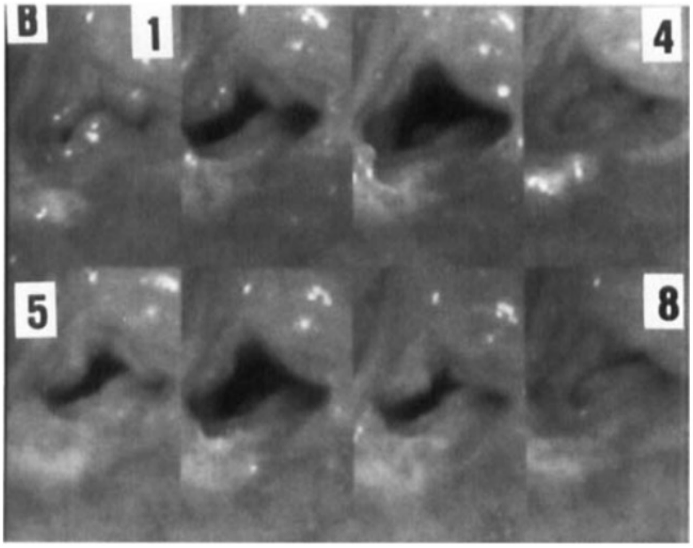

Source – Dworkin et al. (1998).

PES during phonation. Their study contained 35 participants, and they used six categories: circular (with 11% of the participants), triangular (3%), split side-to-side (31%), anterior-posterior split (6%), irregular (29%), and not assessable (17%). It is evident that while the most common shape was in the form of a side-to-side split, it is not possible to indicate a "typical" shape for the cross-section of the oscillating PES. The study of Arenaz Búa et al. (2017) used the same categories as that of van As, Tigges, et al. (1999) with 12 subjects. In this study, the most common shape was the circular one (42% of the participants). The authors do not provide possible explanations for the different shapes observed.

The endoscopic images also show the presence of a mucosal wave (Section 2.1) in some laryngectomees. In the study of van As, Tigges, et al. (1999), the mucosal wave was observed in only half of the participants (18 out of 35), while in the study of Arenaz Búa et al. (2017) eleven (out of twelve) participants presented a mucosal wave in the PES during phonation. These results suggest that the mucosal wave is likely to be far less prevalent in TE speech, when compared to laryngeal phonation. This, in turn, suggests that the "out-of-phase motion" energy transfer mechanism that is of considerable importance to the self-sustained oscillations of the vocal folds (Section 2.1), might not be as significant in TE phonation.

Tracheoesophageal speakers usually present a smaller amount of control of the resulting voice when compared to laryngeal speakers (SCHINDLER et al., 2005). If one compares the level of sophistication of the mechanisms available to position (or posture) the vocal folds (ZHANG, 2016), with what is available for the PES, this is not surprising.

With regard to the control of the oscillation frequency, Moon and Weinberg (1987) conclude from their study that TE speakers are able to control the fundamental frequency of phonation. However, they state that they are not in a position to indicate how this control is made. They hypothesize that it could be due to direct control of the PES, due to indirect control of the PES (by head or neck movements, for instance), or due to variations in properties of the PES mediated by reflexes.

Max, Steurs, and Bruyn (1996) conducted a study in which they asked 10 TE speakers to speak the vowel /a/ as low as they could, then as high as they could. The difference between the frequency in the high condition and the low condition ranged from 42 Hz to 162 Hz, with an average value of 83.8 Hz.

Schindler et al. (2005) asked subjects to speak in a comfortable register, then to speak a perfect fifth above that register (1.5 times previous the frequency). There are not many details on the experiment (for instance, whether the higher frequency was played for the subjects), but the authors state that the participants had a certain difficulty in producing the higher pitch.

Onofre et al. (2013) in a study with five participants, observed that after musical training, the vocal ranges observed varied from 6 semitones (the minimum in the group) to 27 semitones (the maximum in the group) when saying the vowel /a/. These values varied little when different vowels were considered. The report of 27 semitones is quite remarkable in that it indicates a vocal range of over two octaves (over four times the initial frequency). The median was 15 semitones, which is still above one octave. The study is obviously limited by the very small sample size, but it suggests laryngectomees could potentially reach a range quite larger than the one indicated by Verkerke and Thomson (2014), who indicate that TE speech does not generally allow for a frequency variation of 50%.

Another aspect related with the control of the TE voice is the so-called dynamic range, which is the difference between the minimum and the maximum sound pressure level the speaker is able to produce. Max, Steurs, and Bruyn (1996) measured a range that varied from 13 dB to 29 dB in the group of participants, while Schindler et al. (2005) indicates that the dynamic range in the subjects of their study was about 20 dB, which they indicate is similar to dynamic ranges observed in laryngeal speech.

The duration for which a TE speaker could sustain phonation, called the maximum phonation time has also been measured. Robbins et al. (1984) report a mean value of 12.2 s with a standard deviation of 5.2 s in a group of 15 TE speakers. In the study of Max, Steurs, and Bruyn (1996) the subject with the smallest maximum phonation time was able to sustain phonation for 2 s, while the subject with the largest could sustain phonation for 20 s. van As (2001) also reports measurements of the maximum phonation time. She indicates that the results varied from 3 s to 37 s among the participants, with an average of 12.8 s.

Several studies have reported measurements of useful quantitative data regarding TE speech. To conclude this section, these data are presented below in the form of tables for ease of reference.

Table 1 shows flow rates measured by different studies. The table indicates the number of participants in the study (column labeled N), the number of repetitions each subject performed (Reps.), the vowel that was sustained during measurement (Vowel), the level of effort with which the participant was instructed to vocalize (Effort), the range among the group of participants (Min. and Max.), as well as the overall mean. In the studies where more than one repetition was used for each subject, the mean value is indicated along with the standard deviation.

Table 1 – Measured flow rates in TE speech.

Reference	N	Reps.[a]	Vowel[b]	Effort[c]	Min. [ml/s]	Max. [ml/s]	Mean [ml/s]
Moon and Weinberg (1987)	5	5	/ɑ/	Small	35.27 6.30[d]	210.40 19.49	128.89
				Comfortable	74.01 10.69	336.15 22.94	170.00
				Large	235.66 35.78	577.40 43.59	367.78
Motta, Galli, and Di Rienzo (2001)	6	—	/e/	—	78	240	138 60
Schutte and Nieboer (2002)	18	—	[a] e [i]	Overall	20	800	131 112
Grolman et al. (2007)	8	3	/a/	Minimum	—	—	133 55
				Comfortable	—	—	167 72
				Maximum	—	—	267 122
Kotby et al. (2009)	18	3	/ɑ/	—	34	74	53 11
Ng (2011)	12	5	/i/, /a/, /ɔ/, e /u/	—	87.0 9.3	219.6 37.0	134.2

(a) Number of repetitions used for each participant.
(b) Vowel which the participant was instructed to vocalize.
(c) Effort level the participant was instructed to use.
(d) Standard deviation. In some of the works, however, the standard deviation of the mean was reported.

Table 2 shows pressures measured in the trachea during TE phonation. The columns are similar to those in Table 1.

Table 2 – Pressures measured in the trachea during TE speech.

Reference	N	Reps.[a]	Vowel[b]	Effort[c]	Min. [kPa]	Max. [kPa]	Mean [kPa]
Moon and Weinberg (1987)	5	5	/ɑ/	Small	1.71 0.057[d]	3.08 0.243	2.11
				Comfortable	1.77 0.259	4.81 0.218	2.95
				Large	4.33 0.525	8.27 0.685	6.04
Schutte and Nieboer (2002)	18	—	[a] e [i]	Geral	3.00	17.5	9.9 3.4
Grolman et al. (2007)	8	3	/a/	Minimum	—	—	2.65 0.637
				Comfortable	—	—	3.24 0.863
				Maximum	—	—	6.57 0.716

(a) Number of repetitions used for each participant.
(b) Vowel which the participant was instructed to vocalize.
(c) Effort level the participant was instructed to use.
(d) Standard deviation. In some of the works, however, the standard deviation of the mean was reported.

Table 3 presents pressures measured in the esophagus during TE phonation. Besides the columns that were also present in the two tables above, an additional column labeled "Group" is used to indicate a subgroup within the participants of the given study. Also, the column "Sensor position", as the name implies, indicates the vertical position of the sensor along the conduit pharynx-PES-esophagus.

Table 3 – Pressures measured in the esophagus during TE speech (or attempt at speech).

Reference	N	Reps.[a]	Vowel[b]	Group	Sensor position	Effort[c]	Min. [kPa]	Max. [kPa]	Mean [kPa]
Deshmane et al. (1995)	4	—	Phrases	Speakers	At the PES	Comfortable	2.3	2.9	2.5
Schutte and Nieboer (2002)	18	—	[a] e [i]	—	23–25 cm from the nostrils	Overall	1.00	10.8	4.5 2.4
Grolman et al. (2007)	8	3	/a/	—	Level of prosthesis	Minimum	—	—	1.77 0.765
						Comfortable	—	—	2.16 0.932
						Maximum	—	—	5.10 2.06
Aguiar-Ricz et al. (2010)	25	—	"ah"	Speakers	2 cm below the PES	Comfortable	—	—	5.57 2.95
					12 cm below the PES		—	—	6.56 2.75
					17 cm below the PES		—	—	8.28 3.43
				Non speakers	2 cm below the PES	Comfortable	—	—	4.91 4.00
					12 cm below the PES		—	—	4.19 2.28
					17 cm below the PES		—	—	3.71 1.64
Takeshita et al. (2012)	19	2	/a/	Low proficiency	At the PES	Comfortable	3.25	9.17	5.39
				Medium proficiency			1.33	12.0	4.85
				Good proficiency			1.51	5.96	3.40
Arenaz Búa et al. (2017)	14	—	/ae/ ou /e/	Low proficiency	3 cm above the PES	Comfortable	—	—	0.933 0.267
					At the PES		—	—	5.20 2.00
					3 cm below the PES		—	—	7.73 4.13
					7 cm above LES[e]		—	—	9.07 3.20
				Med./good prof.	3 cm abote the PES do SFE	Comfortable	—	—	2.93 1.47
					At the PES		—	—	5.20 2.40
					3 cm below the PES		—	—	5.20 2.67
					7 cm above the LES		—	—	7.20 2.40

(a) Number of repetitions used for each participant.
(b) Vowel which the participant was instructed to vocalize.
(c) Effort level the participant was instructed to use.
(d) Standard deviation. In some of the works, however, the standard deviation of the mean was reported.
(e) Lower esophageal sphincter.

Table 4 presents published values of fundamental frequency of phonation for TE speech.

Table 4 – Measured fundamental frequencies of phonation for TE speech.

Reference	N	Reps.[a]	Vowel[b]	Effort[c]	Min. [Hz]	Max. [Hz]	Mean [Hz]
Robbins et al. (1984)	15	3	/a/	—	—	—	101.7 54.6[d]
Moon and Weinberg (1987)	5	5	/ɑ/	Small	19.27 1.41	88.32 9.47	51.88
				Comfortable	33.13 1.63	121.12 7.30	72.73
				Large	49.86 3.57	153.92 11.94	102.82
Debruyne et al. (1994)	12	—	"a"	Comfortable	50	110	—
van As, Hilgers, et al. (1998)	21	—	/a/	Comfortable	—	—	115.21 35.43
van As-Brooks et al. (2006)	30	3	/a/	Comfortable	46	229	103 43
Lundström et al. (2008)	5	—	One syllable words	—	86 34	136 46	111 23
Zhang, Cook, et al. (2019)	12	3	/a/	—	145.1	269.8	213.9 44.8

(a) Number of repetitions used for each participant.
(b) Vowel which the participant was instructed to vocalize.
(c) Effort level the participant was instructed to use.
(d) Standard deviation. In some of the works, however, the standard deviation of the mean was reported.

Table 5 presents different measures of the PES resting tone, obtained by esophageal manometry. Columns in this table follow a similar organization as that of previous tables. Additionally, a column indicating whether the study considered esophageal, or TE speakers was included, as was a column which indicated whether some type of average of the spatial distribution of pressure was reported, or whether the peak of the distribution was reported.

Table 5 – Intraluminal pressures in the closed PES.

Reference	N	Reps.[a]	Voice	Value[b]	Group	Min. [kPa]	Max. [kPa]	Mean [kPa]
Winans, Reichbach, and Waldrop (1974)	20	—	E[d]	Average	Low proficiency	≈ 0.93	≈ 6.30	3.95 0.83[c]
					Good proficiency	≈ 0.79	≈ 2.41	1.75 0.183
					Overall	≈ 0.79	≈ 6.30	3.95 0.83
Welch, Gates, et al. (1979)	19	6	E	Peak	Non speakers	2.0 0.27	21.1 1.5	8.1 2.4
					Speakers	3.6 0.27	17.3 2.4	9.3 1.3
					Overall	2.0 0.27	21.1 1.5	8.73
Morgan et al. (1992)	18	—	E	Average	Hypotonic	1.3	1.9	1.51
					Tonic	2.0	2.7	2.44
					Hypertonic	4.7	6.7	6.0
					Spasm	8.0	11	8.83
					Myotomy (before)	6.9	9.3	8.0
					Overall	1.3	11	5.4
Dantas, Aguiar-Ricz, et al. (2002)	25	—	E	Peak	Non speakers	≈ 1.9	≈ 9.5	4.68 3.31
					Speakers	≈ 1.3	≈ 7.4	2.93 1.91
					Overall	≈ 1.3	≈ 9.5	3.81
Chone, Seixas, et al. (2009)	8	—	TE[e]	—	Pre-myotomy	2.20	4.47	3.38
					Post-myotomy	1.63	2.61	1.91
Takeshita et al. (2012)	20	—	TE	—	Low proficiency	0.227	0.880	0.592 0.317
					Medium proficiency	0.44	4.44	2.34 1.21
					Good proficiency	0.707	2.83	1.75 1.53
					Overall	0.227	2.83	1.84 1.29
Arenaz Búa et al. (2017)	14	—	TE	—	Low proficiency	—	—	2.13 1.47
					Med./good prof.	—	—	2.27 1.20
					Overall	—	—	2.27 1.20

(a) Number of repetitions used for each participant.
(b) Which value of the distribution was reported (peak or average).
(c) Standard deviation. In some of the works, however, the standard deviation of the mean was reported.
(d) Esophageal voice.
(e) Tracheoesophageal voice.

2.7 The effect of the tonicity of the PES on tracheoesophageal speech

In Section 1.3, it was indicated that the most commonly cited reason for a laryngectomee not to be able to produce the TE voice was the tonicity of the PES, with hypertonicity being the most common cause (HOFFMAN; MCCULLOCH, 1998). The case of spasm, an involuntary contraction possibly caused by a reflex activated by the airflow, is also a common inhibitor of the TE voice (KNOTT, 2019). Extreme cases of hypotoniciy may also inhibit PES oscillation (MCIVOR et al., 1990).

Several methods have been proposed to address the issue of hypertonicity and spasm. An earlier method that has been proposed was to simply not close the layer of muscle over the mucosa during total laryngectomy (that is, the procedure shown in Figure 37b is not done). While there are advocates to this procedure (TUCKER, 1990), there are also authors that argue against it. Simpson, Smith, and Gordon (1972) assessed how different PES closure techniques during total laryngectomy affected esophageal speech. In their study, the technique where the layer of muscle was not closed led to the worst success rate. More interestingly, Terrell, Lewin, and Esclamado (1995) report a case of a patient in which the layer of muscle was not closed and even still the patient was unable to produce the TE voice due to spasm. This observation, along with reports of fistula formation, has led Hamaker and Cheesman (1998) to stop recommending the method.

The observation that even without closing the layer of muscle the PES is able to contract to the point of precluding phonation merits a digression. The inferior pharyngeal constrictor and the cricopharyngeus are originally connected to the thyroid and cricoid cartilages. Considering the description given by Hixon, Weismer, and Hoit (2020) that these muscles tend to project the posterior wall forward, and the sidewalls forward and inward upon contraction, one would imagine that the cartilages would be used as anchors, and as the muscle contracts, the posterior wall is pulled against the cartilage. However, since even without attaching the sides of these muscles to any structure there might still be a considerable contraction of the PES, one is led to conclude that the posterior wall may project forward without the presence of any anchoring structure. To the best of the author's knowledge, there is no study detailing the mechanics of the contraction of the inferior pharyngeal constrictor and cricopharyngeus.

A second method to address hypertonicity is that of myotomy of the constrictor muscles, in which an incision is made in the muscle layer, from the base of the tongue to the entrance of the esophagus. The incision is made down to the submucosal level. Myotomy of the musculature of the PES is a well established procedure to address hypertonicity of the PES, with positive results (HOFFMAN; MCCULLOCH, 1998). It may be performed during a total laryngectomy or afterwards, as a separate procedure (HAMAKER; CHEESMAN, 1998; HOLSINGER; BHAYANI, 2011).

Some authors express concerns regarding PES myotomy. Laccourreye and Shaha in Holsinger and Bhayani (2011) argue against performing myotomy during the laryngectomy, due to an increased risk of devascularization at the level of the suture line, risk of damaging mucosa of the PES, and little improvement in the resulting voice (in Laccourreye's experience). Hoffman and McCulloch (1998) mention the potential risk of pharyngocutaneous fistula, which happens at a rate of 10–20% when myotomy is done separately, after a total laryngectomy[20] (HAMAKER; CHEESMAN, 1998).

A third method consists of a neurectomy, or a cut of the pharyngeal plexus, which denervates the musculature of the PES. Hoffman and McCulloch (1998) indicate that while the procedure appears to be effective, and with a lower risk of fistula formation than myotomy, it has never become widely disseminated.

Chemical denervation by means of botulinum injections has also been used to treat hypertonicity of the PES (TERRELL; LEWIN; ESCLAMADO, 1995; HOFFMAN; MCCULLOCH, 1998; CHONE; GRIPP, et al., 2005). Hoffman and McCulloch (1998) state that the method constitutes a nonsurgical option that is safe, effective, and with

[20] Based on unpublished data.

lower morbidity than the surgical options. They also indicate that the number of injections required varies, with some laryngectomees requiring only one injection while others need repeated injections.

Mechanical dilation of the PES by the use of a balloon, which is a technique most commonly used to address stricture (HARRIS; GRUNDY; ODUTOYE, 2010), has also been used to treat hypertonicity (HOFFMAN; MCCULLOCH, 1998).

To address hypotonicity, the laryngectomee may press a hand against the neck, or use a device, such as a tightening collar (MAHIEU, 1988). It is interesting to remark that Knott (2019) indicates that it is possible for a laryngectomee who is able to produce the TE voice, but has a weak or "breathy" voice due to hypotonicity, may naturally experience some improvement over time. Knott (2019) speculates this would occur due to increased tone and strength of the PES musculature in an analogous manner to physical exercise[21].

The effect of tonicity on TE speech does not limit itself to pathological cases. Indeed, tonicity varies in a spectrum from extreme hypotonicity to extreme hypertonicity. One effect of tonicity on TE speech has already been discussed in Section 2.6—the different shapes of the PES observed during TE phonation. A second effect would be its influence over the quality of the voice produced.

Different authors have attempted to assess how tonicity affects the quality of alaryngeal speech. This has been done using esophageal manometry data to measure the resting tone of the PES, which gives an indication of the amount of muscle contraction for the PES at rest. This is not a perfect measure of tonicity, since the increase in EMG activity during phonation suggests an increase in muscle contraction above the resting tone. The use of esophageal manometry during phonation, on the other hand, fails to provide an indication of muscle contraction, since the segment is opening and closing. The question of how to quantify the amount of muscle contraction during phonation is far from trivial, and at the moment esophageal manometry data for the PES at rest seems to be the best data that is available.

Winans, Reichbach, and Waldrop (1974) conducted a study with 20 esophageal speakers. They separated the subjects into two groups: one of "good" esophageal speakers, and other with "poor" esophageal speakers. Then they compared esophageal manometry data between the two groups. They observed that, at the cricopharyngeus, the good esophageal speakers presented a smaller intraluminal pressure when compared to the poor esophageal speakers (1.75 kPa and 3.95 kPa, respectively).

The result of Winans, Reichbach, and Waldrop (1974) was not replicated by Welch, Gates, et al. (1979), who conducted an esophageal manometry study with 19 laryngectomees. They separated the subjects between those who acquired esophageal speech, and those who did not. They observed no statistically significant difference between peak in-

[21] This again raises the question regarding voluntary control of the musculature of the PES. It is out of the scope of the present thesis whether it would be possible to increase the tone and strengthen the PES musculature by involuntary contractions.

traluminal pressure of the two groups. It is worth mentioning that esophageal speech does require greater ability than TE speech, therefore it is not clear whether all subjects who did not acquire esophageal speech actually suffered from excessive, or reduced, tonicity of the PES, as opposed to not having developed the proper technique.

In the study of Morgan et al. (1992), esophageal manometry measurements were made after surgery in 12 laryngectomees. The laryngectomees then underwent at least two months of speech therapy for the acquisition of the esophageal voice. They noted that laryngectomees with an intraluminal pressure above 2.67 kPa were those who failed to develop esophageal speech.

Dantas, Aguiar-Ricz, et al. (2002) compared intraluminal pressures of laryngectomees who did acquire esophageal speech, and those who did not. They observed smaller pressures in the group that acquired esophageal speech, though statistical significance was not achieved ($p = 0.146$).

Takeshita et al. (2012) classified 20 TE speakers as good, moderate, or poor speakers. They then performed esophageal manometry measurements on the subjects. It was observed that the poor speakers had the lowest measured PES resting tone, the moderate speakers had the largest, and the good speakers an intermediary resting tones. The results varied greatly between subjects in each group, with some amount of overlap between the values of the different groups (see Table 5). It can be speculated that in this study, the group of poor speakers was composed mainly of participants with a hypotonic PES. The group of moderate speakers, on the other hand, may have been composed, for the most part, of subjects with some degree of hypertonicity; however, at least one subject (see the minimum for that group in Table 5, in comparison to the group of poor speakers) is likely to suffer from hypotonicity of the PES. The subjects in the group of good speakers likely had neither hypotonicity nor hypertonicity.

Arenaz Búa et al. (2017) also performed esophageal manometry measurements of the resting tone of the PES. They present the results classifying the TE speakers as good/moderate speakers (11 participants) or poor speakers (3 participants). The measured results were essentially the same for the two groups.

Other studies have looked upon the effect of PES tonicity on TE speech without actually quantifying tonicity. van Weissenbruch et al. (2000) used cineradiographic images of the PES during phonation to classify the PES of alaryngeal speakers (both esophageal and tracheoesophageal speakers) as normal, hypertonic, hypotonic, spasm, and stricture. They observed that hypertonicity, spasm, strictures, and hypotonicity correlated significantly with poor and moderate alaryngeal speech.

A similar approach was adopted by van As, Op de Coul, et al. (2001), with the difference that only TE speakers were considered, and that the groups consisted of: hypotonic, normotonic, hypertonic, spasm, and stricture. They observed that a good TE voice was associated either with a normotonic or hypertonic PES, and that no subject with

PES hypotonicity was classified as a good speaker. Indeed, participants with hypotonicity comprised the majority of the group of poor speakers (6 out of 10), and reasonable speakers (8 out 14). Participants with hypertonicity were classified in the group of poor speakers in the same rate as those with a normotonic PES (2 out of 10 in each case). In the group of good speakers, the majority was composed of subjects with a normotonic PES (9 out 13), while the rest was of subjects classified with a hypertonic PES.

2.8 The mechanics of tracheoesophageal speech

Unlike the literature on the mechanics of laryngeal speech, which is fairly large, there are not many papers studying the mechanics of TE speech. To the best of the author's knowledge, there are only two previous mathematical models of the PES in TE phonation. The first model is a lumped parameter model that has been used in different works of a research group at the University of Erlangen-Nuremberg. The second is a finite element model described in the proceedings of a conference by Zhang, Bai, et al. (2016).

The lumped parameter model was first described by Lohscheller et al. (2003), and was further developed by Schwarz (2007), Schwarz et al. (2011), and Hüttner et al. (2015). The model consists of two axially aligned rings of masses, one above the other, with the masses being distributed along the perimeter of each ring. The number of masses in each ring varies in the different works. Lohscheller et al. (2003) and Hüttner et al. (2015) use eight masses in each ring, while Schwarz (2007) and Schwarz et al. (2011) use six. The masses are connected to adjacent masses in the same ring, as well as to the corresponding mass in the other ring, by springs and dampers. Each mass is also connected to an anchoring point by a spring and a damper. The movement of each mass is restricted to the plane of the ring to which it belongs, and all the springs and dampers are considered linear (Hüttner et al. (2015) use time dependent parameters).

A collision force is added when one of the masses crosses the perimeter of the polygon formed by the masses. This force was considered as an additional spring-loaded by the distance in which the mass had penetrated the perimeter. The model allows for the area of the rings to be zero and even negative. In these cases, the pressure in the ring of masses is made zero. To preclude a nonphysical rotation of the rings, almost like a rigid-body, additional springs were added to restrict circumferential motion of the masses.

The flow is modeled as inviscid, incompressible, irrotational, and quasi-steady, so that the flow is described by the Bernoulli equation. Flow separation is considered to occur in the minimum area, without any pressure recovery. The subglottal pressure is considered to be constant, and the flow is discharged at atmospheric pressure. Vocal tract coupling is not considered, and the flow forces are considered to act only on the lower ring of masses.

The main idea for this model is to use endoscopic images of the PES along with an optimization procedure to determine the parameters of the model, so that the movement of the upper rings of masses matches the movement of the walls of the PES. Good agreement between the images and the model is obtained for the upper ring of masses; however, as the authors state, only the upper ring of masses is matched to the images, and the motion of the lower ring is left unaddressed (SCHWARZ et al., 2011; HÜTTNER et al., 2015).

Most of the model has been developed by analogy with vocal folds models (for example, the two rings of masses are analogous to the two-mass model of the vocal folds), and many details on the physiology of TE speech have not been taken into account. While a set of parameters that makes the upper ring of masses replicate the movement of the upper constriction can be obtained, making inferences on the mechanics of the PES in terms of these parameters is complicated, since they do not possess a direct physiological interpretation.

The second model, described by Zhang, Bai, et al. (2016), was developed using a commercial finite element package. An axisymmetric tube with varying cross-section (the diameter was smoothly reduced towards the center of the tube) was used to model the PES. The walls of the tube were considered to be made of a linear elastic material, and the lumen was filled with air. No mean flow was considered, only a harmonically varying pressure at the inlet and a zero pressure on the outlet. Therefore, the main physical mechanism by which PES oscillations take place seems to have been misinterpreted.

Other two published works deal with the mechanics of TE speech, the two focused on the flow downstream from the prosthesis. Erath and Hemsing (2016) performed an experiment in which two parallel rigid tubes (one representing the trachea, the other the esophagus) were connected by a small tube representing the prosthesis. On the tube representing the trachea, one side corresponded to the inlet while the other was closed, representing the closed tracheostoma. On the tube representing the esophagus, one extremity was closed while on the other a mechanism was used to periodically change the area of the outlet, in order to represent PES oscillations. Water was used as a working fluid (the experiment was scaled so that the Reynolds, Strouhal, and Euler numbers were similar to those found in TE speech), and Particle image velocimetry (PIV) measurements were made to study flow structures at the entrance of the esophagus.

Santos et al. (2021) also studied the flow downstream from the prosthesis. Steady-state numerical simulations were made using the finite volume method. An approximate geometry of the trachea, prosthesis, and PES was constructed, and the effect of the position and angle of the prosthesis was studied in terms of the flow field through the PES constriction, as well as the pressure distribution on the walls of the PES.

2.9 Collapsible tubes

In the previous sections it was seen that after a total laryngectomy the PES is, in simplified terms, a tube of mucosa surrounded by a layer of muscle. Furthermore, contraction of the muscles tends to close the tube. This description bears an obvious resemblance to that of a collapsible tube.

A collapsible tube is a flexible tube that carries moving fluid and is subjected to an external pressure. Figure 47 illustrates schematically a collapsible tube. In the figure, the extremities of the flexible tube are connected to rigid tubes, and the flexible tube is inside a pressurized chamber. This particular case is often referred to as a Starling resistor.

Figure 47 – Schematic representation of a collapsible tube.

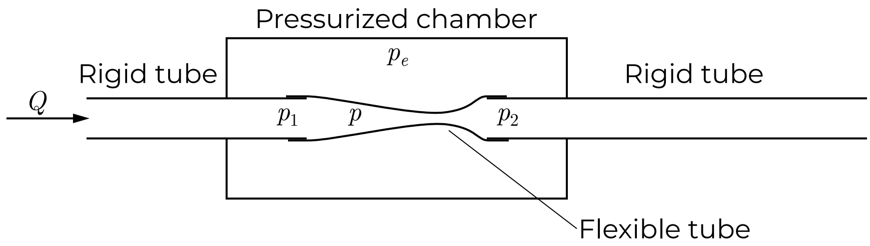

Source – Author.

Collapsible tubes have been an area of interest due to their rich dynamics, and their use in modeling many biological fluid flow phenomena, such as the flow of blood in veins and arteries (SHAPIRO, 1977; FUNG, 1997; GROTBERG; JENSEN, 2004), the flow of air in the respiratory system (BERTRAM, 2008), and even laryngeal phonation (BERKE et al., 1991)[22].

While the Starting resistor was first described over a century ago (KNOWLTON; STARLING, 1912), the interest in the physics of collapsible tubes arose much later (RODBARD; SAIKI, 1953; HOLT, 1941, 1959), when observations of flow limitation (the flow in the flexible tube becomes independent of the pressure difference $p_1 - p_2$) and self-sustained oscillations were noted.

The earliest models for the flow in collapsible tubes consisted of lumped parameter models (CONRAD, 1969; KATZ; CHEN; MORENO, 1969). Not long afterwards, models that sought a continuous formulation for the problem were also proposed. One notable example is that of Shapiro (1977), who shows the analogy between one-dimensional collapsible tube flow, with one-dimensional compressible fluid flow, and one-dimensional free surface flow. For the problem of one-dimensional compressible fluid flow, it is well know that the equation of state of the gas must be considered alongside the continuity equation and the momentum equation to close the problem. The same occurs for the one-dimensional collapsible tube flow, and a "tube law" is added to the problem, which relates $p - p_e$ with the area of the cross-section of the tube, A. The tube law was often obtained experimentally and approximate expressions were used.

At this moment it is worth pointing out that when an elastic tube is subjected to an external pressure larger than the internal (with or without fluid flow), it may buckle if this difference exceeds a given buckling pressure. The shape of the cross-section of the

[22] Collapsible tube models for laryngeal phonation have been met with criticism. See Titze (1988) and Lucero (1993).

tube when buckled may vary, and different modes are possible, as discussed by Flaherty, Keller, and Rubinow (1972). Figure 48 illustrates this. It shows two different buckling modes: $n = 2$, in Figure 48a and $n = 3$ in Figure 48b. In each case, the cross-section is shown for three different $p_e - p$.

Figure 48 – Cross-section of a tube for different $p_e - p$.

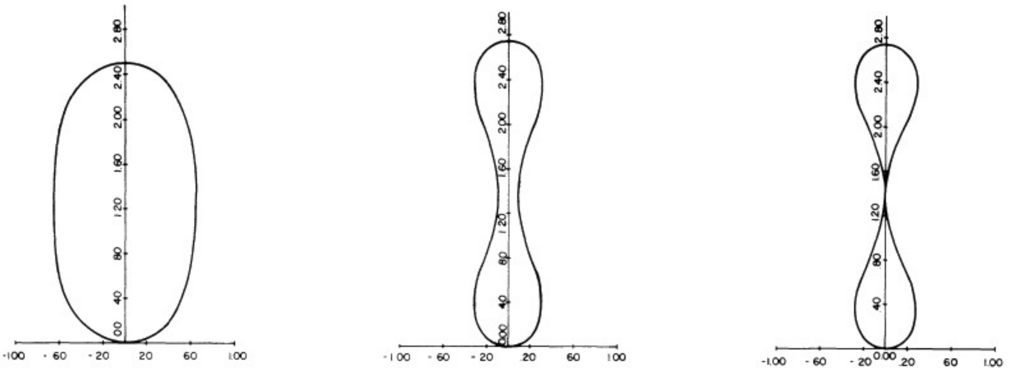

(a) Mode $n = 2$.

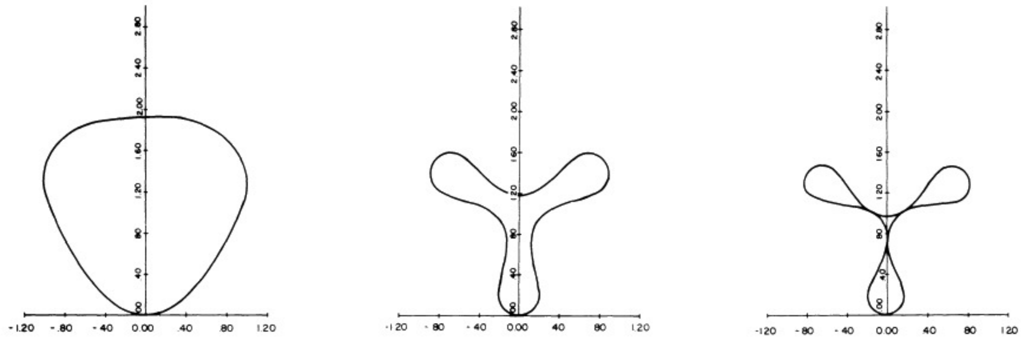

(b) Mode $n = 3$.

Source – Adapted from Flaherty, Keller, and Rubinow (1972).

Most of the works regarding collapsible tubes describe the cross-section closing as in mode $n = 2$ of Figure 48, but this is obviously not universal (see Whittlesey (2013) for instance). It is also interesting to note the analogy to the many shapes of the closed PES observed in endoscopic images (Section 2.6).

In regard to the one-dimensional collapsible tube models, McClurken et al. (1981) argued that the tube law had to include not only the transverse bending stiffness, but also the longitudinal bending stiffness and the axial stiffness. The influential model of Cancelli and Pedley (1985) proposed a tube law in which the axial tension of the membrane was considered, and they used a modified momentum equation to account for flow separation.

The use of *ad hoc* considerations (such as the tube law, or the modified momentum equation) is certainly a drawback of the earlier models. In order to gain insight into the physics of collapsible tubes without having to make use of these assumptions, many authors (LOWE; PEDLEY, 1995; LUO, X.; PEDLEY, T., 1995, 1996; JENSEN; HEIL, 2003; CAI; LUO, 2003; LUO et al., 2008) began studying the analogous problem of a collapsible channel, which corresponds to a two-dimensional channel of rigid walls, but with a flexible membrane replacing part of one of the walls (see Figure 49). This problem is in many ways analogous to that of a collapsible tube, but is far simpler in the sense that it can be addressed from basic principles in a more convenient manner than the full three-dimensional fluid-structure problem.

Other authors conducted studies actually attacking the full three-dimensional problem (SEONG et al., 2002; HAZEL; HEIL, 2003; MARZO; LUO; BERTRAM, 2005; HEIL; BOYLE, 2010). While computing power has grown enough to make this type of simulation viable, the computational time is still a large drawback when it is desired to consider a large number of parameter combinations.

Stewart, Waters, and Jensen (2009) proposed a procedure for the simplification of the two-dimensional problem of collapsible channel. The procedure consists in using dimensional considerations to simplify the governing equations (much like those used for obtaining the boundary layer equations), along with the von Kármán-Pohlhausen integral method. This process is detailed in Section 3. The problem is then reduced to a one-dimensional problem, with two coupled partial differential equations. This procedure has been further studied by Stewart, Heil, et al. (2010), Xu, Billingham, and Jensen (2013), Xu, Billingham, and Jensen (2014), and Stewart (2017). It was also used by Stewart and Foss (2019) in the study of retinal venous pulsations.

Besides mathematical models, several experimental studies have been conducted. The many works of Bertram and colleagues (BERTRAM, C., 1982, 1987; BERTRAM; RAYMOND; PEDLEY, 1990, 1991) are notable examples. In particular, it is worthwhile to mention that Bertram, Raymond, and Pedley (1991) constructed control space diagrams, in which the behavior of the system (low frequency oscillation, high frequency oscillation, irregular oscillations, etc.) was characterized for different combinations of parameters.

For the purposes of the present work, it is interesting to discuss how different authors have dealt with the effect of axial tension in collapsible tube experiments. The relevance of this lies in the likelihood of a longitudinal tension being present in the PES during TE phonation.

C.D. Bertram (1987) investigated how axial strain affected the pressure-area relationship (the tube law) in collapsible tubes. In order to change the axial strain, the distance between the rigid tubes was allowed to take different values, so that the tube could be stretched. Three different loads were applied, leading to three different axial strains. This same procedure was used by Bertram, Raymond, and Pedley (1990), although only one value of axial strain was considered.

This method had been previously adopted by Lyon et al. (1981); however, these authors have also attempted a different procedure. They kept the distance between the rigid tubes constant, and stretched tubes of different lengths before clamping their ends to the rigid tubes. For example, they consider a tube of 4.5 cm stretched to cover a distance of 7.5 cm between the ends of the rigid tubes, and compare the measurement to that of a tube of 7.5 cm. In the study of Xia et al. (2000) the distance between the rigid tubes was also changed, so that different initial axial strains could be considered.

Usually, in other works reviewed, the issue of how to determine the axial tension in the tube is not explored in detail, but a measure of the amount of axial load, or axial deformation is provided. For instance, Podoprosvetova et al. (2021) indicate that in their experiment the tube is stretched axially by 16%.

The brief review presented above does not begin to cover the extensive literature on collapsible tubes. The interested reader is referred to Heil and Jensen (2003), Bertram (2003), Bertram (2008), and Heil and Hazel (2011) for more comprehensive reviews on the subject.

3 Mathematical Model

This chapter describes the mathematical model, which is built upon the review of the anatomy and physiology of TE speech made in the previous chapter. While the following sections will describe the model and the procedure of analysis in detail, it is useful to discuss some points at the outset.

In Section 2.6 it was seen how the PES deforms to a given shape during phonation and roughly maintains this shape, with oscillations occurring around it. Since the shape of the PES during phonation varies considerably among different individuals (depending on the tonicity of the PES), it can not be imposed *a priori*. A PES model should be able to naturally adopt different shapes, depending on the prescribed tonicity.

This is a considerable difference from vocal folds models (Section 2.1), and raises the question of how much is lost by neglecting the part of the PES below the smallest constriction, as was done in the lumped parameter model of Schwarz et al. (2011). Indeed, this model is not ideal for the purposes of the present work, not only due to its limitation in representing the different PES shapes, but mainly due to its reliance on endoscopic images for the determination of the parameters.

Developing a new lumped parameter model, on the other hand, is not feasible at the moment, due to the difficulty in relating its parameters with published data on TE speech, which would require separate experiments to be conducted. On the other hand, more refined continuum-based models capturing the full fluid-structure interaction have the drawback of larger (perhaps prohibitively larger) computational time and resources. These points, as well as the notable resemblance between the PES and a collapsible tube, have led to the choice of modeling the PES as a collapsible channel.

Mathematically, the phenomenon of the oscillations around a roughly steady PES shape may be interpreted as an unstable steady-state solution enclosed by a limit cycle. While there exists a given steady shape for the PES to adopt as air flows through it (the steady-state solution), the equilibrium of this solution is unstable, and any perturbation leads the system to oscillations whose amplitude grows until the system has approached the limit cycle.

Since the focus of the present thesis lies in studying the effect of muscle contraction on TE phonation, it is desired to understand which combination of parameters of the model, specially those related to muscle contraction, allow for self-sustained oscillations to occur. In this sense, a natural approach for analysis is to find steady-state solutions of the model for different combinations of parameters, and characterize their stability. A straightforward procedure for this characterization is to solve the linearized equations of motion of the system around the steady-state solution. These linearized equations generally take the form of an eigenvalue problem. If all eigenvalues have negative real parts, the steady-state solution is stable, otherwise the system is unstable. Eigenvalues with nonzero imaginary part indicate an oscillatory behavior of the system for small perturbations around the steady-state solution.

With regard to the structure of the present chapter, Section 3.1 provides the governing equations of the model. In Section 3.2 the steady-state equation is shown, as are the linearized equations. The question of how the parameters of the model relate with physiological properties of TE speech is explored in Section 3.3. The method used for the discretization and solution of the relevant equations is detailed in Section 3.4. A critical discussion of the model is made in Section 3.5, and the results are presented in Section 3.6.

3.1 Governing equations

Collapsible channel flow corresponds to the flow in a channel of rigid walls, but with a flexible membrane replacing part of one of the walls (Figure 49). An external pressure p_e is applied to the membrane.

Figure 49 – Collapsible channel.

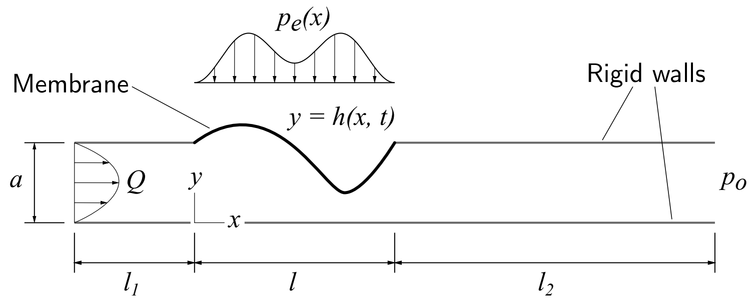

Source – Tourinho et al. (2021).

In the figure, the width of the channel is indicated by a, the length of the membrane by l, the length of the segment of rigid walls upstream of the membrane by l_1, and the one downstream by l_2. The origin of the coordinate system is located on the bottom wall, aligned with the left end of the membrane, as shown in the figure. Coordinates x (horizontal) and y (vertical) are defined with respect to this coordinate system, as is h, the vertical position of the membrane.

The membrane is considered to be thin, under constant tension τ, and to have mass per unit area m. The fluid is newtonian with density ρ and kinematic viscosity ν, both assumed to be constant.

On the inlet, a parabolic velocity profile is imposed, with a prescribed flow per unit breadth (out-of-plane direction) Q or, analogously, with an average velocity $U = Q/a$. On the outlet, the pressure is prescribed as p_o.

The problem is governed by the Navier-Stokes equations (Equations 1a–1c) and the membrane equation (Equation 1d).

$$\begin{cases} \dfrac{\partial u}{\partial x} + \dfrac{\partial v}{\partial y} = 0, & \text{(1a)} \\ \dfrac{\partial u}{\partial t} + u\dfrac{\partial u}{\partial x} + v\dfrac{\partial u}{\partial y} = -\dfrac{1}{\rho}\dfrac{\partial p}{\partial x} + \nu\left(\dfrac{\partial^2 u}{\partial x^2} + \dfrac{\partial^2 u}{\partial y^2}\right), & \text{(1b)} \\ \dfrac{\partial v}{\partial t} + u\dfrac{\partial v}{\partial x} + v\dfrac{\partial v}{\partial y} = -\dfrac{1}{\rho}\dfrac{\partial p}{\partial y} + \nu\left(\dfrac{\partial^2 v}{\partial x^2} + \dfrac{\partial^2 v}{\partial y^2}\right), & \text{(1c)} \\ m\dfrac{\partial^2 h}{\partial t^2} = \tau\kappa + p - p_e. & \text{(1d)} \end{cases}$$

In Equation (1), u and v are the velocity components in the horizontal and vertical directions respectively, p is the pressure in the fluid, and κ is the curvature of the membrane.

The method proposed by Stewart, Waters, and Jensen (2009) is then used to reduce the problem to a pair of coupled differential equations. This procedure is analogous to that used to obtain the boundary layer equations (KUNDU; COHEN, 2008), and will be detailed below in order to show the development of the equations when the inertia of the membrane is considered as well as an external pressure that changes arbitrarily along x. To briefly provide the context, Stewart, Waters, and Jensen (2009) neglect the inertia of the membrane and consider a linearly varying external pressure. Later, Stewart (2017) used a prescribed flux at the inlet, and considered a uniform external pressure on the membrane. Here, in comparison to the formulation of Stewart (2017), the inertia of the membrane is added, and an arbitrary $p_e(x)$ is considered.

First, the following dimensionless variables are defined:

$$\begin{gathered} \hat{x} = \frac{x}{l}, \quad \hat{y} = \frac{y}{a}, \quad \hat{u} = \frac{u}{U}, \quad \hat{v} = \frac{v}{v_c} \\ \hat{p} = \frac{p - p_o}{p_c}, \quad P_e = \frac{p_e - p_o}{p_c}, \quad \hat{h} = \frac{h}{a}, \quad \hat{t} = \frac{t}{t_c}, \end{gathered} \tag{2}$$

where v_c, p_c, and t_c are characteristic values for the vertical component of velocity, pressure, and time respectively.

Substituting the dimensionless variables in the continuity equation (Equation 1a) one obtains

$$\frac{U}{l}\frac{\partial \hat{u}}{\partial \hat{x}} + \frac{v_c}{a}\frac{\partial \hat{v}}{\partial \hat{y}} = 0. \tag{3}$$

For both terms to be of the same order of magnitude,

$$v_c = \frac{Ua}{l}. \tag{4}$$

After substitution of the dimensionless variables, and some rearranging, Equations (1) may be written as Equations (5),

$$\begin{cases} \dfrac{\partial \hat{u}}{\partial \hat{x}} + \dfrac{\partial \hat{v}}{\partial \hat{y}} = 0, & \text{(5a)} \\ \dfrac{l}{t_c U}\dfrac{\partial \hat{u}}{\partial \hat{t}} + \hat{u}\dfrac{\partial \hat{u}}{\partial \hat{x}} + \hat{v}\dfrac{\partial \hat{u}}{\partial \hat{y}} = -\dfrac{p_c}{\rho U^2}\dfrac{\partial \hat{p}}{\partial \hat{x}} + \dfrac{\nu l}{U}\left(\dfrac{1}{l^2}\dfrac{\partial^2 \hat{u}}{\partial \hat{x}^2} + \dfrac{1}{a^2}\dfrac{\partial^2 \hat{u}}{\partial \hat{y}^2}\right), & \text{(5b)} \\ \dfrac{l}{t_c U}\dfrac{\partial \hat{v}}{\partial \hat{t}} + \hat{u}\dfrac{\partial \hat{v}}{\partial \hat{x}} + \hat{v}\dfrac{\partial \hat{v}}{\partial \hat{y}} = -\dfrac{p_c l^2}{\rho U^2 a^2}\dfrac{\partial \hat{p}}{\partial \hat{y}} + \dfrac{\nu l}{U}\left(\dfrac{1}{l^2}\dfrac{\partial^2 \hat{v}}{\partial \hat{x}^2} + \dfrac{1}{a^2}\dfrac{\partial^2 \hat{v}}{\partial \hat{y}^2}\right), & \text{(5c)} \\ \dfrac{ma}{p_c t_c^2}\dfrac{\partial^2 \hat{h}}{\partial \hat{t}^2} = \dfrac{\tau a}{p_c l^2}\dfrac{\partial^2 \hat{h}/\partial \hat{x}^2}{[1+(a/l)^2(\partial \hat{h}/\partial \hat{x})^2]^{3/2}} + \hat{p} - P_e. & \text{(5d)} \end{cases}$$

In Equation (5d) we have imposed that the material points along the membrane are constrained to move in the vertical direction only, leading to the well-known formula for the curvature of a single spatial variable function.

Defining

$$t_c = \frac{l}{U}, \quad p_c = \rho U^2, \tag{6}$$

Equation (5) becomes:

$$\begin{cases} \dfrac{\partial \hat{u}}{\partial \hat{x}} + \dfrac{\partial \hat{v}}{\partial \hat{y}} = 0, & \text{(7a)} \\ \dfrac{\partial \hat{u}}{\partial \hat{t}} + \hat{u}\dfrac{\partial \hat{u}}{\partial \hat{x}} + \hat{v}\dfrac{\partial \hat{u}}{\partial \hat{y}} = -\dfrac{\partial \hat{p}}{\partial \hat{x}} + \dfrac{\nu l}{Ua^2}\left(\dfrac{a^2}{l^2}\dfrac{\partial^2 \hat{u}}{\partial \hat{x}^2} + \dfrac{\partial^2 \hat{u}}{\partial \hat{y}^2}\right), & \text{(7b)} \\ \dfrac{\partial \hat{v}}{\partial \hat{t}} + \hat{u}\dfrac{\partial \hat{v}}{\partial \hat{x}} + \hat{v}\dfrac{\partial \hat{v}}{\partial \hat{y}} = -\dfrac{l^2}{a^2}\dfrac{\partial \hat{p}}{\partial \hat{y}} + \dfrac{\nu l}{Ua^2}\left(\dfrac{a^2}{l^2}\dfrac{\partial^2 \hat{v}}{\partial \hat{x}^2} + \dfrac{\partial^2 \hat{v}}{\partial \hat{y}^2}\right), & \text{(7c)} \\ \dfrac{ma}{\rho l^2}\dfrac{\partial^2 \hat{h}}{\partial \hat{t}^2} = \dfrac{\tau a}{\rho U^2 l^2}\dfrac{\partial^2 \hat{h}/\partial \hat{x}^2}{[1+(a/l)^2(\partial \hat{h}/\partial \hat{x})^2]^{3/2}} + \hat{p} - P_e. & \text{(7d)} \end{cases}$$

The following dimensionless parameters are then defined. The relationship of these parameters with physiological values, as well as their physical interpretation, is given in Section 3.3.

$$M = \frac{ma}{\rho l^2}, \quad R = \frac{Ua}{\nu}\left(\frac{a}{l}\right), \quad T = \frac{a\tau}{\rho U^2 l^2}, \quad L_1 = \frac{l_1}{l}, \quad L_2 = \frac{l_2}{l}. \tag{8}$$

Substituting the parameters of Equation (8) in Equation (7), and dropping terms of second order in the ratio a/l, the following system of partial differential equations is obtained:

$$\begin{cases} \dfrac{\partial \hat{u}}{\partial \hat{x}} + \dfrac{\partial \hat{v}}{\partial \hat{y}} = 0, & \text{(9a)} \\ \dfrac{\partial \hat{u}}{\partial \hat{t}} + \hat{u}\dfrac{\partial \hat{u}}{\partial \hat{x}} + \hat{v}\dfrac{\partial \hat{u}}{\partial \hat{y}} = -\dfrac{\partial \hat{p}}{\partial \hat{x}} + \dfrac{1}{R}\dfrac{\partial^2 \hat{u}}{\partial \hat{y}^2}, & \text{(9b)} \\ \dfrac{\partial \hat{p}}{\partial \hat{y}} = 0, & \text{(9c)} \\ M\dfrac{\partial^2 \hat{h}}{\partial \hat{t}^2} = T\dfrac{\partial^2 \hat{h}}{\partial \hat{x}^2} + \hat{p} - P_e. & \text{(9d)} \end{cases}$$

The similarity with the boundary layer equations is evident in Equations (9a)–(9c). We note that the vertical component of the momentum equation (Equation 9c) merely indicates that the pressure is not a function of $\hat{y}$, and does not need to be considered any further. Also, hats will be dropped from now on and every term should be understood to be in its dimensionless form, unless stated otherwise.

Following Stewart, Waters, and Jensen (2009), the von Kármán-Pohlhausen method is used to further simplify the set of equations. Equations (9a) and (9b) are integrated in y, from the bottom wall to the membrane. By defining the dimensionless flux per unit breadth,

$$q = \int_0^h u\,dy, \tag{10}$$

the set of equations becomes Equation (11).

$$\begin{cases} \dfrac{\partial q}{\partial x} + v|_{y=h} - v|_{y=0} = 0, & \text{(11a)} \\ \dfrac{\partial q}{\partial t} + \displaystyle\int_0^h \left(u\frac{\partial u}{\partial x} + v\frac{\partial u}{\partial y} \right) dy = -h\frac{\partial p}{\partial x} + \frac{1}{R}\left(\left.\frac{\partial u}{\partial y}\right|_{y=h} - \left.\frac{\partial u}{\partial y}\right|_{y=0} \right), & \text{(11b)} \\ M\dfrac{\partial^2 h}{\partial t^2} = T\dfrac{\partial^2 h}{\partial x^2} + p - P_e. & \text{(11c)} \end{cases}$$

The integral on the left-hand side of Equation (11b) can be written as

$$\int_0^h \left(u\frac{\partial u}{\partial x} + v\frac{\partial u}{\partial y} \right) dy = \int_0^h u\frac{\partial u}{\partial x}\,dy + [uv]_0^h - \int_0^h u\frac{\partial v}{\partial y}\,dy. \tag{12}$$

At $y = 0$, u and v are zero. Since we restricted the membrane to move in the vertical direction only, at $y = h$, u will be zero as well. Also, by the continuity equation (Equation 9a), $\partial v/\partial y = -\partial u/\partial x$. Therefore the integral on the left-hand side of Equation (11b) further simplifies to

$$\int_0^h \left(u\frac{\partial u}{\partial x} + v\frac{\partial u}{\partial y} \right) dy = 2\int_0^h u\frac{\partial u}{\partial x}\,dy = \int_0^h \frac{\partial u^2}{\partial x}\,dy. \tag{13}$$

Using Leibniz integral rule, the last integral above may be written as

$$\int_0^h \frac{\partial u^2}{\partial x}\,dy = \frac{\partial}{\partial x}\int_0^h u^2\,dy - u^2(x, h, t)\frac{\partial h}{\partial x}. \tag{14}$$

Finally, since $u = 0$ at $y = h$ the last term in the right-hand side of Equation (14) is zero. Therefore,

$$\int_0^h \left(u\frac{\partial u}{\partial x} + v\frac{\partial u}{\partial y} \right) dy = \frac{\partial}{\partial x}\int_0^h u^2\,dy. \tag{15}$$

Using Equation (15), noting that v is zero at $y = 0$ ($v|_{y=0} = 0$), and that at $y = h$, v must be equal to the membrane velocity ($v|_{y=h} = \partial h/\partial t$), the system of partial differential equations in Equation (11), simplifies to

$$\begin{cases} \dfrac{\partial q}{\partial x} + \dfrac{\partial h}{\partial t} = 0, & \text{(16a)} \\ \dfrac{\partial q}{\partial t} + \dfrac{\partial}{\partial x}\displaystyle\int_0^h u^2\, dy = -h\dfrac{\partial p}{\partial x} + \dfrac{1}{R}\left(\dfrac{\partial u}{\partial y}\bigg|_{y=h} - \dfrac{\partial u}{\partial y}\bigg|_{y=0}\right), & \text{(16b)} \\ M\dfrac{\partial^2 h}{\partial t^2} = T\dfrac{\partial^2 h}{\partial x^2} + p - P_e. & \text{(16c)} \end{cases}$$

Following the von Kármán-Pohlhausen method, we impose a polynomial velocity profile on u. In particular, a parabolic flow profile is used,

$$u(y,t) = a_0(t) + a_1(t)y + a_2(t)y^2. \tag{17}$$

Using the conditions $u(0,t) = u(h,t) = 0$, and the definition of q (Equation 10), it is straightforward to show that

$$u = \frac{6qy}{h^3}(h-y). \tag{18}$$

This expression may be substituted in Equation (16). After working out the integral and the derivatives one obtains,

$$\begin{cases} \dfrac{\partial q}{\partial x} + \dfrac{\partial h}{\partial t} = 0, & \text{(19a)} \\ \dfrac{\partial q}{\partial t} + \dfrac{\partial}{\partial x}\left(\dfrac{6q^2}{5h}\right) = -h\dfrac{\partial p}{\partial x} - \dfrac{12q}{Rh^2}, & \text{(19b)} \\ M\dfrac{\partial^2 h}{\partial t^2} = T\dfrac{\partial^2 h}{\partial x^2} + p - P_e. & \text{(19c)} \end{cases}$$

It is noted that p does not need to appear explicitly in the system of equations, since the membrane equation may be differentiated in x and substituted in Equation (19b). Following this procedure, one obtains the following system of equations:

$$\begin{cases} \dfrac{\partial q}{\partial x} + \dfrac{\partial h}{\partial t} = 0, & \text{(20a)} \\ \dfrac{\partial q}{\partial t} + \dfrac{\partial}{\partial x}\left(\dfrac{6q^2}{5h}\right) = -Mh\dfrac{\partial^3 h}{\partial x \partial t^2} + Th\dfrac{\partial^3 h}{\partial x^3} - h\dfrac{\mathrm{d}P_e}{\mathrm{d}x} - \dfrac{12q}{Rh^2}. & \text{(20b)} \end{cases}$$

In order to solve the system in Equation (20), the boundary conditions need to be established. Two of them are immediately determined—since the membrane is fixed at its ends, we have that:

$$h(0,t) = 1, \quad h(1,t) = 1. \tag{21}$$

To determine the remaining two, we note that Equations (19a) and (19b) are valid for the rigid-wall segments upstream and downstream from the membrane. In these segments h is constant and equal to 1. Therefore, for the rigid segments:

$$\begin{cases} \dfrac{\partial q}{\partial x} = 0, & \text{(22a)} \\ \dfrac{\partial q}{\partial t} + \dfrac{\partial}{\partial x}\left(\dfrac{6q^2}{5}\right) = -\dfrac{\partial p}{\partial x} - \dfrac{12q}{R}. & \text{(22b)} \end{cases}$$

Equation (22a) implies that in the rigid segments q is a function of time only, $q = q(t)$. This in turn means that the spatial derivative on the left-hand side of Equation (22b) is zero. Using this information and rearranging Equation (22b),

$$\frac{\partial q}{\partial t} + \frac{12q}{R} = -\frac{\partial p}{\partial x}. \tag{23}$$

Since the left-hand side is a function of time only, one concludes that the pressure gradient cannot be a function of x, and the pressure varies linearly in the rigid segments (as one would expect from the parabolic flow profile assumption). Defining the left-hand side of Equation (23) as $f_1(t)$ for convenience, and integrating in x, from x_1 to x_2 (with x_1 and x_2 being both in the upstream rigid segment, or both in the downstream rigid segment),

$$p(x_2, t) - p(x_1, t) = f_1(t)(x_2 - x_1). \tag{24}$$

The rigid segment downstream from the membrane is considered first. Choosing $x_1 = 1$ (the right end of the membrane) and $x_2 = 1 + L_2$ (the outlet), noting that $p(1 + L_2, t) = 0$, and that $p(1, t)$ may be assessed from Equation (19c), Equation (24) can be written as

$$T \left.\frac{\partial^2 h}{\partial x^2}\right|_{x=1} = -L_2 \left.\left(\frac{\partial q}{\partial t} + \frac{12}{R}q\right)\right|_{x=1} + P_e(1), \tag{25}$$

providing the third boundary condition.

Furthermore, since at the inlet ($x = -L_1$) there is a prescribed constant flow Q, q will be constant in the entire rigid segment upstream of the membrane. Considering the definition of q (Equation 10), it is concluded that $q = 1$ for the entire rigid segment upstream of the membrane[1]. Therefore, the final boundary condition is established:

$$q(0, t) = 1 \tag{26}$$

It is worth pointing out that the same procedure outlined above for the rigid segment downstream from the membrane may also be used for the rigid segment upstream from the membrane. Choosing $x_1 = -L_1$, and $x_2 = 0$ in Equation (24), and using Equation (19c) to rewrite $p(0, t)$, one obtains:

$$T \left.\frac{\partial^2 h}{\partial x^2}\right|_{x=0} - P_e(0) + p(-L_1, t) = L_1 \left(\frac{\mathrm{d}q}{\mathrm{d}t} + \frac{12}{R}q\right). \tag{27}$$

Since in the rigid segments the dimensionless flow rate q does not vary in x, and since $q = 1$ (constant in time) at the inlet, the pressure at the inlet $p(-L_1, t)$, which will be denoted p_i for convenience, may be calculated by

$$p_i = \frac{12L_1}{R} - T\left.\frac{\partial^2 h}{\partial x^2}\right|_{x=0} + P_e(0). \tag{28}$$

[1] Briefly returning to the use of hats to denote dimensionless quantities, in the rigid segment upstream from the membrane:

$$q = \int_0^1 \hat{u}\, d\hat{y} = \int_0^a \frac{u}{Ua} dy = \frac{1}{Q}\int_0^a u\, dy = 1.$$

To conclude this section, the full set of equations and boundary conditions will be stated, for ease of future reference. However, one small adjustment will be made in the membrane inertia term of the momentum equation. From the continuity equation (Equation 19a),

$$\frac{\partial h}{\partial t} = -\frac{\partial q}{\partial x},$$

which implies that

$$\frac{\partial^3 h}{\partial x \partial t^2} = -\frac{\partial^3 q}{\partial x^2 \partial t}. \tag{29}$$

Making the substitution indicated above, the set of equations and boundary conditions are those shown in Equation (30).

$$\begin{cases} \dfrac{\partial h}{\partial t} + \dfrac{\partial q}{\partial x} = 0, & \text{(30a)} \\ \dfrac{\partial q}{\partial t} + \dfrac{\partial}{\partial x}\left(\dfrac{6q^2}{5h}\right) = Mh\dfrac{\partial^3 q}{\partial x^2 \partial t} + Th\dfrac{\partial^3 h}{\partial x^3} - h\dfrac{\mathrm{d}P_e}{\mathrm{d}x} - \dfrac{12q}{Rh^2}, & \text{(30b)} \\ h(0,t) = 1, & \text{(30c)} \\ h(1,t) = 1, & \text{(30d)} \\ q(0,t) = 1, & \text{(30e)} \\ T\left.\dfrac{\partial^2 h}{\partial x^2}\right|_{x=1} = -L_2\left.\left(\dfrac{\partial q}{\partial t} + \dfrac{12}{R}q\right)\right|_{x=1} + P_e(1). & \text{(30f)} \end{cases}$$

3.2 Linearization around steady-state

As mentioned previously, a linear stability analysis will be performed on the system. Steady-state solutions will be obtained, and the governing equations will be linearized around these steady-state solutions. The linearized equations comprise an eigenvalue-eigenfunction problem, with the eigenvalue providing information on the behavior of the system for small perturbations around the steady-state.

The vertical position of the membrane in steady-state will be denoted by $h_s(x)$, while $q_s(x)$ will indicate the flux at steady-state. In order to obtain them, the time derivatives in Equation (30) are set to zero,

$$\begin{cases} \dfrac{\mathrm{d}q_s}{\mathrm{d}x} = 0 & \text{(31a)} \\ \dfrac{d}{dx}\left(\dfrac{6q_s^2}{5h_s}\right) = Th_s\dfrac{\mathrm{d}^3h_s}{\mathrm{d}x^3} - h_s\dfrac{\mathrm{d}P_e}{\mathrm{d}x} - \dfrac{12q_s}{Rh_s^2} & \text{(31b)} \\ h_s(0) = 1 & \text{(31c)} \\ h_s(1) = 1 & \text{(31d)} \\ q_s(0) = 1 & \text{(31e)} \\ T\left.\dfrac{\mathrm{d}^2h_s}{\mathrm{d}x^2}\right|_{x=1} = -L_2\left.\left(\dfrac{12}{R}q_s\right)\right|_{x=1} + P_e(1). & \text{(31f)} \end{cases}$$

First it is noted that the continuity equation (Equation 31a) together with the boundary condition given by Equation (31e), imply that $q_s = 1$ everywhere, as one would expect from the conservation of mass.

Using this information and rearranging the momentum equation, the system to be solved reduces to

$$\begin{cases} Th_s^3\dfrac{\mathrm{d}^3h_s}{\mathrm{d}x^3} + \dfrac{6}{5}\dfrac{\mathrm{d}h_s}{\mathrm{d}x} - h_s^3\dfrac{\mathrm{d}P_e}{\mathrm{d}x} - \dfrac{12}{R} = 0 & \text{(32a)} \\ h_s(0) = 1; & \text{(32b)} \\ h_s(1) = 1; & \text{(32c)} \\ T\left.\dfrac{\mathrm{d}^2h_s}{\mathrm{d}x^2}\right|_{x=1} = -\dfrac{12L_2}{R} + P_e(1). & \text{(32d)} \end{cases}$$

The solution to the ordinary differential equation given by Equation (32a) provides the vertical position of each point of the membrane at steady-state.

Next, we consider small perturbations from the steady-state solution. These take the form:

$$\begin{cases} h(x,t) = h_s(x) + \theta\tilde{h}(x)\mathrm{e}^{\lambda t}, & \text{(33a)} \\ q(x,t) = 1 + \theta\tilde{q}(x)\mathrm{e}^{\lambda t}, & \text{(33b)} \end{cases}$$

where it is understood that the real part of the perturbations must be taken to obtain physically meaningful quantities (λ, $\tilde{h}$, and $\tilde{q}$ are generally complex), and θ is small ($\theta \ll 1$).

Substituting Equation (33) in the continuity equation (Equation 30a), we obtain:

$$\frac{\partial h}{\partial t} + \frac{\partial q}{\partial x} = \theta\mathrm{e}^{\lambda t}\left(\lambda\tilde{h} + \frac{\mathrm{d}\tilde{q}}{\mathrm{d}x}\right) = 0. \tag{34}$$

Since in general $\theta\mathrm{e}^{\lambda t} \neq 0$, we obtain the linearized equation of continuity:

$$\lambda\tilde{h} + \frac{\mathrm{d}\tilde{q}}{\mathrm{d}x} = 0. \tag{35}$$

Next, the momentum equation (Equation 30b) is considered. First, the advective term is rewritten by working out the derivatives.

$$\frac{\partial q}{\partial t} + \frac{\partial}{\partial x}\left(\frac{6q^2}{5h}\right) = Mh\frac{\partial^3 q}{\partial x^2 \partial t} + Th\frac{\partial^3 h}{\partial x^3} - h\frac{\mathrm{d}P_e}{\mathrm{d}x} - \frac{12q}{Rh^2}, \tag{36}$$

$$\frac{\partial q}{\partial t} + \frac{6}{5}\left(-\frac{q^2}{h^2}\frac{\partial h}{\partial x} + \frac{2q}{h}\frac{\partial q}{\partial x}\right) = Mh\frac{\partial^3 q}{\partial x^2 \partial t} + Th\frac{\partial^3 h}{\partial x^3} - h\frac{\mathrm{d}P_e}{\mathrm{d}x} - \frac{12q}{Rh^2}. \tag{37}$$

Then, both sides of the equation are multiplied by h^2,

$$\underbrace{\frac{\partial q}{\partial t}h^2}_{\text{(a)}} - \underbrace{\frac{6}{5}q^2\frac{\partial h}{\partial x}}_{\text{(b)}} + \underbrace{\frac{12}{5}q\,h\frac{\partial q}{\partial x}}_{\text{(c)}} = \underbrace{Mh^3\frac{\partial^3 q}{\partial x^2 \partial t}}_{\text{(d)}} + \underbrace{Th^3\frac{\partial^3 h}{\partial x^3}}_{\text{(e)}} - \underbrace{h^3\frac{\mathrm{d}P_e}{\mathrm{d}x}}_{\text{(f)}} - \underbrace{\frac{12q}{R}}_{\text{(g)}}, \tag{38}$$

where each term of the equation has been labeled to be considered separately.

Making the substitution of Equation (33), Term (a) becomes:

$$\begin{aligned}\frac{\partial q}{\partial t}h^2 &= \theta\lambda\tilde{q}\mathrm{e}^{\lambda t}\left(h_s^2 + 2\theta h_s\tilde{h}\mathrm{e}^{\lambda t} + \theta^2\tilde{h}^2\mathrm{e}^{2\lambda t}\right), \\ &= \theta\lambda h_s^2\,\tilde{q}\,\mathrm{e}^{\lambda t} + O(\theta^2).\end{aligned} \tag{39}$$

The same is done for Term (b):

$$\begin{aligned}\frac{6}{5}q^2\frac{\partial h}{\partial x} &= \frac{6}{5}\left(1 + 2\theta\tilde{q}\mathrm{e}^{\lambda t} + \theta^2\tilde{q}^2\mathrm{e}^{2\lambda t}\right)\left(\frac{\mathrm{d}h_s}{\mathrm{d}x} + \theta\frac{\mathrm{d}\tilde{h}}{\mathrm{d}x}\mathrm{e}^{\lambda t}\right) \\ &= \frac{6}{5}\left(\frac{\mathrm{d}h_s}{\mathrm{d}x} + \theta\frac{\mathrm{d}\tilde{h}}{\mathrm{d}x}\mathrm{e}^{\lambda t} + 2\theta\frac{\mathrm{d}h_s}{\mathrm{d}x}\tilde{q}\mathrm{e}^{\lambda t}\right) + O(\theta^2);\end{aligned} \tag{40}$$

Term (c):

$$\begin{aligned}\frac{12}{5}q\,h\frac{\partial q}{\partial x} &= \frac{12}{5}\left(1 + \theta\tilde{q}\mathrm{e}^{\lambda t}\right)\left(h_s + \theta\tilde{h}\mathrm{e}^{\lambda t}\right)\left(\theta\frac{\mathrm{d}\tilde{q}}{\mathrm{d}x}\mathrm{e}^{\lambda t}\right) \\ &= \frac{12}{5}\left(\theta\frac{\mathrm{d}\tilde{q}}{\mathrm{d}x}\mathrm{e}^{\lambda t} + \theta^2\tilde{q}\frac{\mathrm{d}\tilde{q}}{\mathrm{d}x}\mathrm{e}^{2\lambda t}\right)\left(h_s + \theta\tilde{h}\mathrm{e}^{\lambda t}\right) \\ &= \frac{12}{5}\theta h_s\frac{\mathrm{d}\tilde{q}}{\mathrm{d}x}\mathrm{e}^{\lambda t} + O(\theta^2);\end{aligned} \tag{41}$$

Term (d):

$$\begin{aligned}Mh^3\frac{\partial^3 q}{\partial x^2 \partial t} &= M\left(h_s^3 + 3h_s^2\theta\tilde{h}\mathrm{e}^{\lambda t} + 3h_s\theta^2\tilde{h}^2\mathrm{e}^{2\lambda t} + \theta^3\tilde{h}^3\mathrm{e}^{3\lambda t}\right)\left(\theta\lambda\frac{\mathrm{d}^2\tilde{q}}{\mathrm{d}x^2}\mathrm{e}^{\lambda t}\right) \\ &= M\left(h_s^3\theta\lambda\frac{\mathrm{d}^2\tilde{q}}{\mathrm{d}x^2}\mathrm{e}^{\lambda t}\right) + O(\theta^2);\end{aligned} \tag{42}$$

Term (e):

$$\begin{aligned}Th^3\frac{\partial^3 h}{\partial x^3} &= T\left(h_s^3 + 3h_s^2\theta\tilde{h}\mathrm{e}^{\lambda t} + 3h_s\theta^2\tilde{h}^2\mathrm{e}^{2\lambda t} + \theta^3\tilde{h}^3\mathrm{e}^{3\lambda t}\right)\left(\frac{\mathrm{d}^3 h_s}{\mathrm{d}x^3} + \theta\frac{\mathrm{d}^3\tilde{h}}{\mathrm{d}x^3}\mathrm{e}^{\lambda t}\right) \\ &= Th_s^3\frac{\mathrm{d}^3 h_s}{\mathrm{d}x^3} + T\left(\theta h_s^3\frac{\mathrm{d}^3\tilde{h}}{\mathrm{d}x^3}\mathrm{e}^{\lambda t} + 3h_s^2\theta\tilde{h}\frac{\mathrm{d}^3 h_s}{\mathrm{d}x^3}\mathrm{e}^{\lambda t}\right) + O(\theta^2);\end{aligned} \tag{43}$$

Term (f):

$$h^3 \frac{\mathrm{d}P_e}{\mathrm{d}x} = \left(h_s^3 + 3h_s^2 \theta \tilde{h} \mathrm{e}^{\lambda t}\right) \frac{\mathrm{d}P_e}{\mathrm{d}x} + O(\theta^2); \tag{44}$$

and Term (g):

$$\frac{12}{R} q = \frac{12}{R} + \frac{12}{R} \theta \tilde{q} \mathrm{e}^{\lambda t}. \tag{45}$$

Terms (a)–(g) are then substituted in Equation (38) and second order terms in θ are dropped.

$$\begin{aligned} \theta \lambda h_s^2 \, \tilde{q} \, \mathrm{e}^{\lambda t} - \frac{6}{5} \left(\frac{\mathrm{d}h_s}{\mathrm{d}x} + \theta \frac{\mathrm{d}\tilde{h}}{\mathrm{d}x} \mathrm{e}^{\lambda t} + 2\theta \frac{\mathrm{d}h_s}{\mathrm{d}x} \tilde{q} \mathrm{e}^{\lambda t} \right) + \frac{12}{5} \theta h_s \frac{\mathrm{d}\tilde{q}}{\mathrm{d}x} \mathrm{e}^{\lambda t} \\ = M \left(h_s^3 \theta \lambda \frac{\mathrm{d}^2 \tilde{q}}{\mathrm{d}x^2} \mathrm{e}^{\lambda t} \right) + T h_s^3 \frac{\mathrm{d}^3 h_s}{\mathrm{d}x^3} + T \left(\theta h_s^3 \frac{\mathrm{d}^3 \tilde{h}}{\mathrm{d}x^3} \mathrm{e}^{\lambda t} + 3 h_s^2 \theta \tilde{h} \frac{\mathrm{d}^3 h_s}{\mathrm{d}x^3} \mathrm{e}^{\lambda t} \right) \\ - \left(h_s^3 + 3 h_s^2 \theta \tilde{h} \mathrm{e}^{\lambda t} \right) \frac{\mathrm{d}P_e}{\mathrm{d}x} - \frac{12}{R} - \frac{12}{R} \theta \tilde{q} \mathrm{e}^{\lambda t}. \end{aligned} \tag{46}$$

Rearranging,

$$\begin{aligned} \theta \mathrm{e}^{\lambda t} \left(\lambda h_s^2 \, \tilde{q} - \frac{6}{5} \frac{\mathrm{d}\tilde{h}}{\mathrm{d}x} - \frac{12}{5} \frac{\mathrm{d}h_s}{\mathrm{d}x} \tilde{q} + \frac{12}{5} h_s \frac{\mathrm{d}\tilde{q}}{\mathrm{d}x} \right) = \underbrace{\frac{6}{5} \frac{\mathrm{d}h_s}{\mathrm{d}x} + T h_s^3 \frac{\mathrm{d}^3 h_s}{\mathrm{d}x^3} - h_s^3 \frac{\mathrm{d}P_e}{\mathrm{d}x} - \frac{12}{R}}_{=0 \text{ (Equation 32a)}} \\ + \theta \mathrm{e}^{\lambda t} \left(M h_s^3 \lambda \frac{\mathrm{d}^2 \tilde{q}}{\mathrm{d}x^2} + T h_s^3 \frac{\mathrm{d}^3 \tilde{h}}{\mathrm{d}x^3} + 3 T h_s^2 \tilde{h} \frac{\mathrm{d}^3 h_s}{\mathrm{d}x^3} - 3 h_s^2 \tilde{h} \frac{\mathrm{d}P_e}{\mathrm{d}x} - \frac{12}{R} \tilde{q} \right), \end{aligned} \tag{47}$$

where it should be noted that the braced term on the right-hand side is zero due to the steady-state equation (Equation 32).

After dividing by $\theta h_s^2 \mathrm{e}^{\lambda t}$, the linearized momentum equation is obtained.

$$\begin{aligned} \lambda \tilde{q} - \frac{6}{5h_s^2} \frac{\mathrm{d}\tilde{h}}{\mathrm{d}x} - \frac{12}{5h_s^2} \frac{\mathrm{d}h_s}{\mathrm{d}x} \tilde{q} + \frac{12}{5h_s} \frac{\mathrm{d}\tilde{q}}{\mathrm{d}x} \\ = M h_s \lambda \frac{\mathrm{d}^2 \tilde{q}}{\mathrm{d}x^2} + T h_s \frac{\mathrm{d}^3 \tilde{h}}{\mathrm{d}x^3} + 3 T \tilde{h} \frac{\mathrm{d}^3 h_s}{\mathrm{d}x^3} - 3 \tilde{h} \frac{\mathrm{d}P_e}{\mathrm{d}x} - \frac{12}{R h_s^2} \tilde{q}. \end{aligned} \tag{48}$$

Equation (48) can be put in a more convenient form. First, it is noted that:

$$-\frac{12}{5h_s^2} \frac{\mathrm{d}h_s}{\mathrm{d}x} \tilde{q} + \frac{12}{5h_s} \frac{\mathrm{d}\tilde{q}}{\mathrm{d}x} = \frac{6}{5} \left(-\frac{2}{h_s^2} \frac{\mathrm{d}h_s}{\mathrm{d}x} \tilde{q} + \frac{2}{h_s} \frac{\mathrm{d}\tilde{q}}{\mathrm{d}x} \right) = \frac{6}{5} \frac{\mathrm{d}}{\mathrm{d}x} \left(\frac{2\tilde{q}}{h_s} \right), \tag{49}$$

and that:

$$\frac{6}{5h_s^2} \frac{\mathrm{d}\tilde{h}}{\mathrm{d}x} = \frac{6}{5} \frac{\mathrm{d}}{\mathrm{d}x} \left(\frac{\tilde{h}}{h_s^2} \right) + \frac{12}{5} \frac{\tilde{h}}{h_s^3} \frac{\mathrm{d}h_s}{\mathrm{d}x}. \tag{50}$$

Both of these equations may be substituted in Equation (48), which may then be rearranged to give:

$$\begin{aligned} \lambda \tilde{q} - \frac{6}{5} \frac{\mathrm{d}}{\mathrm{d}x} \left(\frac{\tilde{h}}{h_s^2} - \frac{2\tilde{q}}{h_s} \right) \\ = M h_s \lambda \frac{\mathrm{d}^2 \tilde{q}}{\mathrm{d}x^2} + T h_s \frac{\mathrm{d}^3 \tilde{h}}{\mathrm{d}x^3} + \tilde{h} \left(3T \frac{\mathrm{d}^3 h_s}{\mathrm{d}x^3} - 3 \frac{\mathrm{d}P_e}{\mathrm{d}x} + \frac{12}{5h_s^3} \frac{\mathrm{d}h_s}{\mathrm{d}x} \right) - \frac{12}{R h_s^2} \tilde{q}. \end{aligned} \tag{51}$$

However, from the steady-state equation (Equation 32):

$$T\frac{\mathrm{d}^3 h_s}{\mathrm{d}x^3} - \frac{\mathrm{d}P_e}{\mathrm{d}x} + \frac{6}{5h_s^3}\frac{\mathrm{d}h_s}{\mathrm{d}x} = \frac{12}{Rh_s^3}. \tag{52}$$

This equation may be used to substitute the last term in the parenthesis of the right-hand side of Equation (51) to give the linearized momentum equation:

$$\lambda\left(\tilde{q} - Mh_s\frac{\mathrm{d}^2\tilde{q}}{\mathrm{d}x^2}\right) = \frac{6}{5}\frac{\mathrm{d}}{\mathrm{d}x}\left(\frac{\tilde{h}}{h_s^2} - \frac{2\tilde{q}}{h_s}\right) + Th_s\frac{\mathrm{d}^3\tilde{h}}{\mathrm{d}x^3} + T\frac{\mathrm{d}^3 h_s}{\mathrm{d}x^3}\tilde{h} - \frac{\mathrm{d}P_e}{\mathrm{d}x}\tilde{h} - \frac{12}{R}\left(\frac{\tilde{q}}{h_s^2} - \frac{2\tilde{h}}{h_s^3}\right). \tag{53}$$

The boundary conditions must go through the same procedure, that is, Equation (33) must be substituted in Equations (30c)–(30f).

For Equation (30c),

$$\begin{aligned} h(0,t) = h_s(0) + \theta\tilde{h}(0)\mathrm{e}^{\lambda t} &= 1, \\ 1 + \theta\tilde{h}(0)\mathrm{e}^{\lambda t} &= 1, \\ \tilde{h}(0) &= 0. \end{aligned} \tag{54}$$

For Equation (30d),

$$\begin{aligned} h(1,t) = h_s(1) + \theta\tilde{h}(1)\mathrm{e}^{\lambda t} &= 1, \\ 1 + \theta\tilde{h}(1)\mathrm{e}^{\lambda t} &= 1, \\ \tilde{h}(1) &= 0. \end{aligned} \tag{55}$$

For Equation (30e):

$$\begin{aligned} q(0,t) = 1 + \theta\tilde{q}(0)\mathrm{e}^{\lambda t} &= 1, \\ \tilde{q}(0) &= 0. \end{aligned} \tag{56}$$

Substitution of Equation (33) in Equation (30f) results in

$$T\left(\left.\frac{\mathrm{d}^2 h_s}{\mathrm{d}x^2}\right|_{x=1} + \theta\left.\frac{\mathrm{d}^2\tilde{h}}{\mathrm{d}x^2}\right|_{x=1}\mathrm{e}^{\lambda t}\right) = -L_2\left[\lambda\tilde{q}(1)\theta\mathrm{e}^{\lambda t} + \frac{12}{R}\left(1 + \theta\tilde{q}(1)\mathrm{e}^{\lambda t}\right)\right] + P_e(1). \tag{57}$$

Rearranging,

$$\underbrace{T\left.\frac{\mathrm{d}^2 h_s}{\mathrm{d}x^2}\right|_{x=1} + \frac{12L_2}{R} - P_e(1)}_{=0 \text{ (Equation 32d)}} + T\theta\left.\frac{\mathrm{d}^2\tilde{h}}{\mathrm{d}x^2}\right|_{x=1}\mathrm{e}^{\lambda t} = -\lambda\tilde{q}(1)L_2\theta\mathrm{e}^{\lambda t} - \frac{12}{R}\tilde{q}(1)\theta\mathrm{e}^{\lambda t}. \tag{58}$$

Dividing by $\theta\mathrm{e}^{\lambda t}$, the last linearized boundary condition is obtained,

$$T\left.\frac{\mathrm{d}^2\tilde{h}}{\mathrm{d}x^2}\right|_{x=1} = -\lambda\tilde{q}(1)L_2 - \frac{12}{R}\tilde{q}(1)L_2. \tag{59}$$

The linearized equations, as well as the linearized boundary conditions, are shown in Equation (60)

$$
\begin{cases}
\lambda \tilde{h} = -\dfrac{d\tilde{q}}{dx}, & \text{(60a)}\\
\lambda\left(\tilde{q} - Mh_s\dfrac{d^2\tilde{q}}{dx^2}\right) = \dfrac{6}{5}\dfrac{d}{dx}\left(\dfrac{\tilde{h}}{h_s^2} - \dfrac{2\tilde{q}}{h_s}\right) - \tilde{h}\dfrac{dP_e}{dx} & \\
\qquad + Th_s\dfrac{d^3\tilde{h}}{dx^3} + T\dfrac{d^3h_s}{dx^3}\tilde{h} - \dfrac{12}{R}\left(\dfrac{\tilde{q}}{h_s^2} - \dfrac{2\tilde{h}}{h_s^3}\right), & \text{(60b)}\\
\tilde{h}(0) = 0, & \text{(60c)}\\
\tilde{h}(1) = 0, & \text{(60d)}\\
\tilde{q}(0) = 0, & \text{(60e)}\\
\lambda L_2\tilde{q}(1) = -T\left.\dfrac{\mathrm{d}^2\tilde{h}}{\mathrm{d}x^2}\right|_{x=1} - \dfrac{12L_2}{R}\tilde{q}(1). & \text{(60f)}
\end{cases}
$$

These equations constitute an eigenvalue-eigenfunction problem to be solved for the eigenvalue λ, and the eigenfunctions $\tilde{h}$ and $\tilde{q}$.

As mentioned before, and discussed by Paidoussis (2014), the eigenvalue will provide valuable information on the behavior of the system. An eigenvalue with negative real part indicates a stable mode—any small perturbation to the steady-state solution tends to be damped, and the system tends to return to the steady-state solution (see Equation 33). If the eigenvalue has a positive real part, the mode is unstable and any small perturbation tends to move the system further and further away from the steady-state solution. Eigenvalues with a nonzero imaginary part indicate an oscillatory response of the system upon a small perturbation. If the real part is negative, the system tends to move back towards the steady-state solution by damped oscillations. On the other hand, if the real part is positive (and the imaginary part is not zero), the oscillation amplitude tends to grow, and self-sustained oscillations are possible. It is important to note that not much beyond the initial tendency of the system can be assessed by the linearized equations in the case of an unstable mode, since the growth in the amplitudes quickly moves the system away from the condition of small perturbations.

3.3 Parameters of the model

In order to conduct the analyses, the parameters of the model have to be determined. These parameters include the five dimensionless quantities of Equation (8): M, R, T, L_1, and L_2; as well as an additional parameter used to characterize the external pressure distribution $P_e(x)$.

While an arbitrary number of parameters could be used to define $P_e(x)$, it was chosen to use only one, for the sake of simplicity. The detailed description of how $P_e(x)$

was defined will be given below, in Subsection 3.3.1; for now, it suffices to say that the mean value of $P_e(x)$ over the domain will be used as the parameter:

$$\bar{P}_e = \frac{1}{x_1 - x_0} \int_{x_0}^{x_1} P_e(x) \mathrm{d}x = \int_0^1 P_e(x)\, \mathrm{d}x. \tag{61}$$

Since it is desired to study how tonicity affects TE phonation, a range of values is considered for the parameter most representative of tonicity ($\bar{P}_e$). Also, two different distributions of $P_e(x)$ will be compared at times.

The question of how well the external pressure represents the contraction of the musculature of the PES is certainly pertinent. A discussion on this point is postponed to Section 3.5, where several limitations of the model are considered.

It is reasonable to infer that another effect of muscle contraction (not necessarily the PES musculature) is a longitudinal tension on the PES. A range of values is also considered for the parameter most related to this: the dimensionless membrane tension, T. Additionally, different values of R will also be considered. For all other parameters, only one value was used throughout the analysis.

Evidently, all these parameters must be determined based on physiological values of TE speech. The relationship made between physiological quantities and each parameter of the model is detailed in the subsections below.

The indication of how the parameters were swept will be given along with each result in Section 3.6, since different results consider different parameter ranges, or different sweeping methods.

3.3.1 Dimensionless external pressure, $P_e(x)$

As stated before, the dimensionless external pressure is directly associated with the tonicity of the PES. Even though its definition was already presented in Section 3.1, it is repeated here, for convenience.

$$P_e = \frac{p_e - p_o}{\rho U^2}. \tag{62}$$

It was seen in Section 2.6 that Welch, Luckmann, et al. (1979) measured the spatial distribution of the intraluminal pressure of the PES of laryngectomees. They observed that this distribution was roughly axisymmetric, and possessed two lobes of higher pressure, separated by a valley. Near the esophagus, the pressure seemed to become nearly uniform.

In the present thesis, a rough approximation of the results of Welch, Luckmann, et al. (1979) was used for $P_e(x)$, which is given by Equation (63).

$$P_e(x) = \frac{4\bar{P}_e}{3} \left(\frac{1}{2} \sin^2 \pi x + \sin^2 2\pi x \right). \tag{63}$$

This function is shown graphically in Figure 50.

Figure 50 – Plot of $P_e(x)$.

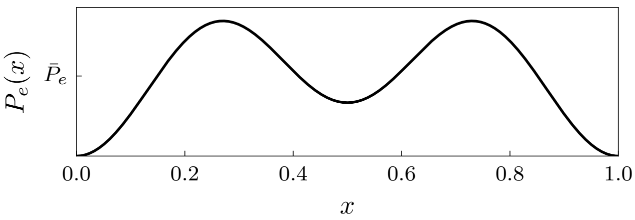

Source – Author.

While some characteristics of Figure 39 are present in Figure 50, the approximate nature of $P_e(x)$ is evident. For instance, the almost constant pressure near the esophagus has been omitted. This was done mainly for convenience. The function is simple, without any kinks, and without regions of very large derivative. Since $\mathrm{d}P_e/\mathrm{d}x$ appears in the governing equations, any region where this derivative is very large, or discontinuous, would have a large impact on the behavior of the system. Therefore, it was decided to use a simplified representation.

Nonetheless, it is reasonable to argue that the main features of the distribution reported by Welch, Luckmann, et al. (1979) are the two lobes of higher pressure, which are reproduced by Equation (63). Considering the lack of a physiological explanation for the shape verified by Welch, Luckmann, et al. (1979), the approximation given by Equation (63) seems reasonable, given its simplicity.

It should be mentioned that the pressure distribution given by Welch, Luckmann, et al. (1979) corresponds to a distribution of the resting tone of the PES. During phonation, this distribution may change. As no indication of how this distribution would be during phonation has been found, it is assumed that the PES contracts roughly the same way as for the resting tone.

Given these limitations, some simulations will also be conducted considering an uniform pressure distribution $P_e(x) = \bar{P}_e$.

To calculate $\bar{P}_e$, ρ and U need to be determined. In order to determine U, it is considered that the mean inlet velocity in the two-dimensional channel U is the same as the mean velocity obtained by the volumetric flow rate (which we will denote by Q_v) through a circular cross-section of diameter equal to the channel width a. Therefore, a is interpreted as an equivalent diameter of the cross-section of the three-dimensional problem, and the mean inlet velocity U, is determined by:

$$U = \frac{4Q_v}{\pi a^2}. \tag{64}$$

The volumetric flow rate Q_v associated with TE phonation has been measured in different works (Table 1), with published values ranging from 20 ml/s to 800 ml/s. A value of 50 ml/s will be considered, mainly for two reasons. First, it is intuitively expected that someone who produces lower flow rates would be more susceptible to difficulties in producing the TE voice. Second, given the assumptions of the model (the neglect of flow separation for instance), its accuracy is likely to degrade as the Reynolds number increases.

The determination of a cannot be made from the CT scans, since while the subject is at rest, the PES is closed, and during phonation the PES is deformed due to the airflow. Additionally, it would not be entirely correct to determine a as the diameter of the esophagus, since during surgery part of the wall of the tube of mucosa is removed, reducing the internal dimensions after closure. However, it is common for the cricopharyngeus muscle to wrap around the layer of mucosa (Figure 37b). Therefore, the total length can be used to estimate a by considering a perimeter equal to this total length. Mu and Sanders (MU; SANDERS, 2002) indicate that the cricopharyngeus muscle is about 25 mm long, which leads to $a = 8\,\text{mm}$.

The flow rate of 50 ml/s used together with an equivalent diameter of 8 mm results in a mean velocity at the inlet of $U = 0.995\,\text{m/s}$. The density of air is considered to be $\rho = 1.2\,\text{kg/m}^3$.

3.3.2 Ratio of lengths of the upstream rigid section and the membrane, L_1

The parameter L_1 (Equation 65) may be set apart from the rest, since it does not appear neither in the equations nor the boundary conditions of the steady-state boundary value problem (Equations 32), and of the linearized equations (Equation 60).

$$L_1 = \frac{l_1}{l}. \tag{65}$$

This parameter is therefore irrelevant for the solution of the steady-state equation, and the linearized equations. L_1 is only necessary if one wishes to calculate the pressure at the inlet, p_i.

Nonetheless, as seen from the CT scans (Figures 40 and 41), the prosthesis is placed at the level of the PES for Subject 1, and slightly below for Subject 2. Therefore, it is reasonable to consider $l_1 = 0$, and therefore $L_1 = 0$.

3.3.3 Ratio of lengths of the downstream rigid section and the membrane, L_2

There are only two dimensional quantities that need to be determined for calculating L_2: l_2, and l (Equation 66).

$$L_2 = \frac{l_2}{l}. \tag{66}$$

The value of l, which should correspond to the length of the PES, may be estimated from the CT images shown in Figures 40 and 41, considering the images for the subjects at rest. For Subject 1, the PES is clearly seen, and its length is about 50 mm. On the other hand, for Subject 1 the closed region is rather short, leading to the question of whether in this case the tonicity of the PES just inferior to the closed region is not sufficient to fully close the tube of mucosa. Given the typical lengths for the PES reported by the literature (Section 2.2.1), which range from 20 mm to 60 mm, the adoption of a length of 50 mm seems reasonable.

The length l_2 will be taken as roughly the length of the pharynx and oral cavity. Based on the CT scans, a length of 150 mm was adopted. The use of these values results in $L_2 = 3$.

3.3.4 Dimensionless membrane inertia, M

The dimensionless membrane inertia M is given by Equation (67) below.

$$M = \frac{ma}{\rho l^2} \tag{67}$$

All the dimensional terms in the equation above have already been discussed, with the exception of m. In order to estimate m, the density of the walls of the PES is considered to be $1040\,\mathrm{kg/m^3}$, which is a reasonable approximation for soft tissue (MAST, 2000). It is also considered that the muscle layer is responsible for the mass of the walls. The thickness of the cricopharyngeus muscle is about 4 mm (MU; SANDERS, 2002), therefore $m = 4.16\,\mathrm{kg/m^2}$. Using the dimensional values described above, $M = 11$.

3.3.5 Modified Reynolds number, R

Parameter R is defined by Equation 68 below:

$$R = \frac{Ua}{\nu}\left(\frac{a}{l}\right) = Re\frac{a}{l}. \tag{68}$$

The relationship with the Reynolds number Re is evident, and R will be referred as a modified Reynolds number, following Stewart, Waters, and Jensen (2009).

Except for ν, all dimensional quantities have been discussed before. The kinematic viscosity of air is considered to be $\nu = 1.5\,(10^{-5})\,\mathrm{m^2/s}$. Using the values described above, $R = 85$.

3.3.6 Dimensionless membrane tension, T

The dimensionless membrane tension is given by Equation (69):

$$T = \frac{a\tau}{\rho U^2 l^2} \tag{69}$$

The dimensional quantities ρ, U, and l have already been discussed. The (dimensional) membrane tension τ still needs to be determined. Of all dimensional quantities, it is the most troublesome to determine. To the best of the author's knowledge, there is no previous study on the longitudinal tension in the PES. Therefore, no quantitative measure that could be used to provide a direct estimate of this quantity has been found.

As was the case for $\bar{P}_e$, several different values of the dimensionless membrane tension will be considered. However, a relationship with the physiology must still be establish.

To obtain an estimate of what would be a reasonable value for τ, it is considered that if the membrane were *in vacuo*, it would possess a wave speed within the range of typical values reported for low frequency surface waves in soft tissue.

Titze, Jiang, and Hsiao (1993) report mucosal wave velocities in vocal folds of excised larynges ranging from 0.587 m/s to 2.177 m/s. Zhang, Osborn, and Kalra (2016) measured surface wave propagation in the lungs at functional residual capacity, and at total lung capacity. They report measured velocities of 1.71 ± 0.20 m/s at residual capacity, and 2.36 ± 0.33 m/s at total capacity.

The value for the *in vacuo* wave speed that is adopted here is 1.5 m/s. Using this value, together with the estimate of m made earlier, results in a dimensional membrane tension of $\tau = 9.36$ N/m. With the above considerations, when T is fixed, it will be fixed at $T = 25$.

3.4 Numerical method

Having described the mathematical formulation and the parameters to be considered, it still remains to show how the steady-state equation and the eigenvalue-eigenfunction problem will be solved.

In the present work, an integral-based spectral collocation method will be used. Greengard (1991) was the first to use what is essentially the same method. This method has been explored by different authors since (MAI-DUY, 2005; MAI-DUY; TANNER, 2007; DRISCOLL, 2010). In the present section, the general method will be presented following Mai-Duy (2005). The detailed descriptions of how the method was implemented to solve the steady-state equation (Equation 32), and the eigenvalue-eigenfunction problem (Equation 60) are found in Appendices A and B.

The main idea of the method is to consider the derivative of highest order in the problem (say, $\mathrm{d}^p y/\mathrm{d}x^p$) as a truncated series of Chebyshev polynomials.

$$\frac{\mathrm{d}^p y}{\mathrm{d}x^p} = \sum_{j=0}^{N} a_j \, \psi_j^0(x). \tag{70}$$

The domain of the problem is $-1 \leq x \leq 1$, and $\psi_j^0(x)$ is the Chebyshev polynomial of order j, defined by[2]:

$$\psi_j^0(x) = \cos\left(j \arccos x\right). \tag{71}$$

[2] A brief introduction to Chebyshev polynomials is given by Hamming (1986).

Any derivative of lower order (and the function y itself) may be determined from Equation (70) by direct integration:

$$\frac{\mathrm{d}^{p-1}y}{\mathrm{d}x^{p-1}} = \sum_{j=0}^{N} a_j\, \psi_j^1(x) + a_{N+1}, \tag{72a}$$

$$\frac{\mathrm{d}^{p-2}y}{\mathrm{d}x^{p-2}} = \sum_{j=0}^{N} a_j\, \psi_j^2(x) + a_{N+1}x + a_{N+2}, \tag{72b}$$

$$\frac{\mathrm{d}^{p-3}y}{\mathrm{d}x^{p-3}} = \sum_{j=0}^{N} a_j\, \psi_j^3(x) + a_{N+1}\frac{x^2}{2} + a_{N+2}x + a_{N+3}, \tag{72c}$$

$$\vdots$$

where $\psi_j^m(x)$ is the m-th integral of the Chebyshev polynomial $\psi_j^0(x)$ (Equation 73). These integrals may be obtained by recurrence relations, or by integrating the series expansion of the Chebyshev polynomials themselves (MAI-DUY, 2005).

$$\psi_j^1(x) = \int \psi_j^0(x)\mathrm{d}x, \tag{73a}$$

$$\psi_j^2(x) = \int \psi_j^1(x)\mathrm{d}x = \int\int \psi_j^0(x)\mathrm{d}x\,\mathrm{d}x, \tag{73b}$$

$$\psi_j^3(x) = \int \psi_j^2(x)\mathrm{d}x = \int\int \psi_j^1(x)\mathrm{d}x\,\mathrm{d}x = \int\int\int \psi_j^0(x)\mathrm{d}x\,\mathrm{d}x\,\mathrm{d}x, \tag{73c}$$

$$\vdots$$

The use of a truncated series means that when the proposed approximation to the derivatives of y, as well as y itself (Equations 70 and 72), are substituted in an ordinary differential equation, or an eigenvalue-eigenfunction problem, there will be a residual. As is the case for most spectral collocation methods, this residual is then set to zero at the Gauss-Chebyshev-Lobatto points (Equation 74).

$$x_i = \cos\left(\frac{i\pi}{N}\right) \quad (i = 0, 1, \ldots, N). \tag{74}$$

Since the Chebyshev polynomials (Equation 71) and their integrals (Equation 73) can be readily computed at the Gauss-Chebyshev-Lobatto points, the only unknown terms are the coefficients of the Chebyshev series a_j $(j = 0, 1, \ldots, N)$, and the integration constants $a_{N+1}, a_{N+2}, \ldots, a_{N+p}$.

In the case of an ordinary differential equation, one is left with an algebraic system of $N+1$ equations (one for each Gauss-Lobatto-Chebyshev point) and $N+p+1$ unknowns. In order to complete the system, one applies the same approximations of Equations (70) and (72) to the boundary conditions of the problem. The resulting system of $N+p+1$ equations and $N+p+1$ unknowns may then be solved numerically.

In the case of an eigenvalue-eigenfunction problem the same idea is applied, that is, the approximations of Equations (70) and (72) are substituted both in the eigenvalue-eigenfunction equation, as well as in the boundary conditions. After some matrix algebra[3] one is left with a generalized eigenvalue problem that can also be solved by established numerical methods.

This method has been chosen over well-known, differentiation-based, pseudospectral methods (BOYD, 2001) mainly due to its ease and efficiency in handling multiple boundary conditions at one of the boundaries[4]. A second point is that in pseudospectral methods, the Chebyshev differentiation matrices tend to become more ill-conditioned as N increases (GREENGARD, 1991), and this worsens in problems with high order derivatives. Since a derivative of third order appears in the present problem, and a large N is desired to resolve the constriction of the channel, this is also a considerable disadvantage in using pseudospectral methods. In comparison to other solution methods (finite differences, finite element method, etc.) the method described above has been chosen due to its accuracy, high convergence rate, and ease of implementation.

After applying the integral-based spectral collocation method to solve the steady-state equation (Equation 32), one obtains a nonlinear algebraic system of equations, given by (see Appendix A for a detailed derivation):

$$\begin{cases} \{0\} = 8T\left([\psi^3]\{a\}\circ[\psi^3]\{a\}\circ[\psi^3]\{a\}\right)\circ[\psi^0]\{a\} & \text{(75a)} \\ \qquad -2\left([\psi^3]\{a\}\circ[\psi^3]\{a\}\circ[\psi^3]\{a\}\right)\circ\{P_e'\} + \dfrac{12}{5}[\psi^2]\{a\} - \dfrac{12}{R}\{1\}, & \\ 0 = \left([\psi^3]\{a\}\right)_N - 1, & \text{(75b)} \\ 0 = \left([\psi^3]\{a\}\right)_0 - 1, & \text{(75c)} \\ 0 = \left(4T[\psi^1]\{a\}\right)_0 - \{P_e\}_0 + \dfrac{12L_2}{R}, & \text{(75d)} \end{cases}$$

where $[\psi^0]$ is the matrix of Chebyshev polynomials evaluated at the Gauss-Chebyshev-Lobatto points, with three additional columns to account for the integration constants when multiplying by $\{a\}$, which is a vector containing the coefficients of the Chebyshev polynomials and the integration constants. Matrices $[\psi^1]$, $[\psi^2]$, and $[\psi^3]$ follow a similar pattern; however, they contain the integrals of the Chebyshev polynomials, $\psi_j^1(x_i)$, $\psi_j^2(x_i)$, and $\psi_j^3(x_i)$, respectively. Vectors $\{P_e\}$ and $\{P_e'\}$ indicate the external pressure P_e, and its first derivative, evaluated at the Gauss-Chebyshev-Lobatto points. Subscript 0 is used to indicate the first row of the vector (which is associated with point $x_0 = 1$), while subscript N is used to indicate the last element of the vector, associated with point $x_N = -1$.

[3] The interested reader is referred to Mai-Duy (2005) for an illustration of the manipulations required for the case of a simple fourth-order eigenvalue eigenfunction problem. For the problem to be solved in this thesis, the detailed procedure is shown in Appendix B.

[4] See Fornberg (2006) for an overview of the problem, and different approaches that can be used to deal with the issue of spurious eigenvalues in high order boundary value problems when using a pseudospectral approach.

Vector $\{1\}$ is a vector of ones, and $\{0\}$ denotes the null vector. The symbol "$\circ$" is used to denote the element-wise, or Hadamard, product.

Equation (75a) is due to the application of the series approximations to the differential equation in the Gauss-Chebyshev-Lobatto points. All the vectors are of dimension $N+1$. Equations (75b)–(75d) result from the application of the series approximations to the boundary conditions. The system is therefore composed of $N+4$ equations. The unknowns are the elements of vector $\{a\}$, which consist of the $N+1$ coefficients of the series and the 3 integration constants, totaling $N+4$ unknowns. With the coefficients of the series and the integration constants, the solution (in this case h_s) at the Gauss-Chebyshev-Lobatto points can be calculated (see Equations 70 and 72).

In order to solve the system, a Python program was developed. The matrices of Chebyshev polynomials at the Gauss-Chebyshev-Lobatto points, as well as the matrices of integrals of the Chebyshev polynomials, were constructed using the *Chebyshev Series* module of the NumPy library (HARRIS; MILLMAN, et al., 2020). The nonlinear system was solved using SciPy's (VIRTANEN et al., 2020) function *root*, from the *optimize* module, with method *hybr*, which is based on a modification of Powell's hybrid method that is implemented in Minpack (MORE; GARBOW; HILLSTROM, 1980).

The lower limit on the norm residual was set arbitrarily low, so that the stop criteria was effectively a test used by the algorithm of Minpack to decide whether no improvement on the solution was possible. This was done to obtain as accurate a solution as possible, since h_s is also needed for the linear stability analysis, so that errors in h_s also affect the approximate solution to the eigenvalue-eigenfunction problem. Additionally, an upper limit of 500 function evaluations was set.

The accuracy of the solution was assessed by the maximum of the absolute value of the residuals (infinity norm of the residual vector). Also, as suggested by Boyd (2001) for pseudospectral methods, the solution was interpolated to an equally-spaced grid, and the residuals were also calculated by finite differences (a fourth-order scheme, with lower order approximations near the boundaries was used).

When considering the linearized equations (Equation 60), application of the spectral collocation method leads to a generalized eigenvalue problem of the form:

$$[A]\{u\} = \lambda[B]\{u\}. \tag{76}$$

Matrices $[A]$ and $[B]$ are derived in Appendix B, as is the vector $\{u\}$, which is a vector composed of coefficients of the polynomials and integration constants of the series approximations of the eigenfunctions $\tilde{h}$ and $\tilde{q}$. By means of $\{u\}$, the corresponding eigenfunctions to a given eigenvalue λ may be reconstructed. In order to solve the generalized eigenvalue problem SciPy's functions *eig* (or *eigvals* if only the eigenvalue was of interest), from the Linear Algebra module were used. In order to avoid spurious eigenvalues, the generalized eigenvalue problem was always solved twice, each time with a different N (both usually smaller than the one used for the steady-state solution). Eigenvalues whose magnitude changed considerably between the two discretizations were judged to be spurious, and discarded from the analysis. The difference between the two discretizations was quantified by the "nearest scaled difference" proposed by Boyd (2001). This difference is defined as:

$$\delta_j = \min_{k \in [1, N_2]} \frac{|\lambda(N_1) - \lambda(N_2)|}{\sigma_j}, \tag{77}$$

where σ_j is an "intermodal separation", defined as:

$$\sigma_1 = |\lambda_1 - \lambda_2|$$
$$\sigma_j = \frac{1}{2}\left(|\lambda_j - \lambda_{j-1}| + |\lambda_{j+1} - \lambda_j|\right), \quad j > 0.$$

As a verification of the implemented algorithms, some of the results published by Stewart (2017) for a massless membrane under uniform external pressure were reproduced.

3.5 Discussion on the proposed model

Now that the model has been presented, as well as the relationship between its parameters and physiological quantities, a critical assessment of the model has to be made. The first point that merits discussion is the choice of this particular model over a lumped parameter model; either one like that used by Schwarz et al. (2011) and Hüttner et al. (2015), or any other type of lumped parameter model.

Even though a lumped parameter model can be constructed to be quite simple, establishing the relationship of each parameter (the masses, springs, and dampers) with physiological quantities would not be as direct as it was for the present model (Section 3.3). In the laryngeal speech literature, it is possible to find several experiments intended at measuring values of mechanical properties of the vocal folds (sometimes relating directly with a given model); however, no such studies were found for the post-laryngectomy PES. In fact, this is likely the reason for the use of an optimization procedure to determine the parameters in the model by Schwarz et al. (2011).

Additionally, the number of parameters to vary may become considerably large. For instance, in the model of Schwarz et al. (2011) there are 12 masses. Each of these is connected to adjacent masses and anchoring points, which leads to 18 springs (not even counting the ones used to restrict rigid-body rotation). Should one consider that the effect of tonicity is represented by increasing or reducing each spring constant k, or increasing or reducing the undeformed length of each spring, the number of parameters to vary would be certainly large.

Simpler models, with a smaller number of parameters, may be proposed, but the model should be able to replicate the many possible shapes of the PES that are observed during phonation (Section 2.6). Even if one considers that the most important part involved in the vibration is the uppermost constriction, the shape of the part of the PES just upstream of this constriction affects the fluid flow, and consequently the dynamics of the PES. Whether the PES inflates or not, and whether a second bulge is present, are relevant aspects of the problem.

In this sense, it is arguable whether a lumped parameter model with as few as two or three masses could replicate the entire range of observed shapes. One might obviously choose to limit the analysis to one specific shape, and consider the part of the PES upstream from the constriction to have a static shape; however, one would have to know *a priori* which tonicity generates which shape. In the present model this arises naturally, as will be seen in Section 3.6.1. Additionally, the collapsible channel formulation of Stewart, Waters, and Jensen (2009) offers the advantage of being “rationally” derived, without having to add empirical terms, which are not available for the PES in TE phonation.

Another modeling option would be to consider the complete fluid-structural, three-dimensional problem. The main drawback with such model would be the much larger computational time required to obtain a solution. Furthermore, given the scarcity of published works on the mechanics of TE speech, it is fair to question whether the available information is sufficient for such detailed models to be worth the additional complexity. A one-dimensional model seems to be “cost-effective” in this regard.

Even though, in comparison to a lumped parameter model or a more sophisticated continuum model, the collapsible channel formulation offers many advantages, its simplicity comes with a cost, and its drawbacks need to be discussed. The first point concerns the use of the two-dimensional geometry of a collapsible channel to represent flow in the PES, rather than a one-dimensional collapsible tube model which would at least be based on the three-dimensional geometry.

While there is a clear analogy between a collapsible tube and the PES in TE speech, the analogy is not perfect. Collapsible tubes are entirely surrounded by the fluid applying the external pressure. They are essentially free to expand in any direction. The PES is not. The vertebral column is stiff enough to restrict inflation in the posterior direction, as can be clearly noticed in Figures 40b and 41b.

Additionally, even though the intraluminal pressure distribution obtained by Welch, Luckmann, et al. (1979) is nearly axisymmetric, the uppermost constriction appears to be formed with the posterior wall of the PES being projected forward, which seems to suggest that the musculature does not contract uniformly around the perimeter[5].

This point is reinforced when one considers the report by Terrell, Lewin, and Esclamado (1995) of a patient where the layer of muscle was not closed during total laryngectomy, and the patient still suffered from spasm strong enough to preclude phonation. For this to occur, a considerable contraction would have to arise from the posterior part of the PES, since for this particular person this is the only part of the mucosa of the PES that is in contact with the muscles of the PES.

[5] While this does not agree with the nearly axisymmetric results of Welch, Luckmann, et al. (1979), it is consistent with the description by Hixon, Weismer, and Hoit (2020) of how the inferior pharyngeal constrictor contracts (Subsection 2.2.4).

These observations suggest that the uniformity that exists around the circumference in a collapsible tube, does not exist in the PES. The collapsible channel model does remove this circumferential uniformity. The rigid wall at the bottom of the channel provides a resistance to inflation analogous to that of the vertebral column. The projection of the posterior wall of the PES, also seems to be better represented by the collapsible channel, where the external pressure acts in one direction only. It is worthwhile to remember that the height h is to be understood as an equivalent diameter, so the position of rigid wall (on the bottom of the channel) is not particularly significant.

It must be stressed that at the moment it is not entirely clear the extent of this predominance of anterior-posterior direction in closing the PES. Besides the results of Welch, Luckmann, et al. (1979), it must also be remembered that in published endoscopic images there have been observations of the closed PES as an anterior-posterior split (Section 2.6), which does not seem to agree with the closing of the PES by the posterior wall being projected forward.

The discussion above highlights the larger issue of how to appropriately model the muscle contraction on the PES. Besides the issues already discussed above, one may also argue that, unlike the constant pressure used here, the intensity of contraction is likely to vary with the deformation of the PES. The choice of using a constant external pressure represents a compromise. Despite its limitations, it allows the comparison to the only quantitative measure of tonicity found in the literature—esophageal manometry measurements for laryngectomees at rest. Furthermore, longitudinal contraction of the PES is likely to be coupled to tonicity, at least to some extent. In the model, these two effects are completely uncoupled. Once again, given that no discussion on the issue of longitudinal stretching of the PES was found in the literature, a compromise had to be made.

Another point worth mentioning is that it was tacitly assumed that the muscle layer only acts by applying the external pressure and by increasing the mass of the membrane wall. However, on the posterior part of the PES, the muscle layer is at the very least loosely connected to the layer of mucosa, and would increase the bending stiffness of the wall.

This highlights that a membrane under tension is not sufficient to characterize the actual stiffness of the PES. While the use of a layered structural model of the PES would provide a better representation than the collapsible channel model, the process of how to build such model is not trivial. On the anterior part of the PES, the muscle layer is not connected to the mucosa layer, but only wraps around it (if it is even closed over the mucosa, as discussed in Section 2.3). Additionally, other anatomical structures may be sutured to the anterior wall, even a thyroid lobe.

The model used also neglects some points which may be significant in TE phonation. The acoustic coupling with the vocal tract (and the esophagus, if it remains open) has been neglected, as was flow separation. The flow at the inlet of the collapsible channel is also not representative of the flow downstream from a TE prosthesis (ERATH; HEMSING, 2016; SANTOS et al., 2021).

Furthermore, in the derivation of the simplified formulation for the collapsible channel, the ratio a/l was assumed to be small. For the parameters considered in Section 3.3 ($a = 8\,\text{mm}$ and $l = 50\,\text{mm}$) the ratio is 0.16, and might be too large to justify completely neglecting terms of second order in a/l.

These points are drawbacks of the model, which come as a cost for its simplicity. While in principle a detailed model could be constructed covering as much of the physics as possible, in practice, it is questionable if this is the best approach to be taken at the moment.

3.6 Results

3.6.1 Steady-state solutions

Figure 51 shows six different steady-state solutions, with each one being associated with a different $\bar{P}_e$. The two-lobed distribution of Equation (63) was used, and to obtain these solutions, $\bar{P}_e$ was increased from 0 to 5 000 in steps of 10. The value of T was fixed at 25, R was set to 85, and $N = 1\,200$. A dotted line, corresponding to the undeformed membrane ($h = 1$), has been added to the image to highlight regions where $h_s > 1$.

Figure 51 – Steady-state solutions for different $\bar{P}_e$ using the two-lobed pressure distribution.

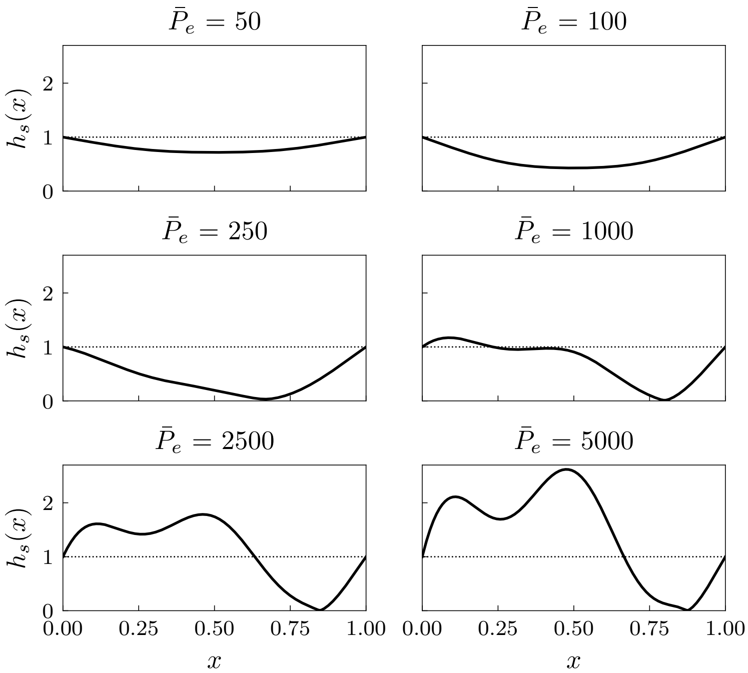

Source – Author.

The figure illustrates the extent to which the steady-state solutions may change with $\bar{P}_e$. For low values of $\bar{P}_e$, the membrane is pushed inwards, symmetrically around $x = 0.5$. At a certain $\bar{P}_e$, the point where the minimum value of h_s occurs starts moving downstream (see $\bar{P}_e = 250$ in the figure). Further increases of $\bar{P}_e$ eventually lead to the most upstream part of the membrane to inflate (see $\bar{P}_e = 1\,000$). The inflated region becomes more prominent for larger $\bar{P}_e$, while the point of minimum h_s continues to move downstream.

This figure also allows for the qualitative comparison with observed shapes of the PES during phonation. It is noted that for the smallest values of $\bar{P}_e$, the membrane deforms very little and there is a wide separation between the membrane and the rigid wall. This relates to the radiographic image of severe hypotonicity, where the walls of the PES remained widely separated during an attempt at phonation (Figure 45a).

With the increase in $\bar{P}_e$, the steady-state solution approximates the condition of Figure 44, where there is no considerable inflation, but a constriction is formed near the uppermost part of the PES. This can be seen for $\bar{P}_e = 250$ in Figure 51. Further increases lead to the inflation of the most upstream part of the membrane, which relates to the inflation of the inferior part of the PES.

The inflated region seen in Figure 51 for $\bar{P}_e = 2\,500$ and $\bar{P}_e = 5\,000$ has a second bulge, near $x = 0.25$, obviously resulting from one of the lobes of the pressure distribution. This relates with the second constriction sometimes observed in the PES. As discussed before, this second constriction could be due to the contraction of the PES musculature, in which case it would be consistent with the intraluminal pressure distribution of Welch, Luckmann, et al. (1979). It is also worthwhile to remember that Omori et al. (1994) relate the uppermost constriction with the inferior pharyngeal constrictor and the lowest with the cricopharyngeus, which also corroborates the possibility of a second constriction arising due to muscle contraction. However, the constriction could also exist due to stricture (Subsection 2.2.5), a case which the model, as used here, would not represent.

Steady-state solutions have also been obtained by considering a uniform external pressure. These are shown in Figure 52 below, which also shows the steady-state solution that was obtained with the two-lobed pressure distribution for the corresponding $\bar{P}_e$.

Overall, the solutions for a uniform external pressure share many of the same general features of the solutions for the two-lobed external pressure. For low $\bar{P}_e$, the membrane is pushed down symmetrically around $x = 0.5$. As $\bar{P}_e$ increases, the point of minimum h_s starts moving downstream. For even higher values, the most upstream part of the membrane begins to inflate. The general resemblance with the observed PES of different tonicities is maintained; however, for obvious reasons, no second constriction can be formed.

It is quite noticeable in the figure that up to $\bar{P}_e = 250$ both solutions are very close to one another, but from $\bar{P}_e = 1\,000$ on, both solutions start to differ more and more.

Figure 52 – Steady-state solutions for a uniform external pressure.

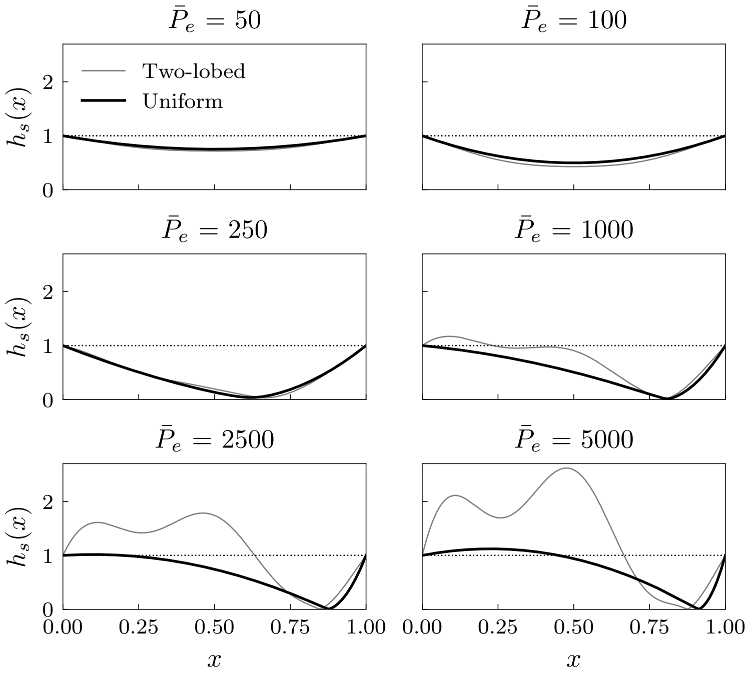

Source – Author.

There is considerably less inflation for the uniform pressure, and the point of minimum $h_s(x)$ happens further downstream when compared to the solutions for the two-lobed pressure distribution.

While at first sight the differences between both solutions for large $\bar{P}_e$ may seem surprising, it should be remembered that only the derivative of the external pressure appears in the steady-state equation (Equation 32a). For the uniform external pressure this term is always zero, while for the two-lobed pressure distribution it is not. As $\bar{P}_e$ increases, the derivative of $P_e(x)$ will generally also increase in magnitude. Therefore, as $\bar{P}_e$ increases, the differences between both solutions will also increase, which is what Figure 52 shows.

While the qualitative behavior of the steady-state solutions of the model has been compared to images of the PES during phonation, it is worthwhile to attempt a quantitative comparison. This can be done with the use of the CT scans.

As discussed before, the most reasonable comparison would be between h_s and an equivalent diameter of each section along the lumen of the PES. It is then necessary to obtain cross-sections of the segmented lumens shown in Figures 42b and 43b. These can be obtained by the use of the *SegmentGeometry* extension (HUIE; SUMMERS; KAWANO, 2022) of the program 3D Slicer (KIKINIS; PIEPER; VOSBURGH, 2014).

Figure 53 shows the equivalent diameter of the lumens of Subject 1 and Subject 2. These curves cover the region from below the prosthesis, where the esophagus was closed, until nearly the oropharynx, well above the PES.

Figure 53 – Equivalent diameters D_{eq} obtained from the CT scans.

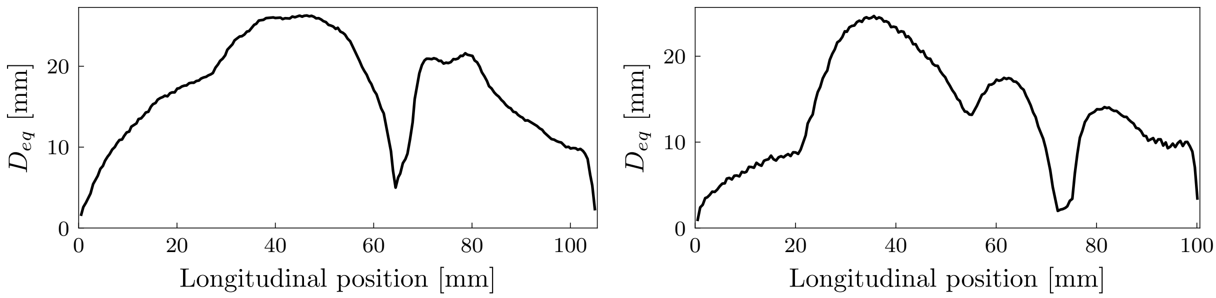

(a) Subject 1.

(b) Subject 2.

Source – Author.

While these curves can be readily related to the CT images, and the reconstructed lumens (Figures 40 and 41), some points need to be discussed. The first one is that for the same longitudinal position along the PES, two separate areas may exist. This is illustrated in Figure 54. The equivalent diameters in the region of the constriction in Figure 53 are misleading in that they account for two separate parts of the PES.

Figure 54 – Illustration of two areas for the same longitudinal position for a subject during phonation.

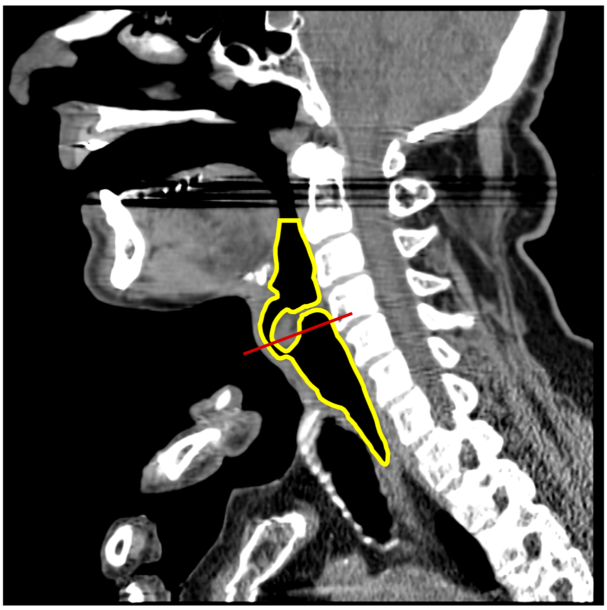

Source – Author.

To provide a better representation of the actual equivalent diameter in the constriction, the segmented lumen was separated in a superior and inferior region, shown in Figure 55 in green and blue respectively. The separation point was defined to be the plane in which two distinct areas first appeared when sweeping the images from the inferior to the superior direction. The equivalent diameters for each region are shown for each subject in Figure 56.

Figure 55 – Segmented lumen separated in a superior (green) and inferior (blue) region.

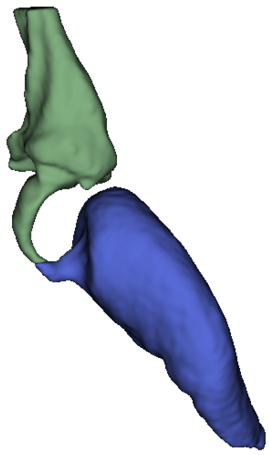

Source – Author.

Figure 56 – Equivalent diameters D_{eq} for the superior and inferior regions.

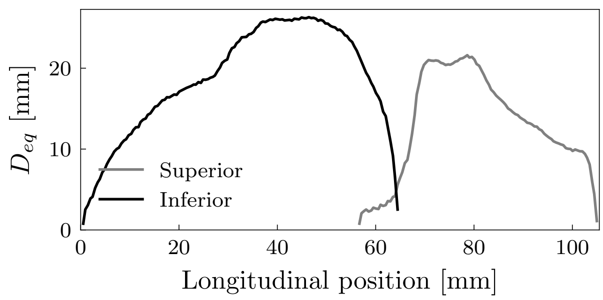

(a) Subject 1.

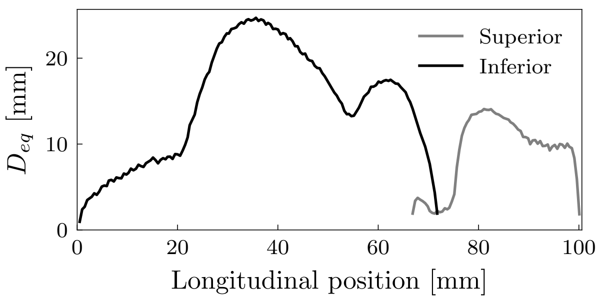

(b) Subject 2.

Source – Author.

A second point that complicates the comparison to the results from the model is that since there are no clear boundaries demarcating the PES, it is not obvious where to set the borders of the PES. It is also not obvious how to determine the characteristic length a, to normalize the equivalent diameters. In order to make the comparisons, the outlet of the prosthesis was identified in the CT scans and its position was associated with $x = 0$. The equivalent diameter in this section was set as the reference to which all the others would be divided. The point that corresponds to the right end of the membrane was chosen as the first point past the constriction where the derivative of the equivalent diameter curves (Figure 53) was zero. The distance between this point and the one at the prosthesis outlet was defined as the longitudinal characteristic length.

Based on the considerations above, Figure 57 compares the steady-state solutions and the equivalent diameters obtained from the CT scans. Since the PES of Subject 2 presents two constrictions, it was compared with the steady-state solution for the two-lobed pressure distribution (Figure 57a), while the PES of Subject 1 was compared to a steady-state solution obtained for the uniform external pressure (Figure 57b). In both cases, $\bar{P}_e$ was set to 5 000.

The curves associated with the CT scans that are shown in the figure are the dimensionless equivalents of Figure 53 (with the overestimated diameters in the constriction). Comparison with the curves shown in Figure 56 is made in Figure 58. In this figure, the curves referring to the inferior part of the PES (Figure 56) were not plotted in the region where there is an overlap with the curves associated with the superior part. This was done to avoid using two curves to represent the CT scan results of each patient. Since the curve associated with the inferior part is less relevant for the comparison to the results of the mathematical model, they have been omitted.

Figure 57 – Comparison of CT scans and steady-state solutions.

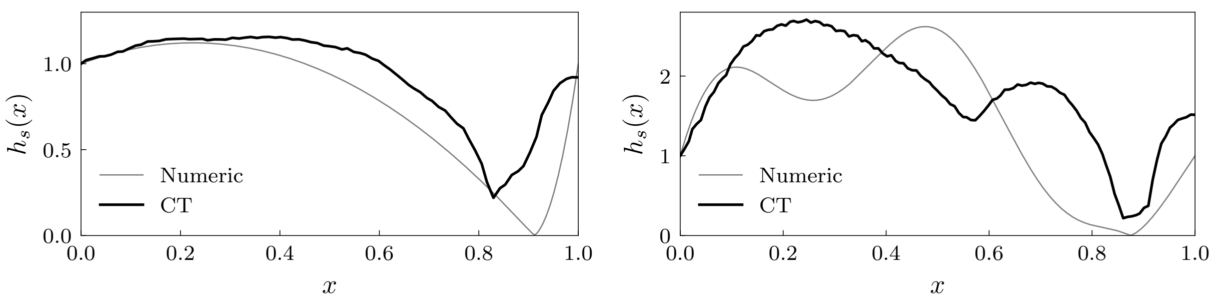

(a) Subject 1. (b) Subject 2.

Source – Author.

Figure 58 – Comparison of the curves obtained by dividing the PES, and the steady-state solutions.

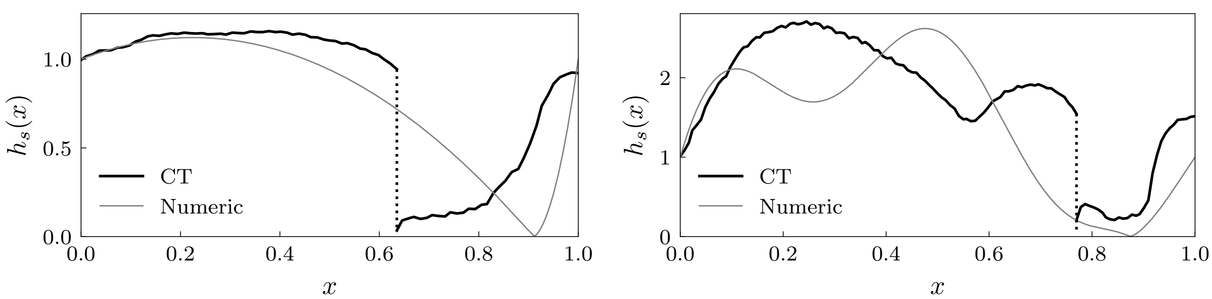

(a) Subject 1. (b) Subject 2.

Source – Author.

There are similarities between the steady-state solutions and the curves obtained from the CT images, but there are also considerable differences, as expected. For Subject 1, the curves are similar up to about $x = 0.3$, where the PES of Subject 1 remains inflated, but h_s starts to decrease. The constriction is far broader than the one predicted by the model, and it does not occur as downstream. A broader constriction could arise in the steady-state solution had a variable $P_e(x)$ had been used. As the steady-state solutions for the two-lobed external pressure show, a lobe in $P_e(x)$ near the downstream end of the membrane may produce such a broader constriction.

The choice of setting the beginning of the pharynx at a point of zero derivative in the CT scan curve may also contribute to the constriction seemingly happening further upstream. This effect is certainly too small to properly explain the discrepancy, but the lack of clear boundaries to the PES does hinder the comparisons.

For Subject 2 the differences are far more prominent, and it can be clearly seen that the two-lobed pressure distribution does not provide an accurate representation of the distribution of tonicity in the PES of this individual. For this participant, the prosthesis is placed below the PES, as can be seen in Figure 41a, and the region where the lumen closes completely is considerably short. It is likely that the PES does not close throughout its entire length, and the tonicity in the region between the two bulges PES must be considerably low[6]. Therefore, it is not surprising that the two-lobed pressure distribution would not provide an accurate representation of the shape of the PES for this subject.

Despite the clear differences between the simulations and the CT scans, it should be remembered that the present work was not concerned with representing the shapes of the PES of these two individuals. The focus was studying the PES in general. Therefore, not much effort was put into trying to approximate the steady-state solutions to curves obtained from the CT scans. An optimization procedure to determine $P_e(x)$ could obviously lead to a better representation of the shapes of the PES of these two subjects. However, it is not clear that this process would lead to a better understanding of the effect of muscle contraction on TE phonation in general. Given the scarcity of works on the mechanics of TE phonation, which hinders the development of a detailed model, this level of accuracy was to be expected.

The transition from the mostly symmetrical collapse of the membrane for low $\bar{P}_e$ to an asymmetrical one is worth an additional discussion. When T is sufficiently low, the system admits multiple steady-state solutions at this transition. This was already described by Stewart (2017) for a membrane under a uniform external pressure, and is shown in Figure 59 for the two-lobed external pressure. In the figure, the minimum of h_s (which is denoted by h_{min}) is plotted for different $\bar{P}_e$.

For $T = 5$ and $\bar{P}_e = 0$ the membrane remains essentially flat, and h_{min} is approximately equal to 1. As $\bar{P}_e$ increases, the membrane collapses towards the inside of the channel, and h_{min} decreases. For $T = 1$, as one moves along the branch, two saddle node bifurcations (SEYDEL, 2010) are encountered. The system admits three steady-state

6 As mentioned previously, since no images have been obtained while the participant swallowed, it is not known whether the second bulge would remain during deglutition, in which case it would exist due to stricture, and not muscle contraction.

Figure 59 – Plot of the minimum of $h_s(x)$ for different $\bar{P}_e$ for the two-lobed external pressure distribution.

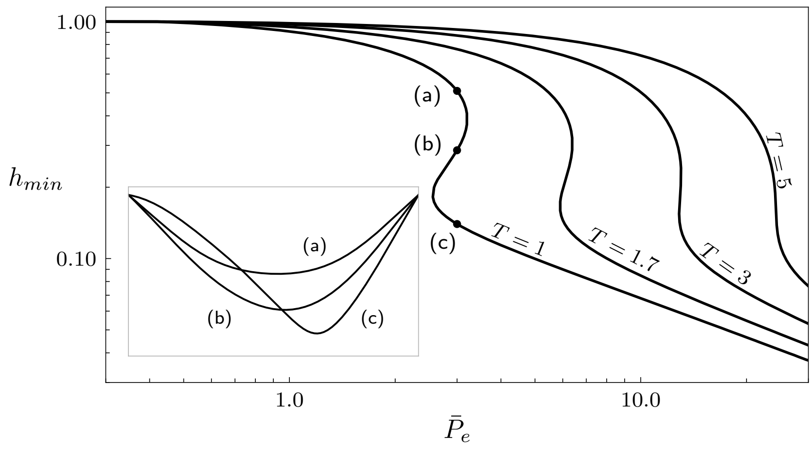

Source – Author.

solutions for the same $\bar{P}_e$. In Figure 59, points (a), (b), and (c) highlight three steady-state solutions for $\bar{P}_e = 3$. The respective membrane configurations of these three points are shown in the inset of the figure. The transition from a symmetrical configuration in (a) to an asymmetrical one in (c) is clear.

3.6.2 Linearized equations

Figure 60 illustrates how the three lowest eigenvalues change as $\bar{P}_e$ is increased. For this figure, the two-lobed pressure distribution was used, with $R = 85$, and $T = 25$. $\bar{P}_e$ was increased from 0 to 150 in steps of 1. The steady-state solution was obtained for $N = 1\,000$, and the linearized equations were solved twice, for $N = 50$ and $N = 100$, in order to identify spurious eigenvalues, which changed considerably between both solutions. The points where the real part of the eigenvalue was zero were estimated by linear interpolation.

For $\bar{P}_e = 0$ the system is stable. No eigenvalue has a positive real part. As $\bar{P}_e$ increases, the lowest eigenvalue moves left, with a continuous decrease in $\text{Re}(\lambda)$. The second and third modes behave differently. The real parts of both start to increase with $\bar{P}_e$, until the system turns unstable through a Hopf bifurcation at $\bar{P}_e = 138.5$ for the third mode. The system begins to admit self-sustained oscillations.

Considering the dimensional parameters discussed in Section 3.3 ($\rho = 1.2\,\text{kg/m}^3$, and $U = 0.995\,\text{m/s}$), and the dimensionless equation for $\bar{P}_e$ (Equation 62), the equivalent dimensional threshold is $\bar{p}_e = 0.165\,\text{kPa}$ (we consider $p_o = 0$). This value is certainly low; however, in Table 5, the lowest intraluminal pressure for the PES at rest is reported by Takeshita et al. (2012), who indicate a pressure of 0.227 kPa for a TE speaker of low proficiency. Considering that this value is for a laryngectomee that is able to speak, albeit

Figure 60 – Eigenvalues in the complex plane for the two-lobed $P_e(x)$.

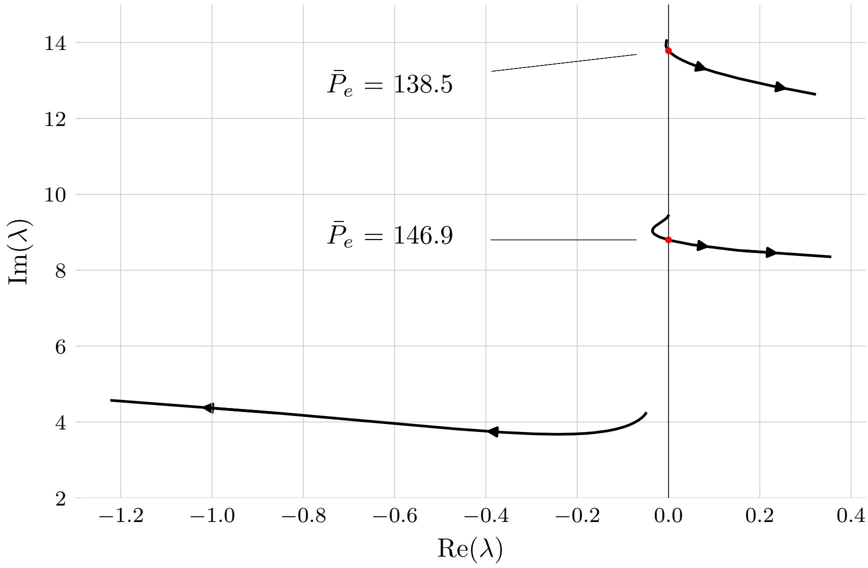

Source – Author.

with a poor voice, a threshold value of $\bar{p}_e = 0.165\,\text{kPa}$ does not seem unreasonable.

Based on the imaginary part of the eigenvalue, the frequency of oscillation at neutral stability may also be calculated. It should be noted that the eigenvalue appears in the exponent when considering the perturbations to the steady-state solution (Equation 33). Briefly returning to the use of hats to denote dimensionless quantities, it is noted that

$$\mathrm{e}^{\mathrm{j}\,\mathrm{Im}(\lambda)\hat{t}} = \mathrm{e}^{\mathrm{j}\,\mathrm{Im}(\lambda)\frac{tU}{l}}, \tag{78}$$

where the characteristic time defined in Equation (6) was used, and j is used to denote the imaginary unit.

It is then clear that $\mathrm{Im}(\lambda)U/l$ is an angular frequency, whose corresponding frequency f is:

$$f = \frac{\mathrm{Im}(\lambda)U}{2\pi l}. \tag{79}$$

At neutral stability, the imaginary part of the eigenvalue of the third mode shown in Figure 60 is $\mathrm{Im}(\lambda) = 13.78$, using $U = 0.995\,\text{m/s}$ and $l = 50\,\text{mm}$, an oscillation frequency of 43.6 Hz is obtained. This frequency is also quite low, but again it is not far from the lowest values reported by Debruyne et al. (1994) and van As-Brooks et al. (2006), which are respectively 50 Hz, and 46 Hz.

Figure 61 shows the steady-state solution at neutral stability. The membrane has a configuration that is nearly symmetric around $x = 0.5$, and the channel is still fairly open, with $h_{min} = 0.187$. With regard to TE phonation, this corroborates the observation that only extreme cases of hypotonicity lead to failure of phonation.

The analysis was repeated for different dimensionless membrane tensions. T was varied from 40 to 5 in steps of 1, while $\bar{P}_e$ was varied from 0 to 250 in steps of 1. To refine

Figure 61 – Steady-state solution at neutral stability ($R = 85$, $T = 25$, and $\bar{P}_e = 138.5$).

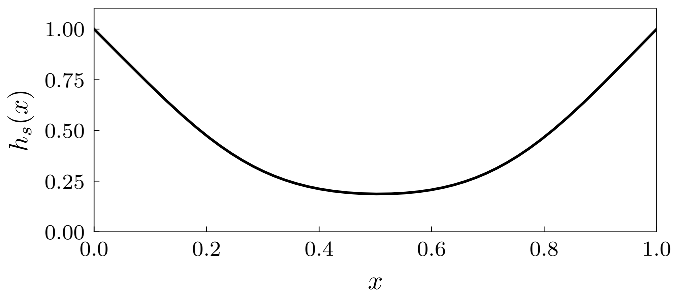

Source – Author.

the estimate of the $\bar{P}_e$ associated with neutral stability for each T, twenty iterations of a bisection procedure were used to approximate $\text{Re}(\lambda) = 0$.

Figure 62 shows curves of the threshold $\bar{P}_e$ for each T considered. Besides the curve for $R = 85$, the figure also shows the curve for $R = 15$, and the inset of the figure shows curves for $R = 50$, and $R = 120$.

Figure 62 – Neutral stability curves in the T–$\bar{P}_e$ plane.

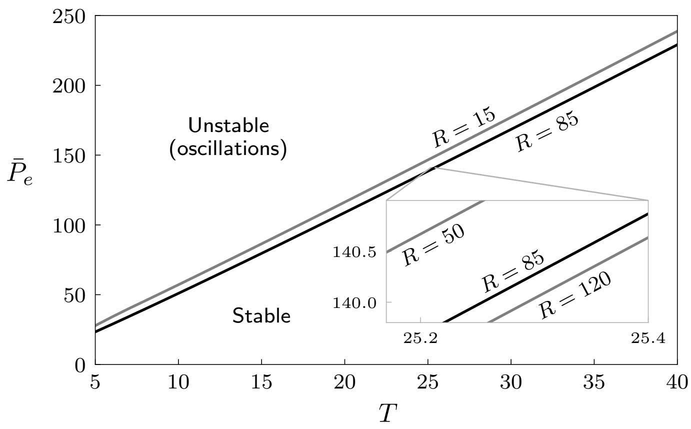

Source – Tourinho et al. (2021).

The figure shows that the neutral stability curves are nearly straight lines, with higher T requiring higher $\bar{P}_e$ for self-sustained oscillations to occur. Also, as R is increased, the neutral stability curve is shifted down, indicating lower thresholds for higher R. However, the amount by which the curve is moved also decreases. The change from $R = 15$ to $R = 85$ is noticeable, however, the curves for $R = 50$, $R = 85$, and $R = 120$ were very close to one another, and were better distinguished only in a detailed view, as shown on the inset of the figure. The inset shows that the shift from $R = 50$ to $R = 85$ is larger than the one from $R = 85$ to $R = 120$, which suggests that the threshold $\bar{P}_e$ becomes almost independent of R for the larger R.

This provides a convenient way to obtain a rough approximation for the tonicity required for self-sustained oscillations to occur, by considering a single straight line. In this approximation, for self-sustained oscillations to occur: $\bar{P}_e > \alpha_1 T - \alpha_0$ (with α_1 and α_0 being greater than zero). In terms of dimensional quantities (with $p_o = 0$),

$$\bar{p}_e > \alpha_1 \frac{a\tau}{l^2} - \alpha_0 \rho U^2. \tag{80}$$

It is seen that larger τ require higher $\bar{p}_e$, while an increase in U decreases the minimum $\bar{p}_e$, which is what is intuitively expected. For the sake of completeness, a linear fit to the curve for $R = 85$ provides $\alpha_1 = 5.9$ and $\alpha_0 = 8.29$.

The inequality given above is evidently not general, since the curves were calculated for specific M and L_2, namely $M = 11$, and $L_2 = 3$. Additionally, the almost linear behavior of the neutral stability curves may not be observed for values outside the range assessed here.

It is also useful to note that, with everything else kept constant, $R = 50$ would be associated with a flow rate of only 29.5 ml/s, and $R = 120$ with a flow rate of 70.7 ml/s, and the curves for the different R considered here would be associated with fairly small flow rates. Given that one expects laryngectomees who produce small flow rates to be more susceptible to having difficulties producing the tracheoesophageal voice, the low flow rates do not seem to be overly restrictive.

It is also useful to look at how the frequency changes along the neutral stability curve. Figure 63 illustrates this relationship. It shows the frequency, calculated by Equation 79, for the points along the neutral stability curve for $R = 85$ in Figure 62.

Figure 63 – Oscillation frequency at neutral stability for $R = 85$.

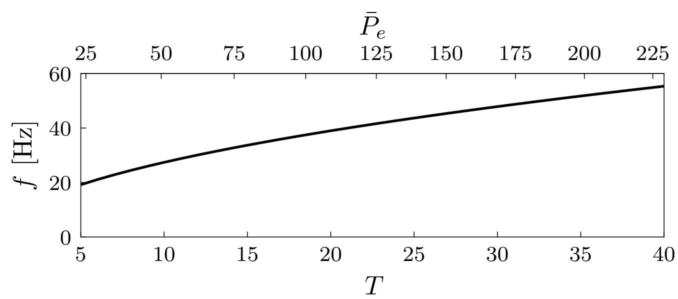

Source – Author.

The frequency increases as T (and consequently, $\bar{P}_e$) increase, as expected. The frequencies are quite low, ranging from 19.2 Hz to 55.4 Hz. The low frequencies point to a limitation in using the collapsible channel model as a representation of TE phonation. However, it is useful to stress that the estimate of the dimensional membrane tension τ was the crudest one among all parameters that were considered. One of the points the literature review on the physiology of TE speech did not properly elucidate was the role of longitudinal contraction of the PES. This could take place by contraction of the pharyngeal musculature (for instance, the palatopharyngeus muscle), or contraction of the longitudinal layer of the esophagus. Furthermore, should the suprahyoid muscles be sutured to the PES during surgery (Section 2.3), they could also stretch the PES. In this case, the estimate of τ based on relating the *in vacuo* wave speed to reported values of surface wave velocities in soft tissue, would possibly lead to an underestimated longitudinal tension.

On the other hand, since this point in the physiology of TE speech is barely touched upon, it is not even possible to discard the possibility of the opposite effect taking place– that is, a shortening of the PES. For instance, the mucosa of the PES is sutured to the root of the tongue during a total laryngectomy (Section 2.3). Should a movement of the root of the tongue towards the back of the pharynx occur during phonation, it would likely lead to some release of longitudinal tension. Granted, this posterior movement is not seen in the CT scans (Figures 40 and 41), and it is not clear whether any change in shape of the root of the tongue is simply due to the airflow. Superficially, movement of the root of the tongue during TE phonation does not seem to be significant; however, the issue is that the role these several anatomical structures play on stretching or shortening the PES is not known at the moment.

To conclude this section, it should be noted that the issue of hypertonicity has not been touched upon. Given the description given by McIvor et al. (1990), that failure in phonation due to spasm occurs with the air being "released in sudden explosive bursts", it is unlikely that failure occurs due to the existence of a stable steady-state configuration of the PES, since in this case the air would be continuously released throughout an attempt at phonation. The study of hypertonicity would then require a study considering the full nonlinear system.

Even though the issue of hypertonicity is certainly of greater importance, it is not clear to what extent should the study of a given model of TE phonation be expanded upon without first having a stronger indication of how well the model actually represents the mechanics of TE phonation. While this type of indication will ultimately have to come from *in vivo* experiments with laryngectomees, or excised PES's, artificial experimental models can expose limitations of a theoretical model, and provide ideas on what to look for in an *in vivo* experiment. The experimental model described in Chapter 4 is proposed with this intention.

4 Experimental model

This chapter describes the experimental model. As was the case for the mathematical model, the experimental model is also based on the idea of a collapsible tube; however, some points have been adapted from the classical experiments in order to better approximate the PES in TE phonation. Also, a procedure to measure the initial longitudinal tension has been attempted.

Section 4.1 describes the experimental setup, while the measurement procedure is laid out in Section 4.2, and the processing of the measurements in Section 4.3. Section 4.4 is concerned with relating properties of the experiment to dimensional parameters of the mathematical model. The results are presented in Section 4.5.

4.1 Experimental setup

4.1.1 Basic description

Figure 64 shows the experimental setup.

Figure 64 – Schematic representation of the experimental setup.

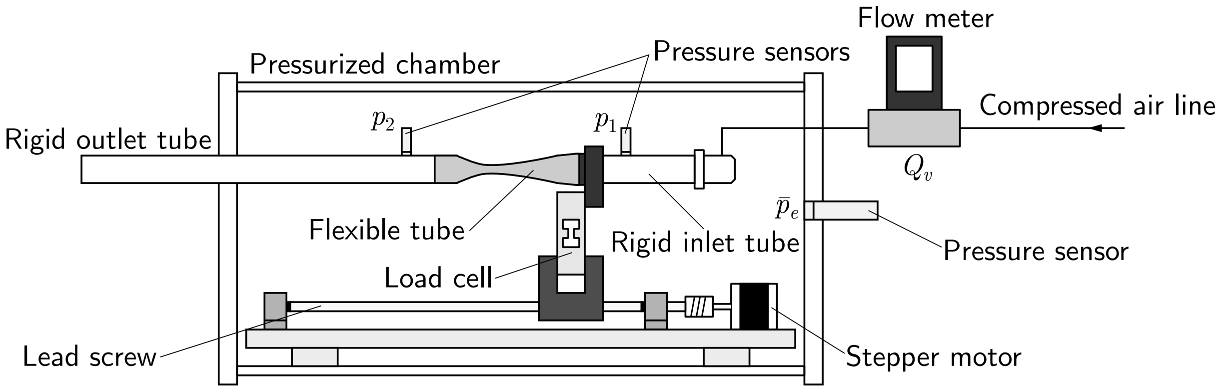

Source – Author.

A flexible tube, representing the PES, is placed inside a pressurized chamber, so that the pressure in the chamber represents the effect of tonicity on the PES. The rigid tubes represent the esophagus and the pharynx. While neither one of these anatomical structures is rigid, they are not subjected to the closing action of the inferior pharyngeal constrictor, the cricopharyngeus, and the uppermost part of the cervical esophagus. The rigid tubes would reflect this, in that they remain open while the flexible tube closes. It should be mentioned, however, that in TE phonation, while the pharynx clearly remains open, the esophagus might close. Closure of the esophagus just below the prosthesis has been observed in the CT scans of both Subject 1 and Subject 2 (see Figure 40 and 41); however, as mentioned in Section 2.6, it is not known whether this occurs for the majority of TE speakers. The rigid tube representing the esophagus cannot be made arbitrarily short for practical reasons, and a compromise had to be made.

The flexible tube is connected directly to the rigid tube at the outlet; however, for the connection to the inlet tube, a procedure to measure the longitudinal tension in the tube has been attempted. The basic idea is to connect the flexible tube to a sliding collar instead of directly to the rigid tube at the inlet. This collar slides over the rigid tube, and stretches the flexible tube over it, as shown in Figure 65.

Figure 65 – Schematic representation of the tensioning mechanism.

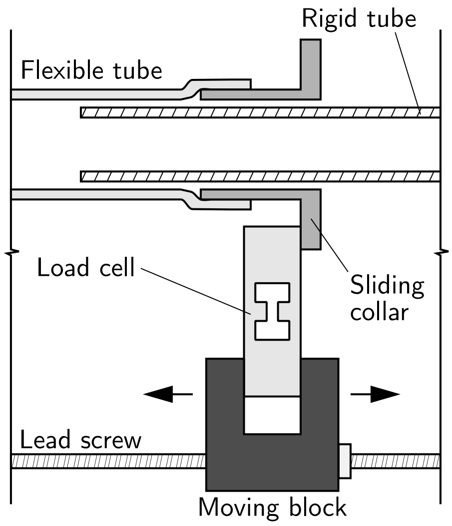

Source – Author.

The movement of the collar is induced by a lead screw connected to a stepper motor. A lead screw nut is fixed to a moving block, so that a rotation of the lead screw results in a linear motion of the block. The connection between the moving block and the collar is made by a load cell, which will give a measure of the force opposing the movement of the collar. This force will be mostly associated with the longitudinal tension in the tube. After the measurement of this initial tension, a clamp is added to seal the flexible tube around the rigid tube. This method to attempt to measure the initial longitudinal tension obviously has drawbacks, but a detailed discussion is postponed to Subsection 4.1.3.

Air is passed through the rigid tubes and the flexible tube, reproducing the airflow through the PES. The air is drawn from a compressed air line, and is regulated by a valve.

Besides the load cell used to estimate the tension in the membrane, four additional measuring instruments are used: three pressure sensors, and a flow meter (see Subsection 4.1.5). One pressure sensor is used to measure the pressure in the chamber relative to the outside pressure, another one is used to measure the pressure upstream of the flexible tube, while the third is used to measure the pressure downstream of the flexible tube. These last two pressure sensors measure the pressure in the flow relative to the pressure in chamber. The flow meter is used just downstream from the valve used to control the flow rate.

The experiment is conducted by adjusting the valve so that the flow rate through the tubes remains constant, and by continuously increasing the pressure in the chamber.

The onset and offset of oscillations are identified, and the oscillatory behavior is registered by the pressure sensors exposed to the airflow.

While the brief description made above provides the general idea of the experiment, several details have obviously been omitted. These will be discussed in the following subsections to provide a more comprehensive picture of the experiment.

4.1.2 Pressurized chamber and rigid tubes

The chamber consisted of a rectangular prism (with internal dimensions of $470 \times 250 \times 250\,\text{mm}^3$), whose walls were made of 10 mm thick plexiglass. Figure 66 shows the constructed chamber. Several sealing components had to be designed for the passage of tubes, hoses, and cables. These are detailed in Appendix C.

Figure 66 – Pressurized chamber.

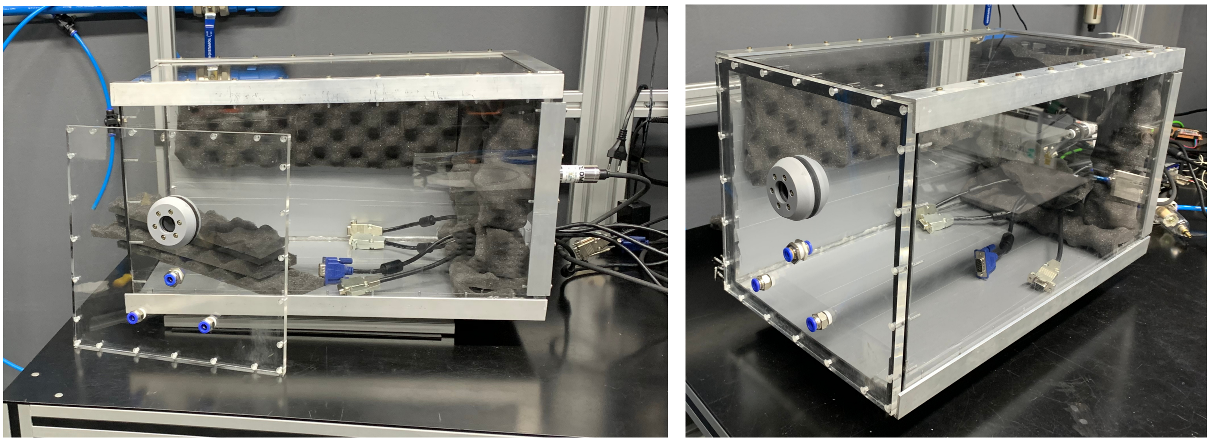

(a) Open. (b) Closed.

Source – Author.

The closed chamber forms an air cavity. During an experiment, when the flexible tube oscillates and generates sound, the acoustic field in the cavity will be excited. For a rectangular acoustic cavity of dimensions $470 \times 250 \times 250\,\text{mm}^3$, a quick estimate indicates that the three lowest natural frequencies are 365 Hz, 686 Hz, and 730 Hz. These estimates are for the acoustic cavity only. In the experimental setup, the walls of the chamber are not perfectly rigid, and the natural frequencies are likely to be lower. This issue is certainly difficult to avoid, since the dimensions of the chamber cannot be made too small, due to practical considerations. In fact, if the chamber were to be made excessively small, one would risk having the deformation of the flexible tube perceptively change the volume of air in the chamber, which therefore would alter its pressure.

Acoustic foam was used inside the chamber to increase sound absorption and attempt to minimize the influence of the acoustic field. Additionally, tape was fixed to the bottom and one of the lateral sides of the chamber as an attempt to increase damping.

The rigid tubes were simple PVC tubes, with external diameter of 20 mm, and internal diameter of 17 mm. An inlet cap and the mounts for the pressure sensors had to be designed and constructed. These are discussed in Appendix C.

The rigid tube upstream was cut so that the distance from the end of the tube to the inlet was 181 mm. The end of the inlet tube was tapered to an external diameter of about 18 mm in order to minimize contact between the flexible tube and the outer wall of the rigid tube during stretching. At the very tip of the tube, the external diameter was kept at about 19 mm, to prevent the clamp from slipping. The pressure sensor was positioned 102 mm of the open end of the rigid tube.

The rigid tube downstream of the flexible tube was cut to a length of 300 mm, and the pressure sensor mount was glued to it, at a distance of 50 mm from the end to which the flexible tube is to be connected.

Aluminum supports were used to maintain the positioning of the tubes on an aluminum V-slot profile frame. The positioning was made so that the ends of the two rigid tubes were kept a distance of 50 mm apart. Figure 67 shows the tubes mounted in the frame.

Figure 67 – Rigid tubes mounted on the frame.

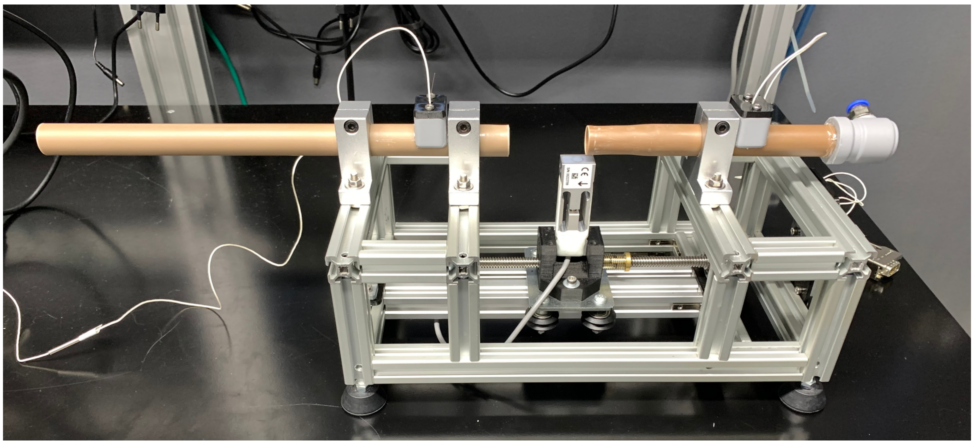

Source – Author.

4.1.3 Longitudinal stretching mechanism

The basic idea for how the measurement of the longitudinal tension will be attempted has been described in Section 4.1.1; however, this measurement is not trivial, and many points still need to be discussed.

In Section 2.9, it was seen that in previous collapsible tube experiments two main methods have been used to change the axial tension in the tube. The first one consisted of clamping the ends of the flexible tube to the rigid tubes, and allowing a given load to change length of the flexible tube. The restoring force provided by the tube can be then associated with the load applied.

While this provides an accurate measure of the longitudinal tension in the tube, it has one large drawback: the length of the flexible tube has to be changed as well. This is particularly troublesome if one wishes to compare experimental results with a theoretical model determined in terms of dimensionless parameters.

For instance, in the model described in Chapter 3, the length of the membrane l appears in five (L_1, L_2, M, R, and T) of a total of six parameters. Each change in the dimensional membrane tension would be related with not only a change in T, the dimensionless membrane tension, but in all five of the dimensionless parameters that involve l. Therefore, the measurements made for the different τ (and correspondingly, different T) would not relate directly to one another, particularly because M, R, and L_2[1] would also be different for each measured T. Instead of assessing the effect of T, what would actually be studied is the effect of T coupled with changes in M, R and L_2.

This problem is not specific to the model considered in the present work, since the length of the flexible tube will likely figure in multiple dimensionless parameters of any continuum-based model. Even though, in a worst case scenario, this effect could even prevent certain regions of the parameter space to be reached experimentally, it should be noted that if changes in l due to the applied tension are small enough to be negligible, approximations could obviously be made.

The second method to characterize longitudinal tension is described by Lyon et al. (1981). In this method, the flexible tube is tensioned before clamping its ends to the rigid tube. While this allows for the tension in the tube to be varied independently of its length, measuring the force applied to the tube in this condition is not trivial. Lyon et al. (1981) for instance, only indicate the lengths of the undeformed tube, and the distance between the ends of the rigid tubes; in other words, the length of the deformed tube.

Considering the potential benefits of measuring the longitudinal tension without changing the length of the flexible tube, the method illustrated in Figure 65 is being proposed.

The implementation of the mechanism was straightforward. The stepper motor is attached to a 300 mm lead screw by a flexible coupler. The lead screw is supported by a pair of rolling bearings, and a moving block is fixed to a gantry system made to move along V-slot aluminum rails. A lead screw nut is also attached to the moving block, so that the rotation of the leadscrew results in a linear motion of the gantry and the moving block. A spring-loaded nut was used to minimize backlash. The stepper motor is controlled by an Arduino microcontroller, used alongside an EasyDriver stepper motor driver. The thread of the lead screw is a TR8×2 thread.

One of the ends of a single point load cell is attached to the moving block, while the other is attached to the sliding collar (Figure 68a). The flexible tube is then strapped to

[1] It should be remembered that L_1 does not figure in the governing equations or the boundary conditions (Section 3.3), and does not affect the solution of the mathematical model. It is only relevant for the calculation of p_i (Section 3.1).

the sliding collar (Figure 68b). The opposite end of the flexible tube may then be clamped to the end of the rigid outlet tube.

Figure 68 – Sliding collar.

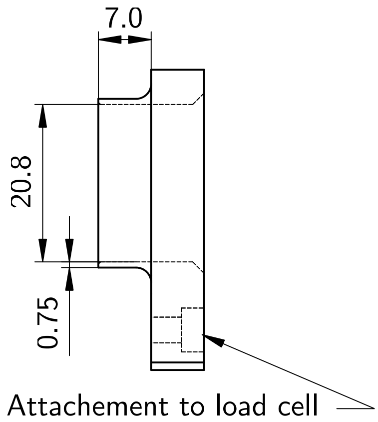

(a) Sliding collar.


(b) Collar strapped to the tube.

Source – Author.

In this mechanism, two parts had to be developed: the sliding collar, and the moving block. These are shown in Appendix C.

While the measurement procedure described above seems straightforward, different obstacles were encountered. The first one is that the distance the collar needs to be moved over the rigid inlet tube has to be sufficiently long to allow room for placing the clamp. The deformation of the tube, with a progressive narrowing of the cross-sections near the middle, makes the flexible tube touch the outer surface of the rigid tube. This contact alters the value of the force read by the load cell. In this case, the force indicated stops being equal to the axial tension in the part of the flexible tube that is between supports, since between this part and the load cell there are additional forces due to the contact between the flexible tube and the rigid tube.

Many attempts to solve this problem were not completely successful. For instance, while it seems reasonable to increase the diameter of the collar, so that the flexible tube is stretched further around the rigid tube, it would not eliminate the issue. As shown in Figure 68b, just after the end of the collar, the flexible tube returns to its undeformed diameter.

Using a flexible tube of larger diameter is not a satisfactory solution either. The next larger diameter offered by the manufacturer of the Penrose drain (which was used as the flexible tube) has an average diameter of 25 mm. Upon clamping of the rigid tube, the tube would wrinkle and fold under the clamp. More importantly, the difference between the internal diameter of the rigid tubes and the flexible tube would be about 47%. Considering that these should ideally be the same, the difference seems too large to be overlooked. For the same reason, it is not adequate to use a rigid tube with the same external diameter, but with a thicker wall, and taper it further.

Another attempt at solving the issue was by the use of lubrication between the rigid tube and the flexible tube. However, the lubricant degraded the flexible tube, so that after some time, the part of the flexible tube that was in contact with the lubricant (and near the clamped region) had undergone considerable permanent deformation. This permanent deformation was not observed when lubrication was not used.

An additional difficulty in measuring the longitudinal tension is the fact that the act of clamping the flexible tube also affects the reading. The problem was quite pronounced when using a conventional worm drive clamp (such as the one visible in Figure 69), but was greatly minimized by the use of a 3–D printed spring clamp (Appendix C). Tests for leakage showed the clamp performed its duty satisfactorily; however, being made of PLA, it is subject to viscoelastic creep, and had to be periodically replaced.

While these sources of uncertainty remain, measurements of the longitudinal tension under different conditions seem to suggest that their effect is not large enough to compromise the measurements. This will be discussed again when considering the measurement procedure (Section 4.2).

4.1.4 Flexible tube

A commercial Penrose drain was used as the flexible tube. The Penrose drain consists of a thin walled latex tube, about 300 mm in length. The manufacturer also indicates a minimum thickness of 0.15 mm, and an average diameter of 19 mm.

It was found that the thickness of the wall of the tube varied along its length, and since the tube is folded for packaging, it has creases in it (Figure 68b), which likely affects the shape of the cross-section of the tube when closing due to the pressure in the chamber.

The tube was cut to a length of 75 mm. This cut was made on the end with the thickest wall, and the thickness was measured to be 0.25 mm at both extremities of the part that was cut. The tube was weighted, and it was found to have a mass of 0.9 g.

The mechanism developed for the longitudinal stretching of the tube, and described in Section 4.1.3 was used to characterize the mechanical behavior of tube under an axial load. The idea behind such characterization is merely to provide a report on how the tube responded, given that the mechanical response of the material certainly plays a role on the dynamics of the system. Being made of a viscoelastic material, one expects the flexible tube to present typical phenomena of this type of material, such as creep and stress relaxation.

In order to carry out the tests, the rigid inlet tube was removed, and the flexible tube was clamped to the rigid outlet tube, so that it was free to stretch without any sort of interference (Figure 69). The tube was clamped over the outlet tube in a way that the measured force was zero when the left end of the collar was 50 mm from the end of the rigid outlet tube.

The first test was conducted to assess the extent to which stress relaxation occurs.

Figure 69 – Setup for the mechanical characterization of the flexible tube.

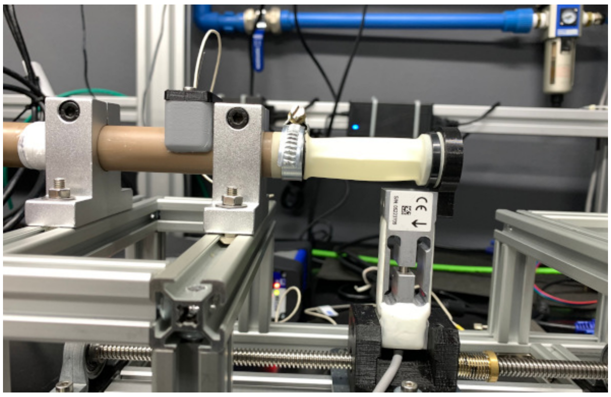

Source – Author.

The tube was stretched a given distance from the original position. It was then held on this position for about 10 min[2]. Subsequently, it was released back to its original position, and was kept at this position for additional 10 min. Four different distances were considered: 2.5 mm, 5.0 mm, 7.5 mm, and 10 mm.

Figure 70 shows the measured forces in time. The sampling rate was set to 600 Hz, and the results were zero-phase filtered with a fourth order Butterworth filter with cutoff frequency of 2 Hz. In the figure, the peak of the force signal was identified in each case, and the results are shown from this point on.

The measured force decreases with time, as does the rate of decrease, as expected. It is seen that the change in absolute value increases with the displacement. For a displacement of 2.5 mm, the decrease in force reached 0.053 N, while for a displacement of 10 mm the decrease reached 0.209 N. Proportionally, these correspond respectively to decreases of 9.52% and 8.65% from the peak value. However, as the plot shows, the change is larger in the first instances of the applied force. For example, for the displacement of 2.5 mm, the force had dropped 6.37% from the peak value in the first minute, while for the displacement of 10 mm, the force dropped to 4.71% of the peak value. For the sake of comparison, the change in force was 0.146 N for the displacement of 7.5 mm, and 0.101 N for the displacement of 50 mm.

As mentioned above, the tube was returned to its original length afterwards. Figure 71 shows the recovery after returning the tube to its initial position. As this position is the same for the four displacements considered, the curves are shown in the same plot. For each curve, the minimum force measured was identified, and the curve was drawn from this point on.

The largest variation occurs from returning the tube from the 10 mm displacement, with an increase of 0.043 N from the minimum.

[2] The 10 min included the time for the moving block to travel from the initial to the final position, so the tube was kept deformed for a few seconds less than 10 min.

Figure 70 – Stress relaxation in the flexible tube.

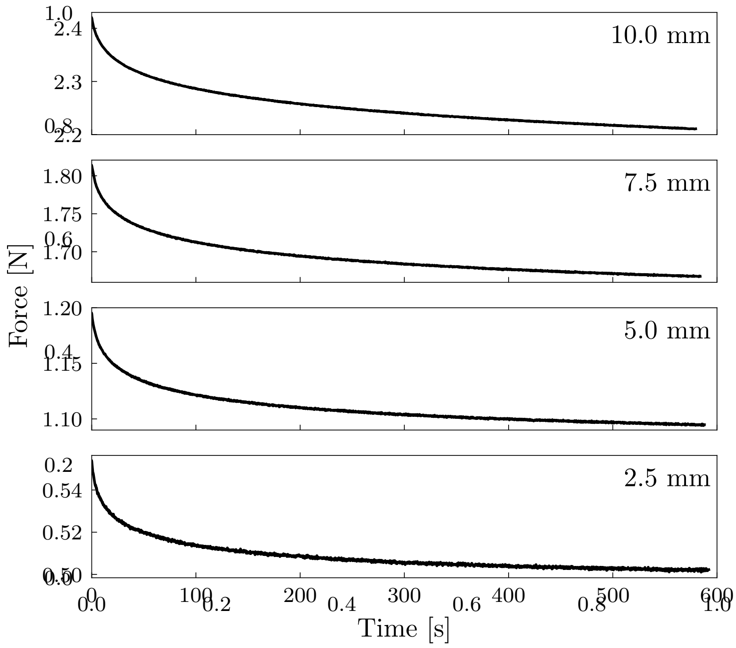

Source – Author.

Figure 71 – Stress recovery in the flexible tube.

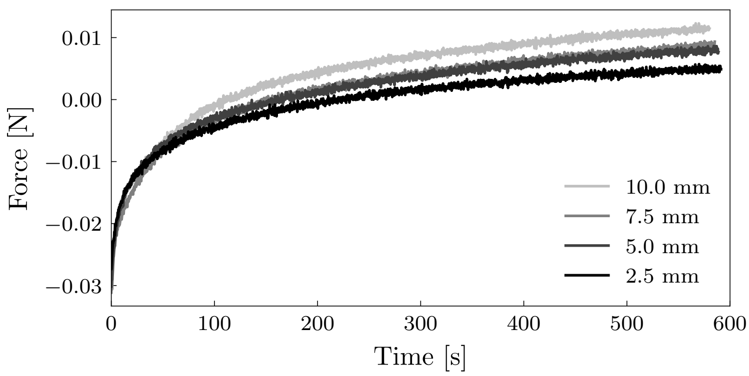

Source – Author.

The time-varying nature of the measured forces upon stretching the tube introduces another factor in the already difficult estimate of the initial longitudinal tension in the tube. It is seen that changes in the measured force due to stress relaxation were most significant for the largest displacements. While they are proportionately small, they certainly are an additional complication to the estimation of the longitudinal tension.

A force-displacement curve was also constructed. The displacement was increased to 15 mm in steps of 0.5 mm. In each step, a waiting period of 30 s was used to allow the force to partially settle. After reaching 15 mm, the collar was moved backwards, once again in steps of 0.5 mm. Only one cycle was completed, since no further analyses would be performed. Figure 72 shows the curve.

Figure 72 – Force-displacement curve for the flexible tube.

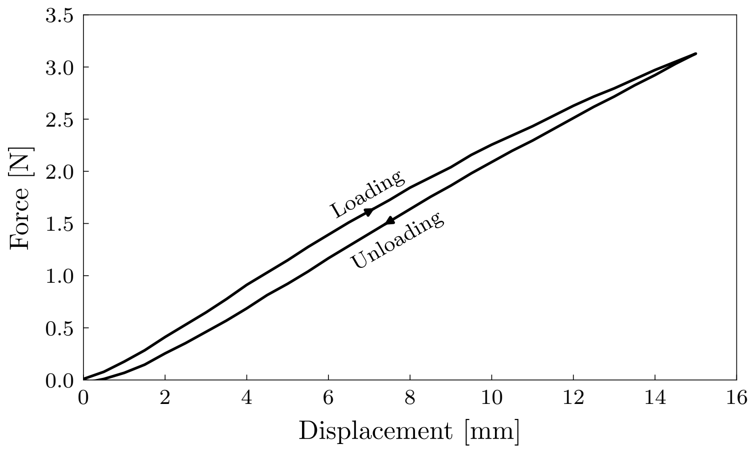

Source – Author.

The hysteresis cycle loop, typical of viscoelastic materials, is evident. The curve is also not linear but, should an approximation need to be made, the errors would be manageable.

4.1.5 Instrumentation

The sensors used in the experiment are those depicted in Figure 64. They are: two pressure sensors for measuring pressures upstream and downstream of the flexible tube; one pressure sensor for measuring the pressure in the chamber; one load cell for the measurement of the longitudinal tension in the tube; and a flow meter to measure the inlet flow rate.

The measurement of the pressures upstream and downstream of the flexible tube were made with two Kulite XCS-093-5D pressure sensors. These are piezoresistive differential pressure sensors, with a pressure range of up to 35 kPa. The manufacturer indicates that the typical accuracy for combined nonlinearity, hysteresis, and repeatability is ±0.1% of the full scale output, while the maximum is ±0.5%. The natural frequency of the sensor is 150 kHz, which is sufficiently high to allow for the measurement of acoustic pressure fluctuations.

To measure the pressure in the chamber, an Omega PXM-409-070HGV was used. This piezoresistive gauge pressure sensor is capable of measuring pressures up to 7 kPa. The reported accuracy (considering linearity, hysteresis, and repeatability combined) is of ±0.08% of the full scale output. The manufacturer indicates a response time smaller than 1 ms, but does not give a precise value. The large response time is not an issue, since what is being measured is the pressure in the chamber, which changes slowly. Additionally, the lower full scale output and improved accuracy allow for more precise measurements than the Kulites.

The tension in the flexible tube was measured with an HBM PW4MC/2KGOP-1 single point load cell, capable of measuring loads up to 2 kgf. The hysteresis, and nonlinearity are both indicated to be ±0.015% of the sensitivity, which is 2 mV/V.

The flow rate was measured with an Omega FMA-1611A mass flow meter, which is capable of measurements of up to 250 SLPM (standard litres per minute). It allows for the measurement of the volumetric flow rate, the mass flow rate, the temperature and absolute pressure of the air. The quoted accuracy is of ±0.8% of the reading, combined with 0.2% of the full scale output. The response time is indicated as being inferior to 10 ms.

An HBM QuantuumX MX-410B was used as the data acquisition (DAQ) board. The board has four input channels, which were used for the pressure sensors and the load cell. The flow meter is capable of outputting a digital RS232 signal, which was used to record measurements provided by it.

A LabVIEW program was used to coordinate the simultaneous acquisition with the DAQ board and the flow meter. To control the DAQ board, the HBM LabVIEW driver was used. A producer-consumer design pattern was implemented with the use of queues. Two producer loops were used, one for the acquisition with the DAQ board, and the other for the acquisition through the flow meter. The consumer loop was used for the plotting and storing of data.

The acquisition between both devices was not perfectly synchronized due to the lack of support for hardware trigger communication between them. There is a small delay (which is expected to be of the order of milliseconds) between the beginning of the acquisition with the DAQ board, and the flow meter. This happens due to differences in time of when the software commands each device to perform the acquisition, as well as inherent timing limitations of using serial communication for the acquisition with the flow meter. In practice, there will be no need for perfect synchronization, and the implemented solution is more than adequate. A sample rate of 4.8 kHz was used for the DAQ board and 20 Hz for the flow meter.

4.2 Measurement procedure

The overall measurement procedure is straightforward. First, the flexible tube is stretched to a desired tension, then the support structure is placed inside the chamber. The flow rate is set to a desired value, and the pressure in the chamber is continuously increased. The behavior of the system is monitored, with special attention to the identification of the pressures in the chamber that lead to the onset of self-sustained oscillations of the flexible tube.

The process of stretching the tube to a desired tension is dictated largely by limitations in the measurement procedure that were exposed in Section 4.1.3. The procedure begins with the rigid inlet tube disassembled and with the flexible tube strapped only to the sliding collar. The collar's initial longitudinal position is set so that its end is in the same position as where the open end of the rigid inlet tube will be. The collar is then moved forward by 8 mm and the flexible tube is clamped to the rigid outlet tube. The amount by which the flexible tube is stretched over the rigid outlet tube is adjusted to approximate a desired longitudinal tension. After this step, the system is essentially as shown in Figure 69.

The rigid inlet tube is then positioned and fixed to the supporting structure. The collar is moved to its initial position, and then it is stretched 8 mm over the rigid tube. This distance is used to allow enough clearance for the clamp. The flexible tube is then pinched around the rigid tube. This is done because as the flexible tube stretches around the rigid tube, any contact between the two leads to frictional forces, which oppose the movement. In comparison to the case where the tube stretches without the presence of the inlet tube, a material point in the flexible tube moves a smaller distance, due to this friction. Therefore, the flexible tube is overstretched in the region between the contact and the collar and understretched in the region between the rigid tubes. By releasing the flexible tube from the wall of the rigid tube and allowing it to return by its elastic forces, this effect is reduced. Repetition of this procedure showed good repeatability in the measured forces. The clamp is then applied, sealing the flexible tube around the rigid one.

The assembled system is then placed inside the chamber, which is subsequently sealed (Figure 73).

Figure 73 – Experimental setup.

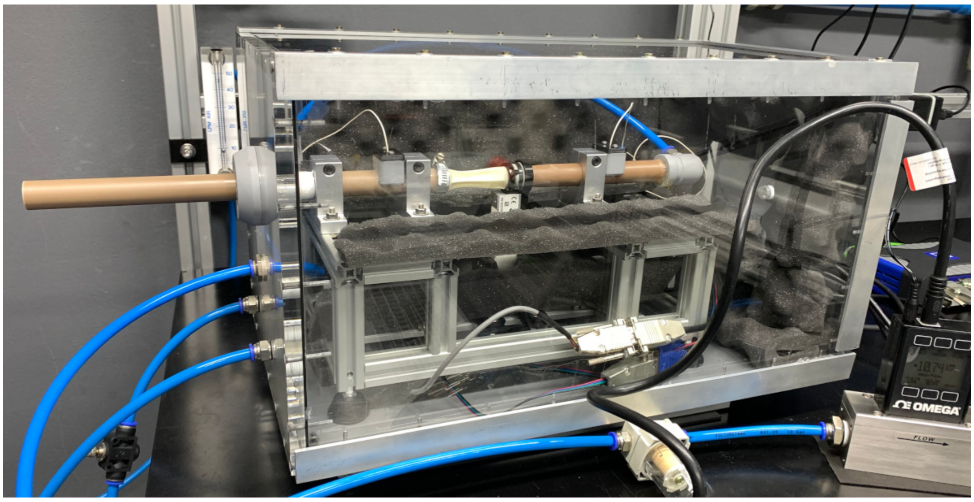

Source – Author.

The flow rate is set to the desired value. As the pressure in the chamber increases, the constriction formed by the flexible tube changes the inlet pressure required to maintain the same flow rate. Therefore, it was not possible to maintain the flow rate perfectly constant, and it had to be continuously adjusted. In the event of a significant change in the behavior of the system as the flow rate was adjusted, the measurement was repeated.

The pressure in the chamber was continuously increased up to 7 kPa. Flow rates that were tested were: 80, 100, 120, 140, 160, 180, 200, 220, 240, 260, 280, and 300 ml/s. Flow rates lower than 80 ml/s did not appear to lead to self-sustained oscillations for pressures in the chamber below 7 kPa, so they were not tested systematically. Five different values of membrane tension were considered. These were 0.025, 0.050, 0.075, 0.100, and 0.125 kgf (0.245, 0.490, 0.735, 0.981, and 1.23 N).

Due to the stretching procedure, these values were not reproduced exactly. The measured values are indicated in Table 6. The force measured when stretching the tube without the inlet tube is indicated along with the force measured when the tube was stretched over the inlet tube (after releasing the flexible tube from the wall and allowing it to return, as described above). The variation caused by clamping is indicated as well. For convenience, the nominal values will be used to refer to each of the tensions considered.

Table 6 – Measured longitudinal tensions [kgf].

Nominal	Without inlet tube	With inlet tube	After clamping
0.025	0.027	0.031	0.037
0.050	0.055	0.056	0.062
0.075	0.079	0.079	0.081
0.100	0.104	0.107	0.110
0.125	0.126	0.133	0.130

4.3 Data processing

The experiment does not require sophisticated processing of the data; however, it was necessary to establish a criterion to define the onset of self-sustained oscillations. Even though the onset can be clearly distinguishable by the sound produced, the onset of oscillation does not follow the same pattern every time. Most of the time, the amplitudes grew very quickly to a nearly constant level; however, there were times when the oscillations began with very small amplitude, producing a very faint sound, which later grew to full fledged oscillations. During these faint oscillations, the sound produced was erratic and seemed to even disappear at times. Therefore, it was considered that they should not be considered as the onset—only completely developed oscillations were considered.

While this consideration narrows down what is considered to be self-sustained oscillations, it is still necessary to determine when exactly the onset occurs. The criterion adopted here was to identify the threshold point as the instant associated with the maximum rate of growth of the oscillation amplitude. The changes of the oscillation amplitude in time can be characterized by the envelope of the signal of the pressure downstream of the flexible tube. The point of maximum rate of growth can be obtained by the time derivative of the envelope.

In order to implement this criterion, first the region where oscillations began was narrowed down (Figure 74).

Figure 74 – Pressure downstream of the flexible tube.

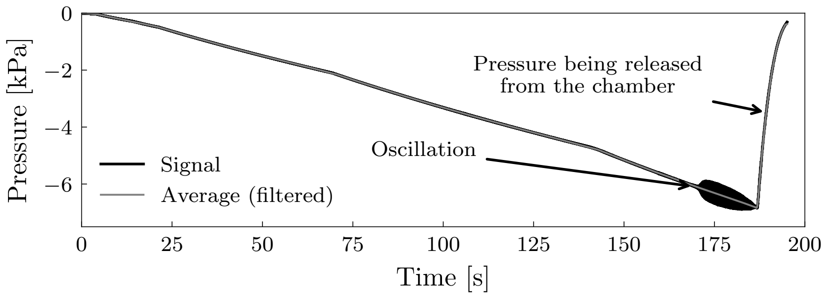

Source – Author.

In interpreting the figure, it should be remembered that the pressure sensor measures the pressure inside the rigid outlet tube in relation to the pressure in the chamber. Therefore, as the pressure in the chamber increases, so does the reference pressure. Therefore, the measured pressure decreases with time.

Furthermore, when oscillations occur, they are seen as fluctuations around a mean value that is continuously decreasing. In order to extract this mean pressure, the raw signal was zero-phase filtered with a Butterworth, fourth order, low-pass filter with a cutoff frequency of 1 Hz. The filtered signal was then subtracted from the raw signal to obtain only the pressure fluctuations (Figure 75). The fluctuations were zero-phase filtered with a low-pass, second order, Bessel filter with cutoff frequency of 2 kHz.

The upper envelope of the pressure fluctuations was then obtained. A rolling window of size of 48 samples was used, and the maximum value in each rolling window was used as the value for the envelope. Since the envelope thus obtained has a “staircase” behavior (as shown in the inset of Figure 75), high values of the derivative may be observed not only due to a general growth of the oscillation amplitude, but also due to a relatively large, but very quick and fleeting, change in the envelope.

Figure 75 – Pressure fluctuations and envelope.

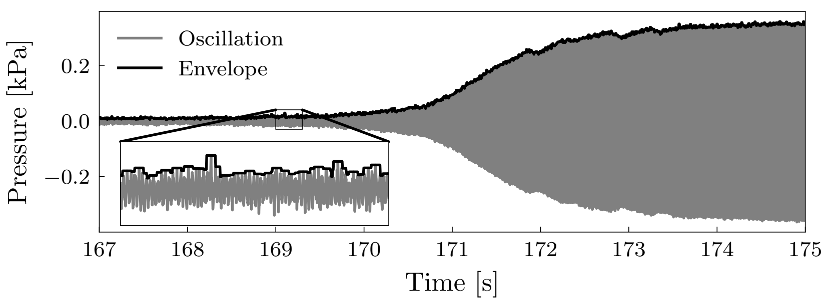

Source – Author.

Since these brief changes in the envelope do not represent amplitude growth, the envelope was smoothed by a fourth order Butterworth low-pass filter, with cutoff frequency of 5 Hz. The derivative of the smoothed envelope was then calculated using second order, centered, finite differences.

Figure 76 – Maximum derivative of smoothed envelope.

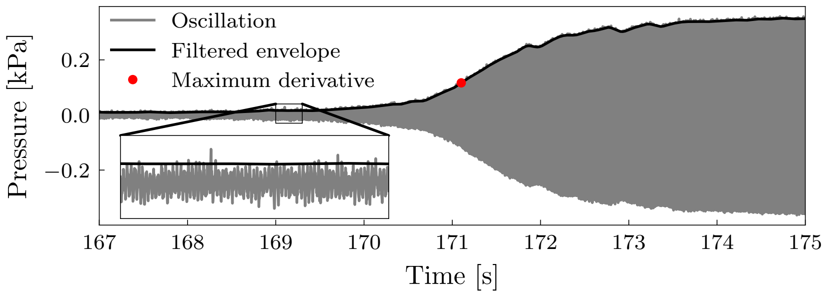

Source – Author.

After determining when the oscillation onset happens, the external pressure associated with this instant can be determined. The external pressure signal was also zero-phase filtered with a Butterworth, fourth order, low-pass filter with a cutoff frequency of 1 Hz, and the pressure associated with the onset was identified. The flow rate associated with this instant was also identified.

The same procedure was also used to determine the offset of self-sustained oscillations. The difference was that the maximum rate of decrease of the oscillation amplitude was used to characterize the threshold point.

The oscillation frequency at onset is also a quantity of interest. One second of the signal was separated, starting from the onset point, and the fundamental frequency in this second of measurement was calculated in two different ways: by the average number of zero crossings, and by a Fast Fourier Transform (FFT). The two estimates were made because the oscillation frequency often changed as the pressure in the chamber increased. If a considerable change occurs within 1 second, the two estimates will likely differ from one another. In this case, signals of shorter lengths were used (0.5 s).

A similar procedure was used when the oscillation frequency for a given chamber pressure was desired. The only difference was when the frequency at 7 kPa was desired. In this case, a sample of 1 s of the signal before reaching 7 kPa was used.

4.4 Relationship to the parameters of the mathematical model

In order to compare the mathematical model to the experiment, the relationship between properties of the experimental setup, and dimensional parameters of the model need to be established.

The lengths a, l, l_1, and l_2 can be determined from the dimensions of the rigid tubes (Subsection 4.1.2). Therefore, $a = 17\,\text{mm}$, $l = 50\,\text{mm}$, $l_1 = 181\,\text{mm}$, and $l_2 = 300\,\text{mm}$. The external pressure $\bar{p}_e$ will be directly related to the pressure in the chamber. Air properties are once again considered to be $\rho = 1.2\,\text{kg/m}^3$ and $\nu = 1.5\,(10^{-5})\,\text{m}^2/\text{s}$.

The relationship between other variables is not as direct, since one is comparing the three-dimensional experiment to the two-dimensional collapsible channel. Approximations have to be made. These will be similar to the ones used when determining appropriate values to represent TE phonation (Section 3.3).

The mass per unit area m, may be determined by estimating the density of the tube from its total mass and dimensions (Section 4.1.4), and multiplying by the thickness of the membrane. One obtains $m = 0.201\,\text{kg/m}^2$.

The mean inlet velocity U is considered to be the same as the mean inlet velocity associated with each flow rate considered. Since the value of a is known, these can be readily calculated for each flow rate that was considered (Section 4.2). The resulting velocities are: 0.352 m/s, 0.441 m/s, 0.529 m/s, 0.617 m/s, 0.705 m/s, 0.793 m/s, 0.881 m/s, 0.969 m/s, 1.06 m/s, 1.15 m/s, 1.23 m/s, and 1.32 m/s.

The dimensional membrane tension per unit breadth τ can be estimated by taking the average of the longitudinal force over the circumference of the flexible tube (Section 4.2). Considering the nominal values, the tensions are 4.11 N/m, 8.21 N/m, 12.3 N/m, 16.4 N/m, and 20.5 N/m.

Given these values, all dimensionless parameters (Section 3.3) may be calculated. Out of all of them, R, T, and $\bar{P}_e$ will change depending on the flow rate, longitudinal tension, and chamber pressure. The parameters M, and L_2; however, remain fixed. These were $M = 1.14$, and $L_2 = 6.00$.

4.5 Results

This section describes the results of the experimental model. In order to better organize the results, the section is divided in four subsections. Subsection 4.5.1 presents qualitative observations on the behavior of the tube. Subsection 4.5.2 presents the behavior of the tube for the longitudinal tensions of 0.025 kgf and 0.050 kgf. Subsection 4.5.3 presents results for the longitudinal tensions of 0.075 kgf, 0.100 kgf, and 0.125 kgf. The separation was made due to the fact that each group presented a general behavior for the onset of self-sustained oscillations that was different from the other. Finally, in Subsection 4.5.4, the analysis of the effect of the longitudinal tension is made, along with comparisons to the mathematical model.

4.5.1 Qualitative observations

Before discussing the results, it is worthwhile to briefly point out some qualitative aspects that were observed regarding the behavior of the flexible tube. As the pressure in the chamber increases, the tube closed with a four-lobed cross-section. This can be seen in Figure 77, which shows the closing of the tube viewed from the open end of the outlet.

Figure 77 – Cross-sections of the tube for increasing (from a to d) chamber pressures.

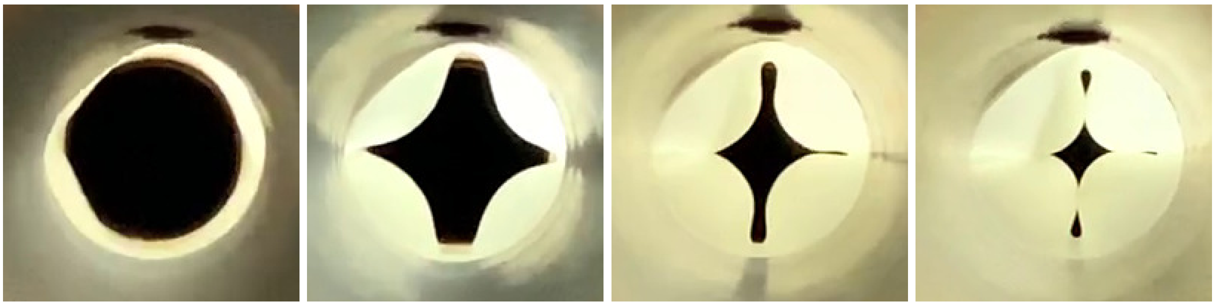

(a) (b) (c) (d)

Source – Author.

The cross-section of the tube is likely related to its buckling modes (Section 2.9). However, the longitudinal creases in the flexible tube (Figure 68b) certainly play a large role in determining the resulting shape for the cross-section.

With regard to TE speech, while the resemblance to endoscopic images is evident, neither van As, Tigges, et al. (1999) nor Arenaz Búa et al. (2017) report observing a four-lobed cross-section of the PES in their endoscopic studies. This is certainly not an indictment on the capacity of the experimental model to represent TE speech, since there could be laryngectomees whose PES closes in a four-lobed shape, but have not been part of these two studies. However, it highlights the need for a better understanding of the physiology of TE speech, in particular, what contributes the most in determining the shape of the cross-section of the PES.

These shapes were observed with and without airflow through the tube, but depending on the flow rate, self-sustained oscillations occurred. Also, while not shown in Figure 77, at even higher pressures than the one for Figure 77d, only a small opening remained, near the center of the tube (Figure 78).

Figure 79 also shows how the tube closes, but from a lateral view. In all instances, the flow rate was 140 ml/s, and there was no oscillation. The only difference between them was the pressure in the chamber.

In Figure 79a, the tube is closed the most near its center. The top and bottom contours of the tube in the figure also suggest that the constriction is not sharp. As the pressure increases to 2.6 kPa, in Figure 79b, the tube has closed more, and the point of minimum area has moved downstream in relation to Figure 79a. The constriction seems

Figure 78 – Flexible tube near complete occlusion.

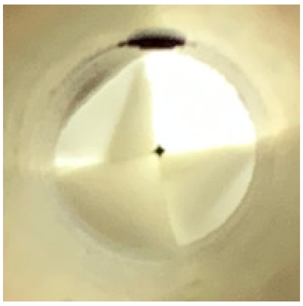

Source – Author.

Figure 79 – Side view of the flexible tube for increasing (from a to c) chamber pressures.

(a) 1.0 kPa. (b) 2.6 kPa. (c) 5.6 kPa.

Source – Author.

narrower and even further downstream for the pressure of 5.6 kPa (Figure 79c).

Overall, the figure illustrates a behavior that is typical of collapsible tubes, and which was also observed in the mathematical model of Chapter 3: for low external pressures the tube collapses near its center, and as the pressure increases, the constriction moves downstream. This behavior was observed throughout the experiment. Unlike the mathematical model, and unlike the CT scans of Figures 40 and 41, inflation of the most upstream part of the membrane was not observed.

4.5.2 Tensions of 0.025 kgf and 0.050 kgf

Results for the longitudinal tension of 0.025 kgf will be considered first. For the lowest flow rates considered, 80 ml/s and 100 ml/s, there were no self-sustained oscillations as the pressure in the chamber was increased up to 7 kPa. Oscillations first occurred for a flow rate of 120 ml/s, and a pressure of 6.34 kPa in the chamber[3]. These oscillations were roughly sinusoidal (Figure 80), with a fundamental frequency of 233 Hz at onset, and only a second harmonic present.

The amplitude of the oscillations shown in Figure 80 decreased as the pressure in the chamber approached 7 kPa (see Figure 74). Since higher pressures would exceed the range of the pressure sensor used, it was not assessed whether the oscillations would stop completely for higher pressures, or would be maintained with a smaller amplitude.

[3] The pressure downstream of the flexible tube, p_2, for this flow rate has already been shown in Figure 74.

Figure 80 – Pressure fluctuations in the time domain (a), and frequency domain (b), for $Q_v = 120\,\mathrm{ml/s}$, $\bar{p}_e = 6.34\,\mathrm{kPa}$, and tension of 0.025 kgf.

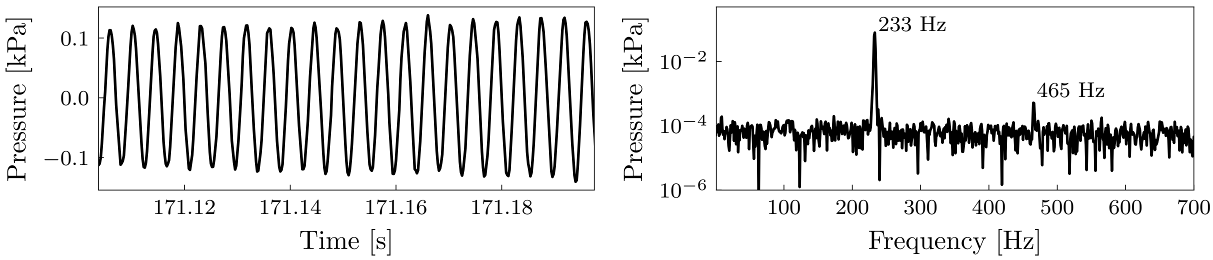

(a) Time domain. (b) Frequency domain.

Source – Author.

For flow rates of 140 ml/s up to 200 ml/s, the tube behaved similarly to what is described above. The main difference was that the threshold pressure decreased as the flow rate increased, and the oscillation frequency decreased as well. These two points will be further discussed shortly in the present section. It is also worth pointing out that the spectrum of the pressure fluctuations for the different flow rates also changed, with additional harmonics appearing in comparison to Figure 80b.

For a flow rate of 220 ml/s the behavior changed considerably. Oscillations began for a much lower external pressure (1.14 kPa), and the fundamental frequency at oscillation onset was also considerably smaller (131 Hz). Figure 81 shows the oscillation shortly after the onset.

Figure 81 – Pressure fluctuations in the time domain (a), and frequency domain (b), for $Q_v = 220\,\mathrm{ml/s}$, $\bar{p}_e = 1.14\,\mathrm{kPa}$, and tension of 0.025 kgf.

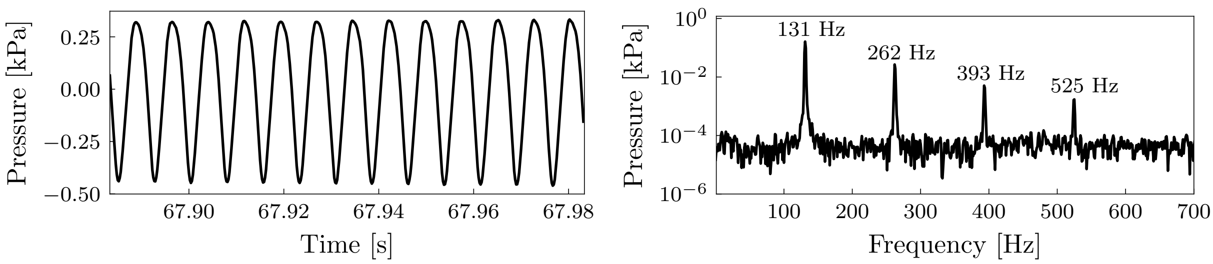

(a) Time domain. (b) Frequency domain.

Source – Author.

Unlike what happened for lower flow rates, the waveform changed continuously as the pressure in the chamber was increased. This is illustrated in Figure 82, which shows the pressure fluctuations downstream of the flexible tube for the flow rate of 220 ml/s.

The fluctuations right after onset are roughly sinusoidal, but with the trough being sharper than the crest. The waveform changes until a small oscillation is seen at the crest (see the frame for $t = 167\,\mathrm{s}$). As $\bar{p}_e$ continues to increase, the waveform returns to being

Figure 82 – Pressure fluctuations for a flow rate of 220 ml/s and tension of 0.025 kgf.

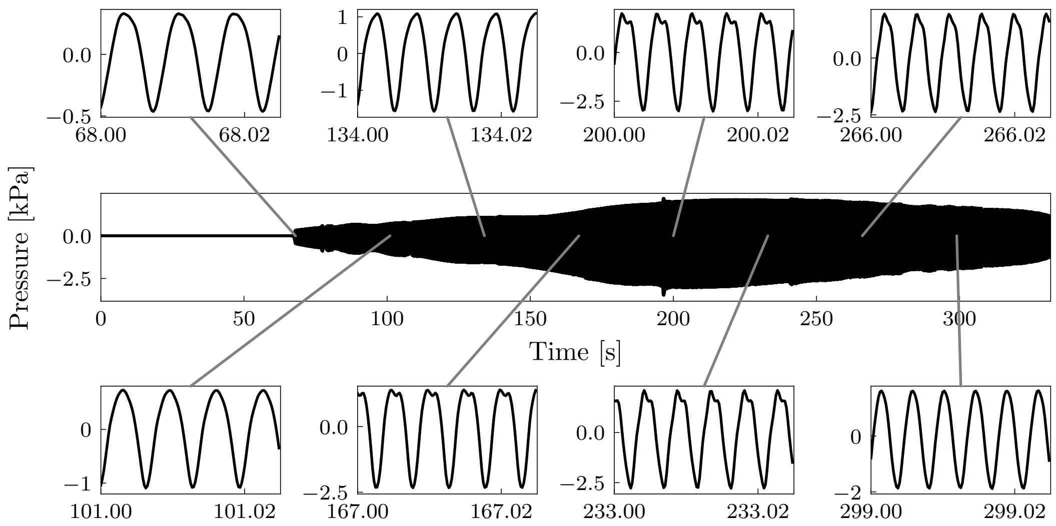

Source – Author.

very similar to the oscillations observed for the flow rates of 120–200 ml/s (Figure 80), even in frequency, since the frequency increased continuously with the pressure in the chamber.

The same general behavior shown for the flow rate of 220 ml/s was observed for higher flow rates; however, the changes in the waveform became more pronounced. This is illustrated in Figure 83, which shows the pressure fluctuations for a flow rate of 300 ml/s.

Figure 83 – Pressure fluctuations for a flow rate of 300 ml/s and tension of 0.025 kgf.

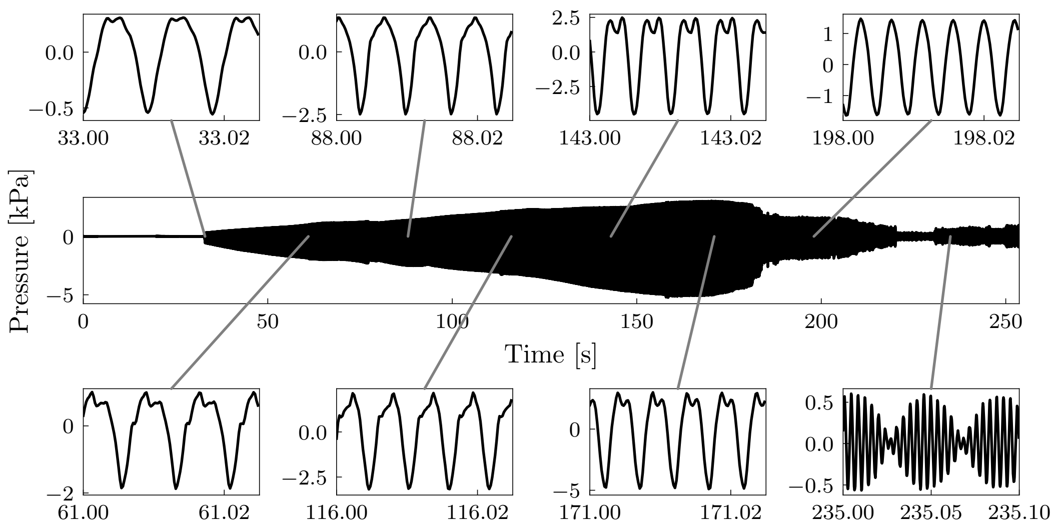

Source – Author.

*Note that the zoomed frame for the oscillations at 235 s is not in the same scale as the others.

Figure 83 also illustrates an additional point that was observed only for flow rates of 280 ml/s and 300 ml/s. In these two cases, as the pressure in the chamber neared 7 kPa, the oscillations became much like an amplitude modulated signal. The sound produced is that of the pitched tone of the "carrier signal" being heard alongside a stream of quick successive bursts associated with the oscillatory envelope. It is not believed that this type of behavior is entirely analogous to the one McIvor et al. (1990) described for TE speech failure, with the air being released in "sudden explosive bursts", but perhaps further increases in pressure would eventually lead the system towards that.

Should the phenomenon be related with hypertonicity, the fact that it occurred only for the highest flow rates tested may lead one to the counter-intuitive hypothesis that if a hypertonic laryngectomee were to exhale the air at a lower flow rate, phonation would be more likely. The reason is that in the experiment, for the same longitudinal tension and chamber pressure, smaller flow rates lead to a pitched sound without the presence of the amplitude modulation (as seen in Figure 82, for example). This could be further indication that the phenomenon is not analogous to failure in TE phonation; however, there is also another possibility. It is quite likely that for pressures higher than 7 kPa, these amplitude modulated oscillations would happen at lower flow rates as well. It might occur that for some sufficiently high pressure, any flow rate would lead to this type of behavior. In this case, a pitched tone that could be associated with phonation would not be possible, regardless of the flow rate. Laryngectomees with hypertonicity could fit this description. On the other hand, laryngectomees with a PES of high tonicity, but where certain flow rates would be conductive to speech, could eventually learn to regulate the exhaled air in a way that allows them to speak. Evidently, this is mere conjecture and further research is necessary.

In Figures 82 and 83 it was seen that the oscillation frequency increases with the pressure in the chamber. This can be better visualized (albeit indirectly) with a spectrogram. Figure 84 shows the spectrograms for the flow rates for which self-sustained oscillations were observed[4].

For flow rates up to 200 ml/s, it is seen that there is a faint curve which then grows strong near the end of the signal, where the frequency is nearly constant. As mentioned before, for these flow rates self-sustained oscillations were identified only for $\bar{p}_e$ near 7 kPa, which would correspond to the higher intensity part of the curve near the end of the measurement. Figure 85 shows the pressure fluctuations in time, as well as the spectrogram for a flow rate of 200 ml/s to better illustrate what happens in the region where the faint curve appears.

While oscillations do occur, their amplitude never grew considerably over the background noise, and were not noticed during measurement. Therefore, they were not considered to be self-sustained oscillations.

One possible explanation for this is that it reflects the change in the real part of the eigenvalue of an oscillatory mode of the system. In this interpretation, the entire

[4] The sudden drop in frequency towards the very end of the signal in some of the spectrograms is due to the pressure in the chamber being released at the end of the measurement.

Figure 84 – Spectrograms for a longitudinal tension of 0.025 kgf.

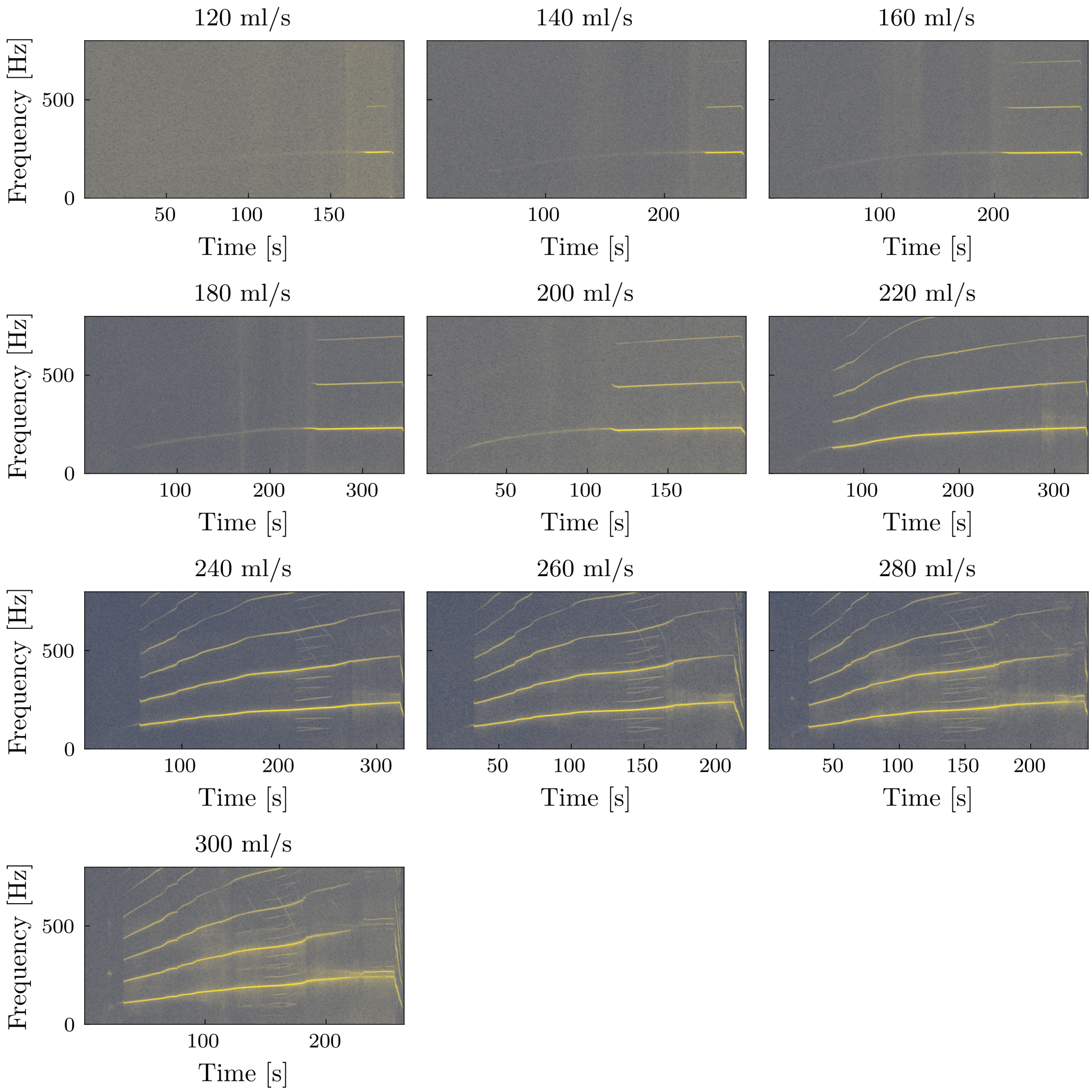

Source – Author.

fundamental frequency curve relates to the same mode of the system. In the region where the curve is faint, the real part of the eigenvalue of this mode would be negative. Any disturbance of the system from steady-state (which continuously occurs, specially since $\bar{p}_e$ is increasing) results in oscillations of the tube. However, since the real part of the eigenvalue is negative, the oscillations are damped and the amplitude never grows sufficiently to make the oscillations more than barely noticeable. Only when the real part turns positive does the amplitude grows, and full-fledged self-sustained oscillations are observed. A second possibility is that these small oscillations result from the acoustic excitation of the conduit composed of rigid inlet tube, flexible tube, and rigid outlet tube.

The spectrograms of Figure 84 show that for flow rates between 120 ml/s and 200 ml/s, self-sustained oscillations occur with an oscillation frequency of roughly 220 Hz that remains nearly constant as the pressure is increased. At a flow rate of 220 ml/s, the

Figure 85 – Pressure fluctuations and spectrogram for a flow rate of 200 ml/s and tension of 0.025 kgf.

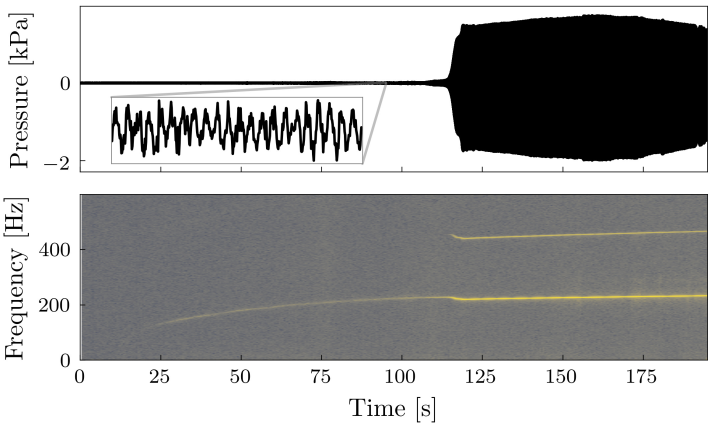

Source – Author.

differences in the behavior of the system that were mentioned previously are seen once again. The onset of oscillations happens much sooner, and now the frequency increases considerably as the pressure in the chamber is increased.

For 240 ml/s, the spectrogram shows a region, between 200 s and 300 s, where several peaks of smaller amplitudes, appear in the spectrum, between the peaks of the harmonics, which are present throughout the self-oscillating behavior. This same behavior also occurs for higher flow rates. Figure 86 shows the pressure fluctuation for this region in the case of a flow rate of 260 ml/s.

Figure 86 – Pressure fluctuations in the time domain (a), and frequency domain (b), for $Q_v = 260\,\text{ml/s}$, $\bar{p}_e = 4.42\,\text{kPa}$, and tension of 0.025 kgf.

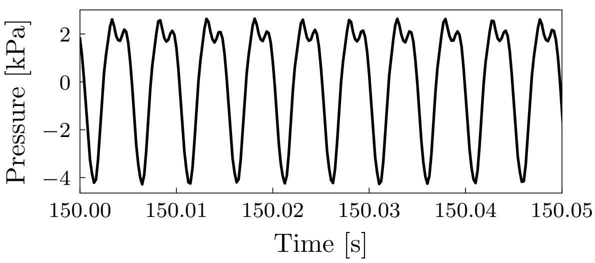

(a) Time domain.

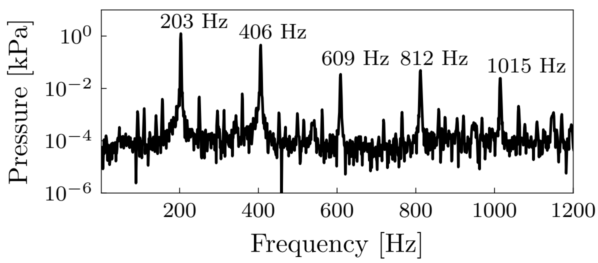

(b) Frequency domain.

Source – Author.

Figure 84 also provides additional information on the nature of the amplitude modulated signal of Figure 83. It is seen that for 280 ml/s and 300 ml/s, near the release of the pressure in the chamber, there are two reasonably close frequencies, which suggests the occurrence of a beat phenomenon that would indeed lead to the amplitude modulated signal. Figure 87 shows the pressure fluctuations for a flow rate of 300 ml/s, and pressure of 6.54 kPa.

Figure 87 – Pressure fluctuations in the time domain (a), and frequency domain (b), for $Q_v = 300\,\text{ml/s}$, $\bar{p}_e = 6.54\,\text{kPa}$, and tension of 0.025 kgf.

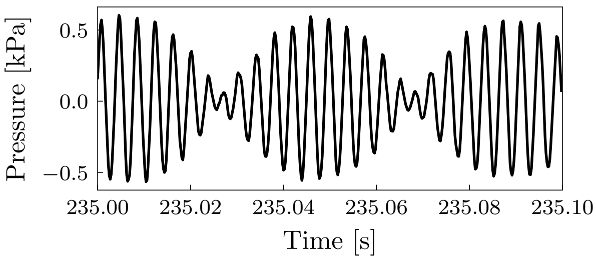

(a) Time domain.

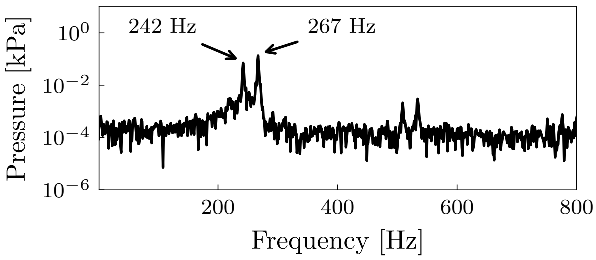

(b) Frequency domain.

Source – Author.

For the case of Figure 87, the beat frequency is 25 Hz. Should the two frequencies be closer together, the beat frequency would be smaller. In this case, perhaps, the air could appear to be released in sudden bursts, as described by McIvor et al. (1990) for failure in phonation due to excessive tonicity.

Three additional points on this matter are worth making. The first is that for the flow rate of 300 ml/s and very high pressures, three close frequencies appeared in the spectrum (Figure 88).

Figure 88 – Pressure fluctuations in the time domain (a), and frequency domain (b), for $Q_v = 300\,\text{ml/s}$, $\bar{p}_e = 6.91\,\text{kPa}$, and tension of 0.025 kgf.

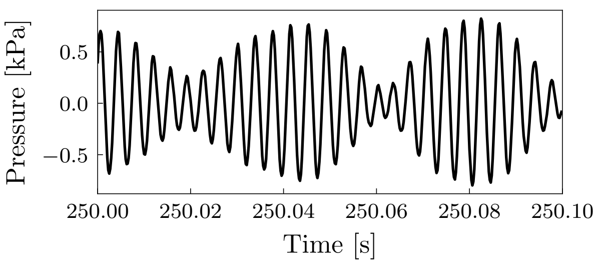

(a) Time domain.

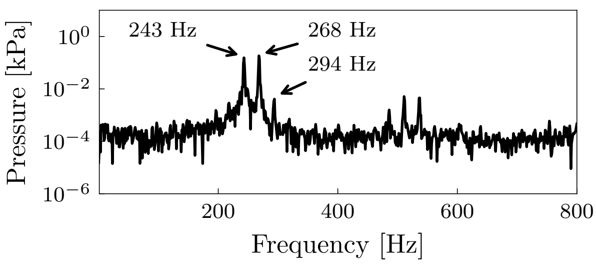

(b) Frequency domain.

Source – Author.

The second point is that, for a flow rate of 260 ml/s, while in the spectrogram of Figure 84 it appears that there is a second frequency near the fundamental one at 200 s, the peak is not well-formed, with a low amplitude (Figure 89). The occurrence of beats is not as prominent due to the large difference in amplitude between both peaks.

The third point is that the frequency of about 268 Hz that appears during the occurrence of beats is close to the acoustic natural frequency of the pipe downstream from the flexible tube. Since for high pressures, the flexible tube collapses and nearly closes the entire cross-section (Subsection 4.5.1), a rough estimate of this natural frequency may be obtained from the natural frequency of a one-dimensional pipe with one end closed

Figure 89 – Pressure fluctuations in the time domain (a), and frequency domain (b), for $Q_v = 260\,\text{ml/s}$, $\bar{p}_e = 6.76\,\text{kPa}$, and tension of 0.025 kgf.

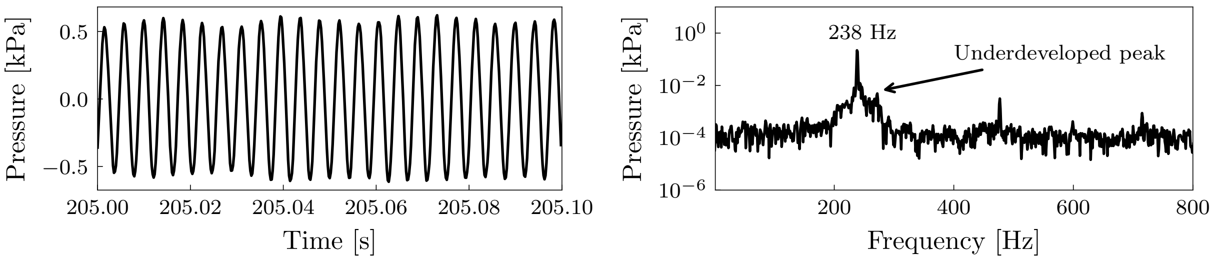

(a) Time domain. (b) Frequency domain.

Source – Author.

and the other opened. In this case, considering the length of 300 mm for the pipe, the first natural frequency would be of about 281 Hz[5]. Since the constriction does not happen exactly at one of the ends of the rigid tube, but further upstream (Figure 79), and since the “closed termination” is not rigid, the actual frequency could be low enough to be near the 268 Hz that appeared in the spectrum, or perhaps even lower.

If failure in phonation happens by an analogous process as in the experimental model here, and if the observed beats are in fact due to the natural frequencies of the rigid tube on the outlet, the acoustic natural frequencies of the vocal tract would play a considerable role in the process. This again raises the question of how good is the analogy between the beats that were observed here, and failure in TE phonation due to hypertonicity. Unfortunately, no recordings of laryngectomees with a hypertonic PES attempting speech have been found (nor were possible to make).

While the spectrograms show how the pressure in the chamber affects the oscillation frequency, it is also useful to compare the extremes—the onset frequency to the frequency at 7 kPa. The importance of this lies in assessing the degree to which tonicity may affect phonation frequency in TE speech. Table 7 shows the frequencies at the onset of self-sustained oscillations, and the frequency at the maximum pressure considered, 7 kPa. The pressure in the chamber associated with the onset of self-sustained oscillations, as well as the ratio between the frequency at 7 kPa and the frequency at onset are also shown. In the table, the flow rates from 120 ml/s to 200 ml/s are separated from those from 220 ml/s and above, since the onset of oscillation happened at a considerably higher pressure, as discussed above.

The table reinforces how little the frequencies change with the increase of the pressure in the chamber for the flow rates below 200 ml/s. It also indicates that for the flow rates of 220 ml/s and above, a change of nearly an octave, or above it, was achieved. It should be noted that, to achieve this change in frequency, the pressure in the chamber

[5] This frequency was estimated by $f = c/4l'_2$, where l'_2 takes into account the end correction for the tube: $l'_2 = l_2 + 0.3a$, with a being the internal diameter of the tube.

Table 7 – Oscillation frequencies for different flow rates, with longitudinal tension of 0.025 kgf.

Q_v [ml/s]	Onset $\bar{p}_e$ [kPa]	Onset f [Hz]	f at 7 kPa [Hz]	f ratio
120	6.34	233	235	1.01
140	6.01	231	234	1.01
160	5.64	230	232	1.01
180	5.31	227	232	1.02
200	4.73	223	233	1.04
220	1.14	131	234	1.79
240	1.01	121	236	1.95
260	0.93	116	239	2.06
280	0.85	112	270*	2.41
300	0.81	110	269*	2.45

* With the occurrence of beats.

had to change by about 6 kPa. Interpreting this result in the light of TE speech, it raises the question of whether changes in tonicity alone could be responsible for the frequency control of TE speakers. At the moment, it seems unlikely that a voluntary control of the tonicity of such magnitude is possible by a laryngectomee, and it is not even clear whether an individual is able to control tonicity at all during TE speech. The result also points to what is reported by Max, Steurs, and Bruyn (1996), Schindler et al. (2005), and Verkerke and Thomson (2014), who indicate that TE speakers have a limited control over phonation frequency.

Table 7 also seems to show a decrease in the onset frequency with the flow rate; however, this decrease is more likely to be associated with the decrease of the onset pressure in the chamber, since there was little variation in the frequencies for a chamber pressure of 7 kPa (except for when beats occurred).

Before concluding the discussion on the tension of 0.025 kgf, it is worth indicating that for flow rates of 280 ml/s and 300 ml/s, there was a brief high frequency oscillation (about 260 Hz for the flow rate of 280 ml/s) that occurred before the onset of self-sustained oscillations. This oscillation was audible, but died out rather quickly, and was not further explored. Figure 90 shows the pressure fluctuations, and indicates the region where this brief oscillation occurred.

The response of the tube for the tension of 0.050 kgf changed significantly when compared to the longitudinal tension of 0.025 kgf. The first difference was that self-sustained oscillations were first observed for the flow rate of 140 ml/s, and essentially at the upper limit for pressure in the chamber (at 6.99 kPa). Figure 91 shows the spectrograms for different flow rates tested.

Other easily noticeable differences are that there are no regions where peaks in the spectrum appear between the harmonics of the fundamental frequency. Beats were also

Figure 90 – Brief oscillation prior to self-sustained oscillations for a flow rate of 280 ml/s and tension of 0.025 kgf.

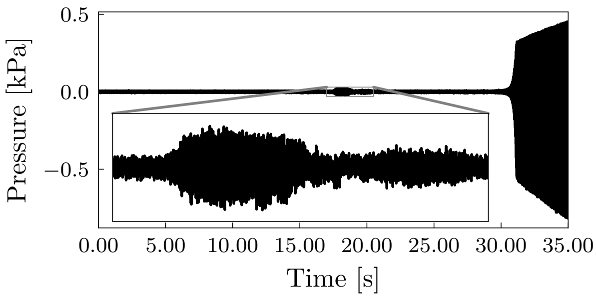

Source – Author.

Figure 91 – Spectrograms for a longitudinal tension near 0.050 kgf.

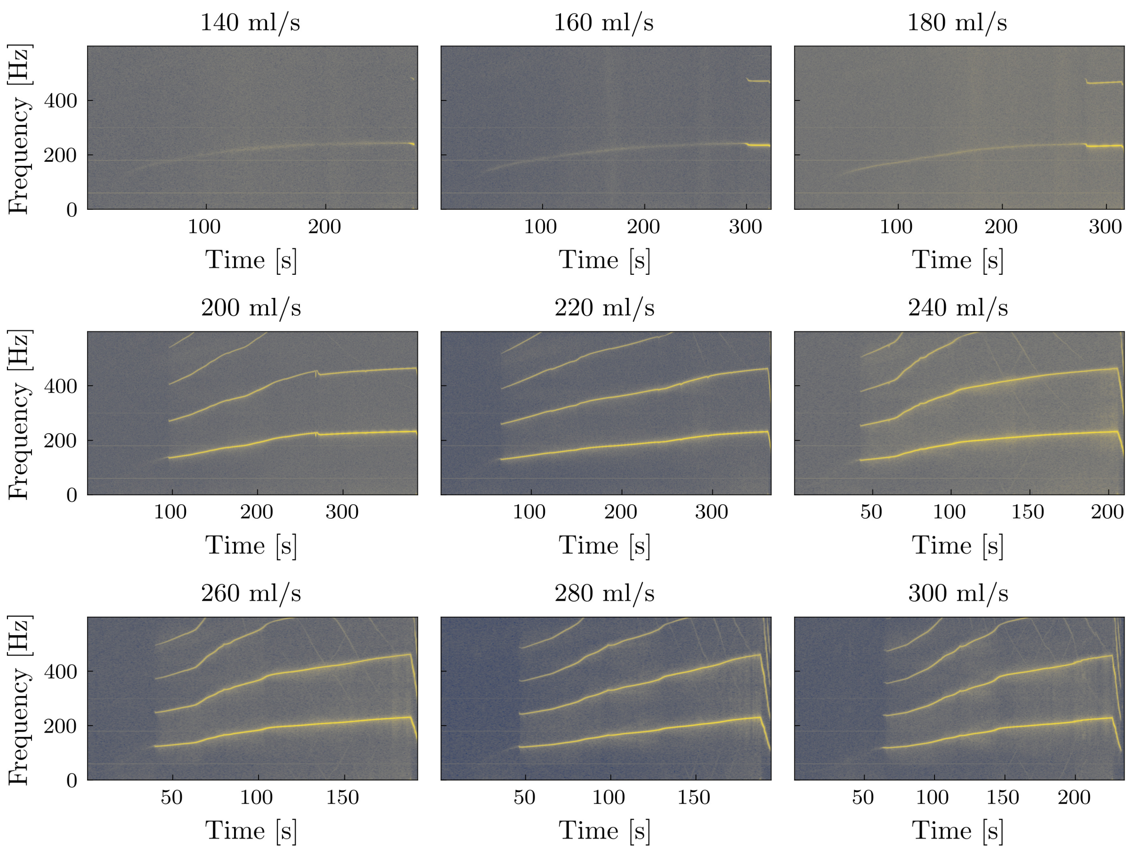

Source – Author.

not observed.

Some similarities to the spectrogram for the tension of 0.025 kgf are also evident. For the lowest flow rates, self-sustained oscillations occur for high pressures and with a relatively high oscillation frequency. At a given flow rate, the oscillations begin for much smaller pressures, and at a lower frequency as well. For this type of oscillation, the frequency increases with the pressure in the chamber.

For the flow rates of 140 ml/s up to 180 ml/s, where the onset happened at high chamber pressures, the oscillation is very similar to that shown in Figure 80. As was the case for the longitudinal tension of 0.025 kgf, for higher flow rates the waveform of the pressure fluctuations changed considerably as the pressure in the chamber was increased. Figure 92 illustrates this for the flow rate of 220 ml/s, while Figure 93 shows the case of 300 ml/s.

Figure 92 – Pressure fluctuations for a flow rate of 220 ml/s and tension of 0.050 kgf.

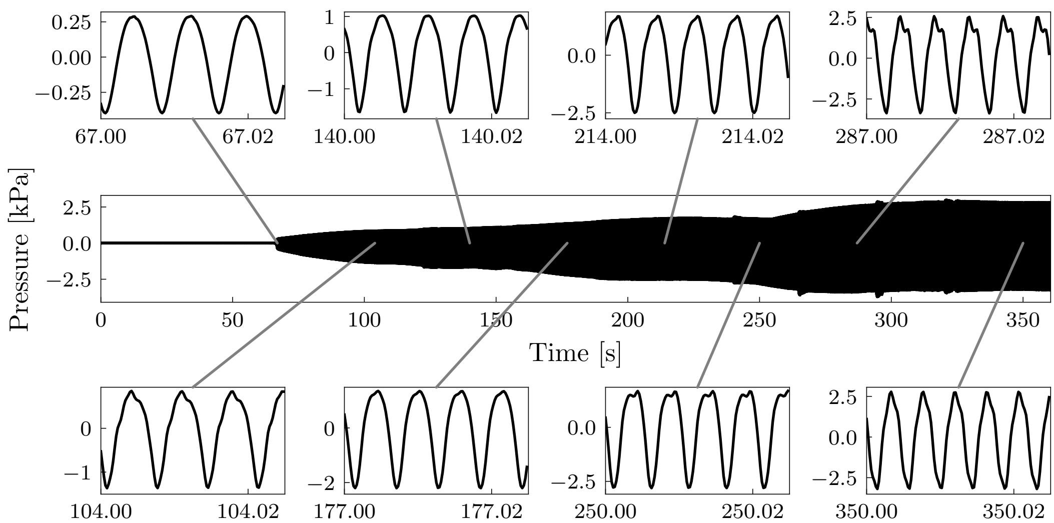

Source – Author.

Figure 93 – Pressure fluctuations for a flow rate of 300 ml/s and tension of 0.050 kgf.

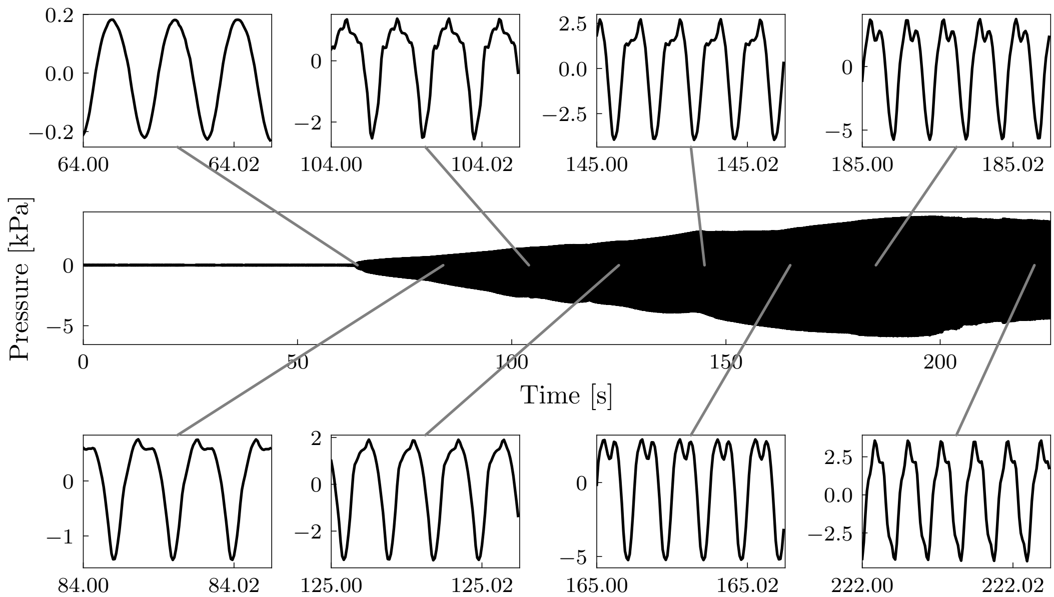

Source – Author.

Table 8 shows the pressure in the chamber at the onset of self-sustained oscillations, the frequency at onset, and the oscillation frequency at 7 kPa, for the longitudinal tension of 0.050 kgf.

Table 8 – Oscillation frequencies for different flow rates, with longitudinal tension of 0.050 kgf.

Q_v [ml/s]	Onset $\bar{p}_e$ [kPa]	Onset f [Hz]	f at 7 kPa [Hz]	f ratio
140	6.99	242	242	1.00
160	6.64	237	235	0.99
180	6.19	232	234	1.01
200	1.32	135	232	1.72
220	1.19	130	231	1.78
240	1.13	126	231	1.83
260	1.09	124	231	1.86
280	1.04	122	228	1.87
300	0.98	119	228	1.92

The table shows the same general pattern as observed for the longitudinal tension of 0.025 kgf (Table 7). The difference in the behavior for when the onset happened at high pressures or at low pressures is maintained, as is the general behavior of each case. However, the flow rate for which the behavior changed is not the same. The changes in frequency for the same flow rate were not as large as they were for the tension of 0.025 kgf—a change of an octave was not observed, for instance.

While already presented in Tables 7 and 8, the threshold $\bar{p}_e$ for each flow rate is shown in Figure 94. To aid visualization, dashed lines have been added connecting the points where a jump occurred, from an onset at high pressures to an onset at low pressures.

Figure 94 – Threshold $\bar{p}_e$ for each flow rate (tensions of 0.025 kgf and 0.050 kgf).

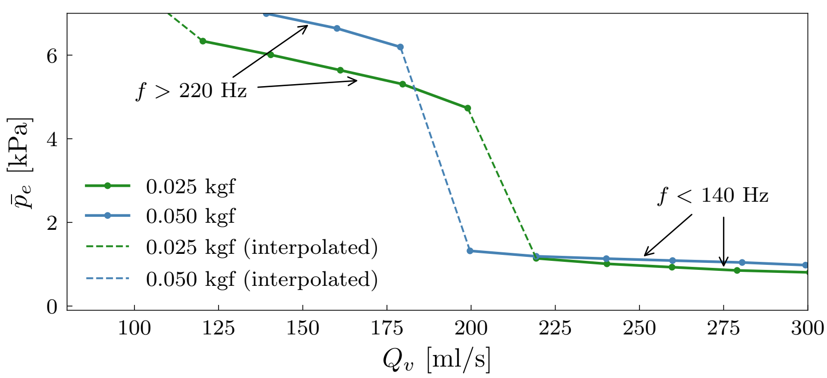

Source – Author.

The figure shows how the increase in longitudinal tension has generally increased the threshold $\bar{p}_e$, with the exception being the flow rate of 200 ml/s. In this case, there is a change in the flow rate for which the jump of high pressure onset to low pressure onset occurs. The reason for this jump is not clear. Thinking in terms of linear stability, the onset for the lower flow rates could be happening at a different mode than for the higher flow rates. The fact that the oscillation frequency barely changes for the lower flow rates is also indicative that different processes may be governing the oscillations in each case.

4.5.3 Tensions of 0.075 kgf, 0.100 kgf, and 0.125 kgf

The overall behavior of the system was essentially the same for the longitudinal tensions of 0.075 kgf, 0.100 kgf, and 0.125 kgf. Unlike what was observed for the lower tensions, the onset of oscillations was never near 7 kPa, nor it took place with high oscillation frequencies (close to 220 Hz). Also, for these tensions, self-sustained oscillations happened only for flow rates of 160 ml/s and above.

Another considerable difference was that the offset of self-sustained oscillations was observed as the pressure in the chamber increased (Figure 95). For all three longitudinal tensions considered in this subsection, this behavior happened only for a flow rate of 160 ml/s.

Figure 95 – Pressure downstream of the flexible tube for a tension of 0.125 kgf, and a flow rate of 160 ml/s.

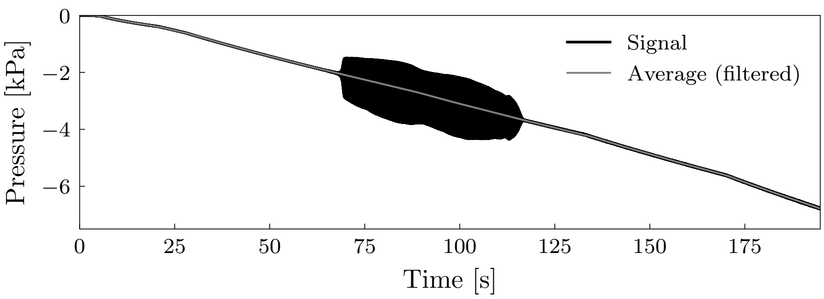

Source – Author.

It is believed that this behavior is not related to failure in phonation due to hypertonicity, since no description of failure happening with a continuous release of air has been found. While the lack of reports of this type of failure does not necessarily preclude the possibility of it happening, the offset of oscillations most likely indicates a limitation of the experimental model in representing TE speech.

Figure 96 shows the spectrograms for the longitudinal tension of 0.100 kgf. Although there were no self-sustained oscillations for the flow rate of 140 ml/s, the spectrogram associated with this flow rate is also shown, to indicate that the same faint curve that was observed in the spectrograms for the tensions of 0.025 kgf and 0.050 kgf also appears here.

In the spectrogram for the flow rate of 160 ml/s, the onset-offset of the self-sustained oscillations is visible. It is seen that self-oscillation happens along the faint curve that has been described above. This is similar to what was observed in the spectrograms of Figures 84 and 91, when self-sustained oscillations began only at higher pressures. The difference is that in those cases, self-sustained oscillations began near the end of the measured pressure range, and here they began and ended in the middle of it. For the

Figure 96 – Spectrograms for the longitudinal tension of 0.100 kgf.

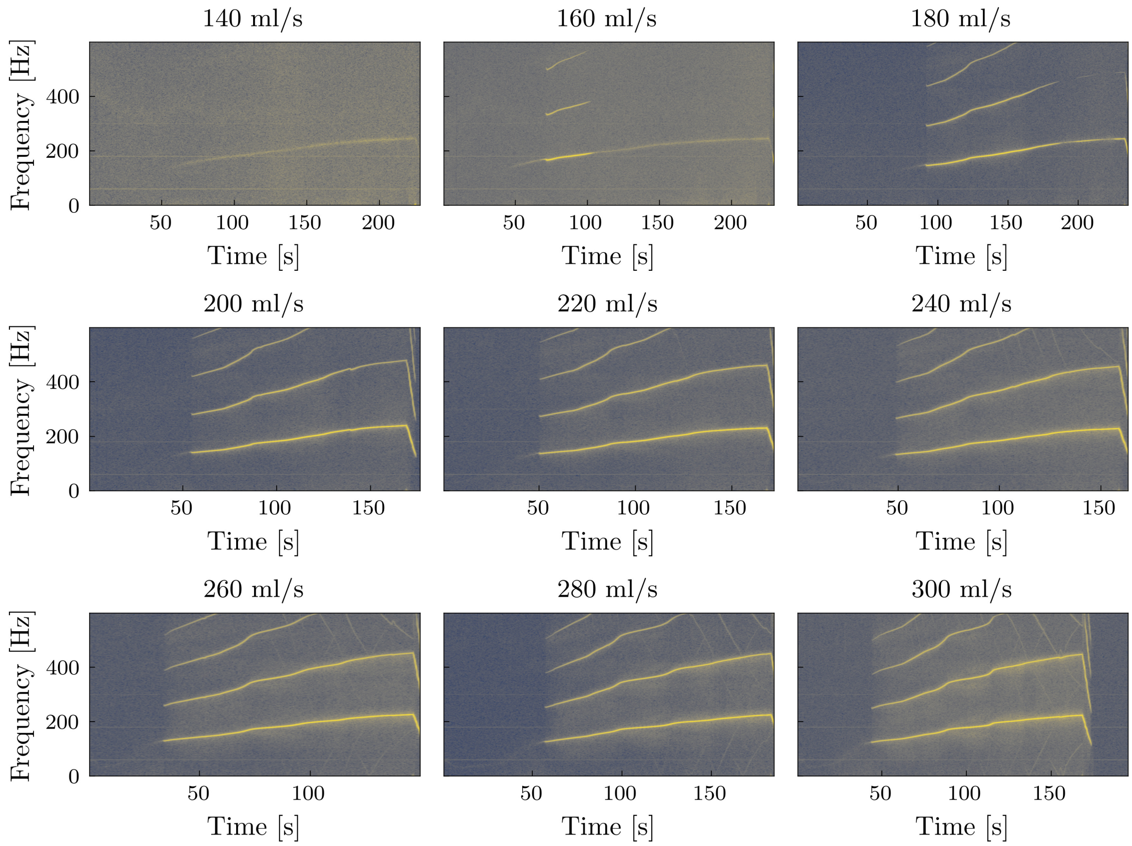

Source – Author.

longitudinal tensions of 0.075 kgf and 0.125 kgf, the behavior of this region was nearly the same.

With regard to the spectrograms for the other flow rates, there was no other substantial difference between the three longitudinal tensions, with one exception. In Figure 96, for the flow rate of 180 ml/s, it is seen that the amplitude of the curve associated with the fundamental frequency decreases considerably just before and just after 200 s. This is highlighted in Figure 97, which shows the pressure fluctuations and the flow rate (to indicate that there was no sudden drop in the flow rate) for this particular measurement.

Despite the noticeable drop in amplitude, the oscillations were still audible (notice there is a difference in amplitude in comparison to the region before the onset of self-oscillations), and it is considered that self-sustained oscillations were maintained.

Tables 9–11 show the onset pressures, the frequencies at onset, the offset pressure, the frequencies at offset, the frequencies at 7 kPa, and the ratio between the frequency at 7 kPa, and at onset, for the longitudinal tensions of 0.075 kgf, 0.100 kgf, and 0.125 kgf.

The tables show many similarities with those presented in Subsection 4.5.2. The threshold pressures decrease, as well as the oscillation frequencies, as the flow rate increases. The decrease in the frequency at the onset is likely related to the decrease of the threshold

Table 9 – Oscillation frequencies for different flow rates, with longitudinal tension of 0.075 kgf.

Q_v [ml/s]	Onset $\bar{p}_e$ [kPa]	Offset $\bar{p}_e$	Onset f [Hz]	Offset f	f at 7 kPa [Hz]	f ratio
160	2.29	3.11	169	191		1.13
180	1.58		142		233	1.64
200	1.43		137		230	1.68
220	1.37		133		228	1.71
240	1.29		129		226	1.75
260	1.21		125		225	1.80
280	1.16		123		224	1.82
300	1.11		120		221	1.84

Table 10 – Oscillation frequencies for different flow rates, with longitudinal tension of 0.100 kgf.

Q_v [ml/s]	Onset $\bar{p}_e$ [kPa]	Offset $\bar{p}_e$	Onset f [Hz]	Offset f	f at 7 kPa [Hz]	f ratio
160	2.30	3.12	166	189		1.14
180	1.70		146		244	1.67
200	1.55		140		239	1.71
220	1.47		137		230	1.68
240	1.39		133		228	1.71
260	1.32		130		226	1.74
280	1.25		127		225	1.77
300	1.22		125		223	1.78

Table 11 – Oscillation frequencies for different flow rates, with longitudinal tension of 0.125 kgf.

Q_v [ml/s]	Onset $\bar{p}_e$ [kPa]	Offset $\bar{p}_e$	Onset f [Hz]	Offset f	f at 7 kPa [Hz]	f ratio
160	2.14	3.75	158	198		1.25
180	1.83		147		241	1.66
200	1.69		142		237	1.68
220	1.58		138		232	1.67
240	1.47		133		228	1.71
260	1.41		130		226	1.74
280	1.36		128		223	1.76
300	1.32		126		221	1.77

Figure 97 – Decrease in amplitude for the tension of 0.100 kgf, and flow rate of 180 ml/s.

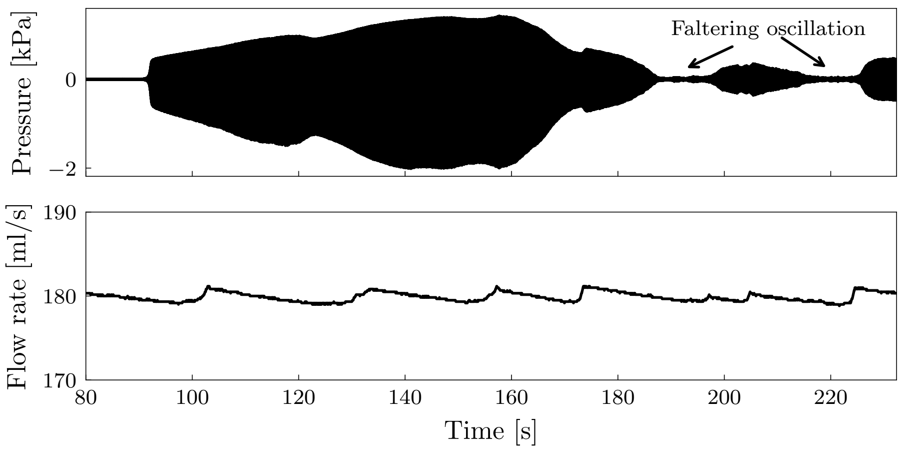

Source – Author.

pressure, as mentioned before. The decrease of the frequency at 7 kPa with the flow rate, while observed for all longitudinal tensions except 0.025 kgf, is not particularly large. In the three tables shown in this subsection, the frequency at 7 kPa for 180 ml/s was at most 9.4% larger than the frequency for 300 ml/s. These changes were far smaller than those induced by the increase of the pressure in the chamber[6]. This suggests that in TE speech, while changes in flow rate may affect the phonation frequency, it is unlikely that these are significant enough to function as a means to control the phonation frequency.

Figure 98 shows the thresholds for the longitudinal tensions of 0.075 kgf, 0.100 kgf, and 0.125 kgf. Additionally, for comparison, the thresholds for the tensions of 0.025 kgf, and 0.050 kgf were also added when they occurred for low pressures.

Figure 98 – Threshold $\bar{p}_e$ for each flow rate.

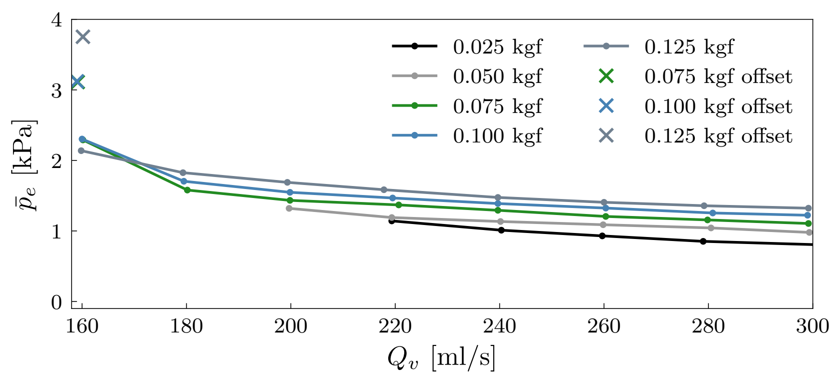

Source – Author.

For high flow rates, the curves follow a well-defined pattern—an increase in the flow rate leads to a decrease in the threshold $\bar{p}_e$, and decreases in the longitudinal tension also

[6] Note that proportionately the changes in pressure were larger than those of the flow rate. However, changes in flow rate during TE speech are not likely to be much larger than the ones considered here. The magnitude of the changes of tonicity in TE speech is not known.

reduce the threshold. For lower flow rates, the pattern is not clear. As already mentioned, for the tensions of 0.075 kgf, 0.100 kgf, and 0.125 kgf, at a flow rate 160 ml/s oscillation offset occurs, and no clear pattern is seen between the longitudinal tension and the threshold $\bar{p}_e$.

4.5.4 Effect of longitudinal tension

The results from the experimental model have already been presented in the previous two subsections; however, it is worthwhile to attempt to highlight the role played by longitudinal tension. This is done in the present subsection.

Figure 99 shows the threshold $\bar{p}_e$ for the onset of the self-sustained oscillations for different longitudinal tensions. The thresholds have been separated into two parts—one for when the onset happened at low pressures (Figure 99a), and the other for when the onset happened at high pressures (Figure 99b).

Figure 99 – Threshold $\bar{p}_e$ for different longitudinal tensions.

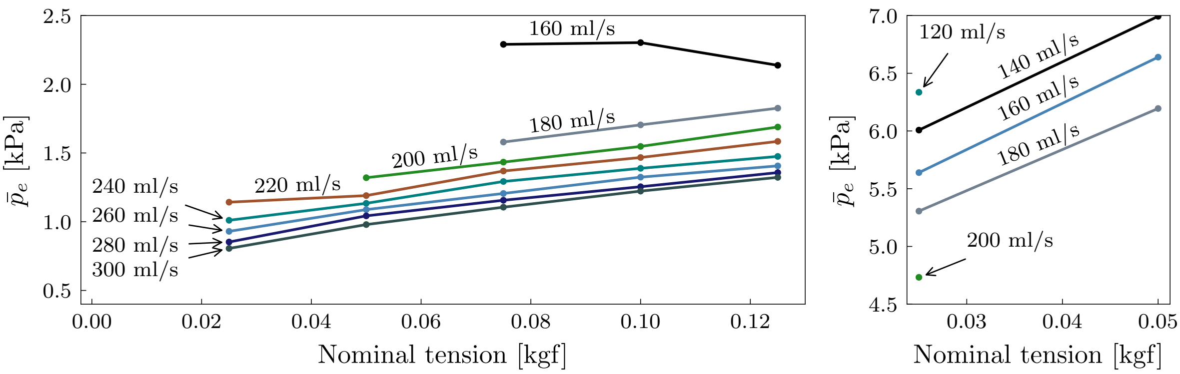

(a) Low pressure onset. (b) High pressure onset.

The figure shows that, for nearly all the flow rates considered, an increase in the longitudinal tension is associated with an increase in the threshold $\bar{p}_e$. The exception to this is the flow rate of 160 ml/s, for the onset at low pressures. The reason for this difference is not clear, and would likely require further investigations. It could simply reflect a change in the dynamic behavior of the system, and the difference in behavior for this particular flow rate was evident (recall that for this flow rate, the self-sustained oscillations actually stopped as $\bar{p}_e$ continued to be increased).

For the onset at low pressures, with the exception of the flow rate of 160 ml/s, the relationship between the two variables seems to be roughly linear, and as the flow rate increases, the threshold curves seem to be shifted down less and less. Such behavior seems analogous to what was observed for the mathematical model (Subsection 3.6.2). To verify this, the data may be plotted in terms of the dimensionless variables T, $\bar{P}_e$, and R. This is done in Figure 100.

Figure 100 – Threshold curves in the T–$\bar{P}_e$ plane.

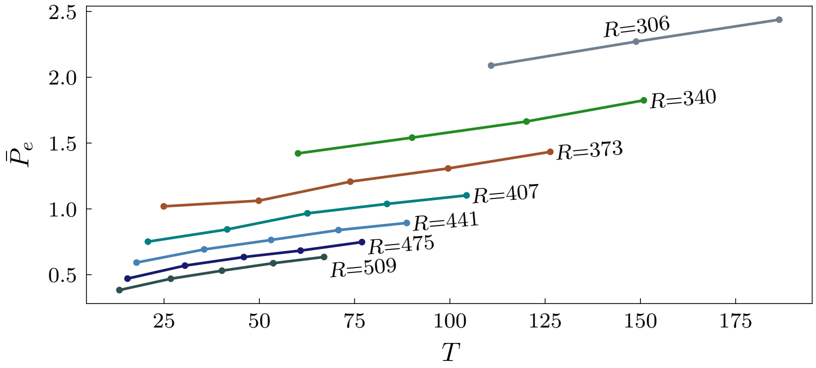

Source – Author.

The threshold curves are roughly straight lines (with nearly the same slope), which are shifted downwards as the modified Reynolds number R is increased. Also, as R increases, the curves seem to move by progressively smaller amounts. Therefore, the same general behavior of the mathematical model is observed here.

Two points regarding this need to be highlighted. First, the data for the flow rate of 160 ml/s (which results in $R = 272$) is not shown in Figure 100 and, as expected, the threshold curve is considerably different from the others (Figure 101a). The second point, illustrated in Figure 101b for high R, is the limitation on the measurement of the initial longitudinal tension[7]. The curves do not follow a perfectly linear behavior, and the large uncertainty in the measurement of the longitudinal tension hinders the interpretation of whether this is due to experimental uncertainty or the actual response of the system.

Figure 101 – Threshold $\bar{P}_e$ for different longitudinal tensions.

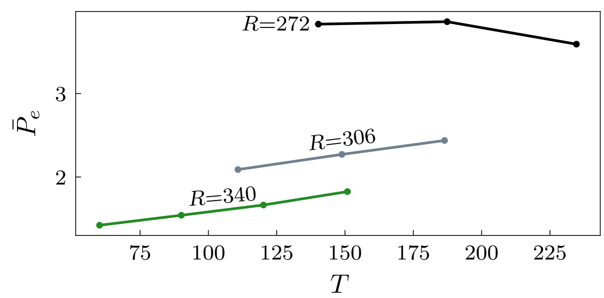

(a) Threshold for $R = 272$.

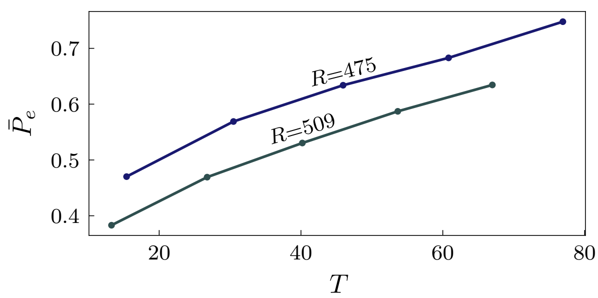

(b) Possible curvature for higher R.

Even though in the experiment, the behavior of the threshold curves is not nearly as accentuated as in the mathematical model, Figure 100 does seem to indicate that for higher flow rates, the threshold $\bar{p}_e$ might be roughly estimated by a relationship of the form of Equation (80), since a single straight line may be used for a rough approximation

[7] Recall that for each point along one of the curves, the entire stretching procedure of the flexible tube had to be performed (Section 4.2).

of the threshold in the T–$\bar{P}_e$ plane. This also adds credence to the possibility that the same type of relationship could hold for the case of hypotonicity in TE speech.

Given the differences in the parameters used for the experiment and those used for the simulations of Subsection 3.6 (including a different external pressure distribution), it is useful to provide a comparison for simulations that make use of parameters that are equivalent to those used in the experiment. This is shown in Figure 102, which provides a comparison between the neutral stability curve obtained with the mathematical model, and the one obtained experimentally for the flow rate of 200 ml/s.

Figure 102 – Comparison of threshold curves obtained with the mathematical and experimental models for the flow rate of 200 ml/s.

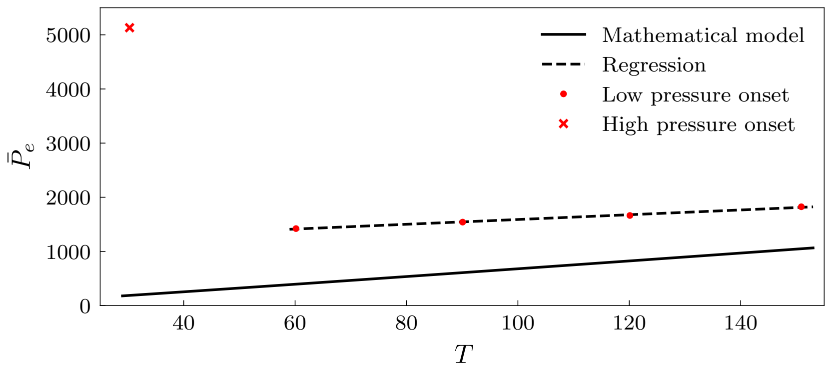

Source – Author.

For the low pressure onset, while the experimental data suggests a linear threshold curve, much like the mathematical model, the curve is significantly different. For $T = 60.2$ the thresholds are different by a factor of 3.59 (the largest besides the high pressure onset). Additionally, while both curves show a positive slope, the slope for the mathematical model is clearly larger than the one suggested by the experiments. Furthermore, the mathematical model does not predict the high pressure onset.

Given the several simplifications made in the mathematical model (Section 3.5), and the fact that the experiment was designed to approximate the PES, not to satisfy the assumptions of the model, these differences are not that surprising.

Another comparison that can be made between the experiment and the mathematical model is between the frequency at the onset of self-sustained oscillations. Figure 103 provides this comparison for the measurements with a flow rate of 200 ml/s.

The figure shows another discrepancy between the mathematical and experimental models, with the difference in frequency reaching nearly 100% for $T = 151$. While in the figure, the experimental frequencies do not appear to increase, this is mostly a matter of scale. There is an increase, but it is far milder than the one observed for the mathematical model, with the difference between the frequencies for $T = 151$ and $T = 60.2$ being less then 10 Hz.

Figure 103 – Comparison of onset frequencies obtained with the mathematical and experimental models for the flow rate of 200 ml/s.

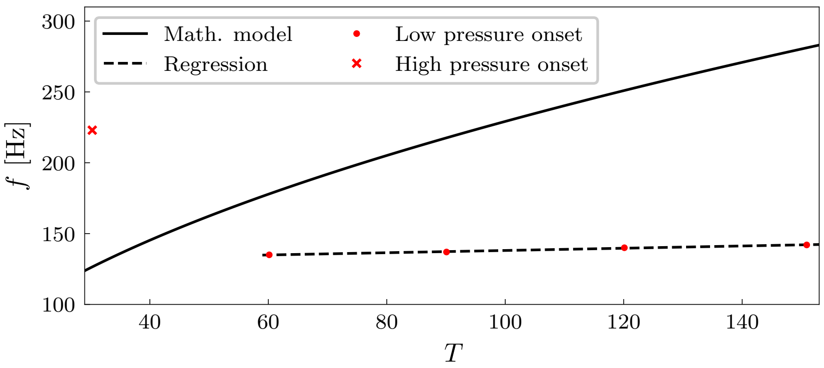

Source – Author.

One considerable difference between the mathematical model and the experiment that could lead to discrepancies is the acoustic effect of the rigid outlet tube (and, perhaps, of the chamber as well). While the fundamental frequency of oscillation of the flexible tube was near the estimated natural frequency of the outlet tube only for the lowest tension and with high flow rates (Section 4.5.2), the harmonics of the fundamental frequency are always present in the signal. How these affect the self-sustained oscillations when near a natural frequency of the outlet tube, is unclear at the moment, but could be further explored in future studies.

To provide a better representation of the changes in the onset frequency with the (dimensional) longitudinal tension, Figure 104 shows this relationship for all the flow rates that were measured.

Figure 104 – Frequencies at onset for different longitudinal tensions.

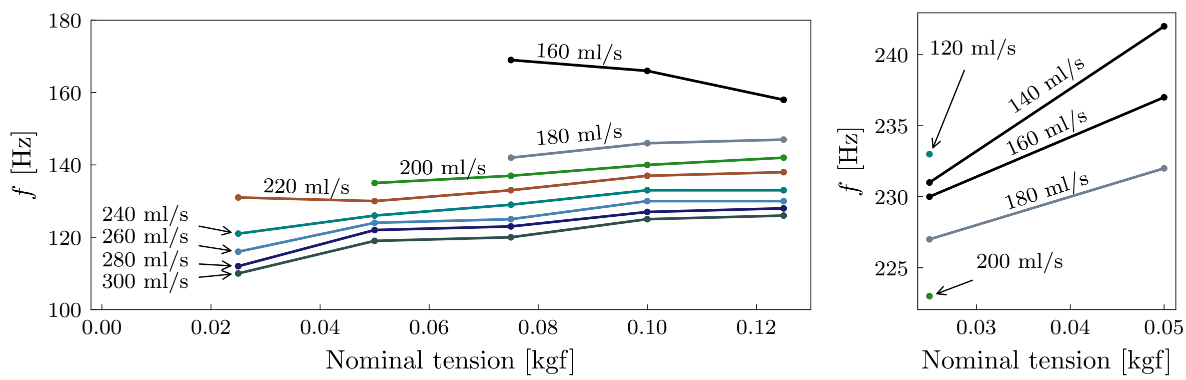

(a) Low pressure onset. (b) High pressure onset.

The figure highlights the behavior that had already been outlined by Tables 7–11. The frequencies at onset seem to increase with the longitudinal tension and decrease with the flow rate; however, it must be remembered that each combination of flow rate and longitudinal tension are associated with a specific value of the threshold $\bar{p}_e$. This threshold pressure should not be ignored in the interpretation of the correlations since, as pointed out previously, the decrease in the frequency at onset could actually result from a decrease in $\bar{p}_e$. It is also worth pointing out that once again the pattern for the flow rate of 160 ml/s is different from the rest in Figure 104a.

In general, interpreting the effect that the longitudinal tension has on oscillation frequency is not trivial. If one considers the oscillation frequencies for a fixed $\bar{p}_e$, and a fixed flow rate for different longitudinal tensions, the frequencies generally do not present a clear pattern, nor change remarkably (this can be seen for the frequencies for the chamber pressure of 7 kPa in Tables 7–11).

The variable that had the clearest impact in the oscillation frequency was $\bar{p}_e$—its increase for a fixed flow rate and fixed longitudinal tension lead to relatively large increases in the frequency. Interpreting this in the light of TE speech, this would suggest that phonation frequency is predominantly controlled by changes in tonicity. However, this point requires further investigation. It is not clear the degree to which a TE speaker is able to voluntarily control tonicity and, as mentioned previously, the changes in $\bar{p}_e$ that were required to change the frequency by about an octave seem large when interpreted in the context of tonicity. Furthermore, using an external pressure to model the tendency of the muscle layer to close the PES and a longitudinal tension to represent its possible stretching might be an oversimplification. The reasons behind this choice have been presented in Section 3.5. Overall, the discussion above reinforces the need for additional research on the physiology and mechanics of TE speech.

5 Conclusions

The present thesis studied the mechanics of TE speech. In particular, the focus was on the role played by muscle contraction on the self-sustained oscillations of the PES. The importance of this lies in the fact that the most commonly cited reason for failure in phonation is an excessive contraction of the musculature of the PES, called hypertonicity. The opposite, an insufficient amount of contraction, or hypotonicity, may also preclude phonation, but is not as common.

Several additional points in TE speech that relate to muscle contraction could be elucidated by further research. For the present work, the most significant is the fact that videofluoroscopic exams have suggested that the observed shape of the PES during phonation may be correlated with its tonicity. While there is one esophageal manometry study that corroborates this, no previous study has assessed the matter on the basis of the mechanics involved.

All of these issues were approached by the use of a mathematical model, and an experimental one. The first step towards the development of these models was a literature review, presented in Chapter 2, to provide the anatomical and physiological foundation for the subsequent work. While it cannot be said that the literature on TE speech is scarce (except for the literature on the mechanics of TE, which is indeed very scarce), many fundamental questions were left unanswered. For instance, the detailed workings of the inferior pharyngeal constrictor, cricopharyngeus, and cervical esophagus upon contraction were not described, and the question of whether additional muscles, capable of longitudinally stretching the PES, are active and significant during phonation has not been answered.

These missing pieces of information steered the development of the models towards a simplified representation, based on collapsible tubes, where tonicity is represented by an external pressure (to allow for comparison to esophageal manometry data).

The mathematical model is described in Chapter 3. It consisted of a collapsible channel and the simplified formulation of Stewart, Waters, and Jensen (2009) and Stewart (2017) was used. The mathematical model corroborates the link between the observed shape of the PES during phonation and its tonicity. Differences in the magnitude of the applied external pressure resulted in changes in the steady-state membrane configuration in essentially the same way as tonicities affect the shape of the PES during phonation. A quantitative comparison with CT scans has shown large differences. This was expected, given that the pressure distribution for each subject was not known. Furthermore, with the mathematical model, a simple relationship (Equation 80) for the minimum tonicity required for phonation was estimated.

The experimental model (Chapter 4) provided a complimentary approach to the mathematical model. The observed behavior of the system was complex, with considerable variation in the waveform of the oscillations. Also, for low flow rates some of the behaviors of the system, such as a jump from an onset of oscillations at high pressures to low pressures, and an oscillation offset as the pressure was increased, are still not fully understood. For higher flow rates, the measurements provide further corroboration of the simplified relationship for estimating the minimum tonicity that was suggested by the mathematical model. However, the experimental results also show that the mathematical model, as used here, is not accurate at predicting the threshold external pressure, nor the frequency at the onset of oscillations. Given the considerable simplifications involved in the model, these discrepancies were to be expected.

Further work could be used to clear up which simplification is having a strong impact in the behavior of the experimental model, but has been neglected in the mathematical one. One possibility is the acoustic effect of the outlet tube. This point is significant not only with regard to discrepancies between the mathematical model and the experimental one, but also in the effect of the vocal tract on TE speech. Different outlets could be used, including an anechoic termination, to assess the degree to which the acoustic coupling affects the self-sustained oscillations. Additionally, improvements could be made on the experimental model. Most notably, the measurement of the longitudinal tension.

The experimental results also highlight another question which is not answered in the literature on TE speech: by what mechanism does a TE speaker adjust the phonation frequency? In the experiments, the variable that was most clearly associated with changes in oscillation frequency was the external pressure; however, large changes in pressure had to be made for changes in frequency to be of the order of one octave or even less. Given that it is not known the degree to which PES tonicity may be changed at will, the results do not seem sufficient to definitively associate changes in tonicity with the control of the phonation frequency.

Even though hypertonicity is the most common cause for failure in TE phonation, it has not been thoroughly studied here. In the mathematical model, the analysis that would be required laid outside the scope of the present work. The full nonlinear equations may be tackled in future works, and a study on the dynamical behavior of the system can be made with the collapsible channel formulation of Stewart (2017). However, for such analysis, a lumped parameter model with few degrees of freedom might prove to be more useful as a first step. One then returns to the problem of how to relate the parameters of the model to physiologically meaningful values. In this sense, it seems unavoidable that experiments with excised PESs, and *in vivo* experiments with TE speakers would have to be conducted.

In the experimental model, the observation of beats in the oscillations for high external pressures and the lowest membrane tension, could be related with hypertonicity but that is certainly not clear at the moment. The use of a different pressure sensor with a higher upper pressure limit would allow for a systematic investigation of the effect. On the other hand, it is worthwhile to question whether the effort would be better spent by characterizing in precise terms the functioning of the muscles of the PES, since this would allow for the development of an experimental model that represents muscle contraction in a more accurate manner than the pressurized chamber used here. The same goes for the longitudinal stretching. It is possible for such stretching to occur by different anatomical structures, but this is not addressed in the literature, and it is not clear whether it is because such effect is judged to be insignificant (the present work suggests otherwise), or if it simply has not been explored yet. A deeper knowledge could inform the design of an improved tensioning mechanism, which was certainly one of the most challenging parts of the experimental model presented here.

Given how many small gaps still exist in the present knowledge on the physiology of TE speech, it seems more than desirable for future work on the mechanics of TE speech to be more closely related with the object of study itself, with greater use of excised parts, and *in vivo* experiments.

References

AGUIAR-RICZ, L. et al. Intraluminal Esophageal Pressures in Speaking Laryngectomees. **Annals of Otology, Rhinology & Laryngology**, v. 119, n. 11, p. 729–735, Nov. 2010. ISSN 0003-4894, 1943-572X. DOI: 10.1177/000348941011901115.

ARENAZ BÚA, B. et al. The Pharyngoesophageal Segment After Total Laryngectomy. **Annals of Otology, Rhinology & Laryngology**, v. 126, n. 2, p. 138–145, Feb. 2017. ISSN 0003-4894, 1943-572X. DOI: 10.1177/0003489416681321.

ASOH, R.; GOYAL, R. K. Manometry and electromyography of the upper esophageal sphincter in the opossum. **Gastroenterology**, v. 74, n. 3, p. 514–520, Mar. 1978. ISSN 00165085. DOI: 10.1016/0016-5085(78)90288-3.

ATOS MEDICAL. **Products**. [S.l.]: Atos Medical. Available from: https://www.atosmedical.com/product_category/laryngectomy-supplies-provox/. Visited on: 6 Mar. 2021.

ATOS MEDICAL. **Provox Vega**. [S.l.: s.n.]. Available from: https://www.atosmedical.com/product/voice-prosthesis-provox-vega/. Visited on: 17 Mar. 2021.

BAILLY, L.; HENRICH, N.; PELORSON, X. Vocal fold and ventricular fold vibration in period-doubling phonation: Physiological description and aerodynamic modeling. **J. Acoust. Soc. Am.**, v. 127, n. 5, p. 12, 2010.

BALM, A. et al. The indwelling voice prosthesis for speech rehabilitation after total laryngectomy: a safe approach. **Otolaryngologia Polska**, v. 65, n. 6, p. 402–409, Nov. 2011. ISSN 00306657. DOI: 10.1016/S0030-6657(11)70731-4.

BASSETT, D. L. **Larynx; medial aspect viewed from right side**. Stanford, CA: Lane Medical Library. Available from: https://lane.stanford.edu/biomed-resources/bassett/raw/bassettLargerView.html?t=largerView&bn=83-6. Visited on: 1 July 2021.

BASSETT, D. L. **Larynx; posterior surface view**. Stanford, CA: Lane Medical Library. Available from: https://lane.stanford.edu/biomed-resources/bassett/raw/bassettLargerView.html?t=largerView&bn=83-2. Visited on: 7 July 2021.

BASSETT, D. L. **Larynx; relation to oral cavity, oral and laryngeal parts of pharynx, left lateral view**. Stanford, CA: Lane Medical Library. Available from: https://lane.stanford.edu/biomed-resources/bassett/raw/bassettLargerView.html?t=largerView&bn=78-1. Visited on: 7 July 2021.

BELAFSKY, P. C.; KUHN, M. A. **The Clinician's Guide to Swallowing Fluoroscopy**. New York, NY: Springer New York, 2014. ISBN 978-1-4939-1108-0 978-1-4939-1109-7. DOI: 10.1007/978-1-4939-1109-7.

BERKE, G. S. et al. Experimental evidence in the *in vivo* canine for the collapsible tube model of phonation. **The Journal of the Acoustical Society of America**, v. 89, n. 3, p. 1358–1363, Mar. 1991. ISSN 0001-4966. DOI: 10.1121/1.400679.

BERTRAM, C. D. Experimental Studies of Collapsible Tubes. In: MOREAU, R.; CARPENTER, P. W.; PEDLEY, T. J. (Eds.). **Flow Past Highly Compliant Boundaries and in Collapsible Tubes**. Dordrecht: Springer Netherlands, 2003. v. 72. P. 51–65. ISBN 978-90-481-6235-2 978-94-017-0415-1. DOI: 10.1007/978-94-017-0415-1_3.

BERTRAM, C. The effects of wall thickness, axial strain and end proximity on the pressure-area relation of collapsible tubes. **Journal of Biomechanics**, v. 20, n. 9, p. 863–876, Jan. 1987. ISSN 00219290. DOI: 10.1016/0021-9290(87)90146-1.

BERTRAM, C. Two modes of instability in a thick-walled collapsible tube conveying a flow. **Journal of Biomechanics**, v. 15, n. 3, p. 223–224, Jan. 1982. ISSN 00219290. DOI: 10.1016/0021-9290(82)90255-X.

BERTRAM, C.; RAYMOND, C.; PEDLEY, T. Application of nonlinear dynamics concepts to the analysis of self-excited oscillations of a collapsible tube conveying a fluid. **Journal of Fluids and Structures**, v. 5, n. 4, p. 391–426, July 1991. ISSN 08899746. DOI: 10.1016/0889-9746(91)90421-K.

BERTRAM, C.; RAYMOND, C.; PEDLEY, T. Mapping of instabilities for flow through collapsed tubes of differing length. **Journal of Fluids and Structures**, v. 4, n. 2, p. 125–153, Mar. 1990. ISSN 08899746. DOI: 10.1016/0889-9746(90)90058-D.

BERTRAM, C. D. Flow-induced oscillation of collapsed tubes and airway structures. **Respiratory Physiology & Neurobiology**, v. 163, n. 1-3, p. 256–265, Nov. 2008. ISSN 15699048. DOI: 10.1016/j.resp.2008.04.011.

BLOM, E. D. Evolution of Tracheoesophageal Voice Prostheses. In: BLOM, E. D.; SINGER, M. I.; HAMAKER, R. C. (Eds.). **Tracheoesophageal voice restoration following total laryngectomy**. San Diego, CA: Singular Publ. Group, 1998. chap. 1, p. 1–8.

BLOM, E. D.; REMACLE, M. Tracheoesophageal Voice Restoration Problems and Solutions. In: BLOM, E. D.; SINGER, M. I.; HAMAKER, R. C. (Eds.). **Tracheoesophageal voice restoration following total laryngectomy**. San Diego, CA: Singular Publ. Group, 1998. chap. 10, p. 73–82.

BOYD, J. P. **Chebyshev and Fourier spectral methods**. 2nd ed., rev. Mineola, N.Y: Dover Publications, 2001. ISBN 978-0-486-41183-5.

BOZEC, A. et al. Current Role of Total Laryngectomy in the Era of Organ Preservation. **Cancers**, v. 12, n. 3, p. 584, Mar. 2020. ISSN 2072-6694. DOI: 10.3390/cancers12030584.

BRASSEUR, J. G.; DODDS, W. J. Interpretation of intraluminal manometric measurements in terms of swallowing mechanics. **Dysphagia**, v. 6, n. 2, p. 100–119, June 1991. ISSN 0179-051X, 1432-0460. DOI: 10.1007/BF02493487.

BROWN, D. H. et al. Postlaryngectomy Voice Rehabilitation: State of the Art at the Millennium. **World Journal of Surgery**, v. 27, n. 7, p. 824–831, July 2003. ISSN 0364-2313, 1432-2323. DOI: 10.1007/s00268-003-7107-4.

CAI, Z.; LUO, X. A fluid–beam model for flow in a collapsible channel. **Journal of Fluids and Structures**, v. 17, n. 1, p. 125–146, Jan. 2003. ISSN 08899746. DOI: 10.1016/S0889-9746(02)00112-3.

CAMPO, E. **The effect of vocal fold geometry on the fluid structure acoustic interactions in an experimental model of the human airway**. Dec. 2012. MA thesis – The Pennsylvania State University, Pennsylvania, USA.

CANCELLI, C.; PEDLEY, T. J. A separated-flow model for collapsible-tube oscillations. **Journal of Fluid Mechanics**, v. 157, n. -1, p. 375, Aug. 1985. ISSN 0022-1120, 1469-7645. DOI: 10.1017/S0022112085002427.

CHAKRAVARTY, P. D. et al. Primary versus secondary tracheoesophageal puncture: systematic review and meta-analysis. **The Journal of Laryngology & Otology**, v. 132, n. 1, p. 14–21, Jan. 2018. ISSN 0022-2151, 1748-5460. DOI: 10.1017/S0022215117002390.

CHAN, R. W.; TITZE, I. R. Dependence of phonation threshold pressure on vocal tract acoustics and vocal fold tissue mechanics. **The Journal of the Acoustical Society of America**, v. 119, n. 4, p. 2351–2362, 2006.

CHAN, R. W.; TITZE, I. R.; TITZE, M. R. Further studies of phonation threshold pressure in a physical model of the vocal fold mucosa. **The Journal of the Acoustical Society of America**, v. 101, n. 6, p. 3722–3727, 1997.

CHEN, A. Y.; FEDEWA, S.; ZHU, J. Temporal Trends in the Treatment of Early- and Advanced-Stage Laryngeal Cancer in the United States, 1985-2007. **Archives of Otolaryngology–Head & Neck Surgery**, v. 137, n. 10, p. 1017, Oct. 2011. ISSN 0886-4470. DOI: 10.1001/archoto.2011.171.

CHONE, C. T.; GRIPP, F. M., et al. Primary versus Secondary Tracheoesophageal Puncture for Speech Rehabilitation in Total Laryngectomy: Long-Term Results with Indwelling Voice Prosthesis. **Otolaryngology–Head and Neck Surgery**, v. 133, n. 1, p. 89–93, July 2005. ISSN 0194-5998, 1097-6817. DOI: 10.1016/j.otohns.2005.02.014.

CHONE, C. T.; SEIXAS, V. O., et al. Computerized manometry use to evaluate spasm in pharyngoesophageal segment in patients with poor tracheoesophageal speech before and after treatment with botulinum toxin. **Brazilian Journal of Otorhinolaryngology**, v. 75, n. 2, p. 182–187, Mar. 2009. ISSN 18088694. DOI: 10.1016/S1808-8694(15)30776-X.

COLLIN, P. H. **Dictionary of medical terms**. London: A & C Black, 2005. OCLC: 865295830. ISBN 978-1-4081-0209-1.

CONRAD, W. A. Pressure-Flow Relationships in Collapsible Tubes. **IEEE Transactions on Biomedical Engineering**, BME-16, n. 4, p. 284–295, Oct. 1969. ISSN 0018-9294. DOI: 10.1109/TBME.1969.4502660.

DAMSTÉ, P. H. **Oesophageal speech after laryngectomy (slokdarmspraak)**. Dec. 1958. PhD thesis – University of Groningen, Gronigen.

DANTAS, R. O.; AGUIAR-RICZ, L. N., et al. Influence of Esophageal Motility on Esophageal Speech of Laryngectomized Patients. **Dysphagia**, v. 17, n. 2, p. 121–125, Apr. 2002. ISSN 0179-051X, 1432-0460. DOI: 10.1007/s00455-001-0111-7.

DANTAS, R. O.; COOK, I. J., et al. Biomechanics of cricopharyngeal bars. **Gastroenterology**, v. 99, n. 5, p. 1269–1274, Nov. 1990. ISSN 00165085. DOI: 10.1016/0016-5085(90)91149-Z.

DEBRUYNE, F. et al. Acoustic analysis of tracheo-oesophageal versus oesophageal speech. **The Journal of Laryngology & Otology**, v. 108, n. 04, Apr. 1994. ISSN 0022-2151, 1748-5460. DOI: 10.1017/S0022215100126660.

DESHMANE, V. H. et al. Pharyngoesophageal segment manometry : Its role in determining post-laryngectomy speech. **Indian Journal of Otolaryngology and Head and Neck Surgery**, v. 47, n. 3, p. 6, July 1995.

DISANTIS, D. J. et al. The neck after total laryngectomy: CT study. **Radiology**, v. 153, n. 3, p. 713–717, Dec. 1984. ISSN 0033-8419, 1527-1315. DOI: 10.1148/radiology.153.3.6494467.

DOLLINGER, M. et al. Experiments on Analysing Voice Production: Excised (Human, Animal) and In Vivo (Animal) Approaches. **Current Bioinformatics**, v. 6, n. 3, p. 286–304, Sept. 2011. ISSN 15748936. DOI: 10.2174/157489311796904673.

DONALD, P. J. **The difficult case in head and neck cancer surgery**. New York: Thieme, 2010. chap. 3. ISBN 978-0-86577-984-6.

DORLAND. **Dorland's Illustrated Medical Dictionary E-Book**. [S.l.: s.n.], 2011. OCLC: 1017901906. ISBN 978-1-4557-0985-4.

DRISCOLL, T. A. Automatic spectral collocation for integral, integro-differential, and integrally reformulated differential equations. **Journal of Computational Physics**, v. 229, n. 17, p. 5980–5998, Aug. 2010. ISSN 00219991. DOI: 10.1016/j.jcp.2010.04.029.

DUVVURI, U.; MYERS, J. N. Contemporary Management of Oropharyngeal Cancer. **Current Problems in Surgery**, v. 46, n. 2, p. 119–184, Feb. 2009. ISSN 00113840. DOI: 10.1067/j.cpsurg.2008.10.003.

DWORKIN, J. P. et al. Videostroboscopy of the pharyngoesophageal segment in total laryngectomees. **The Laryngoscope**, v. 108, n. 12, p. 1773–1781, Dec. 1998. ISSN 0023852X, 15314995. DOI: 10.1097/00005537-199812000-00003.

ERATH, B. D.; HEMSING, F. S. Esophageal aerodynamics in an idealized experimental model of tracheoesophageal speech. **Experiments in Fluids**, v. 57, n. 3, Mar. 2016. ISSN 0723-4864, 1432-1114. DOI: 10.1007/s00348-015-2111-7.

ERATH, B. D.; ZAÑARTU, M., et al. A review of lumped-element models of voiced speech. **Speech Communication**, v. 55, n. 5, p. 667–690, June 2013. ISSN 01676393. DOI: 10.1016/j.specom.2013.02.002.

FANT, G. **Acoustic Theory of Speech Production: With Calculations based on X-Ray Studies of Russian Articulations.** Paris: Mouton, 1970.

FERREIRO-ARGÜELLES, C. et al. CT Findings after Laryngectomy. **RadioGraphics**, v. 28, n. 3, p. 869–882, May 2008. ISSN 0271-5333, 1527-1323. DOI: 10.1148/rg.283075091.

FLAHERTY, J. E.; KELLER, J. B.; RUBINOW, S. I. Post Buckling Behavior of Elastic Tubes and Rings with Opposite Sides in Contact. **SIAM Journal on Applied Mathematics**, v. 23, n. 4, p. 446–455, Dec. 1972. ISSN 0036-1399, 1095-712X. DOI: 10.1137/0123047.

FLANAGAN, J.; LANDGRAF, L. Self-oscillating source for vocal-tract synthesizers. **IEEE Transactions on Audio and Electroacoustics**, v. 16, n. 1, p. 57–64, Mar. 1968. ISSN 0018-9278. DOI: 10.1109/TAU.1968.1161949.

FORASTIERE, A. A. et al. Concurrent Chemotherapy and Radiotherapy for Organ Preservation in Advanced Laryngeal Cancer. **New England Journal of Medicine**,

v. 349, n. 22, p. 2091–2098, Nov. 2003. ISSN 0028-4793, 1533-4406. DOI: 10.1056/NEJMoa031317.

FORNBERG, B. A Pseudospectral Fictitious Point Method for High Order Initial-Boundary Value Problems. **SIAM Journal on Scientific Computing**, v. 28, n. 5, p. 1716–1729, Jan. 2006. ISSN 1064-8275, 1095-7197. DOI: 10.1137/040611252.

FOUQUET, M. L. **A configuração do segmento faringoesofágico no laringectomizado total e sua influência na voz e fala traqueoesofágica**. 2012. PhD thesis – Faculdade de Ciências Médicas da Santa Casa de São Paulo, São Paulo.

FOUQUET, M. L.; BEHLAU, M.; GONÇALVES, A. J. A new proposal for evaluation of the pharyngoesophageal segment and its relation with the narrow-band spectrogram in tracheoesophageal speakers. **CoDAS**, v. 25, n. 6, p. 557–565, Dec. 2013. ISSN 2317-1782. DOI: 10.1590/S2317-17822013.05000010.

FOUQUET, M. L.; GONÇALVES, A. J.; BEHLAU, M. Relation between Videofluoroscopy of the Esophagus and the Quality of Esophageal Speech. **Folia Phoniatrica et Logopaedica**, v. 61, n. 1, p. 29–36, 2009. ISSN 1021-7762, 1421-9972. DOI: 10.1159/000191471.

FREEMAN, S. B.; HAMAKER, R. C. Tracheoesophageal Voice Restoration at Time of Laryngectomy. In: BLOM, E. D.; SINGER, M. I.; HAMAKER, R. C. (Eds.). **Tracheoesophageal voice restoration following total laryngectomy**. San Diego, CA: Singular Publ. Group, 1998. chap. 3, p. 19–25.

FUCHS, A. K.; HAGMULLER, M.; KUBIN, G. The New Bionic Electro-Larynx Speech System. **IEEE Journal of Selected Topics in Signal Processing**, v. 10, n. 5, p. 952–961, Aug. 2016. ISSN 1932-4553, 1941-0484. DOI: 10.1109/JSTSP.2016.2535970.

FULCHER, L. P. et al. Negative Coulomb damping, limit cycles, and self-oscillation of the vocal folds. **American Journal of Physics**, v. 74, n. 5, p. 386–393, May 2006. ISSN 0002-9505, 1943-2909. DOI: 10.1119/1.2173272.

FUNG, Y. C. **Biomechanics**. New York, NY: Springer New York, 1997. ISBN 978-1-4419-2842-9 978-1-4757-2696-1. DOI: 10.1007/978-1-4757-2696-1.

GATES, G. A. Upper esophageal sphincter: Pre and post-laryngectomy - a normative study. **The Laryngoscope**, v. 90, n. 3, p. 454–464, Mar. 1980. ISSN 0023852X, 15314995. DOI: 10.1002/lary.5540900312.

GATES, G. A. et al. Current status of laryngectomee rehabilitation: I. Results of therapy. **American Journal of Otolaryngology**, v. 3, n. 1, p. 1–7, Jan. 1982. ISSN 01960709. DOI: 10.1016/S0196-0709(82)80025-2.

GENDEN, E. M. et al. Evolution of the management of laryngeal cancer. **Oral Oncology**, v. 43, n. 5, p. 431–439, May 2007. ISSN 13688375. DOI: 10.1016/j.oraloncology.2006.08.007.

GRAY, H. **Anatomy of the human body**. Ed. by Warren H. Lewis. 20. ed. Philadelphia and New York: Lea & Febiger, 1918.

GREENGARD, L. Spectral Integration and Two-Point Boundary Value Problems. **SIAM Journal on Numerical Analysis**, v. 28, n. 4, p. 1071–1080, Aug. 1991. ISSN 0036-1429, 1095-7170. DOI: 10.1137/0728057.

GROLMAN, W. et al. Aerodynamic and Sound Intensity Measurements in Tracheoesophageal Voice. **ORL**, v. 69, n. 2, p. 68–76, 2007. ISSN 0301-1569, 1423-0275. DOI: 10.1159/000097401.

GROTBERG, J. B.; JENSEN, O. E. BIOFLUID MECHANICS IN FLEXIBLE TUBES. **Annual Review of Fluid Mechanics**, v. 36, n. 1, p. 121–147, Jan. 2004. ISSN 0066-4189, 1545-4479. DOI: 10.1146/annurev.fluid.36.050802.121918.

GUIDERA, A. K. et al. Head and neck fascia and compartments: No space for spaces: Head and neck fascia and compartments. Ed. by David W. Eisele. **Head & Neck**, v. 36, n. 7, p. 1058–1068, July 2014. ISSN 10433074. DOI: 10.1002/hed.23442.

GUTTMAN, M. R. Rehabilitation of voice in laryngectomized patients. **Arch Otolaryngol**, v. 15, p. 478–479, 1932.

HAAS, J. et al. Study of the Effect of a Moderate Asymmetry on a Replica of the Vocal Folds. **Acta Acustica united with Acustica**, v. 102, n. 2, p. 230–239, Mar. 2016. ISSN 16101928. DOI: 10.3813/AAA.918939.

HALL, J. E. **Guyton and Hall textbook of medical physiology**. 13th edition. Philadelphia, PA: Elsevier, 2016. ISBN 978-1-4557-7005-2.

HAMAKER, R. C.; SINGER, M. I., et al. Primary Voice Restoration at Laryngectomy. **Archives of Otolaryngology - Head and Neck Surgery**, v. 111, n. 3, p. 182–186, Mar. 1985. ISSN 0886-4470. DOI: 10.1001/archotol.1985.00800050076011.

HAMAKER, R. C.; CHEESMAN, A. D. Surgical Management of Pharyngeal Constrictor Muscle Hypertonicity. In: BLOM, E. D.; SINGER, M. I.; HAMAKER, R. C. (Eds.). **Tracheoesophageal voice restoration following total laryngectomy**. San Diego, CA: Singular Publ. Group, 1998. chap. 5, p. 33–39.

HAMMING, R. W. **Numerical methods for scientists and engineers**. 2nd ed. New York: Dover, 1986. ISBN 978-0-486-65241-2.

HARRIS, C. R.; MILLMAN, K. J., et al. Array programming with NumPy. **Nature**, Springer Science and Business Media LLC, v. 585, n. 7825, p. 357–362, Sept. 2020. DOI: 10.1038/s41586-020-2649-2.

HARRIS, R. L.; GRUNDY, A.; ODUTOYE, T. Radiologically guided balloon dilatation of neopharyngeal strictures following total laryngectomy and pharyngolaryngectomy: 21 years' experience. **The Journal of Laryngology & Otology**, v. 124, n. 2, p. 175–179, Feb. 2010. ISSN 0022-2151, 1748-5460. DOI: 10.1017/S0022215109991320.

HAZEL, A. L.; HEIL, M. Steady finite-Reynolds-number flows in three-dimensional collapsible tubes. **Journal of Fluid Mechanics**, v. 486, p. 79–103, June 2003. ISSN 00221120, 14697645. DOI: 10.1017/S0022112003004671.

HEIL, M.; BOYLE, J. Self-excited oscillations in three-dimensional collapsible tubes: simulating their onset and large-amplitude oscillations. **Journal of Fluid Mechanics**, v. 652, p. 405–426, June 2010. ISSN 0022-1120, 1469-7645. DOI: 10.1017/S0022112010000157.

HEIL, M.; HAZEL, A. L. Fluid-Structure Interaction in Internal Physiological Flows. **Annual Review of Fluid Mechanics**, v. 43, n. 1, p. 141–162, Jan. 2011. ISSN 0066-4189, 1545-4479. DOI: 10.1146/annurev-fluid-122109-160703.

HEIL, M.; JENSEN, O. E. Flows in Deformable Tubes and Channels. In: MOREAU, R.; CARPENTER, P. W.; PEDLEY, T. J. (Eds.). **Flow Past Highly Compliant Boundaries and in Collapsible Tubes**. Dordrecht: Springer Netherlands, 2003. v. 72. Series Title: Fluid Mechanics and Its Applications. P. 15–49. ISBN 978-90-481-6235-2 978-94-017-0415-1. DOI: 10.1007/978-94-017-0415-1_2.

HIRANO, M. Morphological Structure of the Vocal Cord as a Vibrator and its Variations. **Folia Phoniatrica et Logopaedica**, v. 26, n. 2, p. 89–94, 1974. ISSN 1421-9972, 1021-7762. DOI: 10.1159/000263771.

HIXON, T. J.; WEISMER, G.; HOIT, J. D. **Preclinical speech science: anatomy, physiology, acoustics, and perception**. Third edition. San Diego, CA: Plural Publishing, 2020. ISBN 978-1-63550-061-5.

HOFFMAN, H. T.; MCCULLOCH, T. M. Botulinum Neurotoxin for Tracheoesophageal Voice Failure. In: BLOM, E. D.; SINGER, M. I.; HAMAKER, R. C. (Eds.). **Tracheoesophageal voice restoration following total laryngectomy**. San Diego, CA: Singular Publ. Group, 1998. chap. 11, p. 83–87.

HOFMANS, G. C. J. et al. Unsteady flow through *in-vitro* models of the glottis. **The Journal of the Acoustical Society of America**, v. 113, n. 3, p. 1658–1675, Mar. 2003. ISSN 0001-4966. DOI: 10.1121/1.1547459.

HOLSINGER, F. C.; BHAYANI, M. K. Total Laryngectomy. In: COHEN, J. I.; CLAYMAN, G. L. (Eds.). **Atlas of Head & Neck Surgery**. 1st. Philadelphia, PA: Saunders, 2011. chap. 37, p. 359–372.

HOLT, J. P. Flow of Liquids Through "Collapsible" Tubes. **Circulation Research**, v. 7, n. 3, p. 342–353, May 1959. ISSN 0009-7330, 1524-4571. DOI: 10.1161/01.RES.7.3.342.

HOLT, J. P. The collapse factor in the measurement of venous pressure. The flow of fluid through collapsible tubes. **American Heart Journal**, v. 22, n. 4, p. 562, Oct. 1941. ISSN 00028703. DOI: 10.1016/S0002-8703(41)90356-3.

HOWE, M. S.; MCGOWAN, R. S. Aerodynamic sound of a body in arbitrary, deformable motion, with application to phonation. **Journal of Sound and Vibration**, v. 332, n. 17, p. 3909–3923, Aug. 2013. ISSN 0022460X. DOI: 10.1016/j.jsv.2012.11.009.

HOWE, M. S.; MCGOWAN, R. S. On the single-mass model of the vocal folds. **Fluid Dynamics Research**, v. 42, n. 1, p. 015001, Feb. 2010. ISSN 0169-5983, 1873-7005. DOI: 10.1088/0169-5983/42/1/015001.

HUIE, J. M.; SUMMERS, A. P.; KAWANO, S. M. SegmentGeometry: A Tool for Measuring Second Moment of Area in 3D Slicer. **Integrative Organismal Biology**, v. 4, n. 1, obac009, Mar. 2022. ISSN 2517-4843. DOI: 10.1093/iob/obac009.

HÜTTNER, B. et al. Development of a time-dependent numerical model for the assessment of non-stationary pharyngoesophageal tissue vibrations after total laryngectomy. **Biomechanics and Modeling in Mechanobiology**, v. 14, n. 1, p. 169–184, Jan. 2015. ISSN 1617-7959, 1617-7940. DOI: 10.1007/s10237-014-0597-1.

INHEALTH TECHNOLOGIES. **Classic™ Indwelling Voice Prostheses, Sterile**. [S.l.: s.n.]. Available from: https://inhealth.com/classic-indwelling-voice-prostheses-sterile-in-1608-so-gr.html. Visited on: 17 Mar. 2021.

INHEALTH TECHNOLOGIES. **Total laryngectomy and voice restoration**: What to expect. [S.l.]: InHealth Technologies, 2018. Available from: https://inhealth.com/media/documents/pdf/Total_Laryngectomy_Brochure.pdf. Visited on: 6 Mar. 2021.

INSTITUTO NACIONAL DE CÂNCER JOSÉ GOMES ALENCAR DA SILVA. **Estimativa 2020**: Incidência de Câncer no Brasil. Rio de Janeiro: Ministério da Saúde, 2019.

ISHIZAKA, K.; FLANAGAN, J. L. Synthesis of Voiced Sounds From a Two-Mass Model of the Vocal Cords. **Bell System Technical Journal**, v. 51, n. 6, p. 1233–1268, July 1972. ISSN 00058580. DOI: 10.1002/j.1538-7305.1972.tb02651.x.

JENSEN, O. E.; HEIL, M. High-frequency self-excited oscillations in a collapsible-channel flow. **Journal of Fluid Mechanics**, v. 481, p. 235–268, Apr. 2003. ISSN 00221120, 14697645. DOI: 10.1017/S002211200300394X.

JIANG, J. J.; ZHANG, Y.; STERN, J. Modeling of chaotic vibrations in symmetric vocal folds. **The Journal of the Acoustical Society of America**, v. 110, n. 4, p. 2120–2128, Oct. 2001. ISSN 0001-4966. DOI: 10.1121/1.1395596.

KAHRILAS, P. et al. Upper esophageal sphincter function during belching. **Gastroenterology**, v. 91, n. 1, p. 133–140, July 1986. ISSN 00165085. DOI: 10.1016/0016-5085(86)90449-X.

KATZ, A. I.; CHEN, Y.; MORENO, A. H. Flow through a Collapsible Tube. **Biophysical Journal**, v. 9, n. 10, p. 1261–1279, Oct. 1969. ISSN 00063495. DOI: 10.1016/S0006-3495(69)86451-9.

KAWAMOTO-HIRANO, A. et al. Submucosal Elastic Laminae of the Middle and Lower Pharynx: A Histological Study Using Elderly Cadaveric Specimens. **Dysphagia**, v. 31, n. 5, p. 635–643, Oct. 2016. ISSN 0179-051X, 1432-0460. DOI: 10.1007/s00455-016-9721-y.

KELLY, J. H.; KUNCL, R. W. Myology of the Pharyngoesophageal Segment: Gross Anatomic and Histologic Characteristics. **The Laryngoscope**, v. 106, n. 6, p. 713–720, June 1996. ISSN 0023852X, 15314995. DOI: 10.1097/00005537-199606000-00009.

KIKINIS, R.; PIEPER, S. D.; VOSBURGH, K. G. 3D Slicer: A Platform for Subject-Specific Image Analysis, Visualization, and Clinical Support. In: JOLESZ, F. A. (Ed.). **Intraoperative Imaging and Image-Guided Therapy**. New York, NY: Springer New York, 2014. P. 277–289. ISBN 978-1-4614-7656-6 978-1-4614-7657-3. DOI: 10.1007/978-1-4614-7657-3_19.

KNOTT, J. Clinical Problem-Solving in Tracheoesophageal Puncture Voice Restoration. In: DOYLE, P. C. (Ed.). **Clinical Care and Rehabilitation in Head and Neck Cancer**. Cham, Switzerland: Springer International Publishing, 2019. chap. 12, p. 189–207. ISBN 978-3-030-04701-6 978-3-030-04702-3. DOI: 10.1007/978-3-030-04702-3.

KNOWLTON, F. P.; STARLING, E. H. The influence of variations in temperature and blood-pressure on the performance of the isolated mammalian heart. **The Journal of Physiology**, v. 44, n. 3, p. 206–219, May 1912. ISSN 00223751. DOI: 10.1113/jphysiol.1912.sp001511.

KOTBY, M. et al. Aerodynamics of the Pseudo-Glottis. **Folia Phoniatrica et Logopaedica**, v. 61, n. 1, p. 24–28, 2009. ISSN 1021-7762, 1421-9972. DOI: 10.1159/000188660.

KRESS, P.; SCHÄFER, P. **Prostheses**. [S.l.]: Stimmprothese.com. Available from: https://stimmprothese.com/1/prostheses/. Visited on: 17 Mar. 2021.

KRESS, P.; SCHÄFER, P. **Swimming devices**. [S.l.]: Stimmprothese.com. Available from: https://stimmprothese.com/1/tracheostoma/swimming-devices/. Visited on: 10 Mar. 2021.

KUNDU, P. K.; COHEN, I. M. **Fluid mechanics**. 4. ed., reprinted. Amsterdam: Elsevier [u.a.], 2008. ISBN 978-0-12-381399-2.

LANG, I. M.; SHAKER, R. Anatomy and Physiology of the Upper Esophageal Sphincter. **The American Journal of Medicine**, v. 103, n. 5, 50s–55s, Nov. 1997. ISSN 00029343. DOI: 10.1016/S0002-9343(97)00323-9.

LANG, I. M. **Upper esophageal sphincter**. [S.l.]: Nature Publishing Group, 2006. Available from: https://www.nature.com/gimo/contents/pt1/full/gimo12.html. Visited on: 7 Apr. 2022.

LEAPER, M.; ZHANG, M.; DAWES, P. J. An Anatomical Protrusion Exists on the Posterior Hypopharyngeal Wall in Some Elderly Cadavers. **Dysphagia**, v. 20, n. 1, p. 8–14, Mar. 2005. ISSN 0179-051X, 1432-0460. DOI: 10.1007/s00455-004-0018-1.

LEWIN, J. S. et al. Device Life of the Tracheoesophageal Voice Prosthesis Revisited. **JAMA Otolaryngology–Head & Neck Surgery**, v. 143, n. 1, p. 65, Jan. 2017. ISSN 2168-6181. DOI: 10.1001/jamaoto.2016.2771.

LEWIS, W. J. B. Clinical Intervention for Airway Improvement: Establishing a New Nose. In: DOYLE, P. C. (Ed.). **Clinical Care and Rehabilitation in Head and Neck Cancer**. Cham, Switzerland: Springer International Publishing, 2019. chap. 8, p. 119–128.

LOHSCHELLER, J. et al. Modelling of the laryngectomee substitute voice. In: PROCEEDINGS of the 3rd International Workshop MAVEBA 2003. Firenze: Firenze University Press, 2003.

LORENZ, K. J. Rehabilitation after Total Laryngectomy—A Tribute to the Pioneers of Voice Restoration in the Last Two Centuries. **Frontiers in Medicine**, v. 4, June 2017. ISSN 2296-858X. DOI: 10.3389/fmed.2017.00081.

LOWE, T.; PEDLEY, T. Computation of Stokes Flow in a Channel with a Collapsible Segment. **Journal of Fluids and Structures**, v. 9, n. 8, p. 885–905, Nov. 1995. ISSN 08899746. DOI: 10.1006/jfls.1995.1050.

LUCERO, J. C. A theoretical study of the hysteresis phenomenon at vocal fold oscillation onset–offset. **The Journal of the Acoustical Society of America**, v. 105, n. 1, p. 423–431, Jan. 1999. ISSN 0001-4966. DOI: 10.1121/1.424572.

LUCERO, J. C. Dynamics of the two-mass model of the vocal folds: Equilibria, bifurcations, and oscillation region. **The Journal of the Acoustical Society of America**, v. 94, n. 6, p. 3104–3111, Dec. 1993. ISSN 0001-4966. DOI: 10.1121/1.407216.

LUCERO, J. C.; KOENIG, L. L. On the relation between the phonation threshold lung pressure and the oscillation frequency of the vocal folds. **The Journal of the Acoustical Society of America**, v. 121, n. 6, p. 3280, 2007. ISSN 00014966. DOI: 10.1121/1.2722210.

LUCERO, J. C.; PELORSON, X.; VAN HIRTUM, A. Phonation threshold pressure at large asymmetries of the vocal folds. **Biomedical Signal Processing and Control**, v. 62, p. 102105, Sept. 2020. ISSN 17468094. DOI: 10.1016/j.bspc.2020.102105.

LUCERO, J. C.; VAN HIRTUM, A., et al. Validation of theoretical models of phonation threshold pressure with data from a vocal fold mechanical replica. **The Journal of the Acoustical Society of America**, v. 125, n. 2, p. 632–635, Feb. 2009. ISSN 0001-4966. DOI: 10.1121/1.3056468.

LUIZARD, P.; PELORSON, X. Threshold of oscillation of a vocal fold replica with unilateral surface growths. **The Journal of the Acoustical Society of America**, v. 141, n. 5, p. 3050–3058, May 2017. ISSN 0001-4966. DOI: 10.1121/1.4979935.

LUNDSTRÖM, E. et al. The pharyngoesophageal segment in laryngectomees—videoradiographic, acoustic, and voice quality perceptual data. **Logopedics Phoniatrics Vocology**, v. 33, n. 3, p. 115–125, Jan. 2008. ISSN 1401-5439, 1651-2022. DOI: 10.1080/14015430701855788.

LUO, X. Y.; PEDLEY, T. J. A numerical simulation of unsteady flow in a two-dimensional collapsible channel. **Journal of Fluid Mechanics**, v. 314, n. -1, p. 191, May 1996. ISSN 0022-1120, 1469-7645. DOI: 10.1017/S0022112096000286.

LUO, X. Y. et al. The cascade structure of linear instability in collapsible channel flows. **Journal of Fluid Mechanics**, v. 600, Apr. 2008. ISSN 0022-1120, 1469-7645. DOI: 10.1017/S0022112008000293.

LUO, X.; PEDLEY, T. A Numerical Simulation of Steady Flow in a 2-D Collapsible Channel. **Journal of Fluids and Structures**, v. 9, n. 2, p. 149–174, Feb. 1995. ISSN 08899746. DOI: 10.1006/jfls.1995.1008.

LYON, C. K. et al. Flow through collapsible tubes at high Reynolds numbers. **CIRCULATION RESEARCH**, v. 49, n. 4, p. 9, 1981.

MACLEAN, J.; COTTON, S.; PERRY, A. Variation in surgical methods used for total laryngectomy in Australia. **The Journal of Laryngology & Otology**, v. 122, n. 7, p. 728–732, July 2008. ISSN 0022-2151, 1748-5460. DOI: 10.1017/S0022215108002119.

MACLEAN, J.; COTTON, S.; PERRY, A. Post-Laryngectomy: It's Hard to Swallow: An Australian Study of Prevalence and Self-reports of Swallowing Function After a Total Laryngectomy. **Dysphagia**, v. 24, n. 2, p. 172–179, June 2009. ISSN 0179-051X, 1432-0460. DOI: 10.1007/s00455-008-9189-5.

MAHIEU, H. F. **Voice and speech rehabilitation following laryngectomy**. 1988. PhD thesis – University of Groningen.

MAI-DUY, N. An effective spectral collocation method for the direct solution of high-order ODEs. **Communications in Numerical Methods in Engineering**, v. 22, n. 6, p. 627–642, Dec. 2005. ISSN 10698299. DOI: 10.1002/cnm.841.

MAI-DUY, N.; TANNER, R. A spectral collocation method based on integrated Chebyshev polynomials for two-dimensional biharmonic boundary-value problems. **Journal of Computational and Applied Mathematics**, v. 201, n. 1, p. 30–47, Apr. 2007. ISSN 03770427. DOI: 10.1016/j.cam.2006.01.030.

MARTINI, F.; TIMMONS, M. J.; TALLITSCH, R. B. **Human anatomy**. 7th ed. Boston: Pearson Benjamin Cummings, 2012. OCLC: ocn636894827. ISBN 978-0-321-68815-6 978-0-321-73064-0.

MARZO, A.; LUO, X.; BERTRAM, C. Three-dimensional collapse and steady flow in thick-walled flexible tubes. **Journal of Fluids and Structures**, v. 20, n. 6, p. 817–835, Aug. 2005. ISSN 08899746. DOI: 10.1016/j.jfluidstructs.2005.03.008.

MAST, T. D. Empirical relationships between acoustic parameters in human soft tissues. **Acoustics Research Letters Online**, v. 1, n. 2, p. 37–42, Oct. 2000. ISSN 1529-7853. DOI: 10.1121/1.1336896.

MATSUMOTO, T. et al. Experimental study of vocal–ventricular fold oscillations in voice production. **The Journal of the Acoustical Society of America**, v. 149, n. 1, p. 271–284, Jan. 2021. ISSN 0001-4966. DOI: 10.1121/10.0003211.

MAX, L.; STEURS, W.; BRUYN, W. de. Vocal Capacities in Esophageal and Tracheoesophageal Speakers. **The Laryngoscope**, v. 106, n. 1, p. 93–96, Jan. 1996. ISSN 0023852X, 15314995. DOI: 10.1097/00005537-199601000-00018.

MCCLURKEN, M. E. et al. Steady, supercritical flow in collapsible tubes. Part 2. Theoretical studies. **Journal of Fluid Mechanics**, v. 109, n. -1, p. 391, Aug. 1981. ISSN 0022-1120, 1469-7645. DOI: 10.1017/S0022112081001134.

MCGOWAN, R. S. An aeroacoustic approach to phonation. **The Journal of the Acoustical Society of America**, v. 83, n. 2, p. 696–704, Feb. 1988. ISSN 0001-4966. DOI: 10.1121/1.396165.

MCGOWAN, R. S.; HOWE, M. S. Comments on single-mass models of vocal fold vibration. **The Journal of the Acoustical Society of America**, v. 127, n. 5, el215–el221, May 2010. ISSN 0001-4966. DOI: 10.1121/1.3397283.

MCIVOR, J. et al. Radiological assessment of post laryngectomy speech. **Clinical Radiology**, v. 41, n. 5, p. 312–316, May 1990. ISSN 00099260. DOI: 10.1016/S0009-9260(05)81691-5.

MCPHAIL, M. J.; CAMPO, E. T.; KRANE, M. H. Aeroacoustic source characterization in a physical model ofphonation. **J. Acoust. Soc. Am.**, v. 146, n. 2, p. 1230–1238, 2019.

MELTZNER, G. S.; HILLMAN, R. E. Impact of Aberrant Acoustic Properties on the Perception of Sound Quality in Electrolarynx Speech. **Journal of Speech, Language, and Hearing Research**, v. 48, n. 4, p. 766–779, Aug. 2005. ISSN 1092-4388, 1558-9102. DOI: 10.1044/1092-4388(2005/053).

MICHAELS, L.; HELLQUIST, H. B. **Ear, Nose and Throat Histopathology**. London: Springer London, 2001. ISBN 978-1-4471-1128-3 978-1-4471-0235-9. DOI: 10.1007/978-1-4471-0235-9.

MILLS, K. R. The basics of electromyography. **Journal of Neurology, Neurosurgery & Psychiatry**, v. 76, suppl_2, p. ii32–ii35, June 2005. ISSN 0022-3050. DOI: 10.1136/jnnp.2005.069211.

MOHRI, M. et al. Neoglottic Activity in Tracheoesophageal Phonation. **Auris Nasus Larynx**, v. 21, n. 1, p. 53–58, Jan. 1994. ISSN 03858146. DOI: 10.1016/S0385-8146(12)80010-1.

MONGEAU, L. et al. Characteristics of a pulsating jet through a small modulated orifice, with application to voice production. **The Journal of the Acoustical Society of America**, v. 102, n. 2, p. 1121–1133, Aug. 1997. ISSN 0001-4966. DOI: 10.1121/1.419864.

MOON, J. B.; WEINBERG, B. Aerodynamic and Myoelastic Contributions to Tracheoesophageal Voice Production. **Journal of Speech Language and Hearing Research**, v. 30, n. 3, p. 387, Sept. 1987. ISSN 1092-4388. DOI: 10.1044/jshr.3003.387.

MORE, J. J.; GARBOW, B. S.; HILLSTROM, K. E. User guide for MINPACK-1. [In FORTRAN], Aug. 1980. DOI: 10.2172/6997568.

MORGAN, D. W. et al. Use of a portable manometer as a screening procedure in voice rehabilitation. **The Journal of Laryngology & Otology**, v. 106, n. 4, p. 353–355, Apr. 1992. ISSN 0022-2151, 1748-5460. DOI: 10.1017/S0022215100119474.

MOTTA, S.; GALLI, I.; DI RIENZO, L. Aerodynamic Findings in Esophageal Voice. **Archives of Otolaryngology–Head & Neck Surgery**, v. 127, n. 6, p. 700, June 2001. ISSN 0886-4470. DOI: 10.1001/archotol.127.6.700.

MU, L.; SANDERS, I. Muscle Fiber-Type Distribution Pattern in the Human Cricopharyngeus Muscle. **Dysphagia**, v. 17, n. 2, p. 87–96, Apr. 2002. ISSN 0179-051X, 1432-0460. DOI: 10.1007/s00455-001-0108-2.

MU, L.; SANDERS, I. Neuromuscular compartments and fiber-type regionalization in the human inferior pharyngeal constrictor muscle. **The Anatomical Record**, v. 264, n. 4, p. 367–377, Dec. 2001. ISSN 0003-276X, 1097-0185. DOI: 10.1002/ar.10020.

MU, L.; SANDERS, I. Neuromuscular Organization of the Human Upper Esophageal Sphincter. **Annals of Otology, Rhinology & Laryngology**, v. 107, n. 5, p. 370–377, May 1998. ISSN 0003-4894, 1943-572X. DOI: 10.1177/000348949810700502.

MU, L.; SANDERS, I. Newly Revealed Cricothyropharyngeus Muscle in the Human Laryngopharynx. **The Anatomical Record: Advances in Integrative Anatomy and Evolutionary Biology**, v. 291, n. 8, p. 927–938, Aug. 2008. ISSN 19328486, 19328494. DOI: 10.1002/ar.20727.

MURRAY, P. R.; THOMSON, S. L. Vibratory responses of synthetic, self-oscillating vocal fold models. **The Journal of the Acoustical Society of America**, v. 132, n. 5, p. 3428–3438, Nov. 2012. ISSN 0001-4966. DOI: 10.1121/1.4754551.

NEUBAUER, J. et al. Coherent structures of the near field flow in a self-oscillating physical model of the vocal folds. **J. Acoust. Soc. Am.**, v. 121, n. 2, p. 18, 2007.

NG, M. L. Aerodynamic characteristics associated with oesophageal and tracheoesophageal speech of Cantonese. **International Journal of Speech-Language Pathology**, v. 13, n. 2, p. 137–144, Apr. 2011. ISSN 1754-9507, 1754-9515. DOI: 10.3109/17549507.2011.534176.

NISHIZAWA, N. et al. Identification of the opener and closer of the pharyngoesophagus in laryngectomees. **Auris Nasus Larynx**, v. 28, s63–s69, May 2001. ISSN 03858146. DOI: 10.1016/S0385-8146(01)00066-9.

OMORI, K. et al. Mechanism of Tracheoesophageal Shunt Phonation. **Archives of Otolaryngology - Head and Neck Surgery**, v. 120, n. 6, p. 648–652, June 1994. ISSN 0886-4470. DOI: 10.1001/archotol.1994.01880300062009.

ONOFRE, F. et al. Effect of singing training on total laryngectomees wearing a tracheoesophageal voice prosthesis. **Acta Cirurgica Brasileira**, v. 28, n. 2, p. 119–125, Feb. 2013. ISSN 0102-8650. DOI: 10.1590/S0102-86502013000200006.

OP DE COUL, B. M. R. et al. A Decade of Postlaryngectomy Vocal Rehabilitation in 318 Patients: A Single Institution's Experience With Consistent Application of Provox Indwelling Voice Prostheses. **Archives of Otolaryngology–Head & Neck Surgery**, v. 126, n. 11, p. 1320, Nov. 2000. ISSN 0886-4470. DOI: 10.1001/archotol.126.11.1320.

PAIDOUSSIS, M. P. **Fluid-structure interactions: slender structures and axial flow**. Second edition. Amsterdam ; Boston [MA]: Academic Press is an imprint of Elsevier, 2014. ISBN 978-0-12-397312-2 978-0-12-397333-7.

PARK, J. B.; MONGEAU, L. Instantaneous orifice discharge coefficient of a physical, driven model of the human larynx. **The Journal of the Acoustical Society of America**, v. 121, n. 1, p. 442–455, Jan. 2007. ISSN 0001-4966. DOI: 10.1121/1.2401652.

PELORSON, X. et al. Theoretical and experimental study of quasisteady-flow separation within the glottis during phonation. Application to a modified two-mass model. **The Journal of the Acoustical Society of America**, v. 96, n. 6, p. 3416–3431, Dec. 1994. ISSN 0001-4966. DOI: 10.1121/1.411449.

PICKUP, B. A.; THOMSON, S. L. Flow-induced vibratory response of idealized versus magnetic resonance imaging-based synthetic vocal fold models. **The Journal of the Acoustical Society of America**, v. 128, n. 3, el124–el129, Sept. 2010. ISSN 0001-4966. DOI: 10.1121/1.3455876.

PODOPROSVETOVA, A. et al. Experimental study of the flow regime effect on the stability of collapsible tubes conveying fluid. **Physics of Fluids**, v. 33, n. 6, p. 064104, June 2021. ISSN 1070-6631, 1089-7666. DOI: 10.1063/5.0050745.

PRUSZEWICZ, A. et al. Electromyography of Cricopharyngeal Muscles in Patients with Oesophageal Speech. **Acta Oto-Laryngologica**, v. 112, n. 2, p. 366–369, Jan. 1992. ISSN 0001-6489, 1651-2251. DOI: 10.1080/00016489.1992.11665435.

RAPHAEL, L. J.; BORDEN, G. J.; HARRIS, K. S. **Speech science primer: physiology, acoustics, and perception of speech**. 6th ed. Baltimore, MD: Wolters Kluwer Health/Lippincott Williams & Wilkins, 2011. OCLC: ocn669122279. ISBN 978-1-60831-357-0.

ROBBINS, J. et al. Selected Acoustic Features of Tracheoesophageal, Esophageal, and Laryngeal Speech. **Archives of Otolaryngology - Head and Neck Surgery**, v. 110, n. 10, p. 670–672, Oct. 1984. ISSN 0886-4470. DOI: 10.1001/archotol.1984.00800360042009.

RODBARD, S.; SAIKI, H. Flow through collapsible tubes. **American Heart Journal**, v. 46, n. 5, p. 715–725, Nov. 1953. ISSN 00028703. DOI: 10.1016/0002-8703(53)90224-5.

RUTY, N. et al. An in vitro setup to test the relevance and the accuracy of low-order vocal folds models. **The Journal of the Acoustical Society of America**, v. 121, n. 1, p. 479–490, Jan. 2007. ISSN 0001-4966. DOI: 10.1121/1.2384846.

SANTOS, F. H. et al. Influence of position and angulation of a voice prosthesis on the aerodynamics of the pseudo-glottis. **Journal of Biomechanics**, v. 125, p. 110594, Aug. 2021. ISSN 00219290. DOI: 10.1016/j.jbiomech.2021.110594.

SCHINDLER, A. et al. Intensity and fundamental frequency control in tracheoesophageal voice. **Acta Otorhinolaryngologica Italica: Organo Ufficiale Della Societa Italiana Di Otorinolaringologia E Chirurgia Cervico-Facciale**, v. 25, n. 4, p. 240–244, Aug. 2005. ISSN 0392-100X.

SCHUTTE, H. K.; NIEBOER, G. Aerodynamics of Esophageal Voice Production with and without a Groningen Voice Prosthesis. **Folia Phoniatrica et Logopaedica**, v. 54, n. 1, p. 8–18, 2002. ISSN 1021-7762, 1421-9972. DOI: 10.1159/000048592.

SCHWARTZ, A. W.; HOLLINSHEAD, W. H.; DEVINE, K. D. Laryngectomy: Anatomy and Technique. **Surgical Clinics of North America**, v. 43, n. 4, p. 1063–1079, Aug. 1963. ISSN 00396109. DOI: 10.1016/S0039-6109(16)37042-6.

SCHWARZ, R. et al. Substitute Voice Production: Quantification of PE Segment Vibrations Using a Biomechanical Model. **IEEE Transactions on Biomedical Engineering**, v. 58, n. 10, p. 2767–2776, Oct. 2011. ISSN 0018-9294, 1558-2531. DOI: 10.1109/TBME.2011.2151860.

SCHWARZ, R. **Model-Based Quantification of Pathological Voice Production**. 2007. PhD thesis – Universität Erlangen-Nürnberg.

SECRETARIA DE ESTADO DA SAÚDE. **Ata Sessão Pública PE-0719/2019**. Santa Catarina: Governo de Santa Catarina, 2019. Available from: https://e-lic.sc.gov.br/. Visited on: 22 Mar. 2021.

SEONG, H. et al. Unsteady flow in a 3-D collapsible tube with uniform wall thickness. In: p. 1480. DOI: 10.1109/IEMBS.2002.1106494.

SEYDEL, R. **Practical Bifurcation and Stability Analysis**. New York, NY: Springer Science+Business Media, LLC Springer e-books, 2010. (Interdisciplinary Applied Mathematics, 5). ISBN 978-1-4419-1740-9.

SHAKER, R.; REN, J.; KERN, M., et al. Mechanisms of airway protection and upper esophageal sphincter opening during belching. **American Journal of Physiology-Gastrointestinal and Liver Physiology**, v. 262, n. 4, g621–g628, Apr. 1992. ISSN 0193-1857, 1522-1547. DOI: 10.1152/ajpgi.1992.262.4.G621.

SHAKER, R.; REN, J.; XIE, P., et al. Characterization of the pharyngo-UES contractile reflex in humans. **American Journal of Physiology-Gastrointestinal and Liver Physiology**, v. 273, n. 4, g854–g858, Oct. 1997. ISSN 0193-1857, 1522-1547. DOI: 10.1152/ajpgi.1997.273.4.G854.

SHAPIRO, A. H. Steady Flow in Collapsible Tubes. **Journal of Biomechanical Engineering**, v. 99, n. 3, p. 126, 1977. ISSN 01480731. DOI: 10.1115/1.3426281.

SHIPP, T. EMG of Pharyngoesophageal Musculature during Alaryngeal Voice Production. **Journal of Speech Language and Hearing Research**, v. 13, n. 1, p. 184, Mar. 1970. ISSN 1092-4388. DOI: 10.1044/jshr.1301.184.

ŠIDLOF, P. et al. Measurement of flow separation in a human vocal folds model. **Experiments in Fluids**, v. 51, n. 1, p. 123–136, July 2011. ISSN 0723-4864, 1432-1114. DOI: 10.1007/s00348-010-1031-9.

SIMPSON, I. C.; SMITH, J. C. S.; GORDON, M. T. Laryngectomy: The influence of muscle reconstruction on the mechanism of oesophageal voice production. **The Journal of Laryngology & Otology**, v. 86, n. 10, p. 961–990, Oct. 1972. ISSN 0022-2151, 1748-5460. DOI: 10.1017/S0022215100076155.

SINGER, M. I.; BLOM, E. D. An Endoscopic Technique for Restoration of Voice after Laryngectomy. **Annals of Otology, Rhinology & Laryngology**, v. 89, n. 6, p. 529–533, Nov. 1980. ISSN 0003-4894, 1943-572X. DOI: 10.1177/000348948008900608.

SINGH, S.; HAMDY, S. The upper oesophageal sphincter. **Neurogastroenterology and Motility**, v. 17, s1, p. 3–12, June 2005. ISSN 1350-1925, 1365-2982. DOI: 10.1111/j.1365-2982.2005.00662.x.

SIVARAO, D.; GOYAL, R. K. Functional anatomy and physiology of the upper esophageal sphincter. **The American Journal of Medicine**, v. 108, n. 4, p. 27–37, Mar. 2000. ISSN 00029343. DOI: 10.1016/S0002-9343(99)00337-X.

SLOANE, P. M. et al. Esophageal insufflation and videofluoroscopy for evaluation of esophageal speech in laryngectomy patients: clinical implications. **Radiology**, v. 181, n. 2, p. 433–437, Nov. 1991. ISSN 0033-8419, 1527-1315. DOI: 10.1148/radiology.181.2.1924785.

SOBOTTA, J. **Atlas of Human Anatomy**: The viscera including the heart. Ed. by Playfair McMurrich. New York: G. E. Stechert & Co., 1928. v. 2.

SOUZA, F. G. R. et al. Quality of life after total laryngectomy: impact of different vocal rehabilitation methods in a middle income country. **Health and Quality of Life Outcomes**, v. 18, n. 1, p. 92, Dec. 2020. ISSN 1477-7525. DOI: 10.1186/s12955-020-1281-z.

STAFFIERI, A. et al. Cost of tracheoesophageal prostheses in developing countries. Facing the problem from an internal perspective. **Acta Oto-Laryngologica**, v. 126, n. 1, p. 4–9, Jan. 2006. ISSN 0001-6489, 1651-2251. DOI: 10.1080/00016480500265935.

STEINECKE, I.; HERZEL, H. Bifurcations in an asymmetric vocal-fold model. **The Journal of the Acoustical Society of America**, v. 97, n. 3, p. 1874–1884, 1995. DOI: 10.1121/1.412061.

STEWART, P. S. Instabilities in flexible channel flow with large external pressure. **Journal of Fluid Mechanics**, v. 825, p. 922–960, Aug. 2017. ISSN 0022-1120, 1469-7645. DOI: 10.1017/jfm.2017.404.

STEWART, P. S.; FOSS, A. J. E. SELF-EXCITED OSCILLATIONS IN A COLLAPSIBLE CHANNEL WITH APPLICATIONS TO RETINAL VENOUS PULSATION. **The ANZIAM Journal**, v. 61, n. 3, p. 320–348, July 2019. ISSN 1446-1811, 1446-8735. DOI: 10.1017/S1446181119000117.

STEWART, P. S.; HEIL, M., et al. Sloshing and slamming oscillations in a collapsible channel flow. **Journal of Fluid Mechanics**, v. 662, p. 288–319, Nov. 2010. ISSN 0022-1120, 1469-7645. DOI: 10.1017/S0022112010003277.

STEWART, P. S.; WATERS, S. L.; JENSEN, O. E. Local and global instabilities of flow in a flexible-walled channel. **European Journal of Mechanics - B/Fluids**, v. 28, n. 4, p. 541–557, July 2009. ISSN 09977546. DOI: 10.1016/j.euromechflu.2009.03.002.

STORY, B. H.; TITZE, I. R. Voice simulation with a body-cover model of the vocal folds. **The Journal of the Acoustical Society of America**, v. 97, n. 2, p. 1249–1260, Feb. 1995. ISSN 0001-4966. DOI: 10.1121/1.412234.

SWEENY, L. et al. Incidence and Outcomes of Stricture Formation Postlaryngectomy. **Otolaryngology–Head and Neck Surgery**, v. 146, n. 3, p. 395–402, Mar. 2012. ISSN 0194-5998, 1097-6817. DOI: 10.1177/0194599811430911.

TAKESHITA, T. K. et al. Relation between the dimensions and intraluminal pressure of the pharyngoesophageal segment and tracheoesophageal voice and speech proficiency. **Head & Neck**, v. 35, n. 4, p. 500–504, 2012. ISSN 10433074. DOI: 10.1002/hed.22921.

TAYLOR, C. J. et al. Magnetic resonance imaging-based measurement of internal deformation of vibrating vocal fold models. **The Journal of the Acoustical Society of America**, v. 145, n. 2, p. 989–997, Feb. 2019. ISSN 0001-4966. DOI: 10.1121/1.5091009.

TERRELL, J.; LEWIN, J.; ESCLAMADO, R. Botulinum toxin injection for postlaryngectomy tracheoesophageal speech failure. **Otolaryngology - Head and Neck Surgery**, v. 113, n. 6, p. 788–791, Dec. 1995. ISSN 01945998. DOI: 10.1016/S0194-5998(95)70023-4.

THOMSON, S. L.; MONGEAU, L.; FRANKEL, S. H. Aerodynamic transfer of energy to the vocal folds. **The Journal of the Acoustical Society of America**, v. 118, n. 3, p. 1689–1700, Sept. 2005. ISSN 0001-4966. DOI: 10.1121/1.2000787.

TIMMERMANS, A. J. et al. Trends in treatment and survival for advanced laryngeal cancer: A 20-year population-based study in The Netherlands: Trends in Treatment and Survival for Advanced Laryngeal Cancer. **Head & Neck**, v. 38, S1, e1247–e1255, Apr. 2016. ISSN 10433074. DOI: 10.1002/hed.24200.

TITZE, I. R. The physics of small-amplitude oscillation of the vocal folds. **The Journal of the Acoustical Society of America**, v. 83, n. 4, p. 1536–1552, Apr. 1988. ISSN 0001-4966. DOI: 10.1121/1.395910.

TITZE, I. R.; JIANG, J. J.; HSIAO, T.-Y. Measurement of Mucosal Wave Propagation and Vertical Phase Difference in Vocal Fold Vibration. **Annals of Otology, Rhinology & Laryngology**, v. 102, n. 1, p. 58–63, Jan. 1993. ISSN 0003-4894, 1943-572X. DOI: 10.1177/000348949310200111.

TITZE, I. R.; SCHMIDT, S. S.; TITZE, M. R. Phonation threshold pressure in a physical model of the vocal fold mucosa. **The Journal of the Acoustical Society of America**, v. 97, n. 5, p. 3080–3084, May 1995. ISSN 0001-4966. DOI: 10.1121/1.411870.

TOURINHO, A. M. d. C. et al. A study on tracheoesophageal phonation based on a collapsible channel model. **The Journal of the Acoustical Society of America**, v. 149, n. 3, p. 1979–1988, Mar. 2021. ISSN 0001-4966. DOI: 10.1121/10.0003817.

TRIEP, M. et al. Optimized transformation of the glottal motion into a mechanical model. **Medical Engineering & Physics**, v. 33, n. 2, p. 210–217, Mar. 2011. ISSN 13504533. DOI: 10.1016/j.medengphy.2010.09.019.

TUCKER, H. M. Total laryngectomy: Technique. **Operative Techniques in Otolaryngology-Head and Neck Surgery**, v. 1, n. 1, p. 42–44, Mar. 1990. ISSN 10431810. DOI: 10.1016/S1043-1810(10)80272-6.

UNIVERSIDADE FEDERAL DE SANTA CATARINA. **Parecer consubstanciado do CEP**. Florianópolis/SC: [s.n.], 2018. Parecer n. 3.054.135.

VAN AS, C. J.; HILGERS, F. J., et al. Acoustical analysis and perceptual evaluation of tracheoesophageal prosthetic voice. **Journal of Voice**, v. 12, n. 2, p. 239–248, Jan. 1998. ISSN 08921997. DOI: 10.1016/S0892-1997(98)80044-1.

VAN AS, C. J.; OP DE COUL, B. M. R., et al. Quantitative Videofluoroscopy: A New Evaluation Tool for Tracheoesophageal Voice Production. **Archives of Otolaryngology–Head & Neck Surgery**, v. 127, n. 2, p. 161, Feb. 2001. ISSN 0886-4470. DOI: 10.1001/archotol.127.2.161.

VAN AS, C. J.; TIGGES, M., et al. High-Speed Digital Imaging of Neoglottic Vibration After Total Laryngectomy. **Archives of Otolaryngology–Head & Neck Surgery**, v. 125, n. 8, p. 891, Aug. 1999. ISSN 0886-4470. DOI: 10.1001/archotol.125.8.891.

VAN AS, C. J. **Tracheoesophageal speech: a multidimensional assessment of voice quality**. Amsterdam: Selbstverl, 2001. OCLC: 248575806. ISBN 978-90-90-15058-1.

VAN AS-BROOKS, C. J. et al. Acoustic Signal Typing for Evaluation of Voice Quality in Tracheoesophageal Speech. **Journal of Voice**, v. 20, n. 3, p. 355–368, Sept. 2006. ISSN 08921997. DOI: 10.1016/j.jvoice.2005.04.008.

VAN DEN BERG, J. Myoelastic-Aerodynamic Theory of Voice Production. **Journal of Speech Language and Hearing Research**, v. 1, n. 3, p. 227, Sept. 1958. ISSN 1092-4388. DOI: 10.1044/jshr.0103.227.

VAN WEISSENBRUCH, R. et al. Cineradiography of the Pharyngoesophageal Segment in Postlaryngectomy Patients. **Annals of Otology, Rhinology & Laryngology**, v. 109, n. 3, p. 311–319, Mar. 2000. ISSN 0003-4894, 1943-572X. DOI: 10.1177/000348940010900314.

VERKERKE, G.; THOMSON, S. Sound-Producing Voice Prostheses: 150 Years of Research. **Annual Review of Biomedical Engineering**, v. 16, n. 1, p. 215–245, July 2014. ISSN 1523-9829, 1545-4274. DOI: 10.1146/annurev-bioeng-071811-150014.

VIRTANEN, P. et al. SciPy 1.0: Fundamental Algorithms for Scientific Computing in Python. **Nature Methods**, v. 17, p. 261–272, 2020. DOI: 10.1038/s41592-019-0686-2.

WANG, Q. et al. Anatomic Continuity of Longitudinal Pharyngeal and Esophageal Muscles: **The Laryngoscope**, v. 117, n. 2, p. 282–287, Feb. 2007. ISSN 0023-852X. DOI: 10.1097/01.mlg.0000249935.81808.df.

WARD, E. et al. Rehabilitation of olfaction post-laryngectomy: a randomised control trial comparing clinician assisted versus a home practice approach. **Clinical Otolaryngology**, v. 35, n. 1, p. 39–45, Feb. 2010. ISSN 17494478, 17494486. DOI: 10.1111/j.1749-4486.2009.02050.x.

WELCH, R. W.; GATES, G. A., et al. Change in the Force-Summed Pressure Measurements of the Upper Esophageal Sphincter Prelaryngectomy and Postlaryngectomy. **Annals of Otology, Rhinology & Laryngology**, v. 88, n. 6, p. 804–808, Nov. 1979. ISSN 0003-4894, 1943-572X. DOI: 10.1177/000348947908800611.

WELCH, R. W.; LUCKMANN, K., et al. Manometry of the Normal Upper Esophageal Sphincter and its Alterations in Laryngectomy. **Journal of Clinical Investigation**, v. 63, n. 5, p. 1036–1041, May 1979. ISSN 0021-9738. DOI: 10.1172/JCI109372.

WHITTLESEY, R. W. **Dynamics and Scaling of Self-Excited Passive Vortex Generators for Underwater Propulsion**. 2013. PhD thesis – California Institute of Technology, California.

WINANS, C. S.; REICHBACH, E. J.; WALDROP, W. F. Esophageal Determinants of Alaryngeal Speech. **Archives of Otolaryngology - Head and Neck Surgery**, v. 99, n. 1, p. 10–14, Jan. 1974. ISSN 0886-4470. DOI: 10.1001/archotol.1974.00780030014002.

WORLD HEALTH ORGANIZATION. **Larynx – Fact sheet**. [S.l.]: World Health Organization. International Agency for Research on Cancer. Global Cancer Observatory, 2020. Available from: https://gco.iarc.fr/today/data/factsheets/cancers/14-Larynx-fact-sheet.pdf. Visited on: 24 Feb. 2021.

XIA, Y. et al. Effect of Initial Axial Strain of Collapsible Tube on Self-Excited Oscillation. **JSME International Journal Series C**, v. 43, n. 4, p. 882–888, 2000. ISSN 1344-7653, 1347-538X. DOI: 10.1299/jsmec.43.882.

XU, F.; BILLINGHAM, J.; JENSEN, O. E. Divergence-driven oscillations in a flexible-channel flow with fixed upstream flux. **Journal of Fluid Mechanics**, v. 723, p. 706–733, May 2013. ISSN 0022-1120, 1469-7645. DOI: 10.1017/jfm.2013.97.

XU, F.; BILLINGHAM, J.; JENSEN, O. E. Resonance-driven oscillations in a flexible-channel flow with fixed upstream flux and a long downstream rigid segment. **Journal of Fluid Mechanics**, v. 746, p. 368–404, May 2014. ISSN 0022-1120, 1469-7645. DOI: 10.1017/jfm.2014.136.

XUE, Q. et al. Subject-specific computational modeling of human phonation. **The Journal of the Acoustical Society of America**, v. 135, n. 3, p. 1445–1456, Mar. 2014. ISSN 0001-4966. DOI: 10.1121/1.4864479.

YAMAMOTO, M. et al. Morphology of the Upper Esophageal Sphincter or Cricopharyngeus Muscle Revisited: A Study Using Adult and Fetal Specimens. **Clinical Anatomy**, v. 33, n. 5, p. 782–794, July 2020. ISSN 0897-3806, 1098-2353. DOI: 10.1002/ca.23506.

ZAÑARTU, M.; MONGEAU, L.; WODICKA, G. R. Influence of acoustic loading on an effective single mass model of the vocal folds. **The Journal of the Acoustical Society of America**, v. 121, n. 2, p. 1119–1129, Feb. 2007. ISSN 0001-4966. DOI: 10.1121/1.2409491.

ZHANG, C.; ZHAO, W., et al. Computational aeroacoustics of phonation, Part II: Effects of flow parameters and ventricular folds. **The Journal of the Acoustical Society of America**, v. 112, n. 5, p. 2147–2154, Nov. 2002. ISSN 0001-4966. DOI: 10.1121/1.1506694.

ZHANG, T.; BAI, S., et al. Modeling of pharyngoesophageal segment during tracheoesophageal phonation in total laryngectomy patients with preliminary validation. In: 2016 38th Annual International Conference of the IEEE Engineering in Medicine and Biology Society (EMBC). Orlando, FL, USA: IEEE, Aug. 2016. P. 2917–2920. DOI: 10.1109/EMBC.2016.7591340.

ZHANG, T.; COOK, I., et al. The relationship between biomechanics of pharyngoesophageal segment and tracheoesophageal phonation. **Scientific Reports**, v. 9, n. 1, p. 9722, Dec. 2019. ISSN 2045-2322. DOI: 10.1038/s41598-019-46223-7.

ZHANG, X.; OSBORN, T.; KALRA, S. A noninvasive ultrasound elastography technique for measuring surface waves on the lung. **Ultrasonics**, v. 71, p. 183–188, Sept. 2016. ISSN 0041624X. DOI: 10.1016/j.ultras.2016.06.012.

ZHANG, Z. Mechanics of human voice production and control. **The Journal of the Acoustical Society of America**, v. 140, n. 4, p. 2614–2635, Oct. 2016. ISSN 0001-4966. DOI: 10.1121/1.4964509.

ZHANG, Z.; NEUBAUER, J.; BERRY, D. A. Aerodynamically and acoustically driven modes of vibration in a physical model of the vocal folds. **The Journal of the Acoustical Society of America**, v. 120, n. 5, p. 2841–2849, 2006.

ZHANG, Z.; NEUBAUER, J.; BERRY, D. A. The influence of subglottal acoustics on laboratory models of phonation. **The Journal of the Acoustical Society of America**, v. 120, n. 3, p. 1558–1569, Sept. 2006. ISSN 0001-4966. DOI: 10.1121/1.2225682.

Glossary

caudal In human anatomy, synonym of inferior. (DORLAND, 2011)

coronal plane Any vertical plane separating the human body into ventral and dorsal parts.

electromyography An exam where the electrical activity in a muscle is measured. (MILLS, 2005)

glottis The space between the vocal folds.

hemilarynx A lateral half of a larynx.

laryngectomee Person who has had his/her larynx surgically removed in a total laryngectomy.

lumen The cavity or channel within a tube or tubular organ. (DORLAND, 2011)

mucosal wave Wave that propagates on the surface of the vocal folds from the inferior part to the superior during phonation.

phonation Flow-induced vibration that produces voice.

platisma muscle A flat muscle running from the collarbone to the lower jaw (COLLIN, 2005). It covers the anterior part of the neck, just beneath the skin.

raphe A seam; in anatomy, the line of union of the halves of any various symmetrical parts. (DORLAND, 2011)

rostral Direction toward the oral and nasal region. (DORLAND, 2011)

saggital plane Any vertical plane separating the human body into left and right parts.

smooth muscle A type of muscle without transverse striations in its constituent fibers that is not under voluntary control (DORLAND, 2011). For this reason, it is also called nonstriated involuntary muscle (MARTINI; TIMMONS; TALLITSCH, 2012).

total laryngectomy A surgical procedure in which the entire larynx is excised.

tracheostoma A surgically created opening in the neck through which the laryngectomee breathes.

transverse plane Any horizontal plane separating the human body into superior and inferior parts.

Appendix

APPENDIX A – Discretization of the steady-state equation

This appendix presents the procedure of discretization of the steady-state equation (Equation 32) following the spectral collocation method discussed in Subsection 3.4.

The problem is rewritten here, for convenience.

$$\begin{cases} T h_s^3 \dfrac{\mathrm{d}^3 h_s}{\mathrm{d}x^3} + \dfrac{6}{5}\dfrac{\mathrm{d}h_s}{\mathrm{d}x} - h_s^3 \dfrac{\mathrm{d}P_e}{\mathrm{d}x} - \dfrac{12}{R} = 0, & \text{(81a)} \\ h_s(0) = 1, & \text{(81b)} \\ h_s(1) = 1, & \text{(81c)} \\ T \left.\dfrac{\mathrm{d}^2 h_s}{\mathrm{d}x^2}\right|_{x=1} = -\dfrac{12L_2}{R} + P_e(1). & \text{(81d)} \end{cases}$$

We begin with a simple change of variables to transform the domain from $[0, 1]$ to $[-1, 1]$. The problem is rewritten in terms of $\hat{x} = 2x - 1$. We obtain

$$\begin{cases} 8T\, h_s^3\, h_s''' + \dfrac{12}{5} h_s' - 2h_s^3\, P_e' - \dfrac{12}{R} = 0, & \text{(82a)} \\ h_s(-1) = 1, & \text{(82b)} \\ h_s(1) = 1, & \text{(82c)} \\ 4T\, h_s''\big|_{\hat{x}=1} = -\dfrac{12L_2}{R} + P_e(1). & \text{(82d)} \end{cases}$$

In Equation (82), primes have been used to denote the derivative with respect to $\hat{x}$. The derivative of highest order, h_s''', is then written as a truncated series of Chebyshev polynomials. Derivatives of lower order, as well as h_s itself, are written in terms of the integrals of Chebyshev polynomials and integration constants[1]:

$$h_s'''(\hat{x}) = \sum_{j=0}^{N} a_j \psi_j^0(\hat{x}), \tag{83a}$$

$$h_s''(\hat{x}) = \sum_{j=0}^{N} a_j \psi_j^1(\hat{x}) + a_{N+1}, \tag{83b}$$

$$h_s'(\hat{x}) = \sum_{j=0}^{N} a_j \psi_j^2(\hat{x}) + a_{N+1}\hat{x} + a_{N+2}, \tag{83c}$$

$$h_s(\hat{x}) = \sum_{j=0}^{N} a_j \psi_j^3(\hat{x}) + a_{N+1}\frac{\hat{x}^2}{2} + a_{N+2}\hat{x} + a_{N+3}, \tag{83d}$$

[1] The same nomenclature is used to denote both the functions h_s, h_s', h_s'', and h_s''', and their series approximations (Equation 83). This is done to avoid an excessively cumbersome notation. Henceforth, h_s, h_s', h_s'', and h_s''' are used to indicate mainly the respective series approximation; however the context should make the proper meaning clear.

where $\psi_j^0(\hat{x})$ is the Chebyshev polynomial of order j, and $\psi_j^1(\hat{x}) = \int \psi_j^0(\hat{x})\mathrm{d}\hat{x}$, $\psi_j^2(\hat{x}) = \int \psi_j^1(\hat{x})\mathrm{d}\hat{x}$, and $\psi_j^3(\hat{x}) = \int \psi_j^2(\hat{x})\mathrm{d}\hat{x}$.

Equations (83) may be applied to the boundary value problem (Equation 82); however, due to the use of the truncated series, the equations are not satisfied exactly, and a residual $r(\hat{x})$ remains.

$$\begin{cases} 8T\, h_s^3\, h_s''' + \dfrac{12}{5} h_s' - 2h_s^3\, P_e' - \dfrac{12}{R} = r, & \text{(84a)} \\ h_s(-1) = 1 + r, & \text{(84b)} \\ h_s(1) = 1 + r, & \text{(84c)} \\ 4T\, h_s''\big|_{\hat{x}=1} = -\dfrac{12L_2}{R} + P_e(1) + r. & \text{(84d)} \end{cases}$$

These series approximations are to be evaluated at the Gauss-Chebyshev-Lobatto points $\hat{x}_i = \cos(i\pi/N)$, with $i = 0, 1, \ldots, N$.

$$h_{s_i}''' = \sum_{j=0}^{N} a_j \psi_j^0(\hat{x}_i), \tag{85a}$$

$$h_{s_i}'' = \sum_{j=0}^{N} a_j \psi_j^1(\hat{x}_i) + a_{N+1}, \tag{85b}$$

$$h_{s_i}' = \sum_{j=0}^{N} a_j \psi_j^2(\hat{x}_i) + a_{N+1}\hat{x}_i + a_{N+2}, \tag{85c}$$

$$h_{s_i} = \sum_{j=0}^{N} a_j \psi_j^3(\hat{x}_i) + a_{N+1}\frac{\hat{x}_i^2}{2} + a_{N+2}\hat{x}_i + a_{N+3}. \tag{85d}$$

In Equation (85), h_{s_i} is defined to be $h_s(\hat{x}_i)$. Likewise, $h_{s_i}' = h_s'(\hat{x}_i)$, $h_{s_i}'' = h_s''(\hat{x}_i)$ and $h_{s_i}''' = h_s'''(\hat{x}_i)$.

These can be written in a more compact form by defining the matrices $[\psi^0]$, $[\psi^1]$, $[\psi^2]$, and $[\psi^3]$,

$$[\psi^0] = \left[\begin{array}{cccc:ccc} \psi_0^0(\hat{x}_0) & \psi_1^0(\hat{x}_0) & \cdots & \psi_N^0(\hat{x}_0) & 0 & 0 & 0 \\ \psi_0^0(\hat{x}_1) & \psi_1^0(\hat{x}_1) & \cdots & \psi_N^0(\hat{x}_1) & 0 & 0 & 0 \\ \vdots & \vdots & \ddots & \vdots & \vdots & \vdots & \vdots \\ \psi_0^0(\hat{x}_N) & \psi_1^0(\hat{x}_N) & \cdots & \psi_N^0(\hat{x}_N) & 0 & 0 & 0 \end{array}\right], \tag{86}$$

$$[\psi^1] = \left[\begin{array}{cccc:ccc} \psi_0^1(\hat{x}_0) & \psi_1^1(\hat{x}_0) & \cdots & \psi_N^1(\hat{x}_0) & 1 & 0 & 0 \\ \psi_0^1(\hat{x}_1) & \psi_1^1(\hat{x}_1) & \cdots & \psi_N^1(\hat{x}_1) & 1 & 0 & 0 \\ \vdots & \vdots & \ddots & \vdots & \vdots & \vdots & \vdots \\ \psi_0^1(\hat{x}_N) & \psi_1^1(\hat{x}_N) & \cdots & \psi_N^1(\hat{x}_N) & 1 & 0 & 0 \end{array}\right], \tag{87}$$

$$[\psi^2] = \left[\begin{array}{cccc:ccc} \psi_0^2(\hat{x}_0) & \psi_1^2(\hat{x}_0) & \cdots & \psi_N^2(\hat{x}_0) & \hat{x}_0 & 1 & 0 \\ \psi_0^2(\hat{x}_1) & \psi_1^2(\hat{x}_1) & \cdots & \psi_N^2(\hat{x}_1) & \hat{x}_1 & 1 & 0 \\ \vdots & \vdots & \ddots & \vdots & \vdots & \vdots & \vdots \\ \psi_0^2(\hat{x}_N) & \psi_1^2(\hat{x}_N) & \cdots & \psi_N^2(\hat{x}_N) & \hat{x}_N & 1 & 0 \end{array}\right], \tag{88}$$

$$[\psi^3] = \left[\begin{array}{cccc:ccc} \psi_0^3(\hat{x}_0) & \psi_1^3(\hat{x}_0) & \cdots & \psi_N^3(\hat{x}_0) & \hat{x}_0^2/2 & \hat{x}_0 & 1 \\ \psi_0^3(\hat{x}_1) & \psi_1^3(\hat{x}_1) & \cdots & \psi_N^3(\hat{x}_1) & \hat{x}_1^2/2 & \hat{x}_1 & 1 \\ \vdots & \vdots & \ddots & \vdots & \vdots & \vdots & \vdots \\ \psi_0^3(\hat{x}_N) & \psi_1^3(\hat{x}_N) & \cdots & \psi_N^3(\hat{x}_N) & \hat{x}_N^2/2 & \hat{x}_N & 1 \end{array}\right], \tag{89}$$

as well as the vectors $\{h_s\} = \{\, h_{s_0}\ h_{s_1} \cdots h_{s_N} \,\}^T$, $\{h'_s\} = \{\, h'_{s_0}\ h'_{s_1} \cdots h'_{s_N} \,\}^T$, $\{h''_s\} = \{\, h''_{s_0}\ h''_{s_1} \cdots h''_{s_N} \,\}^T$, $\{h'''_s\} = \{\, h'''_{s_0}\ h'''_{s_1} \cdots h'''_{s_N} \,\}^T$, and $\{a\} = \{\, a_0\ a_1 \cdots a_N\ a_{N+1}\ a_{N+2}\ a_{N+3} \,\}^T$. One obtains:

$$\{h'''_s\} = [\psi^0]\{a\}, \tag{90a}$$

$$\{h''_s\} = [\psi^1]\{a\}, \tag{90b}$$

$$\{h'_s\} = [\psi^2]\{a\}, \tag{90c}$$

$$\{h_s\} = [\psi^3]\{a\}. \tag{90d}$$

$$\tag{90e}$$

Equations (90) may be substituted in the differential equation,

$$\begin{aligned} \{r\} = {} & 8T\left([\psi^3]\{a\} \circ [\psi^3]\{a\} \circ [\psi^3]\{a\}\right) \circ [\psi^0]\{a\} \\ & - 2\left([\psi^3]\{a\} \circ [\psi^3]\{a\} \circ [\psi^3]\{a\}\right) \circ \{P'_e\} + \frac{12}{5}[\psi^2]\{a\} - \frac{12}{R}\{1\}, \end{aligned} \tag{91}$$

where $\{r\}$ is a vector of the residuals evaluated at the Gauss-Chebyshev-Lobatto points, $\{P'_e\} = \{\, P'_e(\hat{x}_0)\ P'_e(\hat{x}_1) \cdots P'_e(\hat{x}_N) \,\}$, and $\{1\} = \{\, 1\ 1 \cdots 1 \,\}$. Additionally, the operator "$\circ$" represents the element-wise, or Hadamard, product of vectors.

The approximations of Equation (90) can also be substituted in the boundary conditions. One obtains:

$$([\psi^3]\{a\})_N - 1 = r_{N+1}, \tag{92a}$$

$$([\psi^3]\{a\})_0 - 1 = r_{N+2}, \tag{92b}$$

$$(4T[\psi^1]\{a\})_0 - \{P_e\}_0 + \frac{12L_2}{R} = r_{N+3}, \tag{92c}$$

where r_{N+1}, r_{N+2}, and r_{N+3} are the residuals associated with the boundary conditions.

The residuals are then set to zero at the Gauss-Chebyshev-Lobatto points, including those associated with the boundary conditions. The following nonlinear system of $N + 4$

equations and $N+4$ unknowns is obtained.

$$\begin{cases} \{0\} = 8T\left([\psi^3]\{a\} \circ [\psi^3]\{a\} \circ [\psi^3]\{a\}\right) \circ [\psi^0]\{a\} \\ \qquad - 2\left([\psi^3]\{a\} \circ [\psi^3]\{a\} \circ [\psi^3]\{a\}\right) \circ \{P'_e\} + \frac{12}{5}[\psi^2]\{a\} - \frac{12}{R}\{1\}, & \text{(93a)} \\ 0 = ([\psi^3]\{a\})_N - 1, & \text{(93b)} \\ 0 = ([\psi^3]\{a\})_0 - 1, & \text{(93c)} \\ 0 = (4T[\psi^1]\{a\})_0 - \{P_e\}_0 + \frac{12L_2}{R}, & \text{(93d)} \end{cases}$$

where $\{0\}$ is the null vector.

The system in Equation (93) is solved for $\{a\}$. The vertical position of the membrane at steady-state may then be readily reconstructed by means of Equation (90).

For the solution of the system, the Jacobian matrix $[J]$ of the vector of residuals (extended to account for the residuals at the boundary conditions) is used. The components of $[J]$ may be obtained by simple differentiation. For the first $N+1$ rows, the element of the k-th column of the i-th row ($i = 0, 1, \ldots, N$) is given by

$$J_{ik} = \frac{\partial r_i}{\partial a_k} = 8T\, h_{s_i}^3\, \psi_{ik}^0 + 24T\, h_{s_i}^2 \left(\sum_{j=0}^{N+3} \psi_{ij}^0 a_j\right) \psi_{ik}^3 - 6h_{s_i}^2\, \psi_{ik}^3\, P'_{e_i} + \frac{12\, \psi_{ik}^2}{5}. \tag{94}$$

Similarly, for $i = N+1$:

$$J_{N+1,k} = \frac{\partial r_{N+1}}{\partial a_k} = \psi_{N,k}^3, \tag{95}$$

for $i = N+2$:

$$J_{N+2,k} = \frac{\partial r_{N+2}}{\partial a_k} = \psi_{0,k}^3, \tag{96}$$

and for $i = N+3$:

$$J_{N+3,k} = \frac{\partial r_{N+3}}{\partial a_k} = 4T\, \psi_{0,k}^1. \tag{97}$$

APPENDIX B – DISCRETIZATION OF THE LINEARIZED EQUATIONS

The present appendix shows the application of the integral-based spectral collocation method described in Subsection 3.4 to the linearized equations (Equation 60). These equations are repeated below, for convenience.

$$\begin{cases} \lambda\tilde{h} = -\dfrac{d\tilde{q}}{dx}, & \text{(98a)} \\ \lambda\left(\tilde{q} - Mh_s\dfrac{d^2\tilde{q}}{dx^2}\right) = \dfrac{6}{5}\dfrac{d}{dx}\left(\dfrac{\tilde{h}}{h_s^2} - \dfrac{2\tilde{q}}{h_s}\right) - \tilde{h}\dfrac{dP_e}{dx} & \\ \qquad + Th_s\dfrac{d^3\tilde{h}}{dx^3} + T\dfrac{d^3h_s}{dx^3}\tilde{h} - \dfrac{12}{R}\left(\dfrac{\tilde{q}}{h_s^2} - \dfrac{2\tilde{h}}{h_s^3}\right), & \text{(98b)} \\ \tilde{h}(0) = 0, & \text{(98c)} \\ \tilde{h}(1) = 0, & \text{(98d)} \\ \tilde{q}(0) = 0, & \text{(98e)} \\ \lambda L_2\tilde{q}(1) = -T\left.\dfrac{\mathrm{d}^2\tilde{h}}{\mathrm{d}x^2}\right|_{x=1} - \dfrac{12L_2}{R}\tilde{q}(1). & \text{(98f)} \end{cases}$$

The first step consists once again of a change of variables to transform the domain from $[0,1]$ to $[-1,1]$ ($\hat{x} = 2x - 1$). As was done in Appendix A, primes are used to indicate differentiation with respect to the spatial variable. One obtains:

$$\begin{cases} \lambda\tilde{h} = -2\tilde{q}' & \text{(99a)} \\ \lambda\left(\tilde{q} - 4Mh_s\tilde{q}''\right) = \dfrac{6}{5}\left(-\dfrac{4h_s'}{h_s^3}\tilde{h} + \dfrac{2}{h_s^2}\tilde{h}' + \dfrac{4h_s'}{h_s^2}\tilde{q} - \dfrac{4}{h_s}\tilde{q}'\right) - 2P_e'\tilde{h} & \\ \qquad + 8Th_s\tilde{h}''' + 8Th_s'''\tilde{h} - \dfrac{12}{R}\left(\dfrac{1}{h_s^2}\tilde{q} - \dfrac{2}{h_s^3}\tilde{h}\right), & \text{(99b)} \\ \tilde{h}(-1) = 0, & \text{(99c)} \\ \tilde{h}(1) = 0, & \text{(99d)} \\ \tilde{q}(-1) = 0, & \text{(99e)} \\ 4T\tilde{h}''(1) = -L_2\left(\lambda + \dfrac{12}{R}\right)\tilde{q}(1). & \text{(99f)} \end{cases}$$

The Chebyshev series approximation to the functions $\tilde{h}'''$ and $\tilde{q}''$ is considered. Lower derivatives are also approximated, but in terms of the integrals of the Chebyshev polynomials.

$$\tilde{h}'''(\hat{x}) = \sum_{j=0}^{N} a_j \psi_j^0(\hat{x}), \tag{100a}$$

$$\tilde{h}''(\hat{x}) = \sum_{j=0}^{N} a_j \psi_j^1(\hat{x}) + a_{N+1}, \tag{100b}$$

$$\tilde{h}'(\hat{x}) = \sum_{j=0}^{N} a_j \psi_j^2(\hat{x}) + a_{N+1}\hat{x} + a_{N+2}, \tag{100c}$$

$$\tilde{h}(\hat{x}) = \sum_{j=0}^{N} a_j \psi_j^3(\hat{x}) + a_{N+1}\frac{\hat{x}^2}{2} + a_{N+2}\hat{x} + a_{N+3}, \tag{100d}$$

$$\tilde{q}''(\hat{x}) = \sum_{j=0}^{N} b_j \psi_j^0(\hat{x}), \tag{101a}$$

$$\tilde{q}'(\hat{x}) = \sum_{j=0}^{N} b_j \psi_j^1(\hat{x}) + b_{N+1}, \tag{101b}$$

$$\tilde{q}(\hat{x}) = \sum_{j=0}^{N} b_j \psi_j^2(\hat{x}) + b_{N+1}\hat{x} + b_{N+2}. \tag{101c}$$

It can be noted that the process creates 5 integration constants (a_{N+1}, a_{N+2}, a_{N+3}, b_{N+1}, and b_{N+2}). Since there are only four boundary conditions, an additional condition must be used. Consideration of the continuity equation (Equation 99a), together with the boundary condition $\tilde{h}(1) = 0$, provides the required condition.

$$\tilde{q}'(1) = 0. \tag{102}$$

These approximations are then assessed at the Gauss-Chebyshev-Lobatto points. In matrix notation, they become:

$$\{\tilde{h}'''\} = [H^0]\{a\}, \tag{103a}$$

$$\{\tilde{h}''\} = [H^1]\{a\}, \tag{103b}$$

$$\{\tilde{h}'\} = [H^2]\{a\}, \tag{103c}$$

$$\{\tilde{h}\} = [H^3]\{a\}. \tag{103d}$$

$$\{\tilde{q}''\} = [Q^0]\{b\}, \tag{104a}$$

$$\{\tilde{q}'\} = [Q^1]\{b\}, \tag{104b}$$

$$\{\tilde{q}\} = [Q^2]\{b\}. \tag{104c}$$

Here, $\{\tilde{h}'''\} = \{\, \tilde{h}'''(\hat{x}_0)\; \tilde{h}'''(\hat{x}_1) \cdots \tilde{h}'''(\hat{x}_N) \,\}^T$, $\{\tilde{h}''\} = \{\, \tilde{h}''(\hat{x}_0)\; \tilde{h}''(\hat{x}_1) \cdots \tilde{h}''(\hat{x}_N) \,\}^T$, $\{\tilde{h}'\} = \{\, \tilde{h}'(\hat{x}_0)\; \tilde{h}'(\hat{x}_1) \cdots \tilde{h}'(\hat{x}_N) \,\}^T$, $\{\tilde{h}\} = \{\, \tilde{h}(\hat{x}_0)\; \tilde{h}(\hat{x}_1) \cdots \tilde{h}(\hat{x}_N) \,\}^T$, $\{\tilde{q}''\} = \{\, \tilde{q}''(\hat{x}_0)\; \tilde{q}''(\hat{x}_1) \cdots \tilde{q}''(\hat{x}_N) \,\}^T$,

$\{\tilde{q}'\} = \{\, \tilde{q}'(\hat{x}_0)\; \tilde{q}'(\hat{x}_1) \cdots \tilde{q}'(\hat{x}_N) \,\}^T$, $\{\tilde{q}\} = \{\, \tilde{q}(\hat{x}_0)\; \tilde{q}(\hat{x}_1) \cdots \tilde{q}(\hat{x}_N) \,\}^T$, $\{a\} = \{\, a_0\; a_1 \cdots a_{N+3} \,\}^T$, and $\{b\} = \{\, b_0\; b_1 \cdots b_{N+2} \,\}^T$. The matrices in Equations (103) and (104) are given by Equations (105)–(111):

$$[H^0] = \left[\begin{array}{cccc:ccc} \psi_0^0(\hat{x}_0) & \psi_1^0(\hat{x}_0) & \cdots & \psi_N^0(\hat{x}_0) & 0 & 0 & 0 \\ \psi_0^0(\hat{x}_1) & \psi_1^0(\hat{x}_1) & \cdots & \psi_N^0(\hat{x}_1) & 0 & 0 & 0 \\ \vdots & \vdots & \ddots & \vdots & \vdots & \vdots & \vdots \\ \psi_0^0(\hat{x}_N) & \psi_1^0(\hat{x}_N) & \cdots & \psi_N^0(\hat{x}_N) & 0 & 0 & 0 \end{array}\right], \tag{105}$$

$$[H^1] = \left[\begin{array}{cccc:ccc} \psi_0^1(\hat{x}_0) & \psi_1^1(\hat{x}_0) & \cdots & \psi_N^1(\hat{x}_0) & 1 & 0 & 0 \\ \psi_0^1(\hat{x}_1) & \psi_1^1(\hat{x}_1) & \cdots & \psi_N^1(\hat{x}_1) & 1 & 0 & 0 \\ \vdots & \vdots & \ddots & \vdots & \vdots & \vdots & \vdots \\ \psi_0^1(\hat{x}_N) & \psi_1^1(\hat{x}_N) & \cdots & \psi_N^1(\hat{x}_N) & 1 & 0 & 0 \end{array}\right], \tag{106}$$

$$[H^2] = \left[\begin{array}{cccc:ccc} \psi_0^2(\hat{x}_0) & \psi_1^2(\hat{x}_0) & \cdots & \psi_N^2(\hat{x}_0) & \hat{x}_0 & 1 & 0 \\ \psi_0^2(\hat{x}_1) & \psi_1^2(\hat{x}_1) & \cdots & \psi_N^2(\hat{x}_1) & \hat{x}_1 & 1 & 0 \\ \vdots & \vdots & \ddots & \vdots & \vdots & \vdots & \vdots \\ \psi_0^2(\hat{x}_N) & \psi_1^2(\hat{x}_N) & \cdots & \psi_N^2(\hat{x}_N) & \hat{x}_N & 1 & 0 \end{array}\right], \tag{107}$$

$$[H^3] = \left[\begin{array}{cccc:ccc} \psi_0^3(\hat{x}_0) & \psi_1^3(\hat{x}_0) & \cdots & \psi_N^3(\hat{x}_0) & \hat{x}_0^2/2 & \hat{x}_0 & 1 \\ \psi_0^3(\hat{x}_1) & \psi_1^3(\hat{x}_1) & \cdots & \psi_N^3(\hat{x}_1) & \hat{x}_1^2/2 & \hat{x}_1 & 1 \\ \vdots & \vdots & \ddots & \vdots & \vdots & \vdots & \vdots \\ \psi_0^3(\hat{x}_N) & \psi_1^3(\hat{x}_N) & \cdots & \psi_N^3(\hat{x}_N) & \hat{x}_N^2/2 & \hat{x}_N & 1 \end{array}\right], \tag{108}$$

$$[Q^0] = \left[\begin{array}{cccc:cc} \psi_0^0(\hat{x}_0) & \psi_1^0(\hat{x}_0) & \cdots & \psi_N^0(\hat{x}_0) & 0 & 0 \\ \psi_0^0(\hat{x}_1) & \psi_1^0(\hat{x}_1) & \cdots & \psi_N^0(\hat{x}_1) & 0 & 0 \\ \vdots & \vdots & \ddots & \vdots & \vdots & \vdots \\ \psi_0^0(\hat{x}_N) & \psi_1^0(\hat{x}_N) & \cdots & \psi_N^0(\hat{x}_N) & 0 & 0 \end{array}\right], \tag{109}$$

$$[Q^1] = \left[\begin{array}{cccc:cc} \psi_0^1(\hat{x}_0) & \psi_1^1(\hat{x}_0) & \cdots & \psi_N^1(\hat{x}_0) & 1 & 0 \\ \psi_0^1(\hat{x}_1) & \psi_1^1(\hat{x}_1) & \cdots & \psi_N^1(\hat{x}_1) & 1 & 0 \\ \vdots & \vdots & \ddots & \vdots & \vdots & \vdots \\ \psi_0^1(\hat{x}_N) & \psi_1^1(\hat{x}_N) & \cdots & \psi_N^1(\hat{x}_N) & 1 & 0 \end{array}\right], \tag{110}$$

$$[Q^2] = \left[\begin{array}{cccc:cc} \psi_0^2(\hat{x}_0) & \psi_1^2(\hat{x}_0) & \cdots & \psi_N^2(\hat{x}_0) & \hat{x}_0 & 1 \\ \psi_0^2(\hat{x}_1) & \psi_1^2(\hat{x}_1) & \cdots & \psi_N^2(\hat{x}_1) & \hat{x}_1 & 1 \\ \vdots & \vdots & \ddots & \vdots & \vdots & \vdots \\ \psi_0^2(\hat{x}_N) & \psi_1^2(\hat{x}_N) & \cdots & \psi_N^2(\hat{x}_N) & \hat{x}_N & 1 \end{array}\right]. \tag{111}$$

Substitution of Equations (103) and (104) in Equation (99) leads to a set of $2N+7$ equations ($N+1$ from the continuity equation, $N+1$ from the momentum equation, four from the boundary conditions, and one from Equation 102). There are $2N+8$ terms to be determined (the $N+4$ components of $\{a\}$, the $N+3$ components of $\{b\}$, and λ). However, the eigenvalue λ does not appear in three of the boundary conditions, and neither in Equation (102). These four equations impose relationships between the components of $\{a\}$ and $\{b\}$ that must hold regardless of the eigenvalue. Therefore, four of the components of $\{a\}$ and $\{b\}$ may be written in terms of the remaining ones.

Here, we choose to write a_{N+2}, a_{N+3}, b_{N+1}, and b_{N+2} in terms of the remaining components. We define $\{\hat{a}\} = \{\, a_0\ a_1\ \cdots\ a_{N+1} \,\}^T$, $\{a^*\} = \{\, a_{N+2}\ a_{N+3} \,\}^T$, $\{\hat{b}\} = \{\, b_0\ b_1\ \cdots\ b_N \,\}^T$, and $\{b^*\} = \{\, b_{N+1}\ b_{N+2} \,\}^T$, so that

$$\{a\} = \begin{Bmatrix} \{\hat{a}\} \\ \{a^*\} \end{Bmatrix}, \tag{112}$$

and

$$\{b\} = \begin{Bmatrix} \{\hat{b}\} \\ \{b^*\} \end{Bmatrix}. \tag{113}$$

Considering first the boundary conditions in which λ does not appear,

$$\tilde{h}(-1) = ([H^3]\{a\})_N = 0, \tag{114a}$$

$$\tilde{h}(1) = ([H^3]\{a\})_0 = 0, \tag{114b}$$

$$\tilde{q}(-1) = ([Q^2]\{b\})_N = 0, \tag{114c}$$

$$\tilde{q}'(1) = ([Q^1]\{b\})_0 = 0. \tag{114d}$$

The first two equations may be rewritten as

$$\left[\begin{array}{cccc:cc} \psi_0^3(\hat{x}_N) & \psi_1^3(\hat{x}_N) & \cdots & \psi_N^3(\hat{x}_N) & \hat{x}_N^2/2 & \hat{x}_N & 1 \\ \psi_0^3(\hat{x}_0) & \psi_1^3(\hat{x}_0) & \cdots & \psi_N^3(\hat{x}_0) & \hat{x}_0^2/2 & \hat{x}_0 & 1 \end{array}\right] \begin{Bmatrix} \{\hat{a}\} \\ \{a^*\} \end{Bmatrix} = \{0\}, \tag{115}$$

while the last two may be rewritten as

$$\left[\begin{array}{cccc:cc} \psi_0^2(\hat{x}_N) & \psi_1^2(\hat{x}_N) & \cdots & \psi_N^2(\hat{x}_N) & \hat{x}_N & 1 \\ \psi_0^1(\hat{x}_0) & \psi_1^1(\hat{x}_0) & \cdots & \psi_N^1(\hat{x}_0) & 1 & 0 \end{array}\right] \begin{Bmatrix} \{\hat{b}\} \\ \{b^*\} \end{Bmatrix} = \{0\}. \tag{116}$$

Defining sub-matrices $[C_{a1}]$, $[C_{a2}]$, $[C_{b1}]$, and $[C_{b2}]$:

$$[C_{a1}] = \begin{bmatrix} \psi_0^3(\hat{x}_N) & \psi_1^3(\hat{x}_N) & \cdots & \psi_N^3(\hat{x}_N) & \hat{x}_N^2/2 \\ \psi_0^3(\hat{x}_0) & \psi_1^3(\hat{x}_0) & \cdots & \psi_N^3(\hat{x}_0) & \hat{x}_0^2/2 \end{bmatrix}, \tag{117a}$$

$$[C_{a2}] = \begin{bmatrix} \hat{x}_N & 1 \\ \hat{x}_0 & 1 \end{bmatrix}, \tag{117b}$$

$$[C_{b1}] = \begin{bmatrix} \psi_0^2(\hat{x}_N) & \psi_1^2(\hat{x}_N) & \cdots & \psi_N^2(\hat{x}_N) \\ \psi_0^1(\hat{x}_0) & \psi_1^1(\hat{x}_0) & \cdots & \psi_N^1(\hat{x}_0) \end{bmatrix} \tag{117c}$$

$$[C_{b2}] = \begin{bmatrix} \hat{x}_N & 1 \\ 1 & 0 \end{bmatrix} \tag{117d}$$

Equation (115) may then be rewritten in terms of sub-matrices $[C_{a1}]$ and $[C_{a2}]$,

$$\Big[[C_{a1}] \quad [C_{a2}]\Big]\begin{Bmatrix}\{\hat{a}\}\\ \{a^*\}\end{Bmatrix} = \{0\}, \tag{118}$$

$$[C_{a1}]\{\hat{a}\} + [C_{a2}]\{a^*\} = \{0\}. \tag{119}$$

Since $\hat{x}_i = \cos(i\pi/N)$, with $i = 0, 1, \ldots, N$, $\hat{x}_0 = 1$ and $\hat{x}_N = -1$. Therefore, $[C_{a2}]$ is nonsingular, and $\{a^*\}$ may be written in terms of $\{\hat{a}\}$, as was desired.

$$\{a^*\} = -[C_{a2}]^{-1}[C_{a1}]\{\hat{a}\} = [C_a]\{\hat{a}\}, \tag{120}$$

where we define $[C_a] = -[C_{a2}]^{-1}[C_{a1}]$. The same procedure may be applied for Equation (116), to obtain $\{b^*\}$ in terms of $\{\hat{b}\}$:

$$\{b^*\} = -[C_{b2}]^{-1}[C_{b1}]\{\hat{b}\} = [C_b]\{\hat{b}\}, \tag{121}$$

where $[C_b] = -[C_{b2}]^{-1}[C_{b1}]$.

Therefore,

$$\{a\} = \begin{Bmatrix}\{\hat{a}\}\\ [C_a]\{\hat{a}\}\end{Bmatrix}, \tag{122a}$$

$$\{b\} = \begin{Bmatrix}\{\hat{b}\}\\ [C_b]\{\hat{b}\}\end{Bmatrix}. \tag{122b}$$

Another useful step to take before applying the approximations of Equations (103) and (104) to the continuity equation, the momentum equation, and the remaining boundary condition, is to define sub-matrices of the matrices of Equations (105)–(111). Each matrix will be broken down in two parts, always separating the last two columns in one sub-matrix, and the remaining ones in the other. For example, matrix $[H^3]$,

$$[H^3] = \begin{bmatrix} \psi_0^3(\hat{x}_0) & \psi_1^3(\hat{x}_0) & \cdots & \psi_N^3(\hat{x}_0) & \hat{x}_0^2/2 & \hat{x}_0 & 1\\ \psi_0^3(\hat{x}_1) & \psi_1^3(\hat{x}_1) & \cdots & \psi_N^3(\hat{x}_1) & \hat{x}_1^2/2 & \hat{x}_1 & 1\\ \vdots & \vdots & \ddots & \vdots & \vdots & \vdots & \vdots\\ \psi_0^3(\hat{x}_N) & \psi_1^3(\hat{x}_N) & \cdots & \psi_N^3(\hat{x}_N) & \hat{x}_N^2/2 & \hat{x}_N & 1 \end{bmatrix}, \tag{123}$$

may be written as

$$[H^3] = \Big[[H_\psi^3] \quad [H_C^3]\Big], \tag{124}$$

where:

$$[H_\psi^3] = \begin{bmatrix} \psi_0^3(\hat{x}_0) & \psi_1^3(\hat{x}_0) & \cdots & \psi_N^3(\hat{x}_0) & \hat{x}_0^2/2\\ \psi_0^3(\hat{x}_1) & \psi_1^3(\hat{x}_1) & \cdots & \psi_N^3(\hat{x}_1) & \hat{x}_1^2/2\\ \vdots & \vdots & \ddots & \vdots & \vdots\\ \psi_0^3(\hat{x}_N) & \psi_1^3(\hat{x}_N) & \cdots & \psi_N^3(\hat{x}_N) & \hat{x}_N^2/2 \end{bmatrix}, \tag{125}$$

and:

$$[H^3_C] = \begin{bmatrix} \hat{x}_0 & 1 \\ \hat{x}_1 & 1 \\ \vdots & \vdots \\ \hat{x}_N & 1 \end{bmatrix}. \tag{126}$$

It should be noted that the same idea is applied to matrices $[Q^0]$, $[Q^1]$, and $[Q^2]$. For example,

$$[Q^1] = \begin{bmatrix} \psi^1_0(\hat{x}_0) & \psi^1_1(\hat{x}_0) & \cdots & \psi^1_N(\hat{x}_0) & 1 & 0 \\ \psi^1_0(\hat{x}_1) & \psi^1_1(\hat{x}_1) & \cdots & \psi^1_N(\hat{x}_1) & 1 & 0 \\ \vdots & \vdots & \ddots & \vdots & \vdots & \vdots \\ \psi^1_0(\hat{x}_N) & \psi^1_1(\hat{x}_N) & \cdots & \psi^1_N(\hat{x}_N) & 1 & 0 \end{bmatrix}, \tag{127}$$

may be written as:

$$[Q^1] = \Big[[Q^1_\psi] \quad [Q^1_C] \Big], \tag{128}$$

where

$$[Q^1_\psi] = \begin{bmatrix} \psi^1_0(\hat{x}_0) & \psi^1_1(\hat{x}_0) & \cdots & \psi^1_N(\hat{x}_0) \\ \psi^1_0(\hat{x}_1) & \psi^1_1(\hat{x}_1) & \cdots & \psi^1_N(\hat{x}_1) \\ \vdots & \vdots & \ddots & \vdots \\ \psi^1_0(\hat{x}_N) & \psi^1_1(\hat{x}_N) & \cdots & \psi^1_N(\hat{x}_N) \end{bmatrix}, \tag{129}$$

and

$$[Q^1_C] = \begin{bmatrix} 1 & 0 \\ 1 & 0 \\ \vdots & \vdots \\ 1 & 0 \end{bmatrix}. \tag{130}$$

Matrices $[H^0]$, $[H^1]$, $[H^2]$, and $[H^3]$ are all divided in one sub-matrix of dimensions $N+1 \times N+2$ (labeled with subscript ψ) and another with dimensions $N+1 \times 2$ (labeled with subscript "C"). Likewise, matrices $[Q^0]$, $[Q^1]$, and $[Q^2]$ are broken down in one sub-matrix of dimensions $N+1 \times N+1$ (labeled with subscript ψ), and another of dimensions $N+1 \times 2$ (labeled with subscript "C"). These definitions are made to allow for the separation of $\{a^*\}$ and $\{b^*\}$ (both of dimension 2) from $\{\hat{a}\}$ and $\{\hat{b}\}$. For instance, the approximation to $\tilde{h}'$ is

$$\{\tilde{h}'\} = [H^2]\{a\} = \Big[[H^2_\psi] \quad [H^2_C] \Big] \begin{Bmatrix} \{\hat{a}\} \\ \{a^*\} \end{Bmatrix} = [H^2_\psi]\{\hat{a}\} + [H^2_C]\{a^*\}. \tag{131}$$

We then proceed to apply the approximations of Equations (103) and (104) to the continuity equation, the momentum equation, and the boundary condition that contains the eigenvalue λ.

The continuity equation (Equation 98a) becomes

$$\lambda[H^3]\{a\} = -2[Q^1]\{b\}. \tag{132}$$

Separating $\{\hat{a}\}$ from $\{a^*\}$, and $\{\hat{b}\}$ from $\{b^*\}$, as described above:

$$\lambda\Big[[H^3_\psi] \quad [H^3_C]\Big]\begin{bmatrix}\{\hat{a}\}\\ [C_a]\{\hat{a}\}\end{bmatrix} = -2\Big\{[Q^1_\psi] \quad [Q^1_C]\Big\}\begin{Bmatrix}\{\hat{b}\}\\ [C_b]\{\hat{b}\}\end{Bmatrix}, \tag{133}$$

which can be rewritten as

$$\lambda\left([H^3_\psi]+[H^3_C][C_a]\right)\{\hat{a}\} = -2\left([Q^1_\psi]+[Q^1_C][C_b]\right)\{\hat{b}\}. \tag{134}$$

We then move on to the linearized momentum equation. First, the equation is rearranged,

$$\begin{aligned}\lambda\left(\tilde{q}-4Mh_s\tilde{q}''\right) &= \frac{6}{5}\left(-4h_s^{-3}h_s'\tilde{h}+2h_s^{-2}\tilde{h}'\right)-2P_e'\tilde{h}+8T\left(h_s\tilde{h}'''+h_s'''\tilde{h}\right)\\ &\quad+\frac{24}{R}h_s^{-3}\tilde{h}+\frac{6}{5}\left(4h_s^{-2}h_s'\tilde{q}-4h_s^{-1}\tilde{q}'\right)-\frac{12}{R}h_s^{-2}\tilde{q},\\ &= \frac{12}{5}\left(-2h_s^{-3}h_s'\tilde{h}+h_s^{-2}\tilde{h}'+\frac{10}{R}h_s^{-3}\tilde{h}\right)-2P_e'\tilde{h}\\ &\quad+8T\left(h_s\tilde{h}'''+h_s'''\tilde{h}\right)+\frac{12}{5}\left(2h_s^{-2}h_s'\tilde{q}-2h_s^{-1}\tilde{q}'-\frac{5}{R}h_s^{-2}\tilde{q}\right),\end{aligned} \tag{135}$$

then the approximations of Equations (103) and (104) are used:

$$\begin{aligned}\lambda\left([Q^2]\{b\}-4M\{h_s\}\circ[Q^0]\{b\}\right) &= \frac{12}{5}\Big(-2\{h_s^{-3}\}\circ\{h_s'\}\circ[H^3]\{a\}+\{h_s^{-2}\}\circ[H^2]\{a\}\\ &\quad+\frac{10}{R}\{h_s^{-3}\}\circ[H^3]\{a\}\Big)-2\{P_e'\}\circ[H^3]\{a\}\\ &\quad+8T\left(\{h_s\}\circ[H^0]\{a\}+\{h_s'''\}\circ[H^3]\{a\}\right)\\ &\quad+\frac{12}{5}\Big(2\{h_s^{-2}\}\circ\{h_s'\}\circ[Q^2]\{b\}-2\{h_s^{-1}\}\circ[Q^1]\{b\}\\ &\quad-\frac{5}{R}\{h_s^{-2}\}\circ[Q^2]\{b\}\Big),\end{aligned} \tag{136}$$

where $\{h_s\}$ is a vector of the steady-state solution evaluated at the Gauss-Chebyshev-Lobatto. Likewise, $\{h_s^{-m}\}$ $(m=1,2,3)$ corresponds to a vector containing $h_s^{-m}(\hat{x})$ evaluated at the Gauss-Chebyshev-Lobatoo points, and the same idea applies to $\{h_s'\}$. Vector $\{P_e'\}$ consists of $P_e'(\hat{x})$ also evaluated at the Gauss-Chebyshev-Lobatto points.

The next step is to rewrite Equation (136) in terms of $\{\hat{a}\}$ and $\{\hat{b}\}$,

$$\begin{aligned}&\lambda\Big[\left([Q^2_\psi]+[Q^2_C][C_b]\right)\{\hat{b}\}-4M\{h_s\}\circ\left([Q^0_\psi]+[Q^0_C][C_b]\right)\{\hat{b}\}\Big]\\ &\quad=\frac{12}{5}\Big[-2\{h_s^{-3}\}\circ\{h_s'\}\circ\left([H^3_\psi]+[H^3_C][C_a]\right)\{\hat{a}\}+\{h_s^{-2}\}\circ\left([H^2_\psi]+[H^2_C][C_a]\right)\{\hat{a}\}\\ &\qquad+\frac{10}{R}\{h_s^{-3}\}\circ\left([H^3_\psi]+[H^3_C][C_a]\right)\{\hat{a}\}\Big]-2\{P_e'\}\circ\left([H^3_\psi]+[H^3_C][C_a]\right)\{\hat{a}\}\\ &\quad+8T\Big[\{h_s\}\circ\left([H^0_\psi]+[H^0_C][C_a]\right)\{\hat{a}\}+\{h_s'''\}\circ\left([H^3_\psi]+[H^3_C][C_a]\right)\{\hat{a}\}\Big]\\ &\quad+\frac{12}{5}\Big[2\{h_s^{-2}\}\circ\{h_s'\}\circ\left([Q^2_\psi]+[Q^2_C][C_b]\right)\{\hat{b}\}-2\{h_s^{-1}\}\circ\left([Q^1_\psi]+[Q^1_C][C_b]\right)\{\hat{b}\}\\ &\qquad-\frac{5}{R}\{h_s^{-2}\}\circ\left([Q^2_\psi]+[Q^2_C][C_b]\right)\{\hat{b}\}\Big].\end{aligned} \tag{137}$$

This equation may be rearranged further.

$$\lambda\left[\left([Q^2_\psi]+[Q^2_C][C_b]\right)-4M\{h_s\}\circ\left([Q^0_\psi]+[Q^0_C][C_b]\right)\right]\{\hat{b}\}$$
$$=\Bigg\{\frac{12}{5}\Bigg[-2\{h_s^{-3}\}\circ\{h_s'\}\circ\left([H^3_\psi]+[H^3_C][C_a]\right)+\{h_s^{-2}\}\circ\left([H^2_\psi]+[H^2_C][C_a]\right)$$
$$+\frac{10}{R}\{h_s^{-3}\}\circ\left([H^3_\psi]+[H^3_C][C_a]\right)\Bigg]-2\{P_e'\}\circ\left([H^3_\psi]+[H^3_C][C_a]\right)$$
$$+8T\left[\{h_s\}\circ\left([H^0_\psi]+[H^0_C][C_a]\right)+\{h_s'''\}\circ\left([H^3_\psi]+[H^3_C][C_a]\right)\right]\Bigg\}\{\hat{a}\}$$
$$+\frac{12}{5}\Bigg[2\{h_s^{-2}\}\circ\{h_s'\}\circ\left([Q^2_\psi]+[Q^2_C][C_b]\right)-2\{h_s^{-1}\}\circ\left([Q^1_\psi]+[Q^1_C][C_b]\right)$$
$$-\frac{5}{R}\{h_s^{-2}\}\circ\left([Q^2_\psi]+[Q^2_C][C_b]\right)\Bigg]\{\hat{b}\}. \tag{138}$$

The approximation of Equations (103) and (104) are then applied to the boundary condition in which λ appears (Equation 99f).

$$4T[H^1]_0\{a\}=-L_2\left(\lambda[Q^2]_0\{b\}+\frac{12}{R}[Q^2]_0\{b\}\right). \tag{139}$$

Here, the subscript 0 has been used to indicate that only the first row of the matrix (the one associated with $\hat{x}_0$) is being considered. We then rearrange and rewrite in terms of $\{\hat{a}\}$ and $\{\hat{b}\}$ only.

$$\lambda L_2\left([Q^2_\psi]_0+[Q^2_C]_0[C_b]\right)\{\hat{b}\}=-4T\left([H^1_\psi]_0+[H^1_C]_0[C_a]\right)\{\hat{a}\}$$
$$-\frac{12L_2}{R}\left([Q^2_\psi]_0+[Q^2_C]_0[C_b]\right)\{\hat{b}\} \tag{140}$$

Equations (134), (138), and (140) may be considered together:

$$\lambda\begin{bmatrix}[B_{00}] & [0]\\ [0] & [B_{11}]\\ \{0\}^T & \{B_{21}\}^T\end{bmatrix}\begin{Bmatrix}\{\hat{a}\}\\ \{\hat{b}\}\end{Bmatrix}=\begin{bmatrix}[0] & [A_{01}]\\ [A_{10}] & [A_{11}]\\ \{A_{20}\}^T & \{A_{21}\}^T\end{bmatrix}\begin{Bmatrix}\{\hat{a}\}\\ \{\hat{b}\}\end{Bmatrix}, \tag{141}$$

where

$$[A_{01}] = -2\left([Q^1_\psi] + [Q^1_C][C_b]\right), \tag{142a}$$

$$\begin{aligned}[A_{10}] = \frac{12}{5}\Big[&-2\{h_s^{-3}\} \circ \{h_s'\} \circ \left([H^3_\psi] + [H^3_C][C_a]\right) + \{h_s^{-2}\} \circ \left([H^2_\psi] + [H^2_C][C_a]\right) \\ &+\frac{10}{R}\{h_s^{-3}\} \circ \left([H^3_\psi] + [H^3_C][C_a]\right)\Big] - 2\{P_e'\} \circ \left([H^3_\psi] + [H^3_C][C_a]\right) \\ &+ 8T\left[\{h_s\} \circ \left([H^0_\psi] + [H^0_C][C_a]\right) + \{h_s'''\} \circ \left([H^3_\psi] + [H^3_C][C_a]\right)\right],\end{aligned} \tag{142b}$$

$$\begin{aligned}[A_{11}] = \frac{12}{5}\Big[&2\{h_s^{-2}\} \circ \{h_s'\} \circ \left([Q^2_\psi] + [Q^2_C][C_b]\right) - 2\{h_s^{-1}\} \circ \left([Q^1_\psi] + [Q^1_C][C_b]\right) \\ &-\frac{5}{R}\{h_s^{-2}\} \circ \left([Q^2_\psi] + [Q^2_C][C_b]\right)\Big],\end{aligned} \tag{142c}$$

$$\{A_{20}\}^T = -4T\left([H^1_\psi]_0 + [H^1_C]_0[C_a]\right), \tag{142d}$$

$$\{A_{21}\}^T = -\frac{12L_2}{R}\left([Q^2_\psi]_0 + [Q^2_C]_0[C_b]\right), \tag{142e}$$

$$[B_{00}] = [H^3_\psi] + [H^3_C][C_a], \tag{142f}$$

$$[B_{11}] = [Q^2_\psi] + [Q^2_C][C_b] - 4M\{h_s\} \circ \left([Q^0_\psi] + [Q^0_C][C_b]\right), \tag{142g}$$

$$\{B_{21}\}^T = L_2\left([Q^2_\psi]_0 + [Q^2_C]_0[C_b]\right). \tag{142h}$$

Equation (141) is a generalized eigenvalue problem, of the form $\lambda[B]\{u\} = [A]\{u\}$, which is to be solved to obtain the eigenvalue and the approximation to the eigenfunctions $\tilde{h}$ and $\tilde{q}$ in the Gauss-Chebyshev-Lobatto points.

APPENDIX C – Designed components of the experimental model

The present appendix provides details on the experimental components that had to be designed and manufactured.

C.1 Pressurized chamber

A schematic drawing of the chamber is shown in Figure 105. As shown in the figure,

Figure 105 – Pressurized chamber.

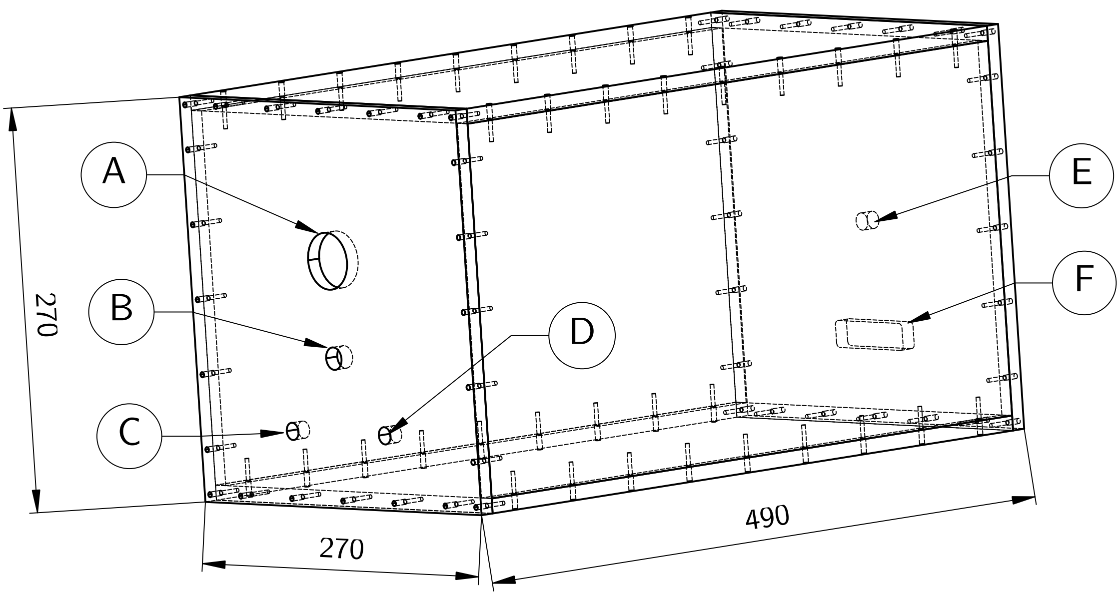

Source – Author.

All dimensions are in millimeters and all sides are made of 10 mm thick plexiglass. The following openings are labeled in the drawing: A, passage of the rigid tube; B, passage of a hose to connect to the inlet rigid tube; C and D, connections used to pressurize the chamber; E, pressure sensor connection; and F, passage of sensor cables.

the walls were held together with screws, but a thermoplastic sealant was used in the interfaces between the walls to avoid leaks. During assembly, aluminum angles were used along the edges of the chamber to improve the distribution of the tightening load. Five walls remained permanently attached with the sealant, while one (the one with openings A, B, C, and D in Figure 105) was left to be assembled and disassembled during the experiments. For this wall, a rubber gasket was used as a seal.

The chamber has six holes that are used for the passage of the rigid tube, hoses, cables, and for connecting the sensor used to read the pressure in the chamber. For the passage of the rigid tube downstream of the flexible tube (A in Figure 105), and for the passage of the cables (F in Figure 105), sealing parts were designed to maintain the pressure in the chamber.

Figure 106 illustrates the seal used for the rigid tube.

Figure 106 – Seal used for the passage of the rigid tube through the wall of the chamber.

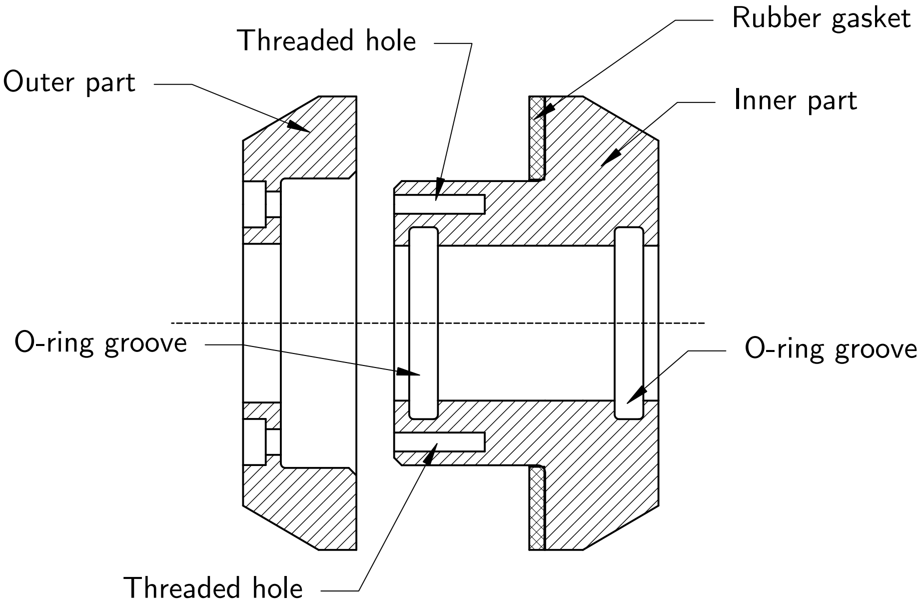

Source – Author.

The seal is composed of two parts. One is located inside the chamber and the other outside it. The part located inside has a cylindrical part and a flange. The cylindrical part is passed through a hole in the wall of the chamber (A in Figure 105). The part of the seal outside the chamber is essentially a cap, which sits in contact with the wall. Screws are passed through this cap, and engage with threaded holes in the inside part. As the screws are tightened, the flange on the inside part presses a rubber gasket against the wall, forming a seal around the flange. The rigid outlet tube passes through a central hole on the inside of both parts. A pair of O-rings provides the seal for the outer wall of the tube.

The seal for the passage of the cables follows the same basic principle. However, the inside and outside parts had to be divided in two (Figure 107), since the connectors of the cables prevented the cables from being slid through, as was the case for the tube. Here, the cables were laid in their respective grooves on the lower part, and upper part was screwed over it, using a silicone adhesive sealant at the interface between them. The sealing of the inside part against the wall of the chamber follows the same idea that was used for the rigid tube—a gasket was used between the flange of the inside part and the wall, and screws were used to force the flange against the wall, compressing the gasket.

Both the seal for the rigid tube, as the seal for the cables were 3–D printed, using PLA as the material. The pieces were sanded, and wood putty was used to fill voids in the print. The piece was sanded again, and a layer of primer was applied.

For the passage of the hose that will provide the airflow through the flexible tube inside the chamber (B in Figure 105), as well as for entrance and release of air from the chamber (C and D in Figure 105), standard pneumatic connectors were used. The

Figure 107 – Seal used for the passage of the cables through the wall of the chamber.

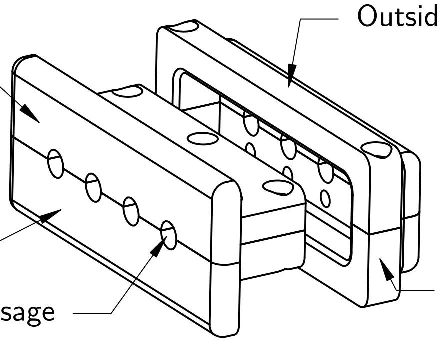

Source – Author.

pressure sensor to measure the pressure in the chamber was threaded directly to hole E of Figure 105.

C.2 Rigid tubes

A 3–D printed cap was designed for the inlet. As was the case for the sealing parts described in Section C.1, the cap was sanded, wood putty was used to fill larger voids in the piece, then the cap was sanded once more (Figure 108a) before applying a layer of primer (Figure 108b). On the side of the cap, a hole was made for the insertion of a pneumatic connector. The entrance was made perpendicular to the axis of the tube in order to approximate the placement of the prosthesis in the esophagus.

Figure 108 – Inlet cap.

(a) After applying wood putty and sanding.

(b) After applying primer.

Source – Author.

As shown in Figure 64, pressure readings are made along the rigid tubes. These are made with small Kulite pressure sensors. For their placement in the tube, mounting pieces were designed, based on similar solutions adopted by Hofmans et al. (2003), and Campo (2012). The pressure sensor is inserted in a silicone plug, and this plug in turn is inserted in the mounting piece, which connects to the rigid tube. A cover is screwed on top of the mounting piece, compressing the silicone plug and sealing any gaps. Figure 109 shows the silicone plug, the mounting piece, and the cover.

Figure 109 – Silicone plug and mounting piece for the Kulite pressure sensors.

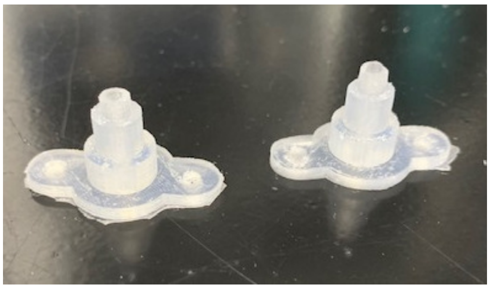

(a) Silicone plugs.

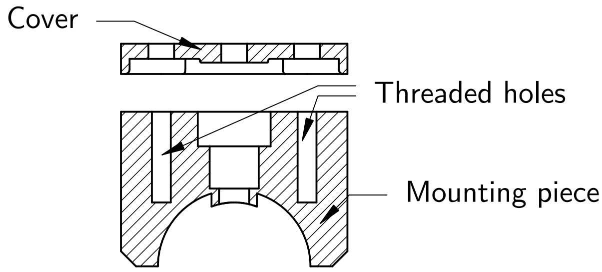

(b) Mounting piece.

Source – Author.

C.3 Longitudinal stretching mechanism

Two parts had to be developed for the longitudinal stretching mechanism: the sliding collar and the moving block. Both were 3–D printed.

The sliding collar has already been shown in Figure 68. Figure 110 shows the moving block. Six screws were used to attach it to the gantry; four of them were extended to the top of the block, in order to increase the stiffness of the block.

Figure 110 – Moving block.

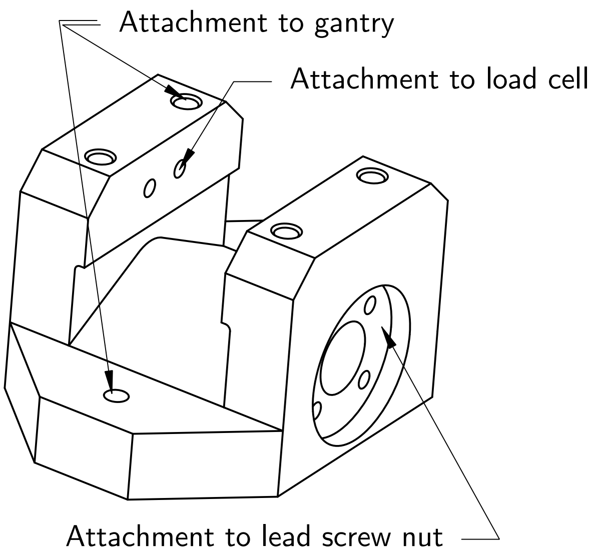

Source – Author.

Additionally, as discussed in Section 4.1.3, a spring clamp was developed to facilitate clamping the flexible tube to the rigid inlet tube. Figure 111 shows this clamp, which was 3–D printed.

Figure 111 – Spring clamp that was used alongside the stretching mechanism.

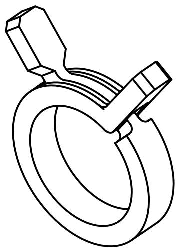

Source – Author.